GABA Receptor and K_{Ca} Channel-mediated Electrical Suppression in Anoxic Cortical Pyramidal Neurons of the Painted Turtle (*Chrysemys picta bellii*)

by

David William Richard Hogg

A thesis submitted in conformity with the requirements
for the degree of Doctor of Philosophy

Cell and Systems Biology

University of Toronto

GABA Receptor and K_{Ca} Channel-mediated Electrical Suppression in Anoxic Cortical Pyramidal Neurons of the Painted Turtle (*Chrysemys picta bellii*)

David William Richard Hogg

Doctor of Philosophy

Cell and Systems Biology
University of Toronto

2015

Abstract

The high energetic cost of neuronal communication requires large amounts of ATP to maintain function. In mammals, oxidative phosphorylation is required to meet these energy demands and without sufficient oxygen supply neuronal hyperexcitability and excitotoxic cell death occurs. This catastrophic cascade of events does not happen in the freshwater painted turtle *Chrysemys picta bellii*, instead there is a coordinated downregulation of cellular ATP consuming processes to match the lower anaerobic ATP supply. To reduce the energetic burden during anoxia turtles have evolved a sophisticated network of neuroprotective mechanisms including channel arrest and spike arrest which combine to prevent membrane depolarization and activation of excessive electrical activity. The aim of my research was to identify and elucidate cellular mechanisms responsible for suppression of electrical activity in anoxic turtle dorsal cortical brain pyramidal neurons. Using electrophysiological and fluorescent imaging techniques I demonstrate for the first time that: 1) in turtle dorsal cortex γ-aminobutyric acid (GABA) release increases during anoxia and enhances a unique $GABA_A$ receptor-mediated giant postsynaptic current, and shifts membrane potential to the GABA reversal potential (E_{GABA}), reducing electrical excitability; 2) endogenous GABAergic

mechanisms responsible for anoxia-tolerance also protect against a debilitating ischemic solution that mimics the cerebral fluid in the penumbral area that surrounds the infarct core; 3) in pyramidal neurons the open probability of Ca^{2+}-activated K^+ channels decreases during anoxia and this is prevented by inhibition of protein kinase C; and 4) anoxia-mediated decreases in mitochondrial reactive oxygen species (ROS) production are sufficient to initiate a redox-sensitive inhibitory GABA signaling cascade that suppresses electrical activity. Together this research significantly contributes to our understanding of the turtle's natural anoxia-tolerant strategy in brain and highlights the integral role of channel arrest and GABAergic spike arrest in prevention of anoxic or ischemic cell damage.

Acknowledgments

The successful completion and defense of a Ph.D. thesis results not only from one person's skill and hard work but also from the support of an entire network of dedicated people. I would like thank everyone who has taken their time to support me in my research, teaching or any other aspect of my graduate studies. This assistance has been critical to my success, and interacting with the intelligent and capable faculty and staff in the Department of Cell and Systems Biology has provided me with much enjoyment.

Firstly, I want to express my sincere gratitude to my supervisor Prof. Les Buck. It has been an absolutely wonderful experience working in your lab and I truly appreciate all the support you have given me over the years. Thank you for all your knowledge and insights into science and life, and thank you for being a great mentor and friend. I would also like to thank Prof. Melanie Woodin for her guidance and insight.

To the Buck lab grad students and post-docs, thanks for all the discussions and laughs. You have made the highs and lows of electrophysiological research an extremely rewarding experience. In particular, I would like to thank Matthew Pamenter and Peter Hawrysh for their important contributions to my research and for their friendship.

I have had the incredible good fortune of being raised by two loving parents who have inspired and supported me from the very start. I always aspire to make you proud and to be as good a parent to my girls as you have been to me. Thank you for everything.

To my incredibly intelligent and beautiful daughters Charlie Gwendolyn and Bailey Patricia, while I can't say that you two have made these last couple of years easier, you have definitely made them the best in my life. I am already so proud of you and I am excited to watch you grow. Just please… not too fast.

And finally, to the love of my life, my amazing wife Patricia. It has been over 27 years since we first met and I am thankful every day for your love and devotion to our family. I am also so very thankful for your unfailing support. You are my everything.

This thesis is dedicated to the memory of my father, Robert Darryl Hogg.

You are my inspiration. I love you and miss you.

Table of Contents

List of Tables

List of Figures

List of Appendices

Table 1. List of abbreviations

aCSF	artificial cerebrospinal fluid
AD	anoxic depolarization
ADP	adenosine diphosphate
AFU	arbitrary fluorescence units
AMP	adenosine monophosphate
AMPA	alpha-amino-3-hydroxy-5-methyl-4-isoxazolepropionic acid
AMPK	AMP-activated protein kinase
AP	action potential
AP_f	action potential frequency
AP_{th}	action potential threshold
ATP	adenosine triphosphate
$[ATP]_i$	intracellular adenosine triphosphate
cAMP	3'-5'-cyclic adenosine monophosphate
Ca_v	voltage-gated Ca^{2+} channels
CNS	central nervous system
DMSO	dimethyl sulfoxide
DNA	deoxyribonucleic acid
E_{Ca}	Ca^{2+} reversal potential
ECD	excitotoxic cell death
EGTA	ethylene glycol tetraacetic acid
E_{ion}	reversal potential of a specific ion or neurotransmitter
EPSP	excitatory postsynaptic potential
ER	endoplasmic reticulum
ETC	electron transport chain
$FADH_2$	flavin adenine dinucleotide
GABA	γ-amino butyric acid
GABA-T	GABA α-oxoglutarate transaminase
GAD	glutamic acid decarboxylase
GAT	GABA uptake transporter
GSH	glutathione
GSSG	glutathione disulfide

GZ	gabazine
HPV	hypoxic pulmonary vasoconstriction
H_2O_2	hydrogen peroxide
$[ion]_e$	extracellular concentration of a specific ion
$[ion]_i$	intracellular concentration of a specific ion
IPSC	inhibitory postsynaptic current
KCC2	K^+/Cl^- cotransporter
mK_{ATP}	mitochondrial ATP-sensitive potassium channel
mPTP	mitochondrial permeability transition pore
mROS	mitochondrial reactive oxygen species
mV	milivolt
NAC	*N*-acetylcysteine
NADH	nicotinamide adenine dinucleotide
NEBs	neuroepithelial bodies
NKCC1	$Na^+/K^+/Cl^-$ cotransporter
NMDA	N-methyl-D-aspartate
$O_2^{\bullet-}$	superoxide
PASMC	pulmonary artery smooth muscle cell
PKC	protein kinase C
PMCA	plasma membrane Ca^{2+} ATPase
P_{open}	open probability
PO_2	partial pressure of oxygen
PTX	picrotoxin
ROS	reactive oxygen species
SERCA	smooth endoplasmic reticular transporters
SOD	superoxide dismutase
TCA	tricarboxylic acid
TTX	tetrodotoxin
Ψ_m	mitochondrial membrane potential

1 General introduction to anoxia-induced stress and mechanisms of anoxia tolerance in turtle

1.1 Energy metabolism in the vertebrate brain

Neuronal communication is an energetically expensive process. This is particularly evident in human brain, which only comprises ~ 2% of the body's weight yet accounts for ~ 20% of the body's resting metabolic rate (Mink *et al.*, 1981). The high energetic demand of human brain is largely the result of neuronal communication between an estimated 80-100 billion neurons with ~ 7000 synaptic connections each (Pakkenberg *et al.*, 2003; Azevedo *et al.*, 2009). The energetic cost by signalling mechanisms at chemical synapses can be broadly divided between the presynaptic and postsynaptic adenosine triphosphate (ATP) requirements. Presynaptically, when an action potential (AP) depolarizes a nerve terminal voltage-gated Ca^{2+} channels are activated and the subsequent Ca^{2+} influx stimulates vesicle release. ATP is consumed by the Na^+/K^+ ATPase which extrudes Na^+ ions to return the membrane potential (V_m) to the resting potential of the cell, and powers Ca^{2+} removal by the Na^+/Ca^{2+} exchanger and Ca^{2+} ATPases (Howarth *et al.*, 2012). In addition, ATP is used to power synaptic vesicle exocytosis and endocytosis as well as for neurotransmitter recycling which requires ATP-dependent ion pumping as well as metabolic processing in astrocytes (e.g. conversion of glutamate to glutamine) (Attwell & Laughlin, 2001; Harris *et al.*, 2012). Postsynaptically, APs and postsynaptic potentials are produced by ion flux through ion channels and ionotropic receptors, and ion concentration gradients are re-established by ATPase pumps, co-transporters and exchangers. The maintenance of cellular ion concentration gradients is achieved either directly or indirectly by the hydrolysis of ATP to adenosine diphosphate (ADP), and in mammalian brain, it is estimated that the total ATP consumption associated with the release of a single vesicle of glutamate is ~ 164,000 ATP molecules (Shulman & Rothman, 2004). Reversal of the glutamate evoked Na^+ and Ca^{2+} fluxes through postsynaptic *N*-methyl-D-aspartate (NMDA) and non-NMDA receptors is particularly costly and has been estimated to account for ~ 50% of ATP consumption at glutamatergic synapses (Harris *et al.*, 2012; Howarth *et al.*, 2012).

The mitochondrion is a cellular organelle that serves as the power-house of the eukaryotic cell (Lane, 2005); and in aerobic organisms, mitochondrial ATP production by oxidative phosphorylation is essential for powering cellular processes and the maintenance of cellular

function. In mammalian brain, sustained neuronal activity is dependent on a steady supply of ATP and only aerobic energy pathways are capable of maintaining this level of ATP generation (Lutz *et al.*, 2003). In neurons, glucose is the preferred energy substrate although lactate and ketone bodies can be oxidized for fuel (for review see Dienel, 2012). Neuronal activity is a major consumer of glucose and accounts for ~ 25% of total body glucose utilization (Belanger *et al.*, 2011). To maintain mitochondrial electron transport the brain consumes ~ 20% of the total body oxygen uptake (Clarke & Sokoloff, 1999), and ~ 95% of the ATP produced is through aerobic glucose oxidation (Erecińska & Silver, 1994). Under aerobic conditions glucose is almost entirely oxidized to CO_2 and water resulting in little metabolic waste build up (Magistretti & Allaman, 2013). First, glucose is converted to pyruvate by the glycolytic pathway. This generates a net 2 ATP, 2 nicotinamide adenine dinucleotide (NADH) and 2 pyruvate molecules per glucose molecule. Using endogenous glycogen as a glucose source rather than exogenous glucose results in a net gain of one ATP (3ATP/glucosyl unit) but brain has limited glycogen reserves (Magistretti & Allaman, 2013). Pyruvate is further oxidized in the tricarboxylic acid (TCA) cycle producing an additional 8 NADH, 2 flavin adenine dinucleotide ($FADH_2$) molecules, and 2 ATP. NADH and $FADH_2$ are then utilized as a source of electrons in the mitochondrial electron transport chain (ETC) to generate a proton gradient by pumping H^+ from the matrix to the inner mitochondrial membrane space (Figure 1.3). The proton gradient is then coupled to ATP synthesis through the ATP synthase and oxygen is used as the terminal electron acceptor of the ETC resulting in the formation of water. The complete aerobic oxidation of one glucose molecule produces ~ 30 ATP depending on the coupling efficiency of oxidative phosphorylation (Magistretti & Allaman, 2013). Under aerobic conditions, mitochondrial ATP generation is sufficient to meet the metabolic demands of AP generation, and neuronal signalling is efficient without accumulation of toxic metabolic end-products (Senior, 1988).

1.2 Anoxic stress in the oxygen-dependent vertebrate brain

Oxygen deprivation compromises mitochondrial ATP generation and without a decrease in ATP consumption aerobic animals are faced with an energy crisis (Staples & Buck, 2009). The dependence of neuronal tissue on oxidative ATP supply means that even brief periods of hypoxia (insufficient oxygen for normal metabolic processes), or anoxia (partial pressure of oxygen (PO_2) = 0 mmHg) can result in neuronal damage and cell death (Siesjo, 1978; Lutz *et al.*, 2003). In brain, local oxygen reserves are limited and are consumed within seconds of anoxia (Hansen, 1985), and

local glycogen stores in astrocytes are minimal and cannot support prolonged neuron function (Magistretti & Allaman, 2013). Therefore, brain depends on a constant supply of oxygenated blood and glucose to maintain neuronal signaling. Under anoxic conditions, without oxygen to accept electrons from cytochrome c oxidase (complex IV of the mitochondrial ETC), electron transfer along the ETC is prevented and the proton gradient is diminished resulting in inhibition of oxidative phosphorylation and aerobic ATP production. Cellular reserves of high energy phosphates are limited and can only maintain normoxic ATP consumption rates for ~ 20 seconds (Lutz *et al.*, 2003). To preserve intracellular [ATP] ($[ATP]_i$) and maintain neuron function the rate of anaerobic glycolysis must increase ~ 10-fold, a process known as the Pasteur effect (Dixon, 1937). This high rate of anaerobic ATP generation is unsustainable and anaerobic glycolysis can only support neuronal ATP demand for a few minutes before decreases in $[ATP]_i$ and accumulation of toxic glycolytic end products. Cell death occurs though a catastrophic cascade of events termed excitotoxic cell death (ECD) which is characteristic of brain damage due to cerebral stroke or whole brain anoxia due to cardiac failure (Lipton, 1999).

1.3 Anoxia-induced excitotoxic cell death in mammalian neurons

Calcium is an important signalling molecule in eukaryotic cells; and therefore, in intracellular [Ca^{2+}] ($[Ca^{2+}]_i$) is maintained at low levels (~ 100 nM free) (Jackson & Redman, 2003; Williams *et al.*, 2013). This is primarily achieved by plasma membrane Ca^{2+} ATPases (PMCA) and smooth endoplasmic reticular (SERCA) transporters (Rizzuto & Pozzan, 2006). Ca^{2+} is also taken up into the mitochondria through the mitochondrial Ca^{2+} uniporter or moved across the plasma membrane by Na^+/Ca^{2+} and the Na^+/Ca^{2+}-K^+ exchangers that harness the Na^+ gradient set up by Na^+/K^+ATPase activity. This creates an ~ 20,000-fold $[Ca^{2+}]_i$ gradient (Ca^{2+} reversal potential (E_{Ca}) ~ +150 mV) between intracellular and extracellular compartments, and this allows for fast Ca^{2+} signaling cascades which are integral for neuron function and communication (Clapham, 2007). Signaling cascades initiated by increases in $[Ca^{2+}]_i$ can broadly activate Ca^{2+} binding proteins, however, the actual Ca^{2+} signal tends to be restricted to local changes due to endogenous buffers surrounding Ca^{2+} entry points (Clapham, 2007). Changes in local but not global $[Ca^{2+}]_i$ permits the faithful initiation of Ca^{2+}-mediated signals but this is contingent on Ca^{2+} extrusion from the cytosol after the signal occurs. Any process that disrupts the proper distribution of $[Ca^{2+}]_i$ risks over activating Ca^{2+}- sensitive proteins which has disastrous consequences.

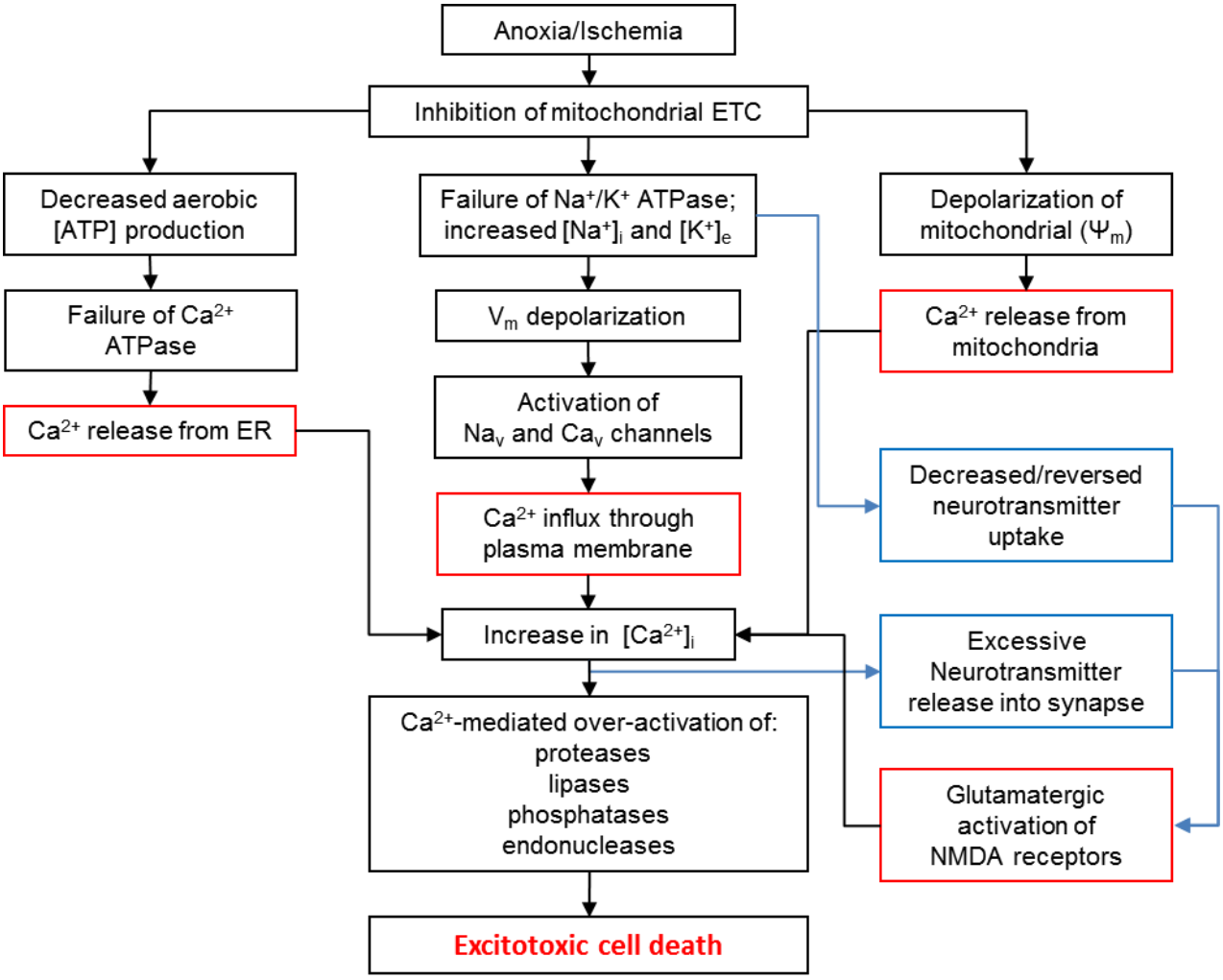

Figure 1.1. Flow chart outlining events associated with excitotoxic cell death in anoxia-intolerant vertebrate neurons.
Red boxes indicate major sources of calcium entry into the cytosol and blue boxes indicate additional effects of oxygen deprivation on presynaptic nerve terminals and glial cells.

In mammalian brain, more than 2 minutes of oxygen deprivation decreases $[ATP]_i$ to less than 15% of normoxic levels, and results in failure of ATP-driven ion transport (Lipton, 1999). Without Na^+/K^+ ATPase activity the Na^+ and K^+ concentration gradients collapse, resulting in depolarization of V_m and over-activation of voltage-gated Na^+ channels (Hansen, 1985; Anderson *et al.*, 2005). This process is termed anoxic depolarization (AD) and it results in electrical hyper-excitability and a drastic increase in $[Ca^{2+}]_i$ due to: 1) over activation of voltage-gated Ca^{2+} channels (Ca_v), 2) inhibition of Ca^{2+} ATPase pumps and Ca^{2+} release from endoplasmic reticulum (ER) stores, and 3) mitochondrial Ca^{2+} release as a result of depolarization of the mitochondrial membrane potential (Ψ_m) (Koopman *et al.*, 2006). In addition, $[Ca^{2+}]_i$ cannot be removed because Ca^{2+} extrusion mechanisms are dependent on ATP and the Na^+ gradient (Stys *et al.*, 1991; Besancon *et al.*, 2008). Membrane depolarization and $[Ca^{2+}]_i$ accumulation enhance the release of amino acid neurotransmitters, including excitatory vesicular glutamate release. This is particularly damaging because ~ 80% of synapses in brain are glutamatergic (Braitenberg & Schüz, 1998; Brady *et al.*, 2005), which leads to activation of NMDA and alpha-amino-3-hydroxy-5-methyl-4-isoxazolepropionic acid (AMPA) receptors and hyperexcitability in synaptically connected and nearby neurons (Choi, 1992). Under aerobic conditions excess synaptic glutamate is rapidly cleared from the synaptic cleft by Na^+ coupled glutamate uptake transporters (Danbolt, 2001; Boudker *et al.*, 2007; Jiang & Amara, 2011); however, under anoxic conditions glutamate uptake is reduced or even reversed further activating glutamate receptors (Abele *et al.*, 1990; Rossi *et al.*, 2000). The end result is a massive derangement of ion concentration gradients which leads to Ca^{2+}-mediated over activation of proteases, lipases, phosphatases, and endonucleases that directly damage cell structure and induce necrotic cell death (Figure 1.1) (Hansen, 1985; Choi, 1992; Arundine & Tymianski, 2004).

1.4 Anoxia-tolerant adaptations in painted turtle

As discussed above, mammals and most air-breathing vertebrates are dependent on a continuous supply of oxygen because they cannot survive without aerobically derived ATP. Anoxia-intolerant mammals attempt to maintain normoxic ATP turnover rates by up-regulating physiological mechanisms to optimize extraction of oxygen and maintain oxidative ATP production (e.g., hyperventilation and tachycardia). Hypoxia tolerant mammals and birds such as deep sea diving seals and penguins have specialized adaptations including: stores of oxygenated erythrocytes and elevated hemoglobin and myoglobin levels to increase body oxygen stores for long dives

(reviewed in Ponganis *et al.*, 2011). These adaptations however, will not protect against prolonged anoxic stress since oxygen stores will eventually need to be replenished. Two of the most hypoxia-tolerant mammals are the naked mole rat (*Heterocephalus glaber*) and the arctic ground squirrel (*Spermophilus parryii*). These animals can survive severe hypoxia because of their ability to depress metabolism; however, these species cannot survive more than 30 min of sustained anoxia (Drew *et al.*, 2004; Larson & Park, 2009). In contrast, there is an exceptional group of vertebrates classified as facultative anaerobes that have the ability to withstand prolonged periods of anoxia. Facultative anaerobes are organisms that produce ATP by aerobic respiration when oxygen is present, but have the capacity to survive on anaerobically derived ATP when oxygen is absent. There are only a few true vertebrate facultative anaerobes and it is a select group of freshwater turtles and cyprinid fish that are the best characterized. These include the painted turtles (*Chrysemys picta*) and red eared sliders (*Trachemys scripta*) and the common carp (*Carassius carassius*) and goldfish (*Carassius auratus*) (Lutz *et al.*, 2003; Bickler & Buck, 2007). These species have evolved the ability to withstand days to months of severe hypoxia or anoxia while overwintering under ice covered water bodies (Nilsson & Renshaw, 2004; Bickler & Buck, 2007). The following section will focus on adaptations that allow the painted turtle to withstand prolonged anoxia

Painted turtles overwinter for months in ponds and lakes where seasonal ice cover insulates the water from fluctuations in temperature and prevents freezing with water temperatures of ~ 3°C. In the winter the water becomes progressively more hypoxic because ice cover prevents atmospheric oxygen from penetrating the water and decomposition of plant material creates a eutrophic environment (Ultsch, 1989; Jackson, 2000). To survive decreasing oxygen levels turtles have evolved a number of adaptations. Under aerobic conditions, turtles acquire oxygen primarily through pulmonary respiration; however, they also have the capacity to absorb oxygen cutaneously, and in severely hypoxic water they can even take up sufficient amounts of oxygen to maintain oxidative ATP production (Koopman *et al.*, 2006). Conventionally, turtles were thought to be inactive while overwintering: however, recent studies have determined that they remain active under the ice and likely move to areas with higher PO_2 levels (Rollinson *et al.*, 2008). This would enable oxidative ATP generation, reduce metabolic acidosis, and prevent substrate (glycogen) depletion, and this indicates that under natural conditions turtles may only be subjected to limited anoxia (~ 2-3 months). Regardless of the natural activity of overwintering turtles, they

have been shown to survive on average 4 months of complete anoxia at 3 °C in the laboratory and up to 6 months in extreme cases (Jackson & Ultsch, 1982)

Painted turtles have evolved a number of protective mechanisms to avoid damage to organs and tissues under anaerobic conditions. Excessive reactive oxygen species (ROS) generation can lead to oxidative damage of lipids and protein and deoxyribonucleic acid (DNA). Transition to anoxia/hypoxia and in particular reoxygenation leads to elevated [ROS] which can overwhelm antioxidant defense mechanisms and is a major component of cell damage in anoxic/ischemic mammals (Warner *et al.*, 2004). To avoid ROS damage freshwater turtles express a variety of constitutively active antioxidant enzymes, including catalase, superoxide dismutase (SOD) and alkyl hydroperoxide reductase (Willmore & Storey, 1997a). Furthermore, turtle organs have higher levels of the antioxidant peptide glutathione compared to mammals (Willmore & Storey, 1997b), and the antioxidant ascorbic acid is 2-3 times higher in turtle than in mammal brain (Rice *et al.*, 1995). In addition, a variety of molecular chaperones, stress responsive transcription factors and pro-survival proteins are naturally upregulated or constitutively active in turtle tissues to maintain functional proteins or prevent against anoxic damage (reviewed in Krivoruchko & Storey, 2010). Together these endogenous protective mechanisms endow turtles with the ability to survive long-term anoxia and make them the most anoxia-tolerant air breathing vertebrate species known.

1.4.1 Metabolic depression as a strategy for surviving long-term anoxia

Under anaerobic conditions, ATP synthesis decreases to ~ 10% of aerobic levels due to inhibition of oxidative phosphorylation (Koopman *et al.*, 2006). In mammals normoxic metabolic rates are maintained during hypoxia by up-regulating anaerobic energy production. This is only a short term solution that rapidly results in a decrease in $[ATP]_i$, tissue and blood acidosis and depletion of glycogen stores (Koopman *et al.*, 2006). In stress tolerant organisms, including mammals, fish, reptiles and insects, a common response to oxygen deprivation or hypothermia is a decrease in metabolic rate (Guppy & Withers, 1999). To explain this phenomenon, Peter Hochachka proposed the metabolic arrest hypothesis which suggests that during periods of hypoxia and/or hypothermia, decreases in ATP consumption must accompany decreased ATP production to maintain substrate stores and ionic homeostasis (Hochachka, 1986). This hypothesis remains valid today and the following section will outline some of the important supporting evidence from turtle studies.

An important component of the turtles overwintering strategy is to take advantage of the naturally depressive effects that cold temperatures have on metabolic rate (Herbert & Jackson, 1985). This approach is very effective, and laboratory studies have demonstrated that the combination of anoxia and cold temperatures (3°C) results in a 90% decrease in whole body metabolic rate (measured by calorimetry) (Jackson, 1968). Typical physiological responses to a decrease in PO_2 and temperature in turtle include: a decrease in heart rate from 30 beats/min at 20 °C to ~ 1 beat/10 min at 3 °C (Herbert & Jackson, 1985), and a greater than 90% decrease in heat output or metabolic rate in hepatocytes (Buck *et al.*, 1993), brain (Doll *et al.*, 1994), and the whole animal (Jackson, 1968). Metabolic depression is in part due to suppression of non-essential energy consuming processes, including protein turnover (~ 90%) and urea synthesis (~ 74%) (hepatocyte; Land *et al.*, 1993). Turtles are ectotherms and thermally conform to ambient temperature. Because of this they have metabolic rates that are 10-20% lower than that of a similar sized mammal at warm temperatures (> 20 °C) (Bennett & Ruben, 1979). As temperatures decrease metabolic rate decreases even further, typically ~ 2 to 3 fold per 10 °C decrease in temperature (Q_{10} = 2-3) (Jackson, 2002). In addition, at temperatures below 15 °C turtles have an exaggerated Q_{10} effect which peaks at a Q_{10} = 8.5 at 3 °C (Herbert & Jackson, 1985). Thus, low temperatures significantly depress metabolic rate and is a noteworthy component of the turtles overwintering strategy. Indeed, the importance of temperature to metabolic depression is supported by field studies which determined that turtles move to colder areas when water PO_2 decreases (Rollinson *et al.*, 2008).

One reason cold temperatures have a depressing effect on metabolic rate is because lipid membranes become more rigid at cold temperatures and this restricts membrane protein movement and enzyme reaction rates (Hazel, 1995). In the anoxia-tolerant crucian carp even mildly cold temperatures (15 °C) significantly decrease plasma membrane bound Na^+/K^+ ATPase activity (Vornanen & Paajanen, 2006), demonstrating the important energy savings that cold temperatures can provide under anoxia conditions. Cytosolic enzyme activity is also directly affected by cold, and in turtle white muscle a decrease in temperature from 20 to 6 °C causes a ~ 60-70% reduction in the activity of the enzyme phosphofructokinase (PFK) (Brooks & Storey, 1990). A major benefit of the depressing effect of cold temperatures on metabolic rate in overwintering turtles is that it prevents the rapid consumption of glycogen and associated lactic acidosis during anoxia and extends survival times (Herbert & Jackson, 1985). It is possible that reduced PFK activity is a component of this because PFK regulates glycolytic rate and reduced activity will help maintain

glycogen stores. When submerged under water at 20 °C the turtle's anoxic survival time is shortened by ~ 200 times (Herbert & Jackson, 1985; Jackson, 2002); indicating that low temperatures are indeed an important component of their anoxic survival strategy. However, even at these warmer temperatures turtles are still able to survive anoxia 1000-10,000 times longer than a typical vertebrate (Bickler & Buck, 2007). In warm acclimatized turtles (20-24°C) anoxia alone induces an ~ 85% decrease in whole body metabolic rate (calorimetry) (Herbert & Jackson, 1985). In isolated brain sheets, anoxia or cyanide (inhibitor of oxidative phosphorylation) decrease metabolic rate by ~ 40-50 % at 25 °C (calorimetry); indicating that there are tissue level mechanisms that depress metabolic rate in brain (Doll *et al.*, 1994). This demonstrates that in anoxic turtles in addition to temperature-mediated effects on metabolic rate there are temperature-independent mechanisms that contribute to depression of metabolism and the ability of all metabolic needs to be met by anaerobic metabolic pathways.

In contrast to intolerant mammals, the painted turtle defends $[ATP]_i$ during anoxia, and metabolic needs can be sustained exclusively by glycolytic pathways (Jackson, 2002). However, glycolytic ATP production still consumes significant amounts of glucose, even at a severely reduced metabolic rate (Koopman *et al.*, 2006). To preserve glycogen and prolong anoxic survival, turtles undergo a large-scale reversible reduction in cellular energy turnover to levels sustainable by anaerobic energy production alone. Anoxic maintenance of $[ATP]_i$ is contingent on a steady supply of the glycolytic substrate glucose. To provide sufficient substrate for long-term anoxic survival turtles amass large amounts of glycogen in the liver (~ 900 μmoles.g-1 wet weight liver) (Hochachka & Somero, 1984). Turtle liver is ~ 15% glycogen by mass which is ten times the capacity of the rat, highlighting the importance of turtle glycogen stores during anoxia (Clark & Miller Jr, 1973). Indeed, after 4 hours of anoxia blood [glucose] increases ~ 10-fold, supplying organs and tissues with low endogenous glycogen stores (e.g., brain) with an essential supply of glucose (Ramaglia & Buck, 2004). Even with a decreased metabolic rate glycolysis results in a significant increase in the production of glycolytic end products during long-term anoxia (e.g., lactate, H^+). As a primary defense against anoxia-mediated acidosis turtle blood has a large buffering capacity due primarily to high blood plasma [bicarbonate] ($[HCO_3^-]$) levels (~ 40 $mmol.l^{-1}$) (Nicol *et al.*, 1983; Herbert & Jackson, 1985). To aid in removal of these acidic anaerobic end products cerebral blood flow is also increased during anoxia (Bickler, 1992; Hylland *et al.*, 1994). However, eventually plasma buffering mechanisms are overcome and during anoxia blood lactate

can increase from 1 to 200 mmol.l^{-1} and pH decrease from 8 units to < 7 units over 3 months submerged in cold (3 °C) anoxic water (Ultsch & Jackson, 1982). To withstand accumulation of lactate and [H^+] in blood and tissue, a unique proton consuming plasma buffering system that utilizes Ca^{2+} carbonates from shell and bone to reversibly sequester lactate in shell and bone has evolved in the turtle (Warren & Jackson, 2008).

1.4.2 Channel arrest as a strategy for surviving long-term anoxia

Electrically active cells, such as neurons, face additional challenges during anoxia due to the high metabolic cost of AP generation. In brain, it is estimated that ~ 50% of the total energy consumption following AP generation is used to re-establish ion concentration gradients. The primary consumer of ATP following AP generation is the Na^+/K^+ ATPase which re-establishes Na^+ and K^+ gradients by pumping three Na^+ out of the cell and two K^+ into the cell against their concentration gradients for every ATP hydrolyzed (Howarth *et al.*, 2012; Yu *et al.*, 2012). ın anoxia-intolerant brain ion pumping cannot be sustained by anaerobic glycolysis primarily due to the high energetic requirements of the Na^+/K^+ATPase, highlighting the importance of this ion pump to neuron function. Maintenance of ionic gradients is also important in turtle, as evidenced by studies of Na^+/K^+ ATPase activity in liver, in which ion pumping was determined to consume 30% of the total ATP turnover during normoxia and up to 75% of total ATP turnover during anoxia (Buck & Hochachka, 1993). Maintenance of the Na^+ electrochemical gradient is therefore a priority in the anoxic turtle brain and indicates an important area in which energy can be saved. One mechanism to reduce the cost of maintaining electrochemical gradients is a decrease in ion movement through ion channels, termed channel arrest (Hochachka, 1986). Reptile membranes are endogenously ~ 5-fold less permeable to Na^+ and K^+ than mammal/endotherm membranes in animals of a similar size at the same temperature (Else & Hulbert, 1987), providing them with an natural advantage under anaerobic conditions. However, in anoxic turtle brain there is an additional decrease in membrane permeability following transition to anoxia. Evidence supporting channel arrest in turtle brain includes, a 42% decrease in voltage-gated Na^+ channel density as determined by [3H]brevetoxin-binding assays (*Pseudemys scripta*) (Perez-Pinzon *et al.*, 1992a) and a 70% decrease in K^+ leakage during anoxia, suggesting inhibition of K^+ channels (*Trachemys scripta*) (Chih *et al.*, 1989; Pék & Lutz, 1997).

In the anoxic mammalian brain, extracellular glutamate accumulates within minutes resulting in over-activation of glutamate receptors, further promoting neuronal hyperexcitability (Koopman *et al.*, 2006). In contrast, in turtle brain extracellular [glutamate] is maintained at basal levels for at least 5 hours of anoxia (Nilsson & Lutz, 1991). This is achieved through inhibition of activity-dependent vesicular glutamate release and the maintenance of glutamate uptake transporters early in anoxia (0-1.5 hours) (Thompson *et al.*, 2007a). In addition to decreased glutamate release, postsynaptic glutamate receptor activity is also decreased. In pyramidal neurons of the cerebrocortex, anoxia leads to a 65% decrease in NMDA receptor open probability (P_{open}) after 60 minutes of anoxia (Buck & Bickler, 1998). Whole-cell NMDA receptor currents decrease by 45-65% following only 30 minutes of anoxia (Shin & Buck, 2003; Pamenter *et al.*, 2008a; Pamenter *et al.*, 2008c) and a reduction in whole-cell AMPA receptor currents by as much as 50-60% (Pamenter *et al.*, 2008b; Zivkovic & Buck, 2010). One possibility for the acute reduction in NMDA receptor currents during anoxia is receptor internalization. This has not directly been assessed in pyramidal neurons; however, the relative abundance of the NR1 subunit in the membrane fraction of whole brain homogenates remains unchanged until after 3 days of anoxia, suggesting that regulation of NMDA receptors by subunit expression occurs only during prolonged anoxia (Bickler *et al.*, 2000). This evidence indicates that in anoxic turtle pyramidal neurons there is an endogenous oxygen sensor that initiates an acute neuroprotective signalling mechanism that causes channel arrest of excitatory glutamate receptors and prevents excessive Ca^{2+} influx (see below for mechanism).

1.4.3 Spike arrest as a strategy for surviving long-term anoxia

In resting brain, ~ 80% of the ATP turnover is consumed by processes associated with AP firing and cycling of γ-amino butyric acid (GABA) and glutamate neurotransmitters (Shulman *et al.*, 2004). Therefore, suppression of electrical activity (e.g., AP firing) during periods of low oxygen is an effective neuroprotective strategy to conserve $[ATP]_i$. In anoxic turtle brain, in addition to channel arrest there is a significant decrease in electrical excitability, termed spike arrest (Perez-Pinzon *et al.*, 1992a). Evidence supporting spike arrest in turtle brain includes a 75 - 95 % suppression of whole brain electrical activity which involves reductions in transmembrane potentials, Na^+ spike thresholds and AP frequency (AP_f) (Perez-Pinzon *et al.*, 1992a; Perez-Pinzon *et al.*, 1992b; Fernandes *et al.*, 1997). In anoxic turtle (*C.picta, Trachemys scripta elegans*) and fish (*C. carassius*, *C. auratus*) brain, the inhibitory neurotransmitter GABA is rapidly elevated 80-

fold during anoxia (Nilsson & Lutz, 1991; Hylland & Nilsson, 1999), indicating that this is the likely cause of electrical suppression in these species. In contrast, in ischemic mammalian neurons [GABA] is elevated only ~30%, GABA receptor subunit mRNA expression is decreased and GABA-evoked currents run down quickly, indicating GABAergic signaling is not neuroprotective (Erecinska et al., 1984; Li et al., 1993). This indicates a divergent and important role for GABAergic mechanisms during anoxic insult in turtle brain.

1.5 GABA-mediated inhibition

GABAergic interneurons have been identified in turtle cerebrocortex and the massive increase in striatal [GABA] under anoxic conditions emphasizes the importance of this inhibitory mechanism to anoxic survival. Understanding how GABA acts to suppress electrical activity in the anoxic turtle brain will be key to elucidating the underlying mechanisms of spike arrest. Since GABAergic neurotransmission is best characterized in mammalian brain, the following section will outline mechanisms of GABAergic inhibition in the mammal.

1.5.1 GABA

GABA is a highly conserved amino acid, it is the primary inhibitory neurotransmitter in vertebrate brain and an estimated 20-30% of the neurons in the mammalian central nervous system (CNS) are GABAergic (Rudolph & Knoflach, 2011). GABA is synthesized *in vivo* by a metabolic pathway termed, the GABA shunt (not to be confused with GABAergic shunting inhibition, see below) (reviewed in Olsen *et al.*, 1999). GABA is produced in the mitochondria primarily from glucose, although pyruvate, other amino acids, and fatty acids can act as precursors. The first step is the transamination of α-ketoglutarate by GABA α-oxoglutarate transaminase (GABA-T) into L-glutamic acid. Glutamic acid decarboxylase (GAD) next catalyzes the decarboxylation of glutamic acid to form GABA. To complete the cycle GABA is metabolized by GABA-T to form succinic semialdehyde which can then be oxidized by succinic semialdehyde dehydrogenase into succinic acid and enter the Krebs cycle. Following vesicular GABA release into the synapse, GABA is removed from the synapse by surrounding glial cells and presynaptic nerve terminals by GABA uptake transporters (GATs). GATs are capable of bidirectional GABA transport which is dependent on the Na^+ and Cl^- gradients (Borden, 1996). GABA taken up into the presynaptic nerve terminal can be reutilized, but GABA taken up into glia is metabolized into succinic semialdehyde and cannot be resynthesized in glia because they lack the enzyme GAD. GABA in glia is converted

into glutamine which is shuttled back into GABAergic neurons. Glutamine is then converted into glutamate and re-entered into the GABA shunt. This metabolic process serves the purpose of producing and conserving GABA.

1.5.2 GABA receptors

Vesicular GABA release activates two main types of receptors; type A ionotropic GABA receptors ($GABA_A$ receptors) and type B metabotropic GABA receptors ($GABA_B$ receptors). $GABA_A$ receptors are ligand-gated heteropentameric transmembrane ion channels, and are structurally similar to the superfamily of Cys loop-type channels that includes the nicotinic acetylcholine, 5-HT_3 (sertonin) and strychnine-sensitive glycine receptors. These ion channels conduct Cl^- and bicarbonate at an ~ 4:1 ratio, and they are the primary mediator of fast synaptic inhibition in the vertebrate brain (Kaila, 1994). To date, 19 $GABA_A$ receptor subunits (α1–6, β1–3, γ1–3, δ, ε, θ, π and ρ1–3) have been identified in the mammalian CNS (Ben-Ari *et al.*, 2007; Rudolph & Knoflach, 2011). The molecular composition of $GABA_A$ receptors has important functional consequences as it determines the properties, pharmacological modulation and targeting of native receptors; and therefore, the large diversity of $GABA_A$ receptor subunits indicates these receptors play a variety of roles in brain (Ben-Ari *et al.*, 2007). The common adult isoform is composed of $2\alpha_1$, 2β2 and $1\gamma_2$ subunits (Sigel & Steinmann, 2012) and the GABA binding site lies at the interface of α- and β- subunits therefore, two GABA molecules are required to fully activate the receptor. Pharmacological agonists include muscimol and isoguvacine, and these sites are antagonized by gabazine and bicuculline, and picrotoxin is a non-competitive antagonist that directly blocks ion flux by binding within the chloride channel. $GABA_A$ receptors are positively modulated by benzodiazepines that bind to a separate high affinity binding site located at the α/γ interface (Figure 1.2A) (Sigel & Steinmann, 2012).

$GABA_A$ receptors are classified into two fundamentally distinct types of receptors, synaptic and extrasynaptic receptors that mediate phasic and tonic inhibition, respectively (Figure 1.2). The γ2 subunit is required for the synaptic clustering of $GABA_A$ receptors and receptors with these subunits typically exhibit fast kinetics, low sensitivity to GABA, and rapid desensitization (Essrich *et al.*, 1998). This enables them to conduct fast inhibitory postsynaptic events, typical of phasic inhibition (Brickley *et al.*, 1999). Phasic (synaptic) GABA neurotransmission is involved in setting the temporal window for synaptic integration (e.g., eliciting an AP) and synchronization of

network oscillation (Cobb *et al.*, 1995; Pouille & Scanziani, 2001). Tonic inhibition is mediated by extrasynaptically located $GABA_A$ receptors containing an α5 or δ subunit instead of a γ subunit (Bright & Smart, 2013). These receptors exhibit a higher sensitivity to GABA which allows them to respond to ambient levels of GABA and generate a persistent, tonic current. Tonic currents increase membrane permeability to Cl^- and therefore, have the ability to alter neuronal gain and firing threshold and regulate neuronal excitability (Mitchell & Silver, 2003; Semyanov *et al.*, 2004). There is accumulating evidence supporting a phasic *slow* type of $GABA_A$ receptor-mediated inhibition that is activated by transmitter spillover onto perisynaptic located $GABA_A$ receptors ($GABA_{A,slow}$ receptor) (reviewed in Capogna & Pearce, 2011). While the exact role of these currents is unknown, it is thought that $GABA_{A,slow}$ currents are involved in modulating synaptic plasticity by inhibiting NMDA receptors and the generation of slow network oscillations (Kanter *et al.*, 1996; Kapur *et al.*, 1997).

$GABA_B$ receptors are heterodimeric seven-transmembrane G-protein coupled receptors that inhibit neurotransmitter release presynaptically, and hyperpolarize V_m postsynaptically (Kornau, 2006). Activation of presynaptic $GABA_B$ receptors reduces neurotransmitter release by inhibiting Ca^{2+} influx through voltage-gated Ca^{2+} channels, by decreasing adenylate cyclase production of cAMP which prevents vesicle fusion, and by directly inhibiting the SNARE complex (soluble *N*-ethylmaleimide-sensitive factor attachment protein receptor) required for vesicle fusion (reviewed in Gassmann & Bettler, 2012). $GABA_B$ receptors have been found to be widely expressed on presynaptic nerve terminals surrounding dendritic spines of glutamatergic neurons suggesting they exert control of excitatory signalling (Kornau, 2006). Postsynaptically, activation of $GABA_B$ receptors results in a slow hyperpolarization of V_m towards the K^+ reversal potential (~ -90 mV), and induces shunting inhibition that can decrease neuronal excitation (Otmakhova & Lisman, 2004). $GABA_B$ receptor-activated Gα-proteins also differentially modulate adenylate cyclases resulting in changes in local 3'-5'-cyclic adenosine monophosphate (cAMP) concentrations (Hashimoto & Kuriyama, 1997; Simonds, 1999). This can regulate cAMP-dependent kinases which modulate various channel activities (Gerber & Gahwiler, 1994).

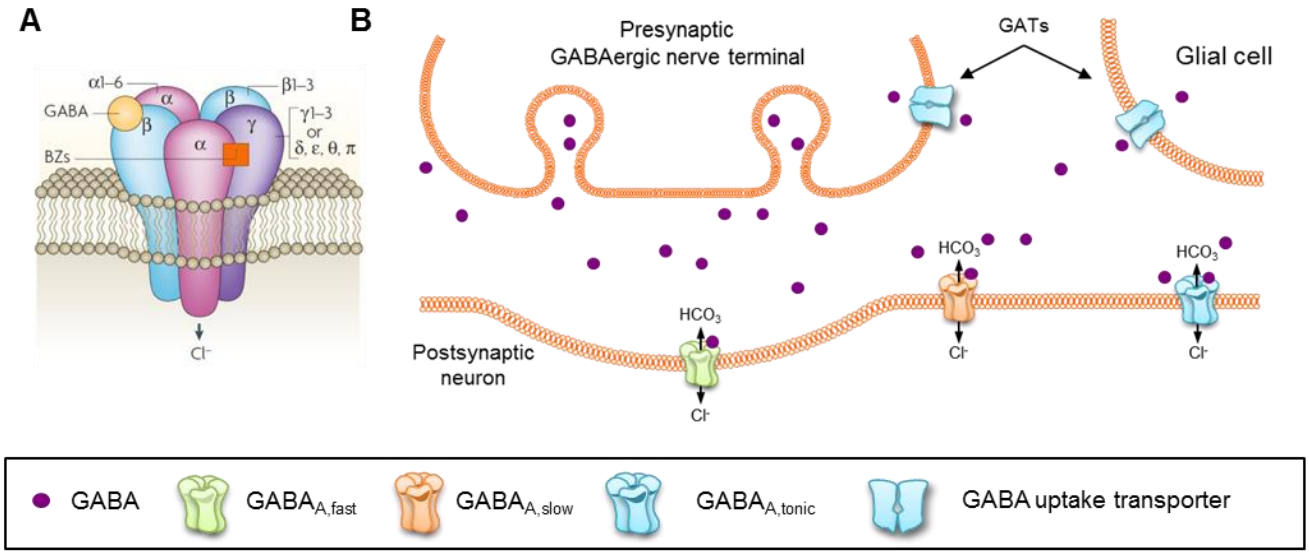

C

GABA$_A$ receptor – mediated inhibition	GABA$_{A,fast}$	GABA$_{A,slow}$	GABA$_{A,tonic}$
Location on neuronal plasma membrane	Synaptic	Perisynaptic	Extrasynaptic
Typical GABA$_A$ receptor currents	100 pA, 50 ms	100 pA, 50 ms	Bicuculline; 40 pA, 20 sec
Typical receptor Kinetics	fast kinetics (τ_{decay} < 10 ms) low GABA sensitivity rapid desensitization	medium kinetics (decay > 30 ms) high GABA sensitivity? slower desensitization	slow kinetics (τ_{decay} > 50 ms) high GABA sensitivity slow desensitization
Typical subunit composition	2α:2β:γ	Similar to GABA$_{A,fast}$ possibly containing α_5	α_4 or α_6 and δ

Figure 1.2. Three types of GABA$_A$ receptors mediate inhibition.

A) Typical GABA$_A$ receptors are heteropentameric Cl^- permeable channels composed of five subunits from seven subfamilies (α, β, γ, δ, ε, θ, π); BZ indicates the site sensitive to benzodiazepines, figure adapted from Jacob et al., 2008. B) Schematic of three types of postsynaptic GABA receptors; synaptic - GABA$_{A,fast}$, perisynaptic - GABA$_{A,slow}$, and extrasynaptic -GABA$_{A,tonic}$ receptors. C) Characteristics of GABA$_{A,fast}$, GABA$_{A,slow}$, and GABA$_{A,tonic}$ receptors; details from Banks & Pearce 2000, Bright & Smart, 2013, and Capogna & Pearce, 2011).

In mature mammalian brain, extracellular [Cl^-] ($[Cl^-]_e$) is higher than the intracellular [Cl^-] ($[Cl^-]_i$) due to the higher relative activity of the Cl^- extrusion transporter KCC2 (K^+/Cl^- cotransporter) compared to the major Cl^- uptake transporter NKCC1 ($Na^+/K^+/Cl^-$ cotransporter) (Rivera *et al.*, 1999). The reversal potential for GABA (E_{GABA}) is ~ -75 mV, and is more depolarized than the Cl^- equilibrium potential (E_{Cl}; ~ -85 mV) due to the influence of the more depolarized HCO_3^- equilibrium potential (E_{HCO3}; ~ -20 mV) (Kaila *et al.*, 1993; Lambert & Grover, 1995). $GABA_A$ receptor-mediated inhibition can occur through two different mechanisms dependent on the electrochemical gradients of Cl^- and HCO_3^-. The classic mode of GABAergic inhibition is dependent on an E_{GABA} that is hyperpolarized relative to V_m, and involves receptor activation, Cl^- influx down its electrochemical gradient, and subsequent V_m hyperpolarization away from resting values (~ -70 mV in mammal neurons) (Kaila, 1994; Williams *et al.*, 2004b). Therefore, $GABA_A$ receptor-mediated inhibition opposes excitatory inputs (e.g., glutamatergic excitation) by hyperpolarizing V_m away from AP threshold (AP_{th}) (spike threshold). The second mode of inhibition is shunting inhibition (Koch & Poggio, 1983; Koch *et al.*, 1983), and occurs when E_{GABA} is equal to or depolarized compared to V_m. Inhibition results from an increase in membrane permeability to Cl^- and shunting of depolarizing input (Koch & Poggio, 1983; Qian & Sejnowski, 1990; Staley & Mody, 1992). $GABA_A$ receptor-mediated shunting inhibition reduces excitability by increasing the Cl^- conductance across the plasma membrane which counters excitatory inputs, preventing V_m depolarization past E_{GABA} (Ben-Ari *et al.*, 2007; Rudolph & Knoflach, 2011).

GABA-mediated signalling is an essential component of neuronal inhibition and the large increase in turtle brain [GABA] suggests that this inhibitory signalling pathway plays an important role in preventing over-excitation under anoxic conditions. In anoxic/ischemic mammal brain GABAergic inhibition is not maintained (Li *et al.*, 1993; Schiene *et al.*, 1996) indicating an important difference between mammals and turtles, and a likely contributing factor to the anoxia-intolerance of mammal brain. If we are to implement endogenous anoxia-tolerant mechanisms learned from the study of turtle brain to prevent ECD in mammals it is necessary that we understand not only the mode of GABA induced electrical inhibition but also the oxygen sensing, and transducing mechanisms responsible for initiating this process.

1.6 Mechanisms of oxygen sensing

The ability to sense changes in environmental oxygen is a fundamental biological process critical for adaptation of living organisms to habitats and physiological situations which encounter variable oxygen levels. A number of specialized tissues are known for their ability to transmit acute responses to decreases in local oxygen tension to the CNS. Most prominent are carotid body glomus (type I) cells, pulmonary artery smooth muscle cells (PASMCs), and neuroepithelial bodies (NEBs) (reviewed in Ward, 2008). Glomus cells respond to decreases in arterial PO_2 by stimulating ventilation and thereby increasing oxygen uptake (Lopez-Barneo *et al.*, 1988). Pulmonary arteries constrict under hypoxic conditions (hypoxic pulmonary vasoconstriction; HPV) leading to optimization of ventilation-perfusion matching and gas exchange in the lung, while systemic arteries dilate, leading to increased oxygen delivery to surrounding tissue (Sylvester *et al.*, 2012). Neuroepithelial bodies (NEBs), which are clusters of neuroendocrine cells located in airway branching points, release neurotransmitters in response to hypoxia; and therefore, likely sense airway oxygen levels (reviewed in Kemp *et al.*, 2002). The cellular and molecular mechanisms underlying the sensing and transduction of body hypoxia/anoxia varies between tissues. Anoxia induces changes in a variety of potential intracellular signals including: $[O_2]$, $[H^+]$, $[CO_2]$, [ROS] and [ATP]. One or a combination of these molecules could be involved in the physiological response to low oxygen. A number of promising oxygen sensing candidate mechanisms have been proposed including: mitochondria (Chandel & Schumacker, 2000; López-Barneo *et al.*, 2001; Wyatt & Buckler, 2004), adenosine monophosphate (AMP)-activated kinase (Wyatt *et al.*, 2007), and haemoxygenase-2 (Williams *et al.*, 2004a); however, none can fully reconcile all the data accumulated over the past two decades. A common factor in the transduction of hypoxia in glomus cells and NEBs is the inhibition of K^+ channels, V_m depolarization and activation of voltage-gated Ca^{2+} channels resulting in the Ca^{2+}-mediated release of neurotransmitters (López-Barneo *et al.*, 2001). However, the situation is different in other oxygen sensitive tissues including PMSCs, where HPV is likely the result of Ca^{2+} entry from voltage dependent and independent sources and Ca^{2+} release from ryanodyne-sensitive stores (Aaronson *et al.*, 2006). Together this indicates that there might not be a unique oxygen sensing system within each cell type and implies that there might be multiple redundant mechanisms to ensure cellular function is not compromised during low oxygen stress. In general, oxygen sensing mechanisms can be divided between those dependent on disruption of oxygen-dependent synthesis or degradation of mediators (e.g., NADPH

oxidases, heme oxygenases and hypoxia inducible factors) and those dependent on disruption of mitochondrial function and energy state (reviewed in Kemp, 2006; Ward, 2008). A variety of mechanisms are likely involved in neuroprotection in turtle; however, since mitochondria are involved in the anoxic response in turtle brain (see below) and the studies presented in this thesis investigate mitochondrial mechanisms of oxygen sensing, the following section will focus on the effects of disruption of mitochondrial function under anoxic conditions.

1.6.1 Mitochondria as oxygen sensors

Cyanobacteria appeared ~ 3 billion years ago and were the first organisms to use photosynthesis and convert light energy into a stable/storable high energy biochemical molecule (Canfield, 2005). As a by-product of the photosynthetic pathway, these organisms released oxygen which accumulated in the atmosphere over the next billion years. This subsequent rise in atmospheric oxygen represents one of the most significant factors influencing the evolution of life on earth. Until this point in earth's history all life was anaerobic and the oxidizing environment presented a toxic problem. However, ~ 1.8 - 1.45 billion years ago an endosymbiosis event occurred that resulted in the precursor to the modern day mitochondrion (Martin & Mentel, 2010). It is currently debated whether an anaerobic host cell engulfed a single-celled obligate anaerobe to detoxify oxygen for the host or a facultative anaerobe to produce energy for the host or the obligate anaerobe was an energy parasite; however, the end result was an extremely effective symbiotic relationship that has powered life on earth for the last billion or so years.

Mitochondria are the largest consumers of oxygen in the cell, and without sufficient oxygen supply they are unable to maintain proper function and generate ATP. This essential role of oxygen in cellular metabolism along with their ability to function as signalling organelles led to the idea that anoxia induced changes in mitochondrial function may serve as an oxygen sensing mechanism ("mitochondrial model of oxygen sensing") (Duchen, 1999; Lahiri *et al.*, 2006). There is wide consensus that inhibition of oxidative phosphorylation affects oxygen sensing in PAMSCs and glomus cells (Chandel & Schumacker, 2000; López-Barneo *et al.*, 2001; Wyatt & Buckler, 2004; Weir *et al.*, 2005); however, controversy still exists over the signalling mechanisms that link mitochondrial function to their effectors. Two of the most prominent hypotheses of the mitochondrial model of oxygen sensing involve changes in energy state of the cell, and cytosolic

redox state/changes in ROS generation. To explain these hypotheses a brief explanation of mitochondrial function is useful.

The citric acid cycle and β-oxidation of fatty acids generates NADH and $FADH_2$, and these reducing equivalents are oxidized by complex I and II, respectively, of the ETC in the inner membrane layer of the mitochondria. Through redox reactions electrons are sequentially passed from complex to complex down the ETC to oxygen, the terminal electron acceptor. Protons are extruded at complexes I, III and IV resulting in generation of the Ψ_m and proton gradient (Δ pH) which drives the F_0F_1 ATP synthase and ATP generation. A consequence of aerobic respiration and a by-product of electron flux through the ETC is the generation of partially reduced and reactive metabolites of O_2 (i.e. superoxide ($O_2^{\bullet -}$)), primarily at complex I and complex III (Figure 1.3) (Adam-Vizi & Starkov, 2010). Superoxide is rapidly dismuted into the more stable hydrogen peroxide (H_2O_2) by cytosolic and mitochondrial superoxide dismutase (CnZnSOD and MnSOD, respectively) (Adam-Vizi & Starkov, 2010). As much as 3% of the electrons moved through the ETC can be lost this way (Turrens, 2003). Under anoxic conditions, the ETC will become more reduced resulting in a buildup of upstream reducing equivalents, an increase in the ratio of reduced glutathione (GSH) to oxidized glutathione disulfide (GSSG), and a more reduced intracellular redox state. Under anoxic conditions mitochondrial ROS generation will stop; however, during the transition to anoxia when there is accumulating electron donors and still some remaining oxygen it is possible that there could be an increase in $[ROS]_i$ (Chandel & Schumacker, 2000). It is important to mention that oxidative ATP generation would only be expected to decrease if Ψ_m and proton Δ pH gradients decreased (Gnaiger, 2003).

1.6.2 Energy state hypothesis of mitochondrial oxygen sensing

Many studies in several tissues have demonstrated that inhibition of oxidative phosphorylation has major effects on oxygen sensing. This led to the idea that changes in the energy state of a cell may be the mechanism responsible for signaling changes in oxygen supply ("energy state hypothesis") (Ward, 2008). One mechanism through which cellular energy status can be sensed is by the activity of AMP-activated protein kinase (AMPK). Under anoxic conditions, maintenance of $[ATP]_i$ is supported by the adenylate kinase reaction which catalyzes the conversion of two molecules of ADP to one molecule of ATP and one molecule of AMP. Without oxidative ATP the AMP/ATP ratio increases and activates AMPK, a ubiquitous cellular

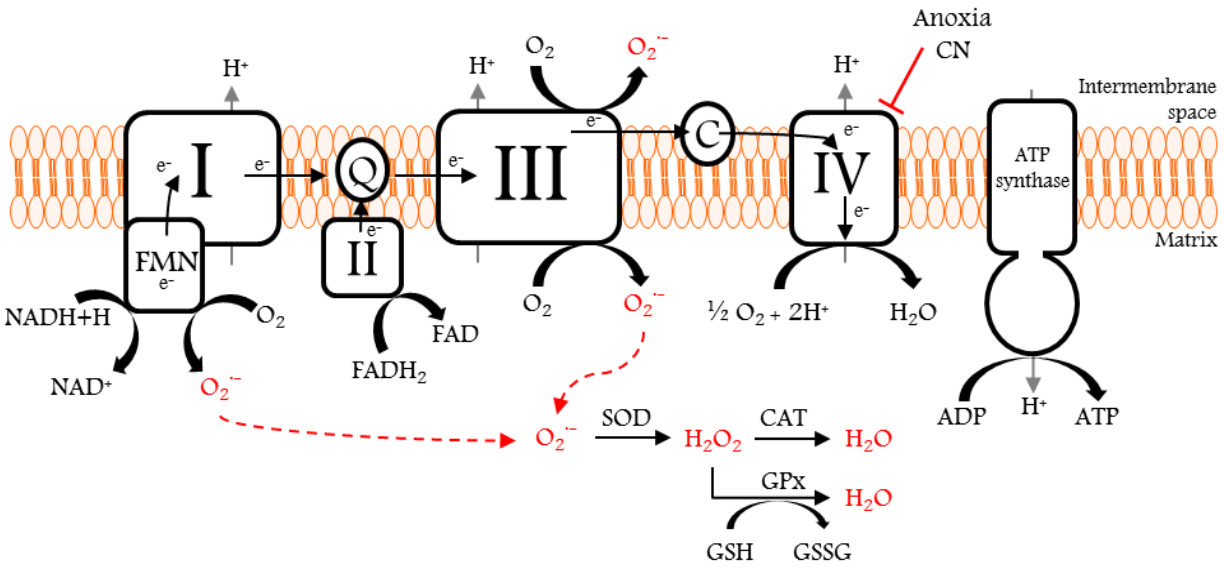

Figure 1.3. Schematic of ROS metabolism and ATP generation in the mitochondria.
Through a series of redox reactions electrons (e^-) donated from NADH (at NADH dehydrogenase; complex I) and $FADH_2$ (at succinate dehydrogenase; complex II) are transferred along the ETC to cytochrome c oxidase (complex IV) where they are used to reduce O_2 to water. This process pumps H^+ out of the matrix generating a H^+ gradient that is coupled to ATP generation by the F_1F_0 ATP synthase. Superoxide ($O_2^{\cdot -}$) is produced from the leakage of electrons at multiple site in the ETC. The primary sites of $O_2^{\cdot -}$ generation are: 1) the flavin mononucleotide (FMN) center of complex I; 2) ubisemiquinone radical of the Q-cycle at the Q_o site of cytochrome bc1 complex (complex III); or 3) at the Q_i sites of complex III. Superoxide is dismuted to hydrogen peroxide (H_2O_2) by superoxide dismutase (SOD) in the matrix and intermembrane space (not shown). H_2O_2 is reduced to water by catalase (CAT) or by a glutathione peroxidase (GPx). Anoxia or cyanide (CN) inhibits cytochrome oxidase (complex IV). Abbreviations: Coenzyme Q_{10} (Q), Cytochrome c (C), Glutathione (GSH), Glutathione disulfide (GSSG).

energy sensor, which modulates a number of cellular functions under hypoxic conditions including, ATP production/consumption, glucose uptake and glycolysis (Hardie *et al.*, 2006). In hypoxic mammalian glomus cells, AMPK has been linked to inhibition of K^+ channels and neurotransmitter release (Wyatt *et al.*, 2007). In turtle tissues, AMPK activity is modulated by anoxia and suppresses protein synthesis in white muscle (Rider *et al.*, 2009), although a role for AMPK in brain is currently unknown. However, in anoxia-tolerant crucian carp brain and heart, anoxic exposure increased phosphorylation of AMPK and kinase inhibition increased ethanol production, indicating metabolic stress (Stensløkken *et al.*, 2008). Together this supports a role for changes in mitochondrial ATP generation as a potential signal of low oxygen in anoxic turtle brain.

Another product of the enzymatic breakdown of ATP is adenosine which increases under energetically stressful conditions by the 5'-nucleotidase-mediated hydrolysis of AMP. In anoxic mammal and turtle this results in elevated intracellular and extracellular [adenosine] (Van Wylen *et al.*, 1986; Nillsson & Lutz, 1992; Lutz & Kabler, 1997). Adenosine is a protective neuromodulator and an important signalling molecule in anoxic mammal and turtle brain. Adenosine exerts its neuroprotective effects by activation of adenosine receptors on both the presynaptic and postsynaptic membranes. In mammalian brain, activation of postsynaptic adenosine receptors decreases neuronal excitability, and activation of presynaptic receptors suppresses neurotransmitter release (Stone, 1981; Cunha, 2001). In turtle brain, anoxic increases in adenosine activate postsynaptic adenosine receptors and have been linked to decreases in K^+ channel and NMDA receptor currents (Pék & Lutz, 1997; Buck & Bickler, 1998).

1.6.3 Mitochondrial Ca^{2+} release is a neuroprotective signal in anoxic turtle pyramidal neurons

Although $[ATP]_i$ remains relatively stable in anoxic pyramidal neurons (Buck *et al.*, 1998), it is likely that there are local decreases in [ATP] within and surrounding the mitochondria because ATP synthesis is inhibited. An anoxic decrease in [ATP] could then act as a signal to alter function of ATP-sensitive proteins and ion channels. The proton-motive force generated by the mitochondria ETC results in a highly negative matrix potential (Ψ_m) (-150 mV to -180mV) which leads to sequestration of Ca^{2+} within the matrix (Nicholls & Budd, 2000). Under normal physiological conditions free matrix $[Ca^{2+}]$ is maintained at 0.3 to 1 μM, making the mitochondria a major Ca^{2+} sink in the cell. Depolarization of mitochondrial Ψ_m leads to Ca^{2+} efflux (Nicholls & Budd, 2000; Gunter *et al.*, 2004); and therefore, one mechanism through which anoxic changes in

mitochondrial energy state can initiate neuroprotective signalling cascades is through depolarization of the mitochondria. A good example of mitochondrial Ca^{2+} release acting as a signal of low oxygen is the Ca^{2+}-mediated channel arrest of NMDA and AMPA receptors that occurs in anoxic turtle pyramidal neurons. This mechanism could potentially be involved in other neuroprotective cascades in anoxic turtle neurons so I will briefly outline our current channel arrest hypothesis for NMDA and AMPA receptors (Figure 1.4) (reviewed in Hogg *et al.*, 2014).

With the onset of anoxia oxidative phosphorylation is prevented and mitochondrial ATP generation is inhibited. Mitochondrial ATP-sensitive potassium (mK_{ATP}) channels which are located on the inner mitochondrial membrane and are normally inhibited by ATP open as a result of decreases in local [ATP]. This causes depolarization of the mitochondrial Ψ_m due to K^+ influx into the matrix and opening of the mitochondrial permeability transition pore (mPTP) in a low conductance state, which leads to a moderate calcium release. We are not entirely certain how mPTP is activated during anoxia; however, local pH (Halestrap, 1991) and adenylate phosphate concentrations (Hunter and Haworth, 1979a) halve been demonstrated to regulate pore opening. In addition, the relatively high intracellular pH in turtle pyramidal neurons (pH ~ 7.4) and maintenance of $[ATP]_i$ near normoxic levels may be the reason behind activation of mPTP in a low-conductance. Intracellular $[Ca^{2+}]$ increases ~ 10-20% (Oregon Green fluorescence; Pamenter *et al.*, 2008c; Hawrysh & Buck, 2013) from ~ 135 to 183 nM (Bickler, 1998), and this activates calmodulin, which competitively antagonizes the binding of α-actinin-2 to the NMDA receptor, resulting in Ca^{2+}-dependent inactivation of NMDA receptors and delocalization from the synapse via dissociation from the cytoskeleton.

1.6.4 Redox state and ROS hypothesis of mitochondrial oxygen sensing

Mitochondrial oxygen sensing mechanisms based on redox state and mitochondrial ROS generation are linked to the effects of the hypoxic or anoxic inhibition of the ETC and mitochondrial ROS generation, not to changes in $[ATP]_i$. The Redox hypothesis of oxygen sensing was developed by Weir and Archer to explain HPV in PASMCs under hypoxic conditions (Archer & Michelakis, 2002). The rationale is that under hypoxic conditions oxidative phosphorylation decreases $[ROS]_i$ and this leads to reduction of the ETC complexes and/or increase in intracellular reducing equivalents (i.e. NADH) from the citric acid cycle. They hypothesize that this reduced cytosol leads to the inhibition of redox-sensitive voltage-gated K^+ channels, V_m depolarization,

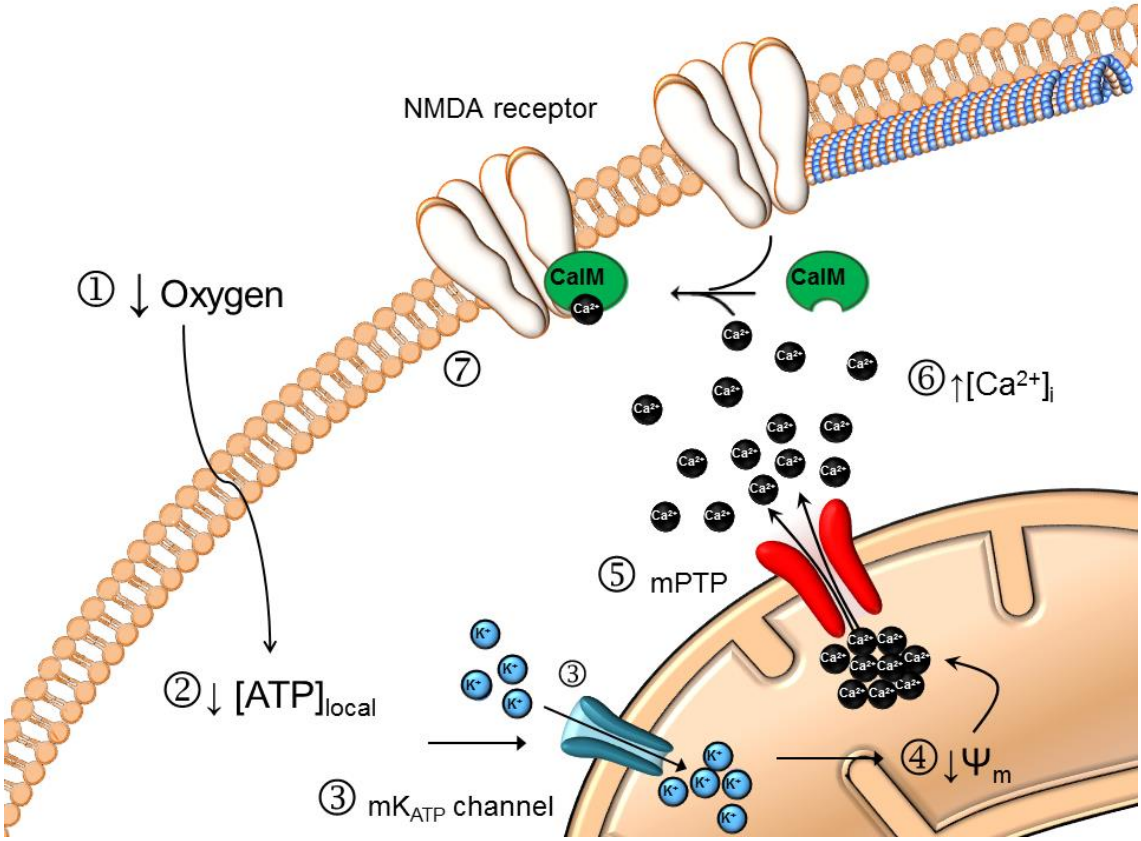

Figure 1.4. Putative anoxia-mediated mitochondrial calcium release mechanism that leads to NMDA receptor silencing.
During anoxia, oxidative phosphorylation halts and ATP production is reduced (1). This leads to local decreases in [ATP] (2), and opening of mitochondrial ATP-sensitive potassium (mK_{ATP}) channels (3). This depolarizes mitochondrial membrane potential (Ψ_m) (4), and opening of the mitochondrial permeability transition pore (mPTP) (5), which leads to release of calcium from mitochondrial stores. This results in a modest rise in $[Ca^{2+}]_i$ (6). The increase in $[Ca^{2+}]_i$ activates calmodulin (CalM), which competitively antagonizes binding of α-actinin-2 to the NMDA receptor, resulting in Ca^{2+}-dependent inactivation of NMDA receptors and delocalization from the synapse via dissociation from cytoskeletal elements (7). This Ca^{2+} signal has the potential to activate other signalling cascades (8). Figure adapted from Hogg et al., 2014.

channels, V_m depolarization, Ca^{2+} entry through Ca_v channels and vasoconstriction. In neonatal adrenomedullary chromaffin cells a similar mechanism for oxygen-sensing has been proposed but instead of a change in redox state it is a decrease in mitochondrial ROS generation and $[H_2O_2]$ that is thought to be responsible for inhibiting K^+ channels and depolarization (Thompson *et al.*, 2007b). In direct opposition, the ROS hypothesis of mitochondrial oxygen sensing developed by Schumaker proposes that under hypoxic conditions there is an increase in ROS generation from complex III of the ETC and this acts as a low oxygen signal (Chandel & Schumacker, 2000).

Little is known about the effects of anoxic decreases in ROS on inhibitory signalling in turtle brain; however, our lab recently investigated the effects of decreases in ROS on excitatory glutamatergic neurotransmission. The data is not included in this thesis but since it is relevant I wanted to briefly outline our findings. We hypothesized that decreases in ROS might be involved in the anoxic inhibition of these receptors; however, we found that NMDA receptors are in fact potentiated by decreases in mitochondrial ROS generation (Dukoff *et al.*, 2014). This is an interesting finding because as mentioned previously under anoxic conditions NMDA and AMPA receptor currents decrease with anoxia. To investigate the contradictory effects of anoxia and decreases in ROS on NMDA and AMPA receptor activity we assessed the effects of manipulation of $[ROS]_i$ and mitochondrial mK_{ATP} channels on NMDA and AMPA receptor function. We found that ROS scavengers increased NMDA receptor currents and application of H_2O_2 decreased these currents. This indicates that similar to mammalian NMDA receptors (Choi & Lipton, 2000), turtle NMDA receptors are redox sensitive. AMPA currents were unaffected by changes in cellular redox/ROS. Activation of mK_{ATP} channels and mitochondrial Ca^{2+} release prior to ROS scavenging prevented the increase in NMDA receptor currents indicating that the timing of the Ca^{2+} versus ROS signals is an important component of anoxia-mediated neuroprotective mechanisms in turtle brain. To confirm the timeline of these events I assessed anoxic changes in bath PO_2 and compared this to changes in fluorescent indicators of Ψ_m (rhodamine), $[Ca^{2+}]_i$ (Oregon green), and $[ROS]_i$ (CM-DCF) (Figure 1.5). I found that mitochondrial Ψ_m depolarization and Ca^{2+} release occurs ~ 1 min before $[ROS]_i$ levels start to decrease, and $[Ca^{2+}]_i$ reaches steady state levels ~ 6 min before $[ROS]_i$. These results demonstrate that there is sufficient time for activation of a Ca^{2+}-mediated inhibition of NMDA receptors before ROS levels decrease and potentiate receptor currents. In addition, this shows that in turtle brain decreases in ROS have physiologically relevant effects on channel currents, indicating ROS signalling could activate of inhibitory GABA signaling.

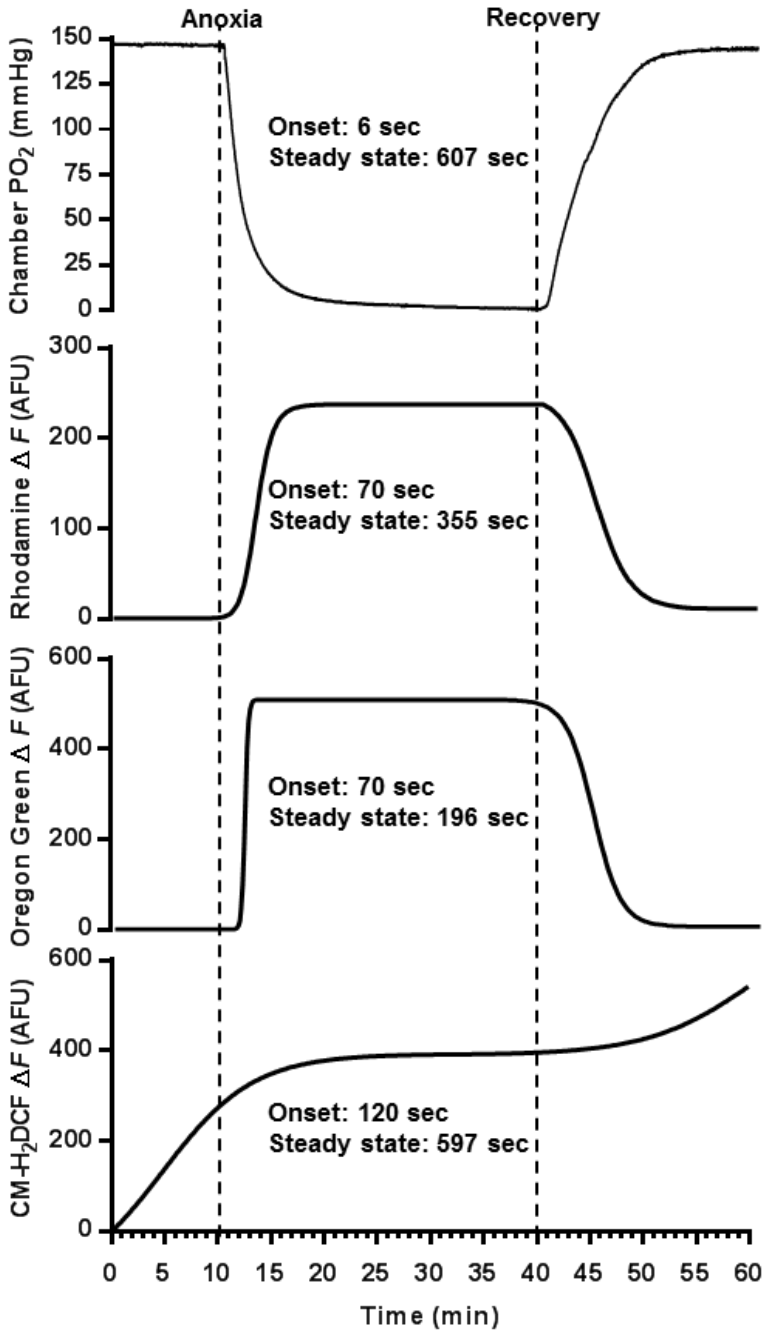

Figure 1.5. Timeline of anoxia-induced changes in bath partial pressure of oxygen (PO_2), and cortical neuron mitochondrial membrane potential (Ψ_m), $[Ca^{2+}]_i$ and $[ROS]_i$.
(A) Sample trace of bath chamber PO_2 during a 30 min anoxic treatment. (B) Rhodamine fluorescence trace demonstrating the timing of Ψ_m depolarization with anoxic treatment. (C) Oregon Green fluorescence trace showing increases in $[Ca^{2+}]_i$ with anoxia. (D) CM-DCF trace outlining decreases in $[ROS]_i$ with anoxia. Time to the onset of the response following the switch to anoxic perfusion and the time to steady state levels are shown in each panel. Each trace in panels B-D represents an average of 10 regions of interest per replicate. The onset and recovery portions of the traces were fitted with a non-linear four parameter curve to reduce noise and highlight the timeline of events. Data in Panel B and C were drift corrected and data in panels B-D were artificially set to a baseline fluorescence of zero to simplify interpretation of the figure. Adapted from Dukoff et al., 2014.

1.7 Turtle cerebrocortex as a model tissue

Although mammals and reptiles have significantly divergent evolutionary histories, they have functionally comparable neurological physiology, at least in terms of AP generation, neurotransmitters, receptors and ion channels (Kriegstein & Connors, 1986b; Larkum *et al.*, 2008). As such, the relative circuitry and energetic requirements of electrical signalling in the turtle brain are likely similar to that of a mammalian brain at the same temperature (Lutz & Nilsson, 1997). The turtle cerebrocortex is an ideal model to use for studying mechanisms of neuronal anoxia-tolerance because it is easy to excise, physiological synaptic connections are largely maintained, and excised brain maintains healthy electrical activity for up to 2 days. In addition to anoxia research, many researchers utilize this model because it is regarded as a precursor of the mammalian neocortex (Shepherd, 2011) and may provide important information regarding the evolution, structure, and synaptic connectivity of the mammalian brain. Throughout this thesis all experiments were performed on turtle *brain sheets* or *cortical sheets*. The region of the brain from which cortical sheets are isolated is the cerebrocortex, or "pallium" (Aboitiz & Zamorano, 2013) (Figure 1.6A). Based on variations in the histology of the cerebrocortex this structure can be divided into four main cytoarchitectonic areas which include the medial cortex, dorsomedial cortex, dorsal cortex and lateral cortex (Ulinski, 2007) (Figure 1.6B). Cortical sheets are isolated by cutting the cerebrocortex free from the anterior dorsal ventricular ridge and the striatum, and in doing so the lateral cortex is removed. The medial and dorsomedial areas correspond to the mammalian hippocampus in terms of their connections to other areas in the brain, while the dorsal cortex is most commonly associated with the visual cortex (Ulinski, 2007; Shepherd, 2011). Electrophysiological and fluorescent studies in this thesis are performed on pyramidal neurons located within the dorsomedial and dorsal cortex of the cerebrocortex. The cerebrocortex of the turtle is a three-layer cortex composed of a molecular layer, cellular layer, and subcellular layer (Connors & Kriegstein, 1986) (Figure 1.6C*i*-*ii*).

Pyramidal neurons account for ~ 80-90% of the neurons in the dorsal cortex, and a similar distribution in the dorsomedial cortex (Ulinski, 2007). In the intact brain, pyramidal neurons receive direct afferent input from the thalamus; however, these connections are severed in the cortical sheet model used in studies in this thesis. Pyramidal neuron somata are located primarily in the cell layer, with expansive apical dendrites that extend through the molecular layer and can

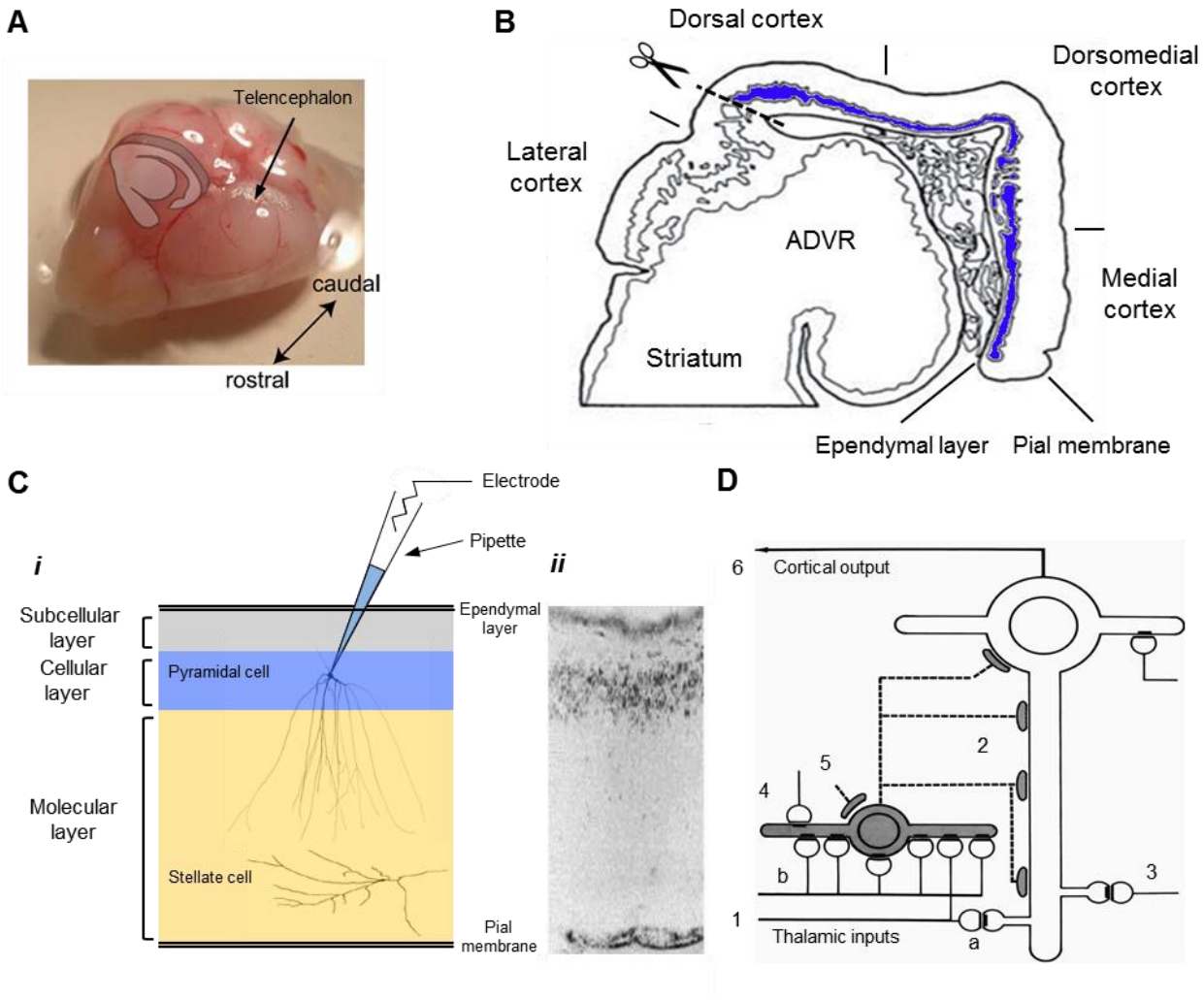

Figure 1.6. Turtle cerebrocortical sheet model used in electrophysiological and fluorescent experiments.

A) Dorsal view of a picture of a dissected turtle brain; coronal section is indicated by the pink schematic diagram. Adapted from Larkum *et al*., 2008. B) Coronal section of turtle telencephalon as indicated in (A); the cerebrocortex is comprised of four cortices: lateral, dorsal, dorsomedial, and medial. Scissors indicate where cerebrocortex is excised. Blue colouring corresponds to the cellular layer populated primarily by pyramidal neurons. Schematic adapted from Ulinski 2007. C*i*) Schematic detailing the three layers of the turtle cerebrocortex. Physiologically the cortex is bordered by the pial membrane dorsally and the ependymal layer ventrally; however, under experimental conditions the cortical sheet is inverted to provide easy access to pyramidal neurons and because pipettes easily penetrate the pial membrane. *ii*) Nissl-stained section of the dorsal cortex illustrating the three-layered organization of the cerebrocortex; this corresponds to (C*i*). Adapted from Connors and Kreigstein, 1986. D) Schematic diagram of the principle intracortical connections in turtle cerebrocortex. Thalamic inputs (1) directly excite pyramidal neuron dendrites (a) and excite inhibitory stellate interneurons (b). Feedforward inhibition is mediated by stellate contact with pyramidal neurons (2). There is reciprocal excitation between pyramidal neurons (3), and presumably GABAergic inhibition of stellate interneurons (5). Pyramidal neurons provide output from the cortex through axons that are located primarily in the subcellular layer (6). Adapted from Shepherd 2011.

reach the pial layer (Ulinski, 2007; Larkum *et al.*, 2008). Axons of pyramidal neurons extend toward the subcellular layer and bifurcate with one branch typically directed medially and the otherlaterally. Pyramidal neurons are glutamatergic and their axons access both AMPA and NMDA receptors on connected cortical neurons, and they also receive feedback excitation from other pyramidal cells (Ulinski, 2007). The remaining 10 - 20% of neurons in the dorsal cortex are non-pyramidal and likely include a mix of both excitatory and inhibitory interneurons. There are several populations of interneurons in the cerebrocortex, however, the most numerous and best characterized are the GABAergic stellate cells. The somata of stellate cells are located in the inner half of the molecular layer bordering the cellular layer (Colombe *et al.*, 2004). Their dendrites extend obliquely through all three cortical layers and their axons ramify throughout all three layers of the dorsal cortex. Stellate cells likely provide both feedforward and feedback inhibition to pyramidal cells, and there is also physiological support for inhibition of stellate interneurons (disinhibition), presumably arising from stellate cell-stellate cell contact (Shepherd, 2011) (Figure 1.6D). Patch clamp recordings of stellate neurons found that they fire bursts of APs and the number of APs/burst increases during anoxia (personal observation). Under patch-clamp conditions pyramidal cells and stellate cells can be differentiated by their responses to somatic current injections which produce trains of APs that accommodate in pyramidal cells but do not in stellate cells (see appendix II, figure A.1.)

1.8 Thesis rationale and hypotheses

Due to seasonal ice cover in the northern part of its range the western painted turtle has evolved to become anoxia tolerant, capable of surviving anaerobic conditions for days to months. Although the turtle brain is functionally comparable to mammal brain it is significantly more tolerant to oxygen deprivation making the turtle brain an ideal model to investigate neuronal mechanisms of anoxia-tolerance. This species has evolved a number of neuroprotective mechanisms to prevent anoxia-induced ECD, including the capacity to regulate ATP supply and demand, a key component of their anoxia-tolerant strategy that prevents the catastrophic cascade of events characteristic of mammalian responses to low oxygen. These adaptations are of particular interest to the field of neurobiology because unraveling the physiological mechanisms that endow the turtle's tolerance to low oxygen could result in therapies that protect mammals from these insults (e.g., stroke tolerance). From a comparative perspective, studying anoxia-tolerant turtles gives us the

opportunity to understand how a brain, an organ extremely sensitive to reduced oxygen availability in mammals, can function without oxygen for long periods.

The overall aim of my research is to elucidate the mechanisms that regulate suppression of neuronal excitability in the anoxic turtle cerebrocortex. This primarily involved the examination of GABAergic signalling in turtle cerebrocortex. Specifically I aimed to test the following hypotheses:

1) Anoxia-mediated spike arrest is the result of increased GABAergic neurotransmission that induces shunting inhibition at the GABA reversal potential (E_{GABA}) (Chapter 2).

2) GABAergic mechanisms that protect turtle brain from anoxic injury will also protect it from damage due to ischemic stress (Chapter 3).

3) Calcium-activated potassium channels (K_{Ca}) are oxygen sensitive and will undergo channel arrest during anoxia (Chapter 4).

4) An anoxia-mediated decrease in mitochondrial ROS generation will enhance GABAergic inhibition through pre- and postsynaptic mechanisms (Chapter 5).

Note on the organization of the thesis: The majority of data in this thesis has been published in peer-reviewed journals and therefore, for simplicity these papers have been presented as chapters in this thesis. These chapters have been presented in the chronological order in which they were performed, and they have been edited for redundancy. The abstracts are presented relatively unedited from their published form. The materials and methods in research chapter 2 contain the general protocols used throughout the thesis. The materials and methods section in each subsequent research chapter only contains new materials and methods specific to that chapter. The vast majority of the research presented in this thesis was conducted by me, and I have included an explanation of author contribution at the beginning of each research chapter. In situations where data sets were co-authored in a manuscript I have attempted to present only my data. However, since science is a collaborative process I have also included a limited amount of data from co-authors if I felt it was necessary to support my research and better explain the findings. For clarity, I have used the pronoun “I” for experiments performed by me and “we” for experiments performed jointly by myself and co-author(s).

2 Enhanced GABA transmission induces electrical suppression in anoxic turtle brain

Preface

A modified version of this chapter was published as Pamenter ME, Hogg DW, Ormond J, Shin DS, Woodin MA and Buck LT (2011). Endogenous $GABA_A$ and $GABA_B$ receptor-mediated electrical suppression is critical to neuronal anoxia tolerance. *Proc. Natl. Acad. Sci.* 108 (27): 11274-11279.

The idea to investigate the role of GABAergic transmission in anoxia-mediated spike arrest came from L. Buck. M. Pamenter performed 50% of the whole-cell conductance measurements (Fig. 2.3A) and 50% of the MEQ fluorescent experiments (Fig. 2.5A). All other data presented was performed and analyzed by D. Hogg.

Abstract

Anoxic insults cause hyperexcitability, neuronal swelling and death in mammalian neurons. Conversely, in anoxia-tolerant turtle cortex, electrical activity in pyramidal neurons is suppressed by anoxia (i.e., spike arrest) and cell death does not occur. The mechanism(s) of spike arrest is unknown; however, it involves GABAergic synaptic transmission because brain GABA concentration dramatically increases with anoxia, GABA application mimics spike arrest, and treatment of anoxic pyramidal neurons with $GABA_{A+B}$ receptor antagonists results in hyperexcitability and cell death. To investigate this unique neuroprotective signaling pathway I used whole-cell and perforated patch-clamp electrophysiology techniques and fluorescent imaging. I demonstrate that there is an increase in GABA release during anoxia and this enhances inhibitory postsynaptic currents on pyramidal neurons. Enhanced GABA transmission increased postsynaptic permeability to Cl^- through a $GABA_A$ receptor dependent-mechanism, and depolarized membrane potential (~ -89 mV) to the GABA receptor reversal potential (~ -81 mV). Anoxic treatment depolarized AP_{th}, and AP_f decreased ~ 70% indicating electrical suppression. Anoxic or GABA treatment resulted in a $GABA_A$ receptor-dependent Cl^- efflux from cortical neurons and a decrease in neuron volume. I conclude that in turtle cerebrocortex anoxic increases in GABA release activate $GABA_A$ receptors on postsynaptic pyramidal neurons and induce shunting inhibition. This $GABA_A$ receptor-mediated current maintains membrane potential hyperpolarized to AP_{th} and prevents hyperexcitability during anoxia.

2.1 Introduction

In mammals, anoxic or ischemic insults are particularly damaging to brain tissue because they elicit ECD. Glutamate receptor over activation is a critical component of ECD; and therefore, has been a major focus of numerous studies aimed at elucidating associated signaling pathways (Muir, 2006). However, clinical interventions which only target these receptors have been largely unsuccessful against anoxic or ischemic damage (Ikonomidou & Turski, 2002). For the successful prevention of ECD induced damage it is therefore important to investigate alternative mechanisms to limit excitability during such insults. A potential therapeutic alternative to directly antagonizing excitatory pathways is to up-regulate inhibitory mechanisms such as those mediated by GABA. GABAergic mechanisms are not strongly recruited in ischemic mammalian neurons. In fact, although [GABA] is elevated by ~ 30% in ischemic murine brain, $GABA_A$ receptor subunit mRNA expression is decreased by ~ 85%, and GABA-evoked currents and [ATP] run down rapidly, suggesting endogenous GABAergic neuroprotection is transient and largely ineffective (Li *et al.*, 1993; Erecińska & Silver, 1994; Allen *et al.*, 2004). Nonetheless, activating GABA receptors pre-insult limits neuronal hyperexcitability in mammalian models of ischemic damage, and AD and cell death are not observed in the afflicted brain region (Galeffi *et al.*, 2000; Costa *et al.*, 2004). Despite these promising results, GABA has received little attention as a clinical stroke intervention and the mode of GABAergic neuroprotection is poorly understood (Ginsberg, 2008).

In anoxia-tolerant turtle, excitatory glutamatergic signaling (via NMDA receptors and AMPA receptors) is downregulated and this is an important neuroprotective mechanism that protects against anoxic insults in this species (Bickler *et al.*, 2000; Pamenter *et al.*, 2008b; Wilkie *et al.*, 2008). In addition, there is a rapid elevation in brain [GABA] (Nilsson & Lutz, 1991), which is likely a primary neuroprotective component of the turtle's anoxia-tolerant strategy since antagonism of $GABA_A$ and $GABA_B$ receptors results in hyperexcitability and cell death similar to anoxic mammalian neurons (Pamenter *et al.*, 2011). Although GABAergic signaling is critical to anoxia tolerance in turtle brain the mechanisms responsible for GABA-mediated spike arrest are unknown. Therefore, the aim of this study is to investigate presynaptic and postsynaptic components responsible for GABA-mediated spike arrest in the anoxic turtle brain. I hypothesize that in turtle cerebrocortex, anoxia will enhance GABA release and this will increase postsynaptic conductance to Cl^- and result in electrical suppression.

2.2 Materials and Methods

2.2.1 Research animals and ethics approval

This study was approved by the University of Toronto Animal Care Committee and conforms to the relevant guidelines issued by the Canadian Council on Animal Care in the Guide to the Care and Use of Experimental Animals, Volume 2, regarding the care and use of experimental animals. Wild-caught adult turtles (*Chrysemys picta bellii*) (carapace diameter >15 cm, 300-600 g) were purchased from Niles Biological Inc. (Sacramento, CA, USA). The animals were housed in large indoor ponds (2 m x 4 m x 1.5 m) equipped with basking platform, heating lamp and a flow-through dechlorinated fresh water system. The water temperature was maintained at approximately 17 ºC and the air temperature at 20 ºC. Turtles were fed three time weekly and maintained on a 12h light : 12h dark photoperiod.

2.2.2 Cortical sheet preparation

Turtles were decapitated and the whole brain was rapidly excised from the cranium (~ 30 sec) as described elsewhere (Blanton *et al.*, 1989b). External vasculature was removed and six cortical sheets of dimensions (~ 5mm x 2mm x 0.7mm) were isolated from the cerebrocortex and collected in chilled turtle artificial cerebrospinal fluid (aCSF) (4 °C) containing (in mM): 107 NaCl, 2.6 KCl, 1 $MgCl_2$, 2 NaH_2PO_4 ($2H_2O$), 26.5 $NaHCO_3$, 10 glucose, 5 Imidazole, 1.2 $CaCl_2$ ($2H_2O$) (pH 7.4, adjusted with 12M HCl; osmolarity 285-290 mOsm/L). Cortical sheets were maintained in aCSF at 4 °C prior to use and for a maximum of 36 hours.

2.2.3 Experimental setup

2.2.3.1 Normoxic setup

All electrophysiological experiments were performed on a vibration isolating laboratory table (TMC - 63-500 Series; Harvard Apparatus Canada) equipped with an isolation stage (ITS-O2; Narishige, Japan). Tissue was visualized using an Olympus BX51W1 upright microscope (Olympus, Richmondhill, Canada) equipped with an Olympus 0.8 N.A., 40X water immersion objective or a 0.1 N.A. 5X objective. For normoxic recordings, individual cortical sheets were placed in a flow-through perfusion chamber and held in place by a slice anchor (RC-26 chamber with P1 platform; Warner Instruments, Hamden, CT). The tissue chamber was gravity - perfused with aCSF from 1 L glass bottles via an intravenous dripper at a rate of 2 - 3 $mL \cdot min^{-1}$. A fast-step

drug perfusion system (VC-6 model perfusion valve controller and SF-77B fast-step perfusion system; Warner Instruments) was used to deliver pharmacological modifiers directly above the cortical sheet. Drugs were solubilised in saline and bubbled according to indicated treatments. All experiments were performed at a room temperature of 22 - 24°C. Isolated cortical sheets are ~ 0.7mm thick and do not have functioning vasculature. Therefore, they are at risk of developing a central anoxic core due to oxygen diffusion limits (Desan, 1984; Jiang *et al.*, 1991). To ensure that the entire cortical sheet remained oxygenated normoxic aCSF was continuously gassed with 95% O_2/5% CO_2 to maintain a high diffusion gradient for O_2 into the sheet. This is important because I am interested in studying the signals that initiate neuroprotection from anoxia. aCSF gassed with 95% O_2 produces hyperoxic aCSF and this can increase $O_2^{\bullet-}$ generation and cell death over 4 hours in 0.3mm thick rat hippocampal slices (Dean *et al.*, 2003; D'Agostino *et al.*, 2007). Elevated $[ROS]_i$ could complicate interpretation of findings so I assessed ROS generation in cortical sheets exposed to aCSF that was gassed with 95% room air/ 5% CO_2 or 95% O_2/5% CO_2. There was no difference in the rate of ROS generation in cortical neurons as measured by the fluorescent ROS sensitive dye CM-DCF (see appendix III, Figure A2). In addition, a variety of other electrophysiological parameters (e.g., V_m, G_w, AP_{th}, GABA IPSC amplitude and frequency; (see appendix III, Table A2) were not different when treated with aCSF gassed with these different gas mixtures.

2.2.3.2 Anoxic setup

Anoxia was achieved by gassing aCSF with 95% N_2/5% CO_2 for a minimum of 30 min prior to commencement of experiments and this was continued throughout the experiment. To maintain anoxic conditions aCSF was delivered through either oxygen impermeable viton tubing and/or perfusion lines were double-jacketed and all air spaces were gassed with 95% N_2/5% CO_2. For anoxic experiments, cortical sheets were placed in a custom made plexiglass perfusion chamber fitted with high-walls (1 cm) and access spaces for electrodes and drug application. To maintain bath anoxia, chamber aCSF was gassed with 95% N_2/5% CO_2 and the top of the chamber was covered with a glass cover slip. The PO_2 of bath aCSF decreased to ~ 0 mmHg in ~ 15 min under these experimental conditions (i.e. bath PO_2 not different from reservoir PO_2; see introduction figure 1.5). The PO_2 of the reservoir and bath was measured using either a fluorescent oxygen analyzer and Witrox-1 v1.6.0 software (Witrox 1; Loligo Systems; Denmark) or an E101 oxygen electrode (Cameron Instruments Co.) connected through a Model 1900 polarographic amplifier (A-M

Systems) to a LabPro interface (Vernier Software and Technology) for data collection. Logger Pro 3.8.4.2 was used for data collection at a sampling rate of 2 seconds.

2.2.4 Electrophysiology

2.2.4.1 Whole-cell patch clamp recordings

Whole-cell patch recordings were made from pyramidal neurons located in the dorsal cortex and dorsal medial cortex (Ulinski, 2007) using fire-polished 4-6 MΩ borosilicate glass pipettes (Harvard Apparatus LTD, Holliston, MA). Physiological pipette solution contained (in mM): 130 K gluconate, 3 NaCl, 5 Na-gluconate, 1 $MgCl_2$, 10 NaHepes, 0.3 NaGTP, 2 NaATP, 0.0001 $CaCl_2$, (adjusted to pH 7.4 with methanesulfonic acid; osmolarity 295-300 mOsm/L). Silver chloride electrodes were used both as the reference and recording electrode. Data were collected using either a CV-4 headstage and an Axopatch-1D amplifier or a CV-7B headstage and MultiClamp 700B amplifier (Molecular Devices, Sunnyvale, CA). Data was digitized using a Digidata 1440A interface and stored on computer using Clampex 10 software (Molecular Devices). A motorized patch-clamp micromanipulator (Burleigh, PCS-6000 series, Thorlabs, Newton, NJ) was used to position pipettes. Cell-attached 5 - 10 GΩ seals were obtained using the blind-patch technique previously described (Blanton *et al.*, 1989b). Upon seal formation, negative pressure was applied to achieve the whole-cell patch clamp-configuration. Following whole-cell capacitance compensation, typical whole-cell access resistances (R_a) were 20 - 30 MΩ. R_a was determined before each measurement of electrical activity (see below) and recordings were discarded if R_a changed by more than 20% or whole-cell leak currents changed > ± 30 pA during the course of the experiment. Pyramidal neurons were differentiated from stellate cells by their responses to somatic current injections which produce trains of APs that accommodate in pyramidal cells but do not in stellate cells (see appendix II, figure A.1) (Connors & Kriegstein, 1986; Shin & Buck, 2003), and only patches onto pyramidal cells were included in this study. When using turtle aCSF in the bath the liquid junction potential (LJP) was experimentally assessed as ~ 14 mV (protocol based on Neher, 1992), and supported by LJP calculations using a generalized version of the Henderson equation (Clampex junction potential calculator; Molecular Devices, Sunnyvale, CA). All data have been corrected for this value offline (raw traces are unaltered)

2.2.4.2 Perforated patch clamp recordings

The gramicidin perforated-patch technique was used to assess neuronal electrical parameters and determine E_{GABA} without disturbing intracellular [Cl^-]. Thin- or thick walled borosilicate glass electrodes were pulled (4 - 5 MΩ), fire polished and backfilled with a high-[Cl^-] pipette solution (150 mM KCl, replacing K-gluconate) containing 25 μg/mL gramicidin. Only patches that had a stable R_a typically < 75 MΩ were used in experiments.

2.2.4.3 Measurement of pyramidal neuron AP_{th}, G_w and E_{GABA}

AP threshold (AP_{th}) was determined by current-clamping cells and ramping voltage in 2 mV increments for 250 ms until an AP was elicited. Threshold was taken to be the first instance of upward voltage deflection. Whole-cell conductance (G_w) was assessed by clamping neurons at voltage steps from -50 to -100 mV in 10-mV increments lasting 250 ms. Current amplitudes were measured between 200 and 220 ms to avoid any capacitance effects, and a slope conductance was determined from the resultant current–voltage (I/V) relationship (Ghai & Buck, 1999). The reversal potential of the GABA-induced current (E_{GABA}) was measured using 2 second ramp voltage steps from −100 to −50 mV applied before and after a 15 sec GABA (2 mM) application. Note: 15 secs of 2 mM GABA application is sufficient to depolarize V_m to E_{GABA}, and V_m recovers rapidly following cessation of GABA drip-perfusion. I/V relationships were analyzed by taking the linear regression of each line before and after 2 mM GABA application, and E_{GABA} was estimated by measuring the voltage at which the I/V relationships before and during GABA application intersected, as described elsewhere (Watanabe *et al.*, 2009). This intersection point is the voltage at which there is no difference in current between the indicated treatment and GABA treatment and is a measure of the cell's background current indicating no effect of GABA perfusion; and therefore, the GABA reversal potential. I measured V_m, G_w and E_{GABA} in both gramicidin-perforated and whole-cell patch configurations and determined that measurements of these parameters were not significantly different between the two techniques. This is reasonable because the pipette [Cl^-] (5 mM) was calculated using the Nernst equation with perforated-patch clamp measurements of E_{GABA}. Since the whole-cell technique has previously been used to determine E_{GABA} in neurons (DeFazio *et al.*, 2000; Hewitt *et al.*, 2009), and there was no significant difference between whole-cell and gramicidin-perforated patch measurements of E_{GABA} or G_w, the data sets were grouped together.

2.2.4.4 Measurement of $GABA_A$ receptor giant IPSCs and tonic currents

To aid in the detection of $GABA_A$ receptor inhibitory postsynaptic potentials (IPSCs), and tonic currents, pyramidal neurons were voltage-clamped at a holding potential of -100 mV and pipette [Cl^-] was increased to 110 mM [Cl^-] by equimolar substitution of KCl for K-gluconate (Chapter 2). To isolate $GABA_A$ receptor currents glutamate receptor antagonists (2R)-amino-5-phosphopentanoate (AP5; 25 μM) and 6-cyano-7-nitroquinoxaline-2, 3-dione (CNQX; 25 μM) were continuously applied. Under these conditions antagonism of glycine receptors with strychnine (2 μM) did not have a detectable effect. After establishing the whole-cell configuration, a 10 min equilibration period was provided for the exchange of ions, stabilization of the patch and for antagonism of non-GABAergic receptors and ion channels. For all GABA-mediated currents only recordings with a stable baseline and distinct IPSCs were used for analysis. Giant IPSCs (gIPSCs) are a unique $GABA_A$ receptor current in turtle cortical pyramidal neurons. Due to the low incidence of gIPSCs they were assessed for 5 min after each treatment period and if required data was normalized to a normoxic 5 min time point (> 15 min after patch formation). Giant IPSCs were analyzed using a threshold search protocol with the trigger level set close to the baseline level to ensure the entire gIPSC was captured. In this chapter, tonic GABA currents were measured by assessing the change in baseline current after gabazine (Gz; 25 μM) was applied.

2.2.5 Fluorescence imaging

2.2.5.1 Upright microscope

Fluorescence experiments were performed using the same microscope and experimental set up as the electrophysiological experiments. All fluorescent indicators used were acetoxymethyl (AM) ester derivatives which can permeate cell membranes. Once inside the cell, the lipophilic blocking groups are cleaved by nonspecific esterases slowing dye leakage. Fluorophores were imaged using indicated filter sets in combination with a monochromonator controlled by Easy Ratio Pro imaging software (Photon Technology international, London, ON, Canada). Fluorescence emissions were detected with an EMCCD camera (Rolera-MG*i*; Q imaging; Burnaby, BC). Neurons were excited for 0.05 seconds every 10 seconds to prevent bleaching of the dye and permit experiments of up to an hour in length. Baseline fluorescence was recorded for 10-15 min until a stable baseline was achieved and then the tissue was exposed to treatment for 20-40 min and then recovered. For statistical analysis of fluorescent imaging data, the average change in regions of interest (ROI)

from the center of the cell body of 10 neurons per cortical sheet were chosen and used as a single replicate. Brightly fluorescing cells were avoided. To assess if endogenous fluorescence of cortical sheets affects fluorescence measurements, control cortical sheets were exposed to each treatment in the absence of fluorophores. The background fluorescence was minimal and remained constant with each treatment and; therefore, background fluorescence was not subtracted from fluorescent data. Sample raw traces were smoothed using Easy Ratio Pro imaging software to reduce noise and simplify interpretation. Some raw traces were drift corrected by fitting stable baseline recordings 5 min before and after treatment onset with a linear regression line. Individual points on the raw trace were then divided by the corresponding points on the regression line (Crowe *et al.*, 1995). Fluorescent indicators were obtained from Invitrogen (Burlington, ON, Canada) and solubilized in either dimethyl sulfoxide (DMSO) or DMSO with 20% pluronic acid. In control experiments DMSO or DMSO with 20% pluronic acid did not affect fluorescence measurements.

2.2.5.2 Fluorometric assessment of $[Cl^-]_i$: MEQ

Chloride changes were assessed using 6-methoxy-N-ethylquinolinium iodide (MEQ). Working stocks of MEQ were prepared daily over nitrogen as previously described (Inglefield & Schwartz-Bloom, 1999). Slices were incubated in 400 μM MEQ for 1 h followed by a 10 min wash in aCSF (22°C). Changes in MEQ fluorescence were calibrated using the Stern–Volmer equation as described elsewhere (Inglefield & Schwartz-Bloom, 1999).

2.2.6 Fluorometric assessment of cell volume: Calcein

Chloride movement induces cell-volume changes; and therefore, cell-volume changes were measured using a calcein fluorescence assay (Hamann *et al.*, 2002). Calcein-AM was excited at 488 nm and emissions were recorded at 520 nm. Maximum cell-volume changes were determined by perfusing cortical sheets with progressively hypo/hyperosmotic aCSF until the osmolarity change was sufficient to induce >10% cell mortality (assessed by complete loss of calcein fluorescence). Minimum fluorescence was observed at 100 mOsm, whereas maximum fluorescence changes occurred at 500 mOsm. Treatment-induced changes in calcein fluorescence are expressed as the percent change relative to this maximum.

2.2.7 Pharmacology and Chemicals

See Table A.1. in the Appendix for a list of all pharmacological modifiers used and their working concentrations. All pharmacological modifiers were drip applied and solutions were made fresh daily. All chemicals were obtained from Sigma-Aldrich Canada Ltd (Oakville, ON), except TTX, which was obtained from Tocris Cookson (Bristol, UK) and CGP55845, which was obtained from Tocris Cookson Inc. (St. Louis, MO, USA). CGP, SKF, SNAP, CNQX, CDZ, CHT and PMA were solubilized in DMSO prior to addition to aCSF. The concentrations of DMSO never exceeded 1% v/v. PTX was solubilized in ethanol (< 1% v/v). Pharmacological modifiers were dissolved in aCSF to their final working concentration and were drip applied with the exception of MPG and CN which were drip and bath applied.

2.2.8 Experimental design and data analysis

Whole-cell, perforated patch and fluorescent experiments were performed in a paired design starting with a 10-15 min normoxic pre-treatment, then a treatment period, and ending with a 30 min normoxic recovery. Two treatment paradigms were generally followed: 1) a 30 min treatment, or 2) a 20 min and 40 min treatment. Analysis of electrophysiological data was performed using Clampfit 10 software (Molecular Devices, Sunnyvale, CA). Analysis of fluorescent data was performed on Easy ratio Pro software (Photon Technology international, London, ON, Canada). In all experiments an individual replicate corresponds to one recording from one brain sheet. Recordings from a maximum of 2 individual brain sheets from a single animal were included for use in statistical comparison. Each sheet was treated only once with pharmacological modifier(s) for the indicated duration.

2.2.9 Statistical analysis

Electrophysiological and fluorescent data were analyzed using SigmaPlot software package version 11.0 (Systat Software, Inc., San Jose, CA). All data was tested for normality and equal variance and data were analyzed using either a one-way analysis of variance (Jaggar *et al.*, 2002), or a two-way repeated measures (RM)-ANOVA with a Tukey's post-hoc test to compare within and against treatment and normoxic values. Significance was determined at $P < 0.05$, and all data are expressed as the mean ± S.E.M. (standard error of mean).

2.3 Results

Spike arrest is dependent on activation of $GABA_A$ receptors.

The first aim of this study was to confirm that spike arrest occurs under the anoxic experimental conditions outlined in the *Materials and Methods*. AP threshold (AP_{th}) and AP frequency (AP_f) were used as measures of pyramidal neuron excitability. Under normoxic conditions, stepwise current injections elicited APs at a threshold of -46.6 ± 2.3 mV (n = 8; figure 2.1A, B*i*) and spontaneous APs fired at a frequency of 1.10 ± 0.1 Hz (n = 8 each; figure 2.1C, D*i*). Anoxic treatment depolarized AP_{th} to -31.3 ± 1.7 mV (n = 4; $p < 0.001$; figure 2.1B*ii*) and AP_f decreased > 60% to 0.4 ± 0.03 Hz (n = 8; $p = 0.001$; figure 2.1C, D*ii*). These changes were reversed by re-oxygenation and are consistent with previous reports of spike arrest in anoxic turtle brain (Feng *et al.*, 1988a; Perez-Pinzon *et al.*, 1992b; Pamenter *et al.*, 2008b). To determine if GABA perfusion mimics anoxia, normoxic brain sheets were treated with 2 mM GABA. GABA treatment depolarized AP_{th} ~ 30 mV to -15.8 ± 1.9 mV (n = 10; $p < 0.001$) and AP_f decreased ~ 90% to 0.09 ± 0.04 Hz (n = 4; $p < 0.001$; figure 2.1C). Co-treatment with anoxia plus GABA did not change AP_{th} or AP_f compared to GABA alone. To assess if decreases in neuron excitability were associated with $GABA_A$ receptors, neurons were treated with GZ. GZ treatment prevented the anoxic depolarization of AP_{th} (-41.7 ± 3.2; n = 4; $p = 0.012$), and increased AP_f under both normoxic and anoxic conditions (11.2 ± 2.5 and 9.1 ± 2.2 Hz; n = 4 each). These data indicate that the anoxic experimental protocols of this study induce spike arrest and that $GABA_A$ receptors are involved because GZ-mediated inhibition causes hyperexcitability.

GABA release increases during anoxia and following inhibition of GABA uptake.

To assess anoxia induced changes in GABA release, pyramidal neurons were whole-cell voltage clamped and $GABA_A$ receptor currents were used as sensors to detect anoxic changes in extracellular [GABA] (figure 2.2A-D). This technique was adapted from elsewhere (Rossi *et al.*, 2000; Allen *et al.*, 2004). $GABA_A$ receptor currents were enhanced with high [Cl^-] pipette solution and a -100 mV holding potential (as described in Materials and Methods). $GABA_A$ receptor currents were isolated with glutamate receptor inhibitors AP5 and CNQX. Under these experimental conditions, when GABA binds to $GABA_A$ receptors, Cl^- leaves the neuron and currents are depolarizing. The turtle brain sheet preparation provides an ideal model for examining GABA release onto pyramidal neurons because synaptic connectivity and endogenous

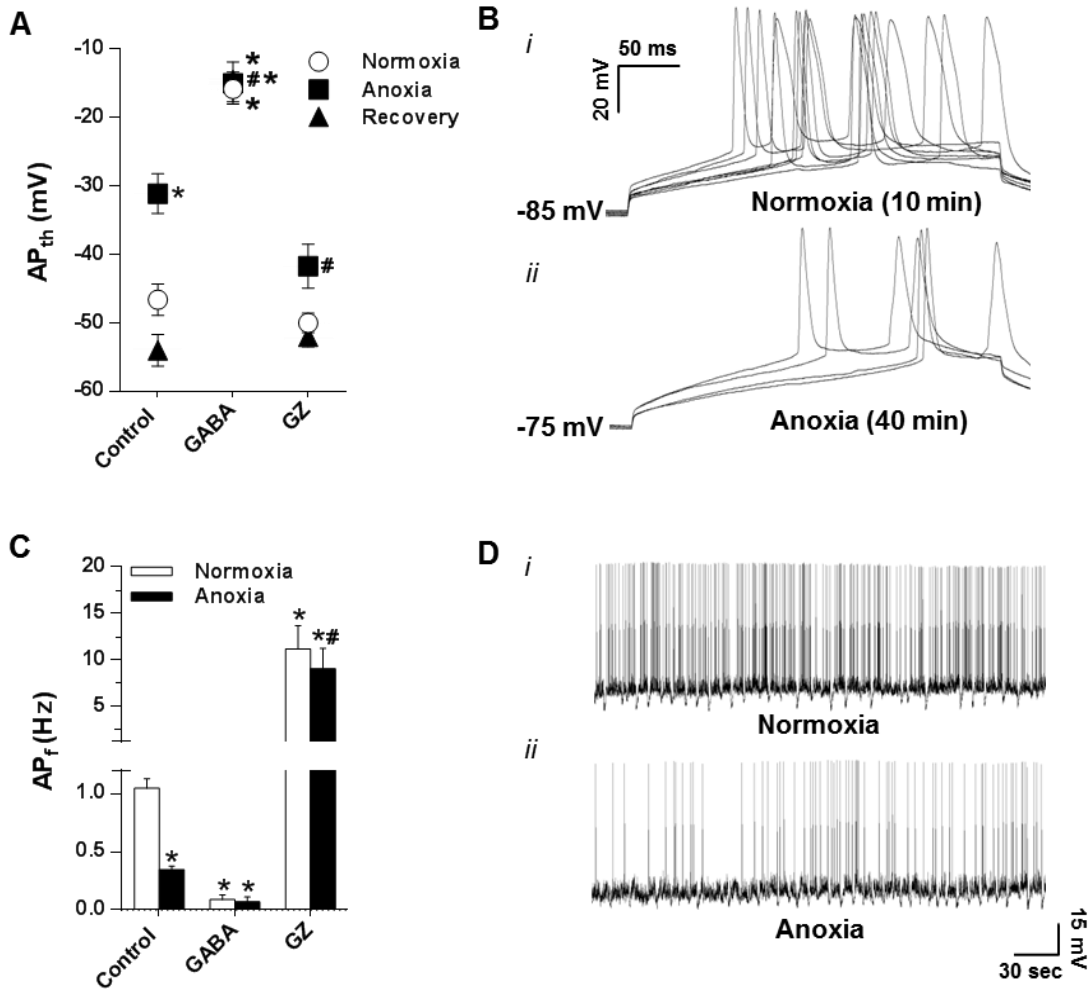

Figure 2.1. Spike arrest is mediated by $GABA_A$ receptors.
(A) Summary of neuronal AP_{th} following normoxic to anoxic transition with recovery (t = 10, 40, and 60 min, respectively). (B) Sample recordings of APs stimulated from electrically quiet neurons by stepwise current injection. (C) Summary of AP_f (Hz) following indicated treatments. (D) Sample free running current-clamp recordings of spontaneously firing pyramidal neurons under normoxic (*i*), and anoxic (*ii*) conditions. Treatments: normoxia 95% O_2/5% CO_2, anoxia 95% N_2/5%, 2 mM GABA, 25 μM gabazine ($GABA_A$ receptor antagonist). Data are mean ± SEM from 4-8 separate experiments. Asterisks (*) indicate significant difference from normoxic controls. Number sign (#) indicates significant difference from anoxic controls ($P < 0.05$).

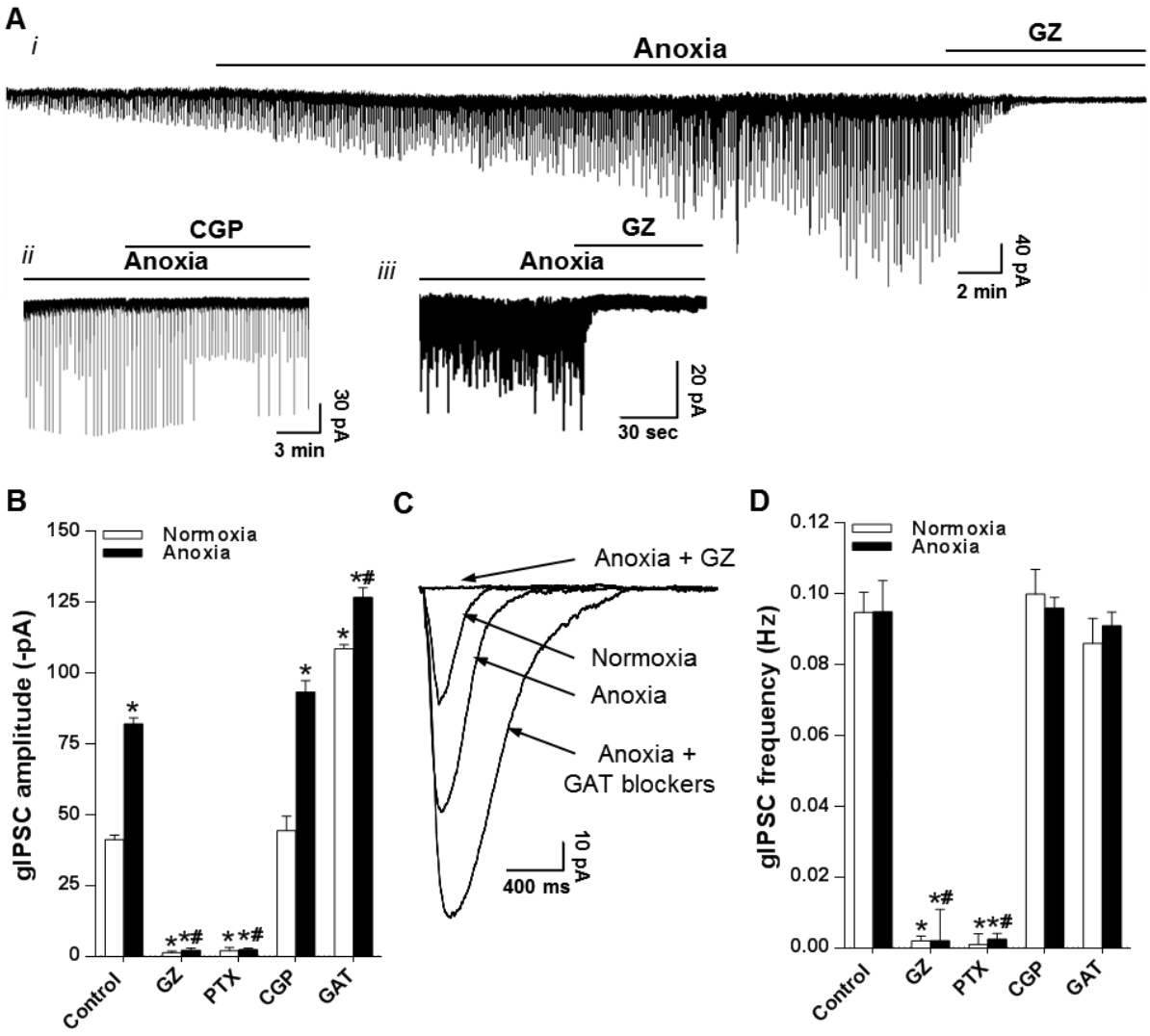

Figure 2.2 Endogenous GABA release is enhanced during anoxia and following inhibition of GABA uptake.

(A) Whole-cell voltage clamp traces of spontaneous GABAergic current activity in pyramidal neurons. (*i*) During transition to anoxia. (*ii*) During anoxia following CGP application. (*iii*) During anoxia following application of GZ to assess tonic GABA activity. To aide current detection, pipette [Cl^-] was increased to 110 mM and neurons were clamped at -100 mV. Cortical sheets were continuously treated with the NMDA receptor antagonist APV (25 μM) and AMPA receptor antagonist CNQX (25 μM). (B) Summary of GABAergic gIPSC amplitude under high [Cl^-] conditions. (C) Superimposed raw spontaneous GABAergic gIPSC recordings averaged from 10 events from three neurons per trace. (D) Summary of GABAergic gIPSC frequency. Black bars represent duration of treatment. Treatments: normoxia 95% O_2/5% CO_2, anoxia 95% N_2/5%, $GABA_A$ receptor antagonists: gabazine (25 μM) and picrotoxin (100 μM), CGP55845 (5 μM; $GABA_B$ receptor antagonist), GABA transport inhibitors: SKF 89976A hydrochloride (40 μM; GAT-1) and (S)-SNAP-5114 (20 μM; GAT-2 and -3). Data are mean ± S.E.M. from 4-19 separate experiments. Asterisks (*) indicate significant difference from normoxic controls. Number sign (#) indicates significant difference from anoxic controls ($P < 0.05$).

neurotransmitter release are maintained (Feng *et al.*, 1988a; Blanton *et al.*, 1989a; Perez-Pinzon *et al.*, 1992b). Under these conditions, a significant tonic inhibitory current was not observed when GZ was applied to normoxic or anoxic neurons (1.6 ± 3.9 and 3.1 ± 2.4 pA respectively; n = 8 each; figure 2.2A*iii*). Spontaneous GABAergic giant IPSCs (gIPSC) were detectable during normoxia, and their amplitude doubled during anoxic perfusion (-41.2 ± 1.6 to -82.1 ± 2.1 pA; n = 10 each; $p < 0.001$; figure 2.2A-C). Giant IPSCs were abolished by $GABA_A$ receptor antagonists (GZ or picrotoxin; PTX) and enhanced by GABA transporter antagonists (GAT; $p < 0.001$; n = 4 each), confirming postsynaptic $GABA_A$ receptor activation by endogenous synaptic GABA release (figure 2.2A*i*- and *iii*, B, C). Application of the $GABA_B$ receptor antagonist CGP did not affect gIPSC amplitude under normoxic conditions (-44.4 ± 5.1 pA; n = 4; figure 2.2B), and treatment with anoxia plus CGP was not different from anoxia alone (-44.4 ± 5.1 to -93.3 ± 4.1 pA; n = 4; figure 2.2A*ii*, B). Giant IPSCs occurred at a frequency ($gIPSC_f$) of 0.1 ± 0.01 Hz under normoxic conditions, and this was unaffected by anoxia, antagonism of GABA uptake or $GABA_B$ receptors (figure 2.2D).

Anoxia increases pyramidal neuron G_w by activating $GABA_A$ receptors.

An anoxia-mediated increase in GABA release and activation of postsynaptic $GABA_A$ receptors should result in an increase in pyramidal neuron whole-cell conductance (G_w). To confirm this, neuronal G_w measurements were performed. As expected, anoxic treatment reversibly increased pyramidal neuron G_w from a normoxic value of 4.8 ± 0.3 to 6.7 ± 0.4 nS (n = 12 each; $p = 0.043$; figure 2.3A, B). Compared to normoxic control, inhibition of $GABA_A$ receptors with GZ prevented the anoxia induced increase in G_w (5.1 ± 0.4 nS; n = 7; figure 2.3A). In contrast, antagonism of $GABA_B$ receptors with CGP did not reduce anoxic G_w (6.4 ± 0.5 nS; n = 7; figure 2.3A). These data are supported by stimulus evoked measurements of input resistance (inverse of G_w) also from turtle pyramidal neurons (Pamenter *et al.*, 2011). These data indicate that pyramidal neuron G_w is modulated by $GABA_A$ but not $GABA_B$ receptor activation during anoxia. Normoxic treatment with 2 mM GABA increased G_w to 15.7 ± 1.8 nS (n = 11; $p < 0.001$; figure 2.3A) and anoxia plus 2 mM GABA did not further increase this value (14.7 ± 2.2 nS; n = 8). To further investigate the effects of GABA on G_w, pyramidal neurons were treated with a range of [GABA] and a dose response curve describing the relationship between G_w and [GABA] was generated (n = 3-13 for each [GABA]; figure 2.3C). Together these findings indicate that a 2 mM GABA perfusion results in maximal activation of $GABA_A$ receptors.

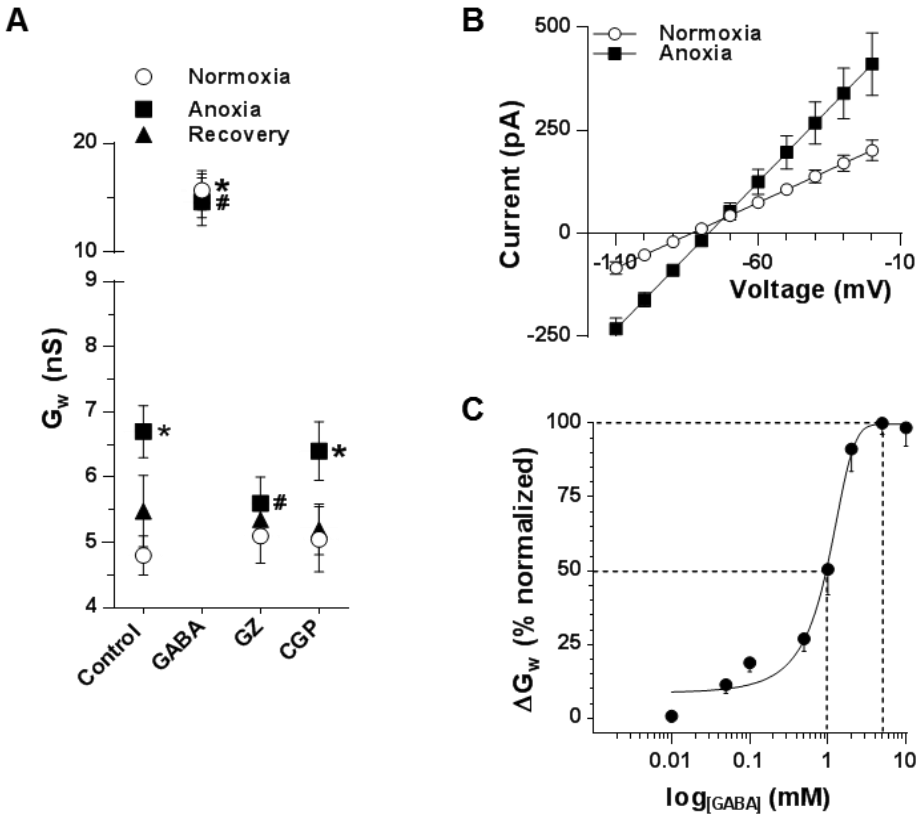

Figure 2.3. Anoxic increases in plasma membrane G_w is $GABA_A$ receptor-dependant.
(A) Summary of G_w measured in the whole-cell configuration. (B) I/V relationships from (A). (C) Dose–response relationship of [GABA] versus ΔG_w. Treatments: normoxia 95% O_2/5% CO_2, anoxia 95% N_2/5%, 2 mM GABA, 25 μM gabazine ($GABA_A$ receptor antagonist), 5 μM CGP55845 ($GABA_B$ receptor antagonist), 25 μM CNQX (AMPA receptor antagonist) and 25 μM APV (NMDA receptor antagonist). Data are mean ± SEM from 3-12 separate experiments. Asterisks (*) indicate significant difference from normoxic controls. Number sign (#) indicates significant difference from anoxic controls ($P < 0.05$).

Anoxic GABA release shifts membrane potential to E_{GABA} by activating $GABA_A$ receptors.

To further investigate the effects of endogenous GABA release on postsynaptic pyramidal neurons, giant inhibitory postsynaptic potentials (gIPSPs) were assessed using free-running current clamp methods, and with regular turtle pipette solution in the presence of CNQX and APV to isolate GABAergic currents. I was interested in investigating gIPSPs under physiological conditions so I measured gIPSP amplitude and frequency during normoxia and following a transition to anoxia. To assess reversibility of gIPSPs I also clamped pyramidal neuron V_m to voltages that were either hyperpolarized (-90 mV) or depolarized (-70 mV) relative to resting V_m. These experiments were initially performed using perforated patch-clamp methods to avoid perturbing intracellular [Cl^-] ($[Cl^-]_i$); however, results were not different from recordings performed under whole-cell patch-clamp conditions so this data set is a combination of the two methods. Under free-running normoxic conditions, gIPSP amplitude was 10.3 ± 1.8 mV, and events were depolarizing relative to V_m (n = 7; figure 2.4A, B). In previous experiments using the high chloride pipette solution I determined that gIPSCs are $GABA_A$ receptor-dependant. To confirm this is also the situation when recorded under physiological conditions I treated neurons with GZ and CGP. GABAergic gIPSPs were abolished by GZ but not by CGP, demonstrating that gIPSPs are $GABA_A$ receptor-mediated (n = 10 - 13 each; not shown). Giant IPSP frequency ($IPSP_f$) occurred at a rate of 0.1 ± 0.01 Hz, and the frequency did not change during anoxia (0.09 ± 0.02 Hz; n = 7; $p < 0.001$; figure 2.4A, summary data not shown); however, anoxic gIPSPs were decreased in amplitude (-1.47 ± 0.7 pA; $p < 0.001$), and their polarity was reversed such that gIPSPs generally are slightly hyperpolarizing relative to V_m. This indicates that anoxic GABA release shifts V_m toward the GABA reversal potential (E_{GABA}). When neurons were current-clamped at -90 mV (near normoxic V_m) or -70 mV (depolarized relative to both normoxic and anoxic V_m), the resulting gIPSPs were not different between conditions, indicating that the mechanism underlying this change is an alteration of V_m homeostasis during anoxia.

In mammalian neurons, $GABA_A$ receptor activation induces Cl^- flux in the direction of the chloride reversal potential (E_{Cl}), which is slightly hyperpolarized compared to E_{GABA} (Blaesse *et al.*, 2009). E_{GABA} has not been previously measured in adult turtle pyramidal neurons; therefore, to more closely examine the relationship between V_m and $GABA_A$ receptor activity I assessed pyramidal neuron E_{GABA} using the gramicidin perforated patch-clamp configuration. Normoxic E_{GABA} was determined to be -80.9 ± 1.4 mV, which is ~ 8 mV depolarized relative to V_m in the

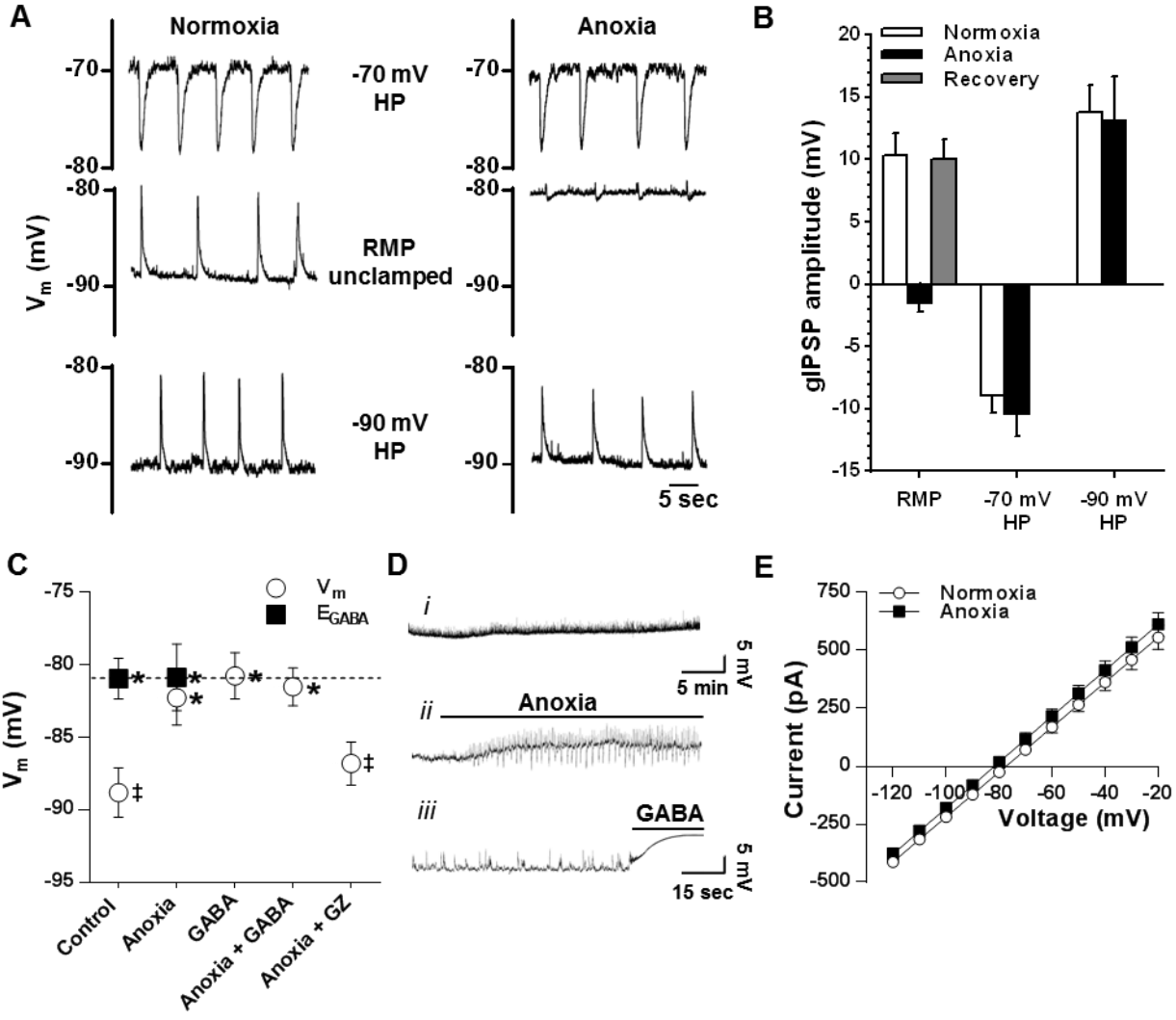

Figure 2.4. Anoxia increases GABAergic activity and shifts V_m to E_{GABA}.
(A) Sample recordings of GABAergic gIPSPs under normoxic and anoxic conditions from neurons voltage-clamped at -70 mV or -90 mV (top and bottom traces, respectively) or free-running (no voltage clamp; middle traces) in the presence of 25 μM CNQX (AMPA receptor antagonist) and 25 μM APV (NMDA receptor antagonist). Resting membrane potential (RMP), Holding potential (HP). (B) Summary of gIPSP amplitudes from (A). (C) Summary of paired V_m and E_{GABA} measured in the perforated-patch configuration. Note: dotted line indicates mean E_{GABA} for comparison. (D) Sample traces from (C). Note: black bars represent duration of treatment. (E) Sample I/V relationship of *pure* GABA currents from (C); E_{GABA} is the x intercept. *Pure* GABA currents were determined by subtracting treatment I/V curves from treatment + GABA I/V curves. Treatments: normoxia 95% O_2/5% CO_2, anoxia 95% N_2/5%, 2 mM GABA. Data are mean ± SEM from 7-17 separate experiments. Asterisks (*) indicate significant difference from normoxic controls. Double daggers (‡) indicate significant difference from E_{GABA} ($P < 0.05$).

same neurons (-88.8 ± 1.7 mV; $p = 0.001$; n = 10; figure 2.4C, E). E_{GABA} was not changed by anoxic treatment (-80.8 ± 2.3 mV; n = 8, figure 2.4C, E); therefore, data is compared to normoxic E_{GABA}. Anoxia depolarized V_m to -80.2 ± 1.9 mV and this was not different from E_{GABA} (figure 2.4C, D*ii*). Consistent with an underlying GABAergic mechanism, in normoxic neurons 2 mM GABA perfusion mimicked anoxia and depolarized V_m to E_{GABA} (-81.0 ± 2.1 mV; n = 12; figure 2.4C, D*iii*). Co-treatment with anoxia plus GABA also depolarized V_m (-81.5 ± 1.2 mV; n = 7), and V_m was not different from E_{GABA} or GABA alone (figure 2.4C, D*iii*). Treatment of neurons with GZ prevented a subsequent anoxia-mediated depolarization in V_m (-86.8 ± 1.5 mV; n = 6; $p = 0.05$), demonstrating that the anoxic activation of $GABA_A$ receptors is responsible for the shift in V_m.

Anoxia or GABA induces $GABA_A$ receptor-mediated Cl^- efflux and cell shrinkage

When E_{GABA} is depolarized relative to V_m, such as in immature mammalian neurons, the Cl^- gradient is such that postsynaptic $GABA_A$ receptor activation induces Cl^- efflux accompanied by reductions in cell volume (Blaesse *et al.*, 2009). To determine if this also happens in anoxic turtle neurons cellular Cl^- movement and neuronal volume regulation was assessed using non-invasive assays [6-methoxy-N-ethylquinolinium iodide (MEQ) and calcein-AM fluorescence, respectively] (Crowe *et al.*, 1995; Inglefield & Schwartz-Bloom, 1999). Anoxia or GABA perfusion reversibly increased MEQ fluorescence 30-40% reflecting Cl^- efflux, because intracellular Cl^- quenches MEQ fluorescence (n = 5 each; $p < 0.001$ for both; figure 2.5A, B*i-iii*). Chloride efflux was confirmed to be through $GABA_A$ receptors because GZ prevented changes in MEQ fluorescence under anoxic conditions and following GABA treatment (n = 5; figure 2.5A, Bv-*vi*). Anoxia plus GABA did not have an additive effect versus anoxia alone indicating anoxia is sufficient to activate this $GABA_A$ receptor-mediated mechanism (n = 5 each; figure 2.5A, B*iv*). Antagonism of $GABA_B$ receptors with CGP did not prevent anoxic increase in MEQ fluorescence (38.3 ± 5.1%; n = 5, figure 2.5A), indicating $GABA_B$ receptors do not regulate pyramidal neuron Cl^- efflux. These fluorescent Cl^- measurements support the electrophysiological assessment of V_m and E_{GABA} because they show that Cl^- leaves the cell down its concentration gradient towards E_{Cl} during anoxia. To assess the effect of anoxic Cl^- movement on neuronal volume cortical sheets were incubated with the fluorophore calcein. Calcein fluorescence intensity is directly proportional to its concentration; and therefore, a decrease in cell volume results in an increase in calcein concentration. GABA treatment increased calcein fluorescence 22.1 ± 4.0 and 9.0 ± 3.0% relative to normoxic control (n

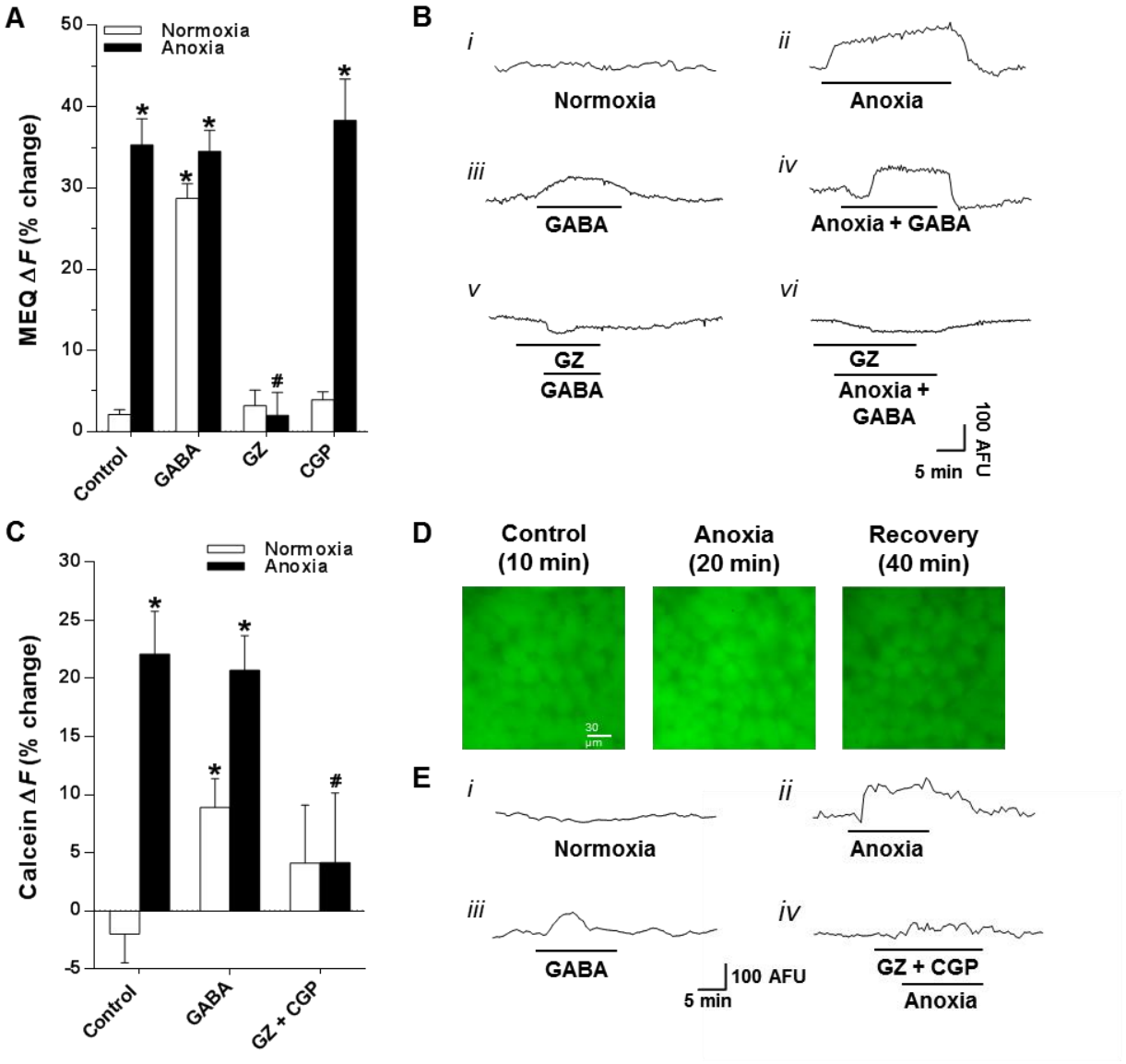

Figure 2.5. Anoxia or GABA induces $GABA_A$ receptor-mediated Cl^- efflux and cell shrinkage.
(A) Summary of MEQ fluorescence. (Note: Increased MEQ fluorescence correspond to reduced intracellular [Cl^-]) (B) Sample MEQ fluorescence recordings from (A). (C) Summary of calcein fluorescence. (Note: Increases in calcein fluorescence correspond to decreased cell volume). (D) Sample calcein fluorescence images of neurons undergoing an anoxic transition with recovery. (E) Sample calcein fluorescence recordings from (C). Note: Changes were assessed after the fluorescent signal stabilized (~ 5 min), and are expressed relative to baseline fluorescence before treatment onset. Black bars represent duration of treatment. Treatments: normoxia 95% O_2/5% CO_2, anoxia 95% N_2/5%, 2 mM GABA, 25 μM gabazine ($GABA_A$ receptor antagonist), and 5 μM CGP55845 ($GABA_B$ receptor antagonist). Data are mean ± S.E.M. from 4-12 separate experiments. Asterisks (*) indicate significant difference from normoxic controls. Number sign (#) indicates significant difference from anoxic controls ($P < 0.05$).

= 4 each; $p < 0.001$ and $p = 0.038$, respectively; figure 2.5C, D, E*i-iii*), reflecting cell shrinkage. Under anoxic conditions, antagonism of $GABA_{A+B}$ receptors reduced the anoxic increase by ~ 80%, to 5.0 ± 7.7% (n = 4 each; $p = 0.002$; figure 2.5C, E*iv*), demonstrating that neuron shrinkage is indeed due to water movement as a result of Cl^- efflux. This data supports the electrophysiological measurements of E_{GABA} being depolarized relative to normoxic V_m in adult turtle cortex.

2.4 Discussion

In this study I investigate GABA-mediated spike arrest in a naturally anoxia-tolerant turtle brain model. I provide evidence that spike arrest is due to the anoxic modulation of both presynaptic and postsynaptic components of GABA transmission. To investigate the presynaptic component of spike arrest I used pyramidal neurons as reporter cells to assess GABA release under anoxic treatment. I demonstrate that anoxia enhances GABA release from presynaptic GABAergic cortical neurons, and this activates a unique $GABA_A$ receptor-mediated phasic current on postsynaptic pyramidal neurons. I have termed these currents giant IPSCs. Under anoxic conditions gIPSCs double in amplitude and this is mimicked by GABA uptake transport blockers. Together these data confirm that GABA release increases during anoxia and indicates that in the cerebrocortex GABAerigc interneurons are oxygen-sensitive. To investigate GABA-mediated spike arrest in postsynaptic pyramidal neurons I assessed the effects of anoxia and GABA receptor modulation on parameters of membrane excitability. Anoxic treatment increased membrane permeability to Cl^- through a $GABA_A$ receptor dependent mechanism, and this Cl^- conductance monopolizes G_w. Increased $GABA_A$ receptor activity depolarized V_m and AP_{th}, resulting in a significantly decreased AP_f. I propose that the principal mechanism behind spike arrest is $GABA_A$ receptor-mediated shunting inhibition that shifts V_m to E_{GABA} and prevents further depolarization to AP_{th}. GABA-mediated spike arrest is an essential component of the turtle's anoxia-tolerance strategy and these results highlight the critical role $GABA_A$ receptors play in cortical pyramidal neurons and identify a unique oxygen-sensitive inhibitory signalling pathway that enables survival during prolonged anoxic stress.

In the mature mammalian brain, $[Cl^-]_i$ is typically low due to high activity of KCC2. Since $GABA_A$ receptors primarily conduct Cl^-, activation of these receptors is inhibitory because Cl^- influx shifts V_m towards E_{Cl} (~ E_{GABA}) and away from AP_{th}. Under normoxic conditions, with a steady supply

of oxidatively derived ATP, maintenance of Na^+ gradients is easily maintained by Na^+/K^+ ATPase activity. However, this is not a particularly effective strategy for surviving long-term anoxia because it results in increased ATP usage (Bickler & Buck, 2007). In contrast to mammals, turtle pyramidal neurons exhibit an E_{GABA} that is depolarized (~ 8 mV) relative to V_m, and anoxia or GABA treatment activate postsynaptic $GABA_A$ receptors resulting in Cl^- efflux and V_m depolarization, not hyperpolarization. While this may seem counter-intuitive, an anoxia-mediated increase in chloride conductance (G_{Cl}) produces an electrical shunt that can prevent excitation by decreasing the temporal and spatial summation of excitatory inputs (Blaesse *et al.*, 2009). Therefore, activation of $GABA_A$ receptors during anoxia will be inhibitory regardless of the value of E_{GABA}. Furthermore, due to the intrinsic outward rectification of $GABA_A$ receptor currents, depolarizing GABA responses can be even more effective than hyperpolarizing response (see below discussion on AP_{th}) (Gray & Johnston, 1985; Verdoorn *et al.*, 1990). The expression/activity of Cl^- co-transporters in adult turtle neurons is unknown; although KCC2 expression is high in retina (*Pseudemys elegans*) (Leitch *et al.*, 2005), indicating a similar mechanism of Cl^- homeostasis. Importantly, normoxic and anoxic E_{GABA} are not different indicating that neither NKCC1 nor KCC2 are modulated during anoxia.

An interesting finding from this study and others (Feng *et al.*, 1988a; Perez-Pinzon *et al.*, 1992b; Pamenter & Buck, 2008) is that anoxic or GABA perfusion depolarizes AP_{th} ~ two-fold more than V_m depolarizes, indicating that under these conditions additional excitatory input is required to elicit an AP. This is supported by measurements of rheobase (i.e., stimulation required to generate an AP) which increases ~ 20-fold during anoxia (Pamenter *et al.*, 2011). This may be the consequence of the $GABA_A$ receptor-mediated depolarizing shunt because V_m depolarization can inactivate voltage-gated sodium channels (Chandel & Schumacker) resulting in fewer Na_v channels available for activation and a depolarized AP_{th} (Henze and Buzsaki, 2001). AP_{th} also depends on the rate of V_m depolarization to threshold with lower rates of depolarization corresponding to more depolarized AP_{th} (Blaesse *et al.*, 2009). Therefore, under anoxic conditions an increase in G_w would not only increase the amount of excitatory current required to depolarize V_m to threshold but would also slow the rate of V_m depolarization. A depolarized AP_{th} could also be the result of anoxia-induced changes in protein kinase expression or activity (Henze & Buzsaki, 2001; Scheuer, 2011), and in particular protein kinase A (PKA) or protein kinase C (PKC) because phosphorylation of Na_v by either of these kinases decreases channel currents and slows inactivation

(Numann *et al.*, 1991). This is relevant to this model because anoxia induces changes in the activity of both these kinases (Brooks & Storey, 1993; Mehrani & Storey, 1995). Another interesting result related to this depolarizing shunting inhibition is that neuron volume decreases along with anoxia or $GABA_A$ receptor-mediated Cl^- efflux. This is in direct contrast to ischemic mammalian neurons where dysregulation of ionic gradients results in cell swelling which can lead to necrotic membrane rupture (Allen *et al.*, 2004). This indicates that in addition to ATP savings during anoxia, depolarizing shunting conductances may prevent osmotic imbalances that contribute to neuron death.

Activation of anoxia-mediated GABAergic shunting inhibition in pyramidal neurons requires an endogenous source of GABA. Although turtle brain [GABA] is known to increase 80-fold in response to anoxia (Nilsson & Lutz, 1991), this study provides the first measurement of anoxia-induced increases in GABA release. The primary GABAergic neurons in the cerebrocortex of the turtle are stellate interneurons. These are the second most abundant type of neuron and they synapse onto and modulate pyramidal neuron activity (Kriegstein & Connors, 1986a; Kriegstein & Connors, 1986b). Recording from these interneurons during a transition to anoxia would be the ideal method of assessing presynaptic GABA release; however, this is difficult to achieve in the brain sheet model due to the low incidence of this type of neuron in the cellular layer that I am recording from. To circumvent this problem I used a high chloride pipette solution and voltage-clamped pyramidal neurons at -100 mV to amplify the GABAA receptor currents. I used changes in the amplitude of pyramidal neuron IPSCs as a proxy for changes in presynaptic GABA release. Using this technique I identified phasic GABA-mediated gIPSCs and used them to measure presynaptic GABA release. Giant IPSCs are the result of activation of $GABA_A$ receptors because GZ completely inhibits them. They are generated at a fixed frequency regardless of treatment, and anoxia or application of GAT blockers more than doubled gIPSC amplitude indicating that GABA release is the result of upstream network activity. Although this data does not indicate the mechanism through which GABA release is enhanced it does demonstrate that in turtle cerebrocortex GABA release is oxygen-sensitive.

A surprising result of this study is the absence of a measureable tonic $GABA_A$ receptor-mediated current in pyramidal neurons. Under anoxic conditions, an increase in GABAergic tone mediated by extrasynaptic GABA receptors would help to clamp V_m at E_{GABA} and increase whole-cell membrane permeability to Cl^-; and this would be an energetically inexpensive mechanism through

which to prevent AP generation. One possible reason no tonic GABA current was measured could be because I used GZ instead of bicuculine (BIC) as the $GABA_A$ receptor antagonist. While both GZ and BIC are competitive antagonists that prevent receptor activation by displacing GABA from its binding site, GZ selectively binds to low affinity $GABA_A$ receptors, and is not as effective at inhibiting tonic GABA currents (Bai *et al.*, 2001; Bright & Smart, 2013).

To initiate ECD in turtle pyramidal neurons both $GABA_A$ and $GABA_B$ receptors need to be blocked (Pamenter *et al.*, 2011). This demonstrates that metabotropic $GABA_B$ receptors are also a critical component of spike arrest; however, their role in shunting inhibition is unknown. Typically activation of presynaptic $GABA_B$ receptors inhibit Ca^{2+} channels while postsynaptic $GABA_B$ receptors activate K^+ channels (Ben-Ari *et al.*, 2007). In this study, antagonism of $GABA_B$ receptors with CGP did not have an effect on anoxic gIPSC amplitude and frequency indicating GABA release in not modulated by $GABA_B$ receptors. CGP application did not decrease anoxic G_w indicating postsynaptic K^+ channels are not modulated by activation of $GABA_B$ receptors. Together this indicates that $GABA_B$ receptors do not play a role in shunting inhibition. In mammals, presynaptic $GABA_B$ receptors are found primarily concentrated around glutamatergic synapses where receptor activation prevents glutamate release (Kornau, 2006). This is likely the situation in turtle cerebrocortex as well because application of CGP during anoxia increased AP_f (Pamenter *et al*., 2011). In addition, CGP application increases AMPA receptor-mediated excitatory postsynaptic potentials (EPSPs) again indicating increased glutamate release (Pamenter *et al.*, 2011). Together this evidence suggests that in turtle cerebrocortex the primary contribution of $GABA_B$ receptors to spike arrest is to prevent excitatory glutamate release and decrease excitatory input into pyramidal neurons.

In summary, I report that in turtle cerebrocortex there is an anoxia-mediated increase in GABA release that activates $GABA_A$ receptors on pyramidal neurons. This leads to an increase in Cl^- conductance and activation of a shunting mechanism that clamps V_m at E_{GABA}. This depolarizes AP_{th} and decreases AP generation which conserves ATP at a crucial time when ATP is limited. Excess GABA likely activates $GABA_B$ receptors located on presynaptic glutamatergic synapses and decreases glutamate release, further reducing AP generation. An important result of this study is the discovery of unique oxygen-sensitive giant $GABA_A$ receptor-mediated IPSCs. These gIPSCs occur at a stable frequency indicating that they are the result of upstream network activity from oxygen-sensitive GABAergic interneurons.

3 GABAergic mechanisms protect painted turtle cerebrocortex from an *in vitro* mimic of the ischemic mammalian penumbra

Preface

A modified version of this chapter was published as Pamenter ME, Hogg DW, Gu XQ, Buck LT and Haddad GG. (2012). Painted turtle cortex is resistant to an in vitro mimic of the ischemic mammalian penumbra. *J. Cereb. Blood Flow Metab*. 32: 2033-2043.

The idea to investigate if GABAergic spike arrest can defend against ischemic stress was conceived jointly by D. Hogg and M. Pamenter. D. Hogg performed all electrophysiology experiments (figures 3.1-3.4), M. Pamenter performed the fluorescent assays (figure 3.5).

Abstract

Anoxia or ischemia causes hyperexcitability and cell death in mammalian neurons. Conversely, in painted turtle brain anoxia increases GABAergic suppression of spontaneous electrical activity and cell death is prevented. To examine ischemia tolerance in turtle neurons, cortical sheets were treated with an *in vitro* mimic of the penumbral region of stroke afflicted mammalian brain (ischemic solution, IS). In sheets treated with IS, neuronal V_m and E_{GABA} depolarized to a similar steady state (-92 ± 2 to -28 ± 3 mV, and -75 ± 1 to -35 ± 3 mV, respectively), and G_w increased > 3-fold (from 4 ± 0.2 to 15 ± 1 nS). These neurons were electrically quiet and changes reversed after reperfusion. GABA receptor antagonism prevented the IS-mediated increase in G_w and neurons exhibited enhanced electrical excitability and rapid and irreversible rundown of V_m during reperfusion. These results suggest that inhibitory GABAergic mechanisms also suppress electrical activity in ischemic turtle cerebrocortex. Indeed, after 4 hours of IS treatment neurons did not exhibit any apparent damage; while at 24 hours, only early indicators of apoptosis were present. I conclude that anoxia-tolerant turtle neurons are also tolerant of exposure to a mammalian ischemic penumbral mimic solution; and therefore, the mechanisms that protect turtle brain from anoxia may also be useful in protecting mammalian brain from ischemic insults.

3.1 Introduction

In Canada, ischemic stroke is a leading cause of death and disability costing on average $3 billion dollars a year (Mittmann *et al.*, 2012). An ischemic stroke occurs when a blocked artery reduces blood supply to the brain, and this results in decreased oxygen supply. In addition to the deleterious effects of anoxia or hypoxia, cerebral blood flow is impaired, which also limits nutrient delivery and slows the removal of signaling molecules, ions, and metabolically derived lactate and CO_2 (Branston *et al.*, 1974). These events enhance cytotoxicity, ionic imbalance, and acute acidification in the occluded region (the infarct core) and the hypoperfused surrounding tissue (the penumbra) (Anderson *et al.*, 1999; Yao *et al.*, 2007). Since freshwater turtles are naturally anoxia-tolerant the mechanisms that have evolved in these animals to withstand oxygen-deprivation may be useful in providing direction in producing therapies for treatment of ischemia in mammals. Similar to mammals, turtle brain also becomes more acidic during anoxia (Wasser *et al.*, 1991; Buck *et al.*, 1998); however, cerebral blood flow is increased (Bickler, 1992), and liver glycogen stores are mobilized and continuously delivered to the brain, facilitating glycolytic ATP production (Bickler & Buck, 2007). This represents a significant systemic advantage relative to ischemic stress in mammals; and indeed, turtles are considerably more tolerant to ischemic stress and survive > 1 hour after cardiac excision at 22°C (Belkin, 1968). Furthermore, mimicking the turtle's endogenous cell-level neuroprotective mechanisms (inhibiting glutamatergic activity – channel arrest, or enhancing GABAergic activity - spike arrest) is neuroprotective against ischemic or hypoxic injury in mammalian brain (Arundine & Tymianski, 2004; Costa *et al.*, 2004). Therefore, the ability of anoxia-tolerant turtle brain to withstand ischemic stress is of interest to better understand how neuroprotective adaptations to low oxygen environments may provide protection against more complex ischemic challenges.

Previous attempts to examine the resistance of anoxia-tolerant turtle neurons to ischemic stress have relied on oxygen-glucose deprivation or chemical mimics of ischemia that model the mammalian infarct core (i.e., iodoacetate and sodium cyanide to inhibit glycolysis and oxidative phosphorylation, respectively) (Doll *et al.*, 1991). However, cells within the infarct core die within minutes of insult onset and while this process is of scientific interest, from a clinical standpoint these cells cannot likely be rescued. Conversely, the penumbral region surrounding the infarct core is hypo-perfused and therefore hypoxic, and cell death here spreads over hours to days post-insult and accounts for the majority of morbidity and mortality after stroke in mammalian models (Lo,

2008). Therefore, mechanisms of neuroprotection in this region are of considerably greater clinical relevance than in the infarct core. Using a physiological saline solution that mimics the key ionic, hypoxic, and acidic parameters of the penumbral milieu, I asked whether anoxia-tolerant turtle cortical neurons are resistant to this clinically relevant ischemic stress. To answer this question, I treated turtle cortical sheets with aCSF or ischemic solution (IS), and examined pyramidal neuron synaptic activity using the whole-cell and perforated-patch electrophysiological techniques. In addition, cortical sheets were treated with aCSF or IS for up to 24 hours, and pyramidal neuron viability was examined using molecular and biochemical viability assays.

3.2 Materials and Methods

3.2.1 Experimental design

For electrophysiological experiments the design of experiments and protocols used in this chapter are similar to those in chapter 1. Only new materials and methods specific to this chapter are included in this section. For viability assays cortical sheets were divided into three groups and treated with either: (1) aCSF at 4°C, (2) aCSF at 22°C, or (3) ischemic solution (IS, Yao et al. 2007) at 22°C (see below). Sheets were treated for up to 24-hrs, as indicated. For experiments in which [ATP] was measured, an additional set of samples were treated with IS for 1- or 24-hrs and allowed to recover in normoxic aCSF for 1-hr before homogenization. For molecular and biochemical assays, cortical sheets were treated simultaneously and in parallel.

3.2.2 Ischemic setup

In experiments investigating the effects of ischemia in turtle cerebrocortex, tissue was perfused with an ischemic penumbral mimic solution (IS) containing (in mM): 47 NaCl, 29 KCl, 35 K-gluconate, 1.5 $MgCl_2$, 3 glucose, 65 sucrose, 0.1 glutamate, 4 $NaHCO_3$, 0.13 $CaCl_2$ (315 mOsM, pH 6.5) (Yao *et al.*, 2007). IS was bubbled with a gas mixture containing 1.5% O_2/15% CO_2/ balance N_2 for a minimum of 30 min prior to commencement of experiments and *ischemia* was maintained by a perfusion system and chamber similar to that used in Chapter 2. In some experiments, cortical sheets were treated with either a high-K^+ aCSF solution containing 64 mM K^+ (to match the K^+ composition of IS). This solution was made by adding 61.4 mM K-gluconate to raise total extracellular [K^+] to 64 mM. In other experiments, sheets were treated with IS containing normal [K^+] (2.6 mM) (to match the aCSF K^+ composition). This solution was made

by substituting 2.6 mM KCl, 26.4 mM choline chloride and 80.4 mM sucrose for K-gluconate in the original IS recipe. All electrophysiological experiments were conducted at 22°C. IS and high-K^+ aCSF were assessed to have a LJP of 4 mV, aCSF and low K^+ aCSF were assessed to have a LJP of 14 mV. All data have been corrected for this value offline.

3.2.3 Fluorescence imaging

3.2.3.1 Confocal microscope

Propidium iodide (PI) exclusion from live cortical sheets was imaged using a Perkin Elmer Ultraview Vox spinning disk confocal microscope, with a 572 nm (TRITC) laser line (Perkin Elmer, Waltham, MA). Samples were maintained at 4 or 24°C and constantly gassed with either normoxic or IS gas mixtures, and images were taken at 30 min intervals for 24 hrs (data presented at 0.5, 1, 2, 4, 8, 12 and 24 hrs). In other experiments, PI uptake and annexin V binding (see below) were imaged in cortical sheets treated for 4- or 24-hrs in aCSF, IS, or aCSF with 5 μM staurosporine (STS) (apoptosis-inducing agent), using an Olympus FV1000 scanning confocal microscope, with 572 nm (TRITC) and 488 nm (FITC) laser lines (Olympus, San Diego, CA). For data collection in both sets of confocal microscopy experiments, the parameters of the microscope such as light intensity, exposure time, camera gain, etc., were determined for the brightest fluorescing sample and standardized for subsequent samples. For analysis, five random sections from each study group were taken at 20x magnification using AxioVision (Carl Zeiss, Thornwood, NY) or Volocity software (Perkin Elmer), and the number of cells staining positive for PI uptake or annexin V translocation was determined by counting FITC- or TRITC-stained cells normalized to tissue area. To quantify cell death in each sheet, images were analyzed using ImageJ software (version 1.37, NIH, USA).

3.2.3.2 Annexin V apoptosis assay

Cortical sheets were treated as indicated in the experimental design section (above) for 4- or 24-hrs. Following treatment, Annexin V translocation was measured using an Annexin V-FITC Apoptosis Detection Kit (Enzo Life Sciences, Plymouth Meeting, PA) as per the manufactures instructions, and annexin V translocation was imaged using a confocal microscope (see above). Experiments were repeated 3-5 times for each treatment.

3.2.3.3 ATP luciferase assay to assess metabolic viability

Cortical sheets were treated as indicated in the experimental design section (above) for 1- or 24-hrs. Following treatment, sheets were rinsed twice in PBS, excess fluid was removed by wicking with a Kimwipe, and sheets were weighed and then rapidly homogenized in cell lysis buffer using a Precellys 24 tissue homogenizer (Bertin Corp, Rockville, MD). The resulting cell suspensions were normalized to wet tissue weight and aliquots were then pipetted into black, solid-bottom 96-well microplates (Corning). Total ATP content was assessed using a Perkin Elmer ATPlite Luminescence Assay System kit as specified by the manufacturers protocol (Perkin Elmer, MA, USA), and a Bio-Tek PowerWave 340 microplate spectrophotometer (Bio-Tek, Winooski, VT, Ex/Em: 485/630 nm), and analyzed using Gen 5 software (Bio-Tek). Standard curves were generated using serial dilutions of a known ATP standard provided in each kit. The sensitivity of the detector was calibrated to the luminescence of the highest [ATP] standard in each experiment, and plates were read at the same intensity. Experiments were repeated 3-5 times for each treatment, and results were normalized to ATP luminescence recorded from control cells assayed at t = 0 hours.

3.2.3.4 Comet DNA fragmentation assay

Cortical sheets were treated as indicated in the experimental design section (above) for 24-hrs. Following treatment, sheets were rinsed twice in PBS and then rapidly homogenized in ice-cold PBS using a tissue homogenizer (Bertin Corp). Purified DNA was extracted from the resulting cortical sheet homogenates using a Qiagen DNAeasy Blood and Tissue kit as specified by the manufacturers protocol (Qiagen, Valencia, CA), and quantified by NanoDrop (Thermo Sci., Wilmington, DE). Equal quantities of DNA were heated at 65°C for 10 mins, and then loaded onto a standard 1.5% agarose gel containing 0.5 mg/ml ethidium bromide. Electrophoresis was performed at 120V for ~ 40 min at room temperature to separate DNA fragments by weight. Specific bands were visualized via UV trans-illumination using a BioRad Chemilab XRS+ gel-dock system (BioRad, Hercules, CA), and densitometry was performed and images were analyzed using BioRad imaging software (BioRad). Experiments were repeated 3 times.

3.2.3.5 Propidium Iodide (PI) membrane integrity assay

Membrane viability was assessed as the ability of cells to exclude the dye PI. PI is a membrane impermeant fluorescent molecule that binds to DNA by intercalating between bases. Therefore, only cells with compromised plasma membranes fluoresce, and this can be used as an indicator of cell viability. Prior to treatment, cortical sheets were incubated overnight with 5 µg/ml of PI at 4°C to ensure penetration of PI into the tissue. Next, each brain sheet was placed into a single well in a 12-well #0 thickness glass-bottom microplate (MatTek), and fresh PI (5 µg/ml) was added to these wells to prevent depletion of the dye. Sheets were treated as indicated in the experimental design section (above), and then imaged using a confocal microscope (see above). Experiments were repeated 3-5 times for each treatment.

3.2.4 Statistical analysis

Data were analyzed using a two-tailed Student *t*-test or one-way ANOVA, followed by a Tukey's post-hoc test.

3.3 Results

Pyramidal neurons are reversibly depolarized during ischemic solution perfusion

Under normoxic conditions pyramidal neurons exhibited a steady resting V_m of -90.3 ± 1.1 mV for up to 2 hours (n = 10, figure 3.1A, B*i*), and voltage ramps elicited APs at a threshold of -51.3 ± 1.0 mV (figure 3.1C, D*i*), values which are similar to previous measurements from normoxic turtle cerebrocortex (Pamenter *et al.*, 2011). Conversely, upon IS perfusion neurons rapidly depolarized ~ 60 mV to 70 mV to a new steady state (V_m = -22.9 ± 1.4 mV and -28.4 ± 2.3 mV after 20 and 60 min of IS perfusion, respectively; n = 26; $p < 0.001$ for both; figure 3.1A, B*ii-iii*). Notably, neurons did not exhibit excitatory events during the initial depolarization and were electrically quiet during the entire period of IS treatment, and APs could not be evoked (n = 26; figure 3.1C, D*ii*). These changes were reversed by washout with normoxic aCSF. V_m hyperpolarized to -68.6 ± 3.9 mV after 20 minutes of reperfusion ($p = 0.005$), and at 40 minutes was not significantly different from pre-IS baseline controls (-85.4 ± 1.5 mV; $p = 1.000$). Neuronal excitability also returned after reperfusion, as evidenced by the firing of evoked APs (recovery AP_{th} = -45.5 ± 3.4 mV; figure 3.1C, D*iii*). In ischemic mammal brain, neuronal

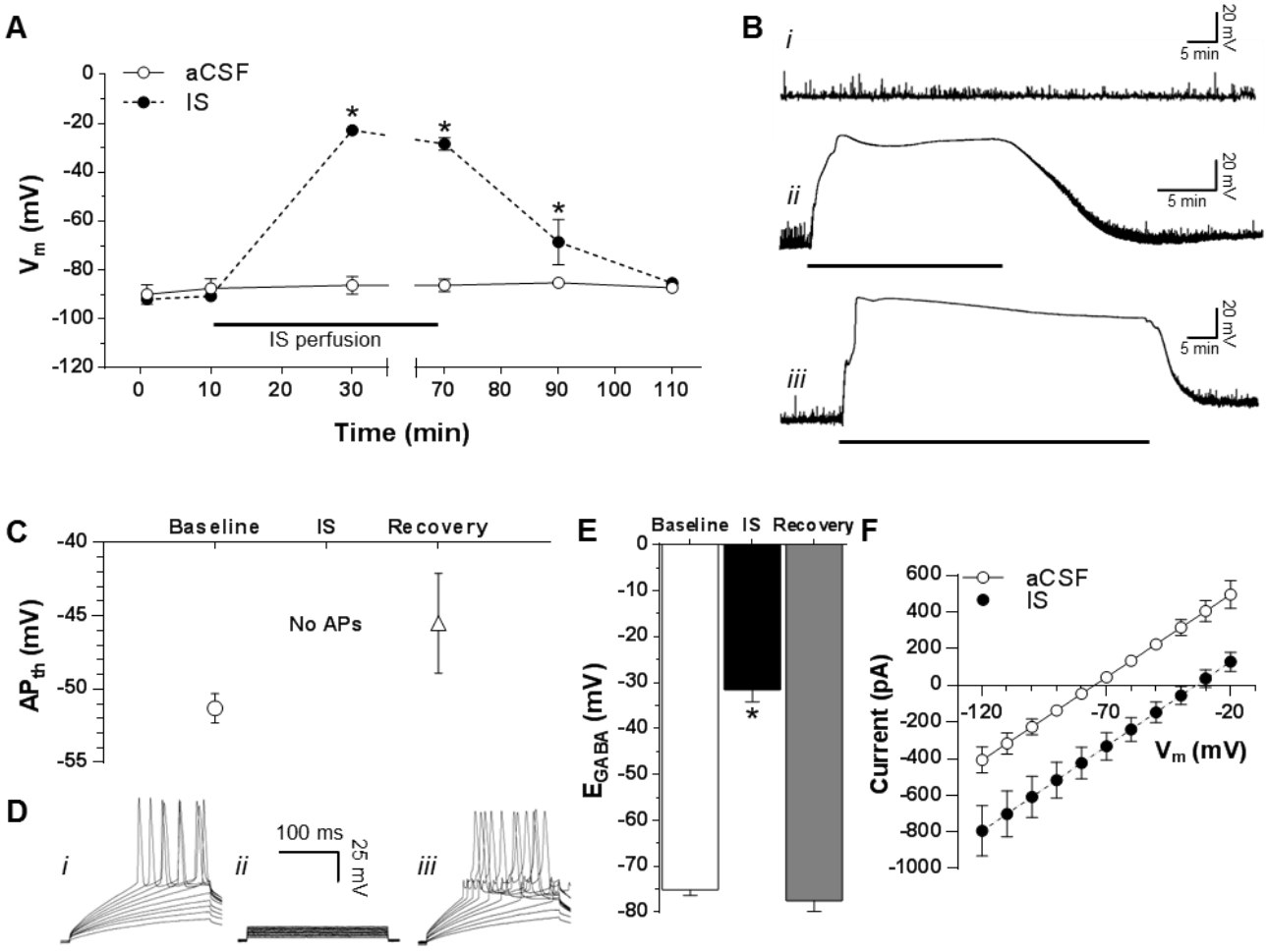

Figure 3.1. V_m depolarizes to E_{GABA} in IS-treated pyramidal neuronal
(A) Summary of V_m recordings from pyramidal neurons treated with normoxic aCSF or a 30 min IS treatment with recovery. (B) Sample V_m recordings from patch-clamped neurons treated with (*i*) aCSF or (*ii*) 20 min IS or (*iii*) 60 min IS perfusion with recovery. Black bars indicate duration of IS perfusion. (C) Summary of AP_{th} from stimulated neurons treated as indicated. APs could not be elicited during IS treatment. (D) Sample recordings of evoked APs recorded during (*i*) baseline control, (*ii*) IS perfusion, and (*iii*) normoxic reperfusion. (E) Summary of E_{GABA} measurements. (F) Summary of *pure* GABA I/V curves used to determine E_{GABA} in aCSF (solid lines) and IS (dashed line) from (E). Treatments: normoxic baseline aCSF 95% O_2/5% CO_2, IS 1.5% O_2/15% CO_2/balanced N_2, 2 mM GABA. Data are mean ± S.E.M. V_m data are from 10-26 separate experiments for each treatment; E_{GABA} data are averaged recordings from 12 separate neurons. Asterisks (*) indicate significant difference from normoxic controls ($P < 0.05$).

depolarization is deleterious and leads to seizure-like events and irreversible anoxic depolarization within minutes of insult onset (Lipton, 1999). Therefore, the lack of similar electrical hyperexcitation in IS-treated turtle neurons, despite a rapid and marked V_m depolarization, suggests that inhibitory mechanisms (i.e., spike arrest) are strongly recruited during IS treatment and reperfusion in this model. In anoxic turtle neurons, V_m is 'clamped' at E_{GABA}, which is largely determined by the distribution of Cl^- across the plasma membrane (E_{Cl}); however, the IS used in this experiment incorporates deleterious ionic imbalances that are characteristic of the penumbral milieu, which would alter this distribution. Therefore, to determine the new set point of Cl^- distribution during IS, and assess a potential role for this in the IS-mediated depolarization of V_m, I measured E_{GABA} using perforated patch-clamp techniques. Under normoxic conditions, E_{GABA} was -75.2 ± 1.2 mV and depolarized relative to control V_m (n = 20; figure 3.1E, F). IS perfusion depolarized E_{GABA} to -31.6 ± 2.6 mV ($p < 0.001$); and was not significantly different from V_m in IS at the same time point ($p = 0.559$). After normoxic reperfusion, E_{GABA} returned to baseline levels (-77.5 ± 2.3 mV). This depolarization represents a significant increase in intracellular ($[Cl^-]_i$). According to the Nernst potential equation $[Cl^-]_i$ in aCSF is ~ 6.3 mM (extracellular chloride ($[Cl^-]_e$) = 113 mM), whereas after the transition to IS, $[Cl^-]_i$ increases to ~ 22.2 mmol/L ($[Cl^-]_e$ = 77.5 mM).

Neuronal membrane conductance is greatly increased during ischemic solution treatment

Under anoxic conditions spike arrest is mediated by an increase in GABA-sensitive Cl^- conductance (G_{Cl}), which resets V_m to E_{GABA} (Pamenter *et al.*, 2011). Since neuronal V_m and E_{GABA} also depolarized to similar levels (~ 30 mV) during IS perfusion I hypothesized that a similar increase in G_{Cl} occurs during ischemia, and that this increase underlies V_m depolarization to E_{GABA}. To test this hypothesis, I examined changes in G_w during IS perfusion. At rest, G_w was 3.9 ± 0.2 nS but increased ~ 4-fold to 14.6 ± 1.3 nS during IS perfusion (n = 31; $p < 0.001$; figure 3.2A, B, C); and G_w recovered to pre-IS control levels upon reperfusion (4.8 ± 0.5 nS; $p = 0.997$). I have previously shown that 2 mM GABA administration induces similar-magnitude changes to G_w in turtle neurons (Pamenter *et al.*, 2011); therefore, in separate experiments I treated cortical sheets with GABA during an aCSF to IS transition with recovery. In these experiments, G_w in neurons pretreated for 15 seconds with 2 mM GABA was 15.1 ± 1.7 nS in normoxic aCSF and 17.1 ± 2.4 nS in IS (n = 14; figure 3.2A). These conductance states were not significantly different from GABA-free IS-treated samples ($p = 1.000$ and 0.721, respectively).

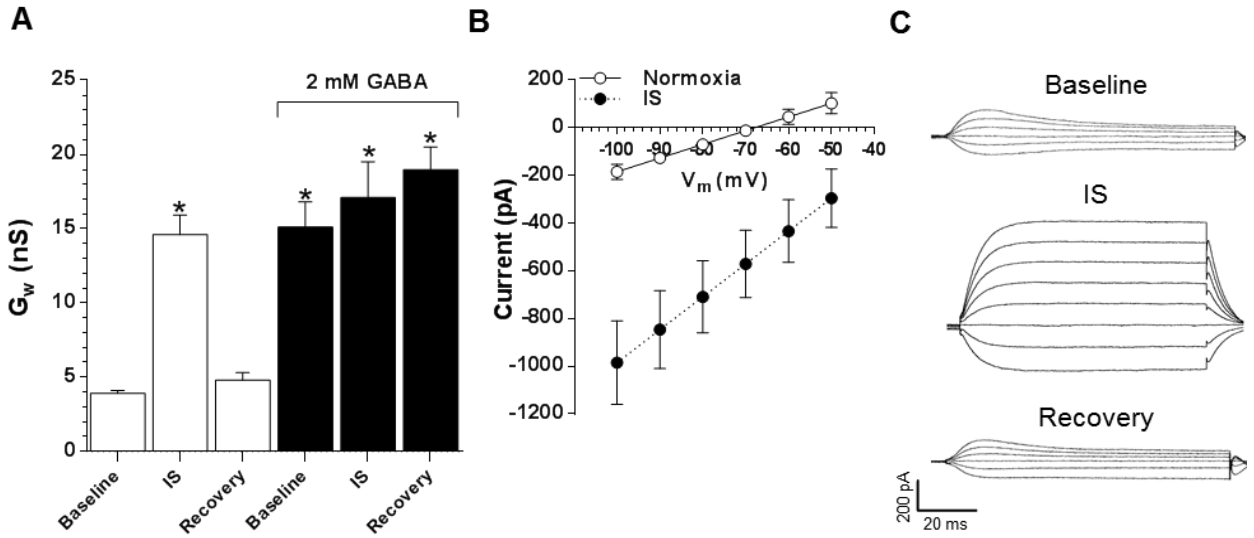

Figure 3.2. Ischemic solution (IS) and GABA increase G_w.
(A) Summary of G_w recordings from cortical pyramidal neurons treated with aCSF or IS alone (white bars) or co-treated with GABA (black bars). (B) Summary I/V curves of G_w in aCSF (solid line) and IS (dashed line) from (A). (C) Sample raw G_w voltage-clamp recordings from (A). Treatments: normoxic baseline aCSF 95% O_2 / 5% CO_2, IS 1.5% O_2, 15% CO_2, balanced N_2, 2 mM GABA. Data are mean ± S.E.M. Data are from 25-31 separate experiments for each treatment, I/V curves are averaged recordings from 10 separate neurons. Asterisks (*) indicate significant difference from normoxic controls ($P < 0.05$).

$GABA_A$ and $GABA_B$ receptors contribute to spike arrest in anoxic turtle cortex (Pamenter *et al.*, 2011); therefore, to examine a role for these receptors under ischemic conditions I next applied the GABA receptor antagonists GZ and CGP during IS perfusion. Under these conditions, pyramidal neurons exhibited electrical excitability during the transition to IS perfusion and also after normoxic reperfusion (n = 5 each; figure 3.3A*i-ii*). In all experiments, V_m was more depolarized during IS perfusion with GABA receptor antagonists than with IS alone (-15.7 ± 0.6 versus -28.4 ± 2.3 mV; n = 5 each; figure 3.3B). And after normoxic reperfusion excessive spontaneous APs were observed and V_m did not recover (figure 3.3A*ii*), whereas in neurons treated with IS alone V_m returned to baseline levels (-19.4 ± 1.5 to -82.0 ± 2.0 mV after 30 minutes normoxic aCSF reperfusion, respectively; n = 5 each; figure 3.3B). Importantly, the IS-mediated increase in G_w was prevented by GABA receptor antagonism (4.5 ± 0.8 and 6.3 ± 1.5 nS before, and during IS+GZ+CGP treatment, respectively; n = 5 each; $p = 0.330$; figure 3.3C)

High external $[K^+]$ increases GABAergic inhibitory tone

Neuronal V_m is determined primarily by the K^+ gradient (Hodgkin & Huxley, 1952). E_{GABA} is also influenced by this gradient through the activity of K^+/Cl^- cotransporters, such that increases in extracellular $[K^+]$ ($[K^+]_e$) are expected to depolarize E_{GABA} (Thompson & Gahwiler, 1989; Rivera *et al.*, 1999). Compared to aCSF, external $[Cl^-]$ is reduced from 113 to 77.5 mM in IS, which would account for an ~ 10 mV depolarizing shift in E_{GABA} (Nernst potential equation). However, during IS perfusion E_{GABA} was much more depolarized (by ~ 30 to 40 mV), indicating that the $[Cl^-]_i$ is altered by IS perfusion in addition to changes to $[Cl^-]_e$. Since K^+ is greatly increased in the mammalian ischemic penumbra and in our penumbral mimic solution, I next examined the impact of altered K^+ on neuronal electrical activity and GABAergic inhibition in normoxia and during IS treatment in turtle brain. First, I treated cortical sheets with a high-K^+ aCSF solution containing 64 m K^+ (to match the K^+ composition of IS). In these experiments, neurons rapidly depolarized ~ 75 mV and V_m was -10.3 ± 2.3 mV after 30 minutes of perfusion (n = 9; $p < 0.001$; figure 3.4A*i*, B). E_{GABA} was similarly depolarized by high-K^+ aCSF to -44.6 ± 2.2 mV (n = 5, data not shown), neurons were electrically quiet during this depolarization (Table 2), and V_m returned to baseline after 30 minutes reperfusion with normal aCSF (-81.7 ± 1.6; n = 9; $p = 0.533$). Similarly, G_w reversibly increased from a normoxic baseline value of 4.6 ± 0.7 to 12.3 ± 1.5 nS when neurons were treated with high-K^+ aCSF (n = 5, $p < 0.001$; figure 3.4C, D), a conductance state that is consistent with that of normoxic neurons during GABA application.

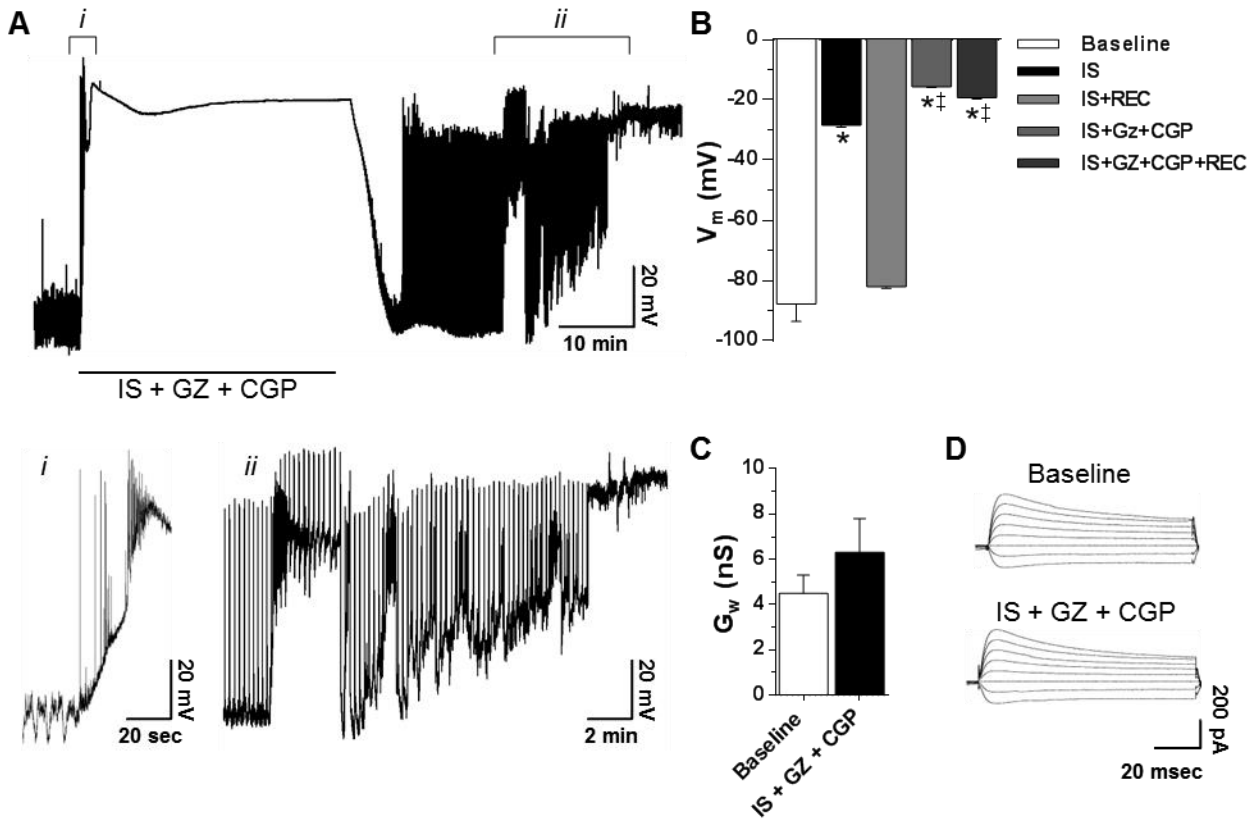

Figure 3.3. GABA receptor antagonism during IS-treatment causes electrical hyperexcitation and V_m depolarization after normoxic reperfusion.
(A) Sample V_m recording from a patch-clamped pyramidal neuron co-treated with IS plus the $GABA_A$ receptor antagonist gabazine (GZ) and the $GABA_B$ receptor antagonist CGP55645 (CGP). Insets (*i* and *ii*) are enlargements of the corresponding time period on the full trace (below). Black bar indicates duration of IS plus GZ and CGP treatment. (B) Summary of V_m changes from (A). (C) Summary of G_w changes from cells in (A). (D) Sample raw G_w voltage-clamp recordings from (C). Treatments: normoxic baseline aCSF 95% O_2 / 5% CO_2, IS 1.5% O_2, 15% CO_2, balanced N_2, 25 μM GZ, 5 μM CGP. Data are mean ± S.E.M. from five separate experiments. Asterisks (*) indicate significant difference from control treatment and double daggers (‡) indicate significant difference from IS alone ($P < 0.05$).

Table 2. Effects of extracellular [K^+] and GABA on AP_{th}

Experimental condition	AP_{th} (mV)		
	Baseline	Treatment	Recovery
High-K^+ aCSF	-48.4 ± 1.2 (9)	No APs (5)*	-46.1 ± 1.7 (9)
High-K^+ aCSF (+) GABA	No APs (5)*†	No APs (5)*	No APs (5)* †
Low-K^+ IS	-44.0 ± 2.4 (8)	6.5 ± 4.5 (5) *‡	-40.1 ± 2.9 (8)
Low-K^+ IS (+) GABA	No APs (5)*†	No APs (5)*	No APs (5)* †

High-K^+ aCSF or 2 mM GABA perfusion prevented AP firing. Data are mean ± S.E.M. Parentheses indicate n-value. Treatments: normoxic baseline aCSF 95% O_2/5% CO_2, high-K^+ aCSF (64 mM K^+) 95% O_2/5% CO_2, IS with low-K^+ (2.6 mM) 1.5% O_2/15% CO_2/balanced N_2, and GABA 2 mM. Asterisks (*) indicate significant difference from normoxic controls; daggers (†) indicate significant difference from normoxia at the same time point; and double daggers (‡) indicate significant difference from IS alone ($P < 0.05$).

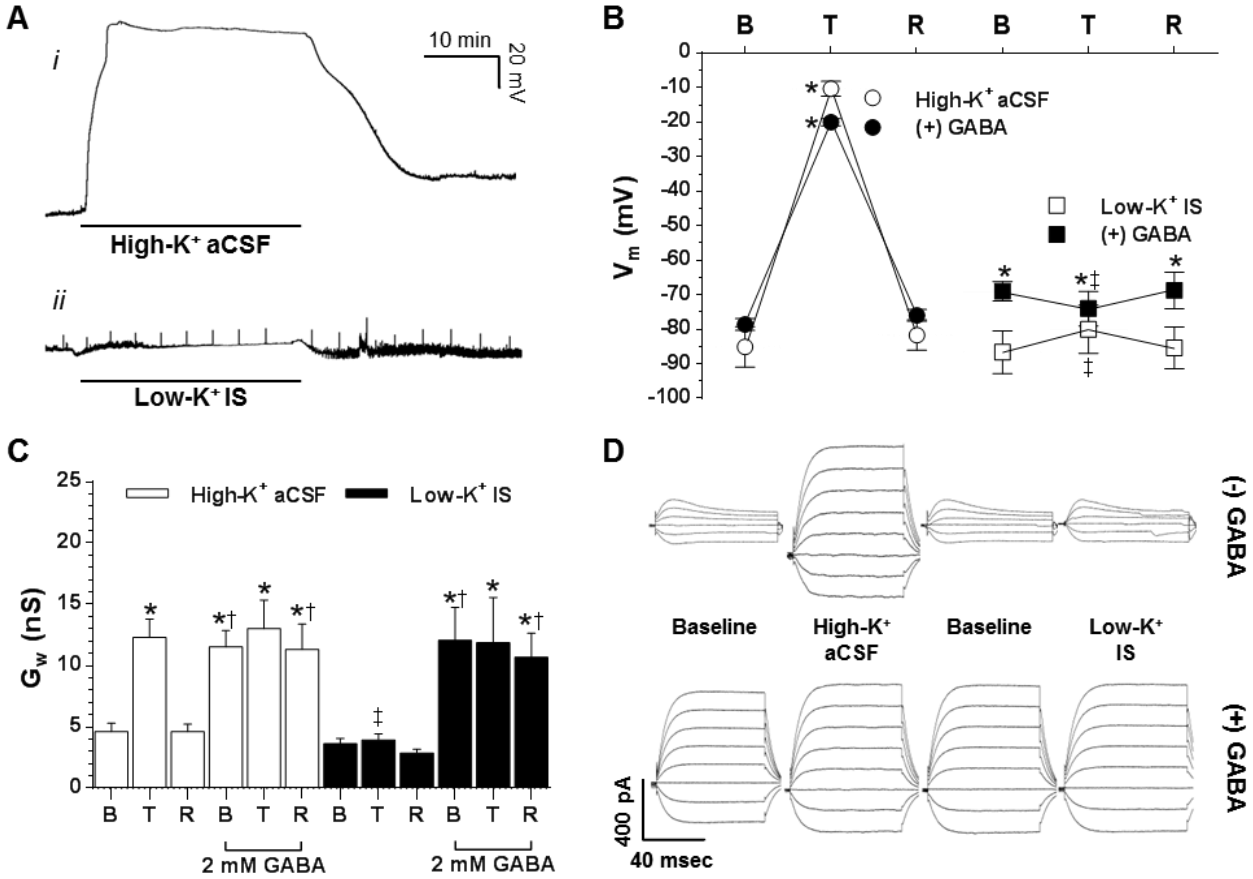

Figure 3.4. Extracellular K^+ underlies the IS-mediated V_m depolarization and increase in G_w.
(A) Sample V_m recordings from patch-clamped pyramidal neurons treated with (*i*) high-K^+ aCSF or (*ii*) low-K^+ IS, and after 30 minutes recovery. Black bars indicate duration of treatment perfusion. (B) Summary of V_m recordings from pyramidal neurons treated as indicated; Baseline (B), treatment (T), and Recovery (R). (C) Summary of G_w changes from cells in (A). (D) Sample raw G_w voltage-clamp recordings from (C). Data are mean ± S.E.M. from 5-9 separate experiments. Treatments: normoxic baseline aCSF 95% O_2/5% CO_2, high-K^+ aCSF (64 mM K^+) 95% O_2/5% CO_2, IS with low-K^+ (2.6 mM) 1.5% O_2/15% CO_2, balanced N_2, and GABA 2 mM. Asterisks (*) indicate significant difference from non-GABA treated baseline; daggers (†) indicate significant difference from non-GABA treated condition at the same time point; and double daggers (‡) indicate significant difference from high-K^+ treatment condition ($P < 0.05$).

To examine the role of GABA in high-K^+-mediated changes, I next applied 2 mM GABA during an aCSF to high-K^+ aCSF transition with recovery. In this analysis, GABA-treated neurons were slightly depolarized with regard to untreated neurons (-78.6 ± 2.5mV), and a 30 min perfusion of high-K^+ aCSF plus GABA reversibly depolarized V_m to -20.0 ± 2.3 mV (n = 5; figure 3.4B). Compared to baseline normoxic aCSF G_w was increased by GABA treatment alone, perfusion of high-K^+ aCSF plus GABA reversibly depolarized V_m to -20.0 ± 2.3 mV (n = 5; figure 3.4B). Compared to baseline normoxic aCSF G_w was increased by GABA treatment alone (13.3 ± 2.3 nS; $p < 0.001$; n = 5 for each; figure 3.4C, D) and the subsequent switch to high-K^+ aCSF with GABA had no additional effects on G_w (13.0 ± 2.3 nS; $p = 0.985$). In addition, APs could not be evoked from neurons treated with high-K^+ aCSF alone or in the presence of GABA (n = 9 and 5, respectively; Table 2). Taken together, these results indicate that inhibitory GABAergic activation (i.e., GABA release), and the depolarizing shift in E_{GABA}, occurs downstream of elevated $[K^+]_e$ accumulation. This is because GABA perfusion alone increases G_w but does not markedly depolarize neurons, whereas high-K^+ aCSF perfusion alone increases G_w to the same degree as GABA perfusion and also depolarizes neurons, while simultaneously preventing electrical excitability.

This relationship was indirectly confirmed in experiments examining the effect of a modified IS perfusate containing low $[K^+]$ (2.6 mM). In these experiments neurons treated with low-K^+ IS did not exhibit significant depolarization of V_m ($p = 0.184$) and G_w did not increase ($p = 1.000$), and APs could be evoked with stimulus injection (n = 8; figures 3.4A-D; Table 2). In addition, E_{GABA} was not depolarized relative to controls (-75.0 ± 0.6 mV; n = 5; data not shown). Conversely, application of GABA to low- K^+ IS treated neurons restored the large increase in G_w observed in control IS experiments and prevented stimulus-evoked potentials but did not restore the depolarization of V_m, indicating that E_{GABA} was not markedly depolarized by low-K^+ IS perfusion. Therefore, increased GABA release and postsynaptic G_w, along with the IS-mediated shift in E_{GABA}, are regulated by high-K^+ in the unmodified IS perfusate. This indicates that the IS-mediated change in V_m and electrical inhibition is due to increased presynaptic release of GABA, while the change in E_{GABA} is due to postsynaptic alterations of neuronal K^+ gradients with a smaller contribution from a reduced driving force on Cl^- due to lower $[Cl^-]_e$.

Turtle neurons tolerate prolonged ischemic solution treatment

To assess how long this natural anoxia-tolerant mechanism can protect against ischemic insults cortical sheets were treated with a prolonged IS regimen. It is not feasible to assay long-term cell viability using electrophysiological approaches; therefore, a variety of biochemical and molecular assays were used to examine the effects of prolonged IS perfusion (0.5 to 24 hours) on turtle cortical sheet viability. Cell death can occur through two distinct processes: necrosis or apoptosis (Edinger & Thompson, 2004). Necrotic cell death is generally characterized by rapid permeability barrier (plasma membrane) rupture in the absence of apoptotic markers (Galluzzi *et al.*, 2007); therefore, membrane viability was measured using a propidium iodide (PI) exclusion assay in live cortical sheets bathed in aCSF or IS treated at 24°C (n = 3 for each; figure 3.5A). The PI fluorescence was assessed at 0.5, 1, 2, 4, 8, 12, and 24 hours, and at each of these time points PI fluorescence was unchanged in either treatment group relative to controls treated in aCSF at 4°C. In other experiments, PI fluorescence was assessed in combination with the translocation of the apoptotic marker annexin V to the outside of neuronal plasma membranes. After 4 hours of IS treatment, there was no significant change in PI or annexin V fluorescence in either aCSF or IS perfused cortical sheets treated at 24°C relative to controls treated with aCSF at 4°C (n = 5 for each; $p = 0.729$ and $p = 0.956$; figure 3.5B, C). Similarly, after 24 hours of treatment neurons in all groups continued to exclude PI; however, the extent of annexin V fluorescence in IS-treated samples significantly increased ~ 6-fold relative to controls ($p < 0.001$), indicating the occurrence of apoptosis in IS-treated cortical sheets. In parallel experiments, cortical sheets were treated with the proapoptotic agent staurosporine in aCSF. Relative to controls staurosporine significantly increased annexin V fluorescence ~ 11- and 15-fold at 4 and 24 hours, respectively (n = 3; $p < 0.001$ respectively; figure 3.5B, C). To further examine cell viability at 24 hours, DNA fragmentation was examined using a DNA gel electrophoresis assay, since laddered oligonucleosomal DNA fragmentation is a hallmark of advanced apoptosis (Galluzzi *et al.*, 2007). In this analysis, fragmentation was not observed in aCSF- or IS-treated samples (n = 3 for each; figure 3.5D), suggesting that the induction of apoptosis in IS-treated cortical sheets at 24 hours is at a very early stage. Finally, total cellular [ATP] was assayed at 1 and 24 hours. Compared to the 4°C aCSF treated neurons, intracellular [ATP] was unchanged after 1 hour of IS treatment (n = 5; $p = 0.100$; figure 3.5E), but decreased ~ 75% in IS-treated samples at 24 hours (n = 3; $p < 0.001$; figure 3.5E). Nonetheless in cortical sheets that were treated with IS for 24 hours and then allowed

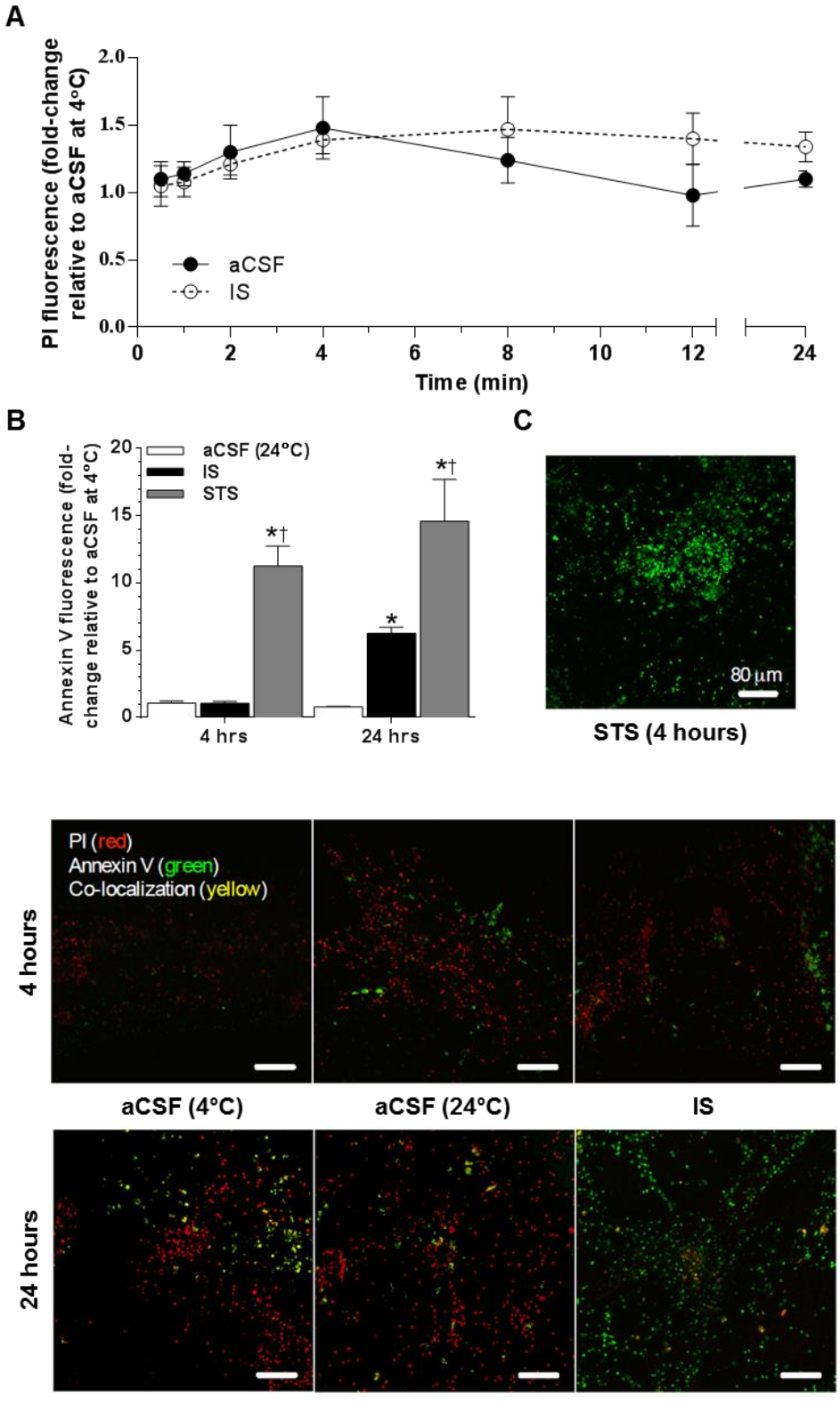
A
PI fluorescence (fold-change relative to aCSF at 4°C)
2.0
1.5
1.0
0.5
0.0
aCSF
IS
0
2
4
6
8
10
12
24
Time (min)
B
Annexin V fluorescence (fold-change relative to aCSF at 4°C)
aCSF (24°C)
IS
STS
20
15
10
5
0
*†
*
*†
4 hrs
24 hrs
C
80 µm
STS (4 hours)
PI (red)
Annexin V (green)
Co-localization (yellow)
4 hours
aCSF (4°C)
aCSF (24°C)
IS
24 hours

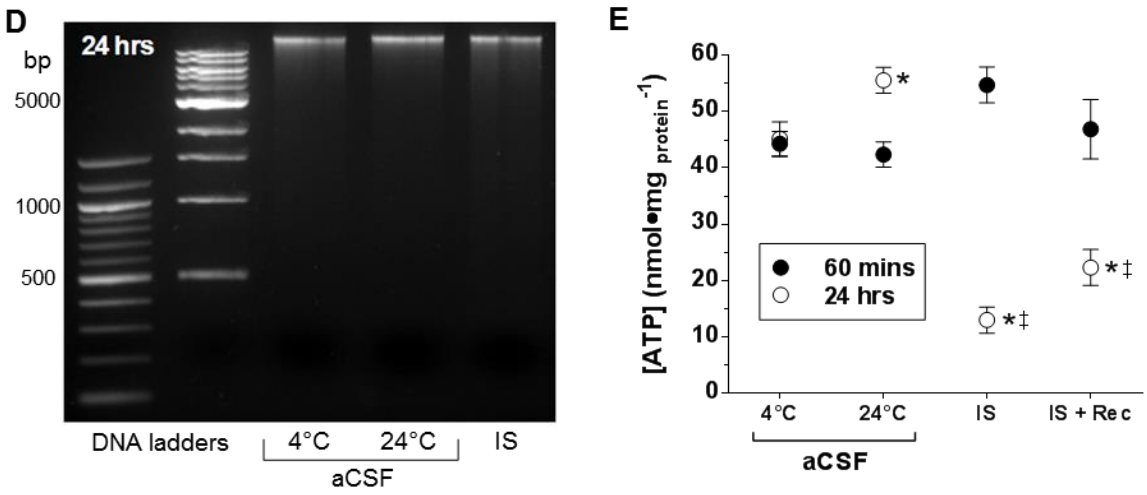

Figure 3.5. Ischemic solution (IS) perfused cortical sheets retain DNA and plasma membrane integrity, but express an early apoptotic marker at 24 hours.
(A) Summary of fold-change of propidium iodide (PI) fluorescence imaged from live cortical sheets treated at 24°C relative to PI fluorescence in control samples treated simultaneously with aCSF at 4°C. (B) Summary of fold-change of apoptotic annexin V fluorescence. (C) Overlain sample images from (B) of PI (red) and annexin V (green) fluorescence in cortical sheets treated as indicated. (D) Gel image of oligonucleosomal DNA fragment separation via electrophoresis on a 1.5% conventional agarose gel. (E) Summary of [ATP] from cortical sheets treated as indicated. Data are mean ± S.E.M. from 3 to 5 separate experiments for each treatment. Treatments: normoxic aCSF 95% O_2/5% CO_2, IS 1.5% O_2/15% CO_2, balanced N_2, and 5 mmol/L staurosporine (STS), control in aCSF at 4°C, and 24 hours IS plus 1-hour recovery. Asterisks (*) indicate significant difference from control treatment; daggers (†) indicate significant difference from IS; and double daggers (‡) indicate significant difference from similar treatment at the same time point ($P < 0.05$).

to recover in normoxic aCSF for 1 hour, [ATP] began to recover, suggesting that samples treated with this paradigm remain viable and recover from prolonged IS exposure.

3.4 Discussion

In addition to being anoxia-tolerant, this study shows that painted turtle cortical neurons are tolerant to an ischemic penumbral mimic solution. This conclusion is supported by observations that turtle pyramidal neurons: 1) depolarize but are electrically quiescent during 1 hour of IS perfusion and recover fully after normoxic reperfusion; 2) defend [ATP] in this time period, and [ATP] recovers from an ischemic low after 24 hours treatment; and 3) maintain plasma membrane and DNA integrity through 24 hours of IS treatment. Although healthy turtles do not experience ischemia naturally this tolerance is nonetheless remarkable and the mechanisms that promote survival may be used to protect tissue in ischemia-sensitive mammals. Here, I report that the electrical response of IS-treated pyramidal neurons is similar to that of anoxia-treated neurons with IS causing a: depolarization of V_m to E_{GABA}; > 3-fold increase in G_w and an inhibition of electrical activity despite extreme depolarization.

The mechanism underlying these postsynaptic changes is likely mediated by GABA receptor activation since: 1) GABA addition during normoxic aCSF perfusion increases neuronal G_w to the same degree as IS and APs cannot be elicited; while 2) co-treatment of IS and GABA does not result in further elevations of G_w; and 3) antagonism of $GABA_{A+B}$ receptors during IS prevents the IS-mediated increase in G_w, and neurons become hyperexcited and V_m runs down within minutes of reperfusion. Therefore, since IS and GABA have similar but not additive effects on G_w and neuronal excitability, and GABAergic inhibition during IS treatment prevents the increase in G_w and induces excitotoxicity characteristic of ischemic mammalian neurons, I conclude that enhanced GABAergic inhibition prevents electrical excitability and at a minimum, underlies early-stage IS tolerance in this model.

GABAergic inhibition and the large depolarizing shift in E_{GABA} are mediated by the high $[K^+]$ of the IS. In mammals a high $[K^+]$ perfusate induces extensive neuronal excitation by shifting the K^+ gradient such that neurons depolarize and become more electrically active within 4 to 5 minutes of perfusion (Zhou *et al.*, 2010). In mammalian slice models excitation leads to depolarization of both presynaptic and postsynaptic neurons, which increases neurotransmitter release,

excitotoxicity and spreading depression (Gardner-Medwin, 1981). Conversely, in turtle brain high-K^+ aCSF causes extensive postsynaptic depolarization, but electrical activity is suppressed and V_m recovers after reperfusion with normal aCSF. GABA-mediated increases in postsynaptic G_w are activated by high-K^+ and this does not occur in neurons treated with low-K^+ IS, indicating that presynaptic GABA release is greatly increased by high-K^+. The observation that turtle neurons are electrically silent in high-K^+ experiments despite significant depolarization is notable as this indicates that inhibitory tone in turtle brain outweighs excitatory tone, as in these experiments the high [K^+] will likely have activated excitatory glutamatergic signaling in addition to inhibitory GABAergic signaling. This may represent a significant adaptive advantage in turtle brain relative to mammal brain. This is supported by the observation that turtle neurons treated with low-K^+ IS do not exhibit increases in G_w because it indicates that GABA transmission is only enhanced under high K^+ conditions. In addition, the lack of electrical hyperexcitability in neurons treated with low-K^+ IS indicates that the remaining deleterious alterations in this solution are not overly damaging to turtle neurons, or are protected against by alternative mechanisms since the inhibitory GABAergic shunt that underlies spike arrest does not appear to be active under these conditions.

In addition to regulating GABA release during IS perfusion, high-K^+ is also responsible for the depolarizing shift in E_{GABA} observed in IS-treated neurons. A rationale for this is: E_{GABA} is primarily determined by the Cl^- gradient, which is in turn determined by the activity of K^+/Cl^- cotransporters (Rivera *et al.*, 1999); therefore, increasing $[K^+]_e$ decreases the driving force on Cl^- and depolarizes E_{GABA}. This relationship is supported by our observations that high-K^+ alone in aCSF was sufficient to depolarize E_{GABA} during normoxia and shift V_m toward this depolarized potential, and that low-K^+ IS did not induce a shift in V_m or E_{GABA}, even when postsynaptic $GABA_A$ receptors were chronically activated in the presence of 2 mM GABA. Conversely, in anoxic turtle cortex GABA release is drastically increased but E_{GABA} is not depolarized and $[K^+]_e$ does not change significantly during prolonged anoxia, suggesting that alternative mechanisms are used to activate endogenous inhibitory GABAergic neuroprotective mechanisms in anoxic turtle brain (Jackson & Heisler, 1983; Nilsson & Lutz, 1991; Pamenter *et al.*, 2011).

Traditionally researchers have used oxygen-glucose deprivation or chemical ischemia to mimic stroke *in vitro*. Although these paradigms accurately model the metabolic consequence of impaired cerebral blood flow, they do not incorporate other deleterious aspects of the ischemic milieu (Yao *et al.*, 2007; Lo, 2008). The ischemic paradigm used in our experiments similarly mimics the

metabolic consequences of reduced cerebral blood flow (low glucose, hypoxia), but also incorporates severe ionic derangements, acidification (~ pH 6.4), and excitatory neurotransmitter accumulation (glutamate) characteristic of ischemic mammalian penumbral tissue (Hansen & Nedergaard, 1988; Siesjö, 1992; Yao *et al.*, 2007). Indeed, many of these alterations alone are sufficient to induce depolarization or death in mammalian neurons. For example, the increase in external $[K^+]$ from 2.6 (in aCSF) to 64 mM (in IS) is sufficient to induce spreading depression in cortex (Zhou *et al.*, 2010), whereas holding external pH at 6.4 for 6 hours causes 50% neuronal and glial cell mortality in forebrain (Nedergaard & Hansen, 1993). Therefore when combined, these alterations present a highly challenging stress, and the ability of turtle cortex to withstand IS treatment for up to 24 hours with minimal apparent damage is remarkable.

Unlike turtle neurons, mammalian cells are intolerant to IS treatment. In hippocampal slice models and in cell cultures, mammalian neurons become electrically excited and rapidly depolarize within minutes of IS onset at 24°C or 37°C, and V_m does not recover after normoxic reperfusion (Yao and Haddad, unpublished observations). Furthermore, after a 24- hour IS treatment ~ 90% of neurons take up PI and > 90% of cellular lactate dehydrogenase is released (Yao *et al.*, 2007), while [ATP] is depleted > 85%, and DNA exhibits extensive oligonucleosomal fragmentation and TUNEL (terminal deoxynucleotidyl transferase- mediated 20-deoxyuridine 50-triphosphatebiotin nick end labeling)-positive staining characteristic of late-stage apoptosis (Galluzzi *et al.*, 2007; Pamenter *et al.*, 2012a; Pamenter *et al.*, 2012b; Pamenter *et al.*, 2012c). Similar results have been reported in a wide variety of *in vivo* and *in vitro* models of the ischemic mammalian penumbra where general ischemic stress induces: electrical hyperexcitation and extreme V_m depolarization within minutes; ionic and neurotransmitter derangements, [ATP] depletion, and necrotic cell rupture or extensive activation of apoptotic mechanisms within < 1 to 4 hours; and extensive or total neuronal cell death within 6 to 24 hours (Hansen & Nedergaard, 1988; Siesjö, 1992; Nedergaard & Hansen, 1993; Broughton *et al.*, 2009).

Comparatively, patch-clamped turtle cortical neurons tolerate at least 60 minutes of IS treatment (i.e., at least 20 to 30 × longer than mammalian neurons) and V_m and synaptic function recovers after reperfusion. Necrosis does not occur through 24 hours of IS treatment as indicated by the maintenance of vital dye exclusion, and DNA does not exhibit fragmentation typical of either necrosis or apoptotic cell degradation at 24 hours (Galluzzi *et al.*, 2007). However, a significant increase in the translocation of annexin V, an early indicator of apoptosis (Galluzzi *et al.*, 2007),

occurred after 24 hours but not 4 hours of IS treatment. This result suggests that cortical sheets are likely reaching the limit of their tolerance and are beginning to undergo programmed cell death. Nonetheless, the recovery of ATP levels after 1-hour of reperfusion following 24 hours of IS treatment suggests that the tissue remains viable and recovers even after prolonged stress. There is evidence that cells damaged by ischemic stress are replaced via neuronal regeneration in this model (Kesaraju & Milton, 2009) and it is tempting to speculate that *in vivo*, damaged cells marked for apoptosis would be replaced. This would enable turtles to tolerate prolonged brain ischemia and recover without long-term detriment, even if some cells are damaged by the initial stress. If this were the case, then the observed annexin V staining at 24 hours may actually be adaptive in turtle brain and indicative of maintenance- related local apoptosis to mark damaged cells for removal, instead of an indication of the onset of widespread apoptosis.

In the present study, temperature differences may contribute to the enhanced ischemia tolerance of turtle brain relative to previously published studies in mammal brain. Experiments with mammal brain are typically conducted between 24-37°C, and hypothermia slows metabolism and extends ischemic or hypoxic survival time (Lampe & Becker, 2011). Conversely, turtles survive months of anoxia at 4°C, and typically tolerate 2 to 3 days of anoxia at room temperature, and hours at 37°C (Bickler & Buck, 2007). Nonetheless, turtles have consistently displayed a remarkable degree of anoxia and ischemia tolerance relative to mammals across a wide range of experimental temperatures (Belkin, 1968; Doll *et al.*, 1991; Bickler, 1992; Bickler & Buck, 2007) and our present results provide further support for this relationship. For example, at temperatures of 22°C to 24°C turtle brain sheets tolerate > 3 hours of anoxic perfusion and > 1 hour of ischemic perfusion, whereas neurons in rat brain slices rapidly depolarize in < 5 minutes of anoxia or ischemia (Doll *et al.*, 1991; Lipton, 1999; present study). Similarly at the whole-organism level, turtles tolerate > 1 hour of ischemia after cardiac excision, while mammals die within minutes of blood flow cessation (Belkin, 1968; Bickler & Buck, 2007).

In summary, this study has shown that turtle cortical neurons tolerate a highly deleterious ischemic stress for up to 24 hours. Electrophysiological studies indicate that one key mechanism underlying this tolerance is a large-scale activation of inhibitory GABAergic G_{Cl}, which clamps V_m at E_{GABA} and prevents excitatory events and cell death during IS onset. A similar mechanism underlies spike arrest in the anoxic turtle cortex but the degree to which inhibitory GABAergic mechanisms are activated in IS-treated neurons is several-fold greater than that observed previously in anoxic

experiments (Pamenter *et al.*, 2011), likely because GABAergic inhibition here is activated by greatly increased extracellular K^+, whereas in the anoxic cortex GABA release is activated by an unknown mechanism that is likely K^+ independent. Nonetheless, these results illustrate that naturally evolved adaptations to survival in anoxic environments can also protect against clinically relevant paradigms of ischemic stress. This study highlights the value of a comparative model in which to elucidate medically relevant protective mechanisms against anoxic and ischemic insults in brain.

4 Oxygen-sensitive reduction in Ca^{2+}-activated K^+ channel open probability in turtle cerebrocortex

Preface

A modified version of this chapter was published as Rodgers-Garlick CI, Hogg DW and Buck LT (2013). Oxygen-sensitive reduction in Ca^{2+}-activated K^+ channel open probability in turtle cerebrocortex. *Neuroscience*. 237: 243–254.

The idea to investigate the effect of anoxia on Ca^{2+}-activated K^+ channels was conceived jointly by D. Hogg and C. Rodgers-Garlick. Characterization of the channel (Fig. 4.1), and anoxic experiments (Fig 4.3 and Fig. 4.4) were performed equally by D. Hogg and C. Rodgers-Garlick. C. Rodgers-Garlick performed the experiments assessing the Ca^{2+}-sensitivity of the K_{Ca} (Fig. 4.2). D. Hogg performed the experiments assessing PKC modulation of the K_{Ca} (Fig. 4.5).

Abstract

In response to low ambient oxygen levels the painted turtle brain undergoes a large depression in metabolic rate which includes a decrease in neuronal AP_f. This involves channel arrest of NMDA and AMPA receptor currents and an increase in GABA receptor currents. In a search for other oxygen-sensitive channels a Ca^{2+}-activated K^+ channel (K_{Ca}) was discovered that exhibited a decrease in open time in response to anoxia. Single-channel recordings of K_{Ca} activity were obtained in cell-attached and excised inside-out patch configurations from neurons in cortical brain sheets bathed in either normoxic or anoxic artificial aCSF. The channel has a slope conductance of 223 pS, is activated by membrane depolarization, and is controlled in a reversible manner by free [Ca^{2+}] at the intracellular membrane surface. In the excised patch configuration anoxia had no effect on K_{Ca} channel open probability (P_{open}); however, in cell-attached mode, there was a reversible 5-fold reduction in P_{open} (from 0.5 ± 0.05 to 0.1 ± 0.03) in response to a 30 min anoxic treatment. The inclusion of the potent PKC inhibitor chelerythrine prevented the anoxia-mediated decrease in P_{open} while application of a phorbol ester PKC activator decreased P_{open} during normoxia (from normoxic 0.4 ± 0.05 to phorbol-12-myristate-13-acetate (PMA) 0.1 ± 0.02). Anoxia results in depolarization of pyramidal neuron V_m to E_{GABA} (~ 8 mV) and an increase in $[Ca^{2+}]_i$; therefore, K_{Ca} arrest is likely important to prevent Ca^{2+} activation during anoxia and to reduce the cost of maintaining ion gradients. We conclude that turtle pyramidal cell Ca^{2+}-activated

K^+ channels are oxygen-sensitive channels regulated by cytosolic factors and are likely the reptilian analog of the mammalian large conductance K_{Ca} channel (BK channels).

4.1 Introduction

Initiation of channel arrest and spike arrest must include oxygen sensors; cells must first sense a change in oxygen tension and then trigger mechanisms to reduce ATP demand. Opening of mitochondrial ATP-sensitive K^+ channels (mK_{ATP}) have been linked to a reduction in both NMDA and AMPA receptor activity in the turtle cortex and may be central to an oxygen-sensing mechanism (Pamenter *et al.*, 2008c; Zivkovic & Buck, 2010). An oxygen-sensing mechanism may consist of a decrease in mitochondrial [ATP] due to the lack of oxidative phosphorylation which activates mK_{ATP}, leading to mitochondrial K^+ influx, mitochondrial membrane potential (Ψ_m) depolarization, Ca^{2+} efflux to the cytosol through the MPTP, protein kinase/phosphatase activation, and ion channel modulation (Shin *et al.*, 2005; Pamenter *et al.*, 2008c; Hawrysh & Buck, 2013). Mitigating a neurotoxic NMDA receptor-mediated increase in $[Ca^{2+}]_i$ is key to preventing ECD in the mammalian central nervous system. The less dramatic increase in $[Ca^{2+}]_i$ associated with mK_{ATP} opening in turtle pyramidal neurons appears to be part of the natural signaling mechanism leading to the anoxic reduction in NMDA receptor activity (Pamenter *et al.*, 2008c; Hawrysh & Buck, 2013).

Elucidation of the oxygen-sensitive signaling molecules and ion channels involved in channel arrest and spike arrest is essential for understanding how turtle brain avoids hyperexcitability and ECD under anoxic conditions. While understanding the mechanisms responsible for the anoxic modulation of glutamatergic and GABAergic transmission is of paramount importance due to the critical role of these neurotransmitter systems in anoxia-tolerance, it is also necessary to identify other oxygen-sensitive ion channels and unravel their contributions to anoxia-tolerance in turtle brain. To this end, we used patch-clamp techniques to record oxygen-sensitive spontaneous single-channel currents in turtle cortical neurons. Single-channel currents were identified in cell-attached and excised inside-out patches using a combination of channel blockers and ion substitution in the recording electrode. We identified a large conductance calcium-activated potassium channel (K_{Ca}) similar to Big potassium or maxi K_{Ca} in mammals (reviewed in Gribkoff *et al.*, 2001; Magleby, 2003), and I directly measured changes in channel open probability in response to anoxia and protein kinase and phosphatase modulators.

4.2 Materials and Methods

4.2.1 Experimental design

The electrophysiological experimental protocols used in this chapter are similar to those in Chapter 2 except where indicated. Only new materials and methods specific to this chapter are included in this section.

4.2.2 Electrophysiology

4.2.2.1 Single-channel patch-clamp recordings

Single-channel recordings were obtained from cell-attached or excised patches using fire-polished 8-10 MΩ borosilicate glass pipettes. Following GΩ seal formation, patches were allowed to stabilize for 5 min before the potential of the membrane patch was clamped to the desired level by polarizing the electrode with respect to ground and single-channel currents of the patch were recorded. Excised inside-out membrane patches were obtained by reversing the recording electrode away from the cortical sheet using the stepper-motor. The tip of the electrode was positioned above the cortical sheet but remained immersed in the bath. All data were collected at 20 kHz, low-pass-filtered at 1 kHz.

4.2.2.2 Single channel K_{Ca} current/voltage relationships

For cell-attached single-channel recordings, electrodes were filled with turtle aCSF and cortical sheets were also bathed in turtle aCSF. Action potentials were suppressed with a 5 min application of the voltage-gated Na^+ channel blocker TTX, which was repeated every 20 min. In the voltage-clamp configuration the initial holding potential was set to -80 mV. Assuming a cellular resting V_m of approximately -80 mV, this resulted in a patch transmembrane potential of 0 mV. The following formula was used to calculate the transmembrane potential of the patch; voltage at intracellular surface of a cell-attached patch) from the electrode holding potential (HP) and a cellular resting V_m of -80 mV:

$$\text{Transmembrane potential} = (-80\ \text{mV}) - (\text{HP})$$

To test for spontaneous single-channel activity, voltage was stepped from -120 mV to +40 mV in 20 mV steps in the cell-attached configuration. The patch was held at each potential for 60 s.

Single-channel currents were observed and could be characterized as outward rectifying. Depolarization of the patch was required to activate the channel and channel open probability (P_{open}) was calculated from amplitude histograms generated from 60 s recordings of single channel activity at transmembrane potentials of -60 mV to +40 mV. To rule out confounding NMDA receptor activity, 3 mM $MgCl_2$ was added to the turtle aCSF electrode solution (4 mM total Mg^{2+}) as well as 30 μM APV. To eliminate AMPA receptor and non-specific K^+ channel activity, 30 μM CNQX, 5 mM CsCl, and 10 mM tetraethylammonium chloride (TEA; voltage-gated K^+ channel antagonist) were added to the electrode solution. To eliminate Ca^{2+}-activated K^+ channel (K_{Ca}) activity, 150 nM iberiotoxin (IbTX; specific K_{Ca} antagonist) was added to the aCSF electrode solution. Cell-attached patches obtained with the above electrode solutions were interspersed among those obtained with a control aCSF electrode solution that did not contain any channel antagonists. Based on the effects of TEA and IbTX, outward rectification, and current responses at depolarized transmembrane potentials, we hypothesized that the channel of interest was a Ca^{2+}-activated K^+ channel.

A full I/V relationship could not be obtained in cell-attached mode because of the outward rectification of the channel. To generate a full I/V relationship, both sides of the excised inside-out membrane patch were bathed with an aCSF solution containing high [K^+] (mM: 100 KCl; 11 NaCl; 1 $MgCl_2$; 2 NaH_2PO_4 ($2H_20$); 26.5 $NaHCO_3$; 10 glucose; 5 imidazole; pH 7.4). The solution was identical on either side of the membrane patch, except with respect to [Ca^{2+}]. It was previously shown that 0.5 μM free [Ca^{2+}] at the inner surface of an excised membrane patch is sufficient to activate K_{Ca} (Pallotta et al. 1981). Thus, 8 μM $CaCl_2$ and 40 μM EGTA were added to the electrode solution (extracellular side of patch) to yield a free [Ca^{2+}] of 10 nM, and 20 μM $CaCl_2$ and 14 μM EGTA were added to the intracellular solution (intracellular side of excised patch) to yield a free [Ca^{2+}] of 5 μM (free [Ca^{2+}] calculations were also based on [Mg^{2+}] using the EGTA/free Ca^{2+} calculator from http://randombio.com/egta.html). Stepping the voltage applied to excised patch-clamped neurons in the manner described above yielded full I/V curves where the current was 0 pA at a holding potential of 0 mV. Because there is no cellular resting V_m for excised patches, the transmembrane potential is simply the holding potential multiplied by -1. When the above 100 mM KCl electrode solution was used, cell-attached I/V relationships were inverted compared to those obtained with 2.6 mM KCl in the electrode; inward currents were observed when the patch was hyperpolarized.

4.2.2.3 Ca^{2+}-dependent activation of K_{Ca}

Using excised inside-out membrane patches, relationships between channel P_{open} and $[Ca^{2+}]_i$ were obtained by manipulating bath $[Ca^{2+}]$ at a fixed transmembrane potential of 40 mV. Electrodes were filled with the same high $[K^+]$ aCSF solution described above with 10 nM free $[Ca^{2+}]$. Upon excision of the membrane patch the intracellular side of the membrane was exposed to a high $[K^+]_i$ solution that was similar to the electrode solution, except that it contained zero Ca^{2+}. This was achieved by adding 50 μM EGTA to the intracellular solution. In the absence of Ca^{2+} no channel activity was observed. The tip of a perfusion apparatus was placed in close proximity to the patch electrode and patches were then perfused with high $[K^+]$ intracellular solutions that contained different $[Ca^{2+}]$'s and [EGTA]'s depending on the desired free $[Ca^{2+}]$. For example, 60 μM $CaCl_2$ and 10 μM EGTA yielded 50 μM free Ca^{2+}. To demonstrate the reversibility of K_{Ca} activation, excised patches were exposed to 50 μM Ca^{2+} for 1-2 min, followed by washout with zero Ca^{2+} bath solution. This process was repeated a second time using the same excised patch. For all of the experiments described above bath aCSF was continuously gassed with 95% O_2/5% CO_2.

4.2.2.4 Normoxic to anoxic transitions and protein kinase C and phosphatase modulation

The effect of anoxia on K_{Ca} P_{open} was examined using cell-attached and excised inside-out patch-clamp techniques. For cell-attached patch experiments, turtle aCSF was used as both the electrode and bath solutions. For excised inside-out patch experiments, the electrode and intracellular solutions contained symmetrical K^+ (100 mM) and electrodes contained 10 nM Ca^{2+}. Prior to patch excision, the cortical sheet was bathed with the 100 mM K^+ solution containing 0 Ca^{2+}. Once the patch was excised, 5 μM free Ca^{2+} was perfused near the electrode tip either for the duration of the experiment or just prior to recordings of single-channel activity and subsequently washed out with the 0 Ca^{2+} solution. During each experiment patches were initially perfused with normoxic aCSF for 10-15 min, followed by a 30 min anoxic perfusion, and then a 30 min normoxic reperfusion. At the end of each perfusion period, a 10 sec recording of single-channel activity was obtained and used for P_{open} comparisons. Cell-attached patches were voltage-clamped at -100 mV (20 mV transmembrane potential) just prior to and for the duration of the 10-s recordings.

To determine if phosphorylation of K_{Ca} channels plays a role in decreasing P_{open} during anoxia turtle brain sheets were pre-incubated for 20 min with the protein kinase C (PKC) inhibitor –

chelerythrine (10 μM; also drip applied throughout the experiment at 0.5 μM to maintain PKC inhibition). Brain sheets were then placed in the recording chamber and P_{open} determined during normoxic and anoxic exposure as described above. The PKC activator phorbol-12-myristate-13-acetate (PMA, 10 μM) was drip applied to brain sheets during normoxic perfusion and P_{open} determined as above. To investigate steady-state normoxic regulation of K_{Ca} P_{open} brain sheets where pre-incubated in the phosphatase 1 and 2A inhibitor – okadaic acid (6 μM) and the Ca^{2+}/ calmodulin inhibitor - calmidazolium (10 μM). Stock solutions of all drugs were prepared in DMSO.

4.2.3 Statistical analysis

Amplitude and P_{open} histograms were generated using Clampex 10.2 software (Molecular Devices) and all other graphs were plotted using SigmaPlot 11.0 (Systat Software, Inc., San Jose, CA). Two-way repeated measures (RM)-ANOVAs were employed using SigmaStat 3.0 statistical analysis software to determine significant differences among multiple groups followed by a *post hoc* Tukey's test to determine differences among two specific groups within the data set. A 95% confidence interval was used to determine significance.

4.3 Results

Identification of a K_{Ca} channel in turtle cortical neurons

Using a cell-attached patch-clamp configuration with aCSF in the bath and pipette we observed spontaneous single-channel activity (figure 4.1; n = 20). Single-channel currents can be described as large and unitary; depolarizing the patch increased the frequency and duration of channel opening, all characteristics of large-conductance K_{Ca} currents. Single-channel activity was not blocked by the addition of NMDA receptor antagonists (4 mM $MgCl_2$, 25 μM APV) or AMPA receptor antagonists (25 μM CNQX) to the pipette solution (n = 10 each; figure 4.1B*i-ii*). Addition of the general K^+ channel antagonist/specific inward-rectifying K^+ channel antagonist CsCl (5 mM) to the pipette solution did not block channel currents (n = 10; figure 4.1B*iii*). When TEA (10 mM) was added to the pipette solution, single-channel activity was completely absent in 100% of patches (n = 10; figure 4.1B*iv*). Addition of the high specificity BK channel antagonist IbTX (150 nM; Candia et al., 1992) to the pipette solution also completely blocked channel activity in 100% of patches (n = 10; figure 4.1B*v*).

Turtle pyramidal neurons have a resting V_m of ~ -80 mV as determined from whole-cell perforated patch recordings (Pamenter *et al.*, 2011; Pamenter *et al.*, 2012b). The channel was inactive at the cell resting V_m of -80 mV, and single-channel currents were observed only when the patch was depolarized relative to the V_m of the cell (n = 20; figure 4.1A, C, D). Depolarization activated the channel in 100% of membrane patches on intact cells and the frequency of channel opening was holding potential dependent (figures 4.1A, C). As the extracellular side of the membrane was made more negative, depolarization of the patch relative to the V_m of the cell resulted in increased open probability (P_{open}) of the channel, larger currents, and increased single-channel slope conductance with each 20 mV voltage step (figure 4.1A, C). The channel was not active at V_m negative to -46 ± 3.2 mV and only outward currents were observed at V_m positive to -46 ± 3.2 mV (figure 4.1C).

Excised inside-out membrane patches were used to obtain a I/V relationship (n = 10; figure 4.1D). The pipette solution and the *intracellular* solution bathing the intracellular side of the patch both contained 100 mM KCl, but free [Ca^{2+}] in the pipette solution was 10 nM and 5 μM in the *intracellular solution*. Full I/V curves were obtained where the reversal potential was 0 mV and the slope conductance was 223 pS, similar to that established for mammal K_{Ca} (figure 4.1D) (Marty, 1981; Pallotta *et al.*, 1981; Tabares *et al.*, 1985; Egan *et al.*, 1993). A sigmoidal curve was fitted to the I/V data, which is appropriate for K_{Ca} channels (figure 4.1D) (Egan *et al.*, 1993). With 5 μM free $[Ca^{2+}]_i$, channels were active in 100% (10/10) of excised membrane patches. In cell-attached patch configuration, increasing electrode [K^+] from 2.6 mM to 100 mM resulted in only inward currents at hyperpolarized patch potentials, indicating that K^+ carried the channel current (n = 10; figure 4.1D). The above features, i.e. silencing effect of IbTX, outward rectification of the channel, increased P_{open} with depolarization, and the slope conductance obtained from excised membrane patches indicated that these are large-conductance K_{Ca} channel currents.

Ca^{2+}-dependent K_{Ca} activation

The P_{open} of the K_{Ca} channel was dependent on both V_m (figure 4.1A, C) and $[Ca^{2+}]_i$ (figure 4.2). Using excised inside-out membrane patches, a Ca^{2+}-activation curve was obtained by exposing the inner membrane surface to a range of [Ca^{2+}]'s (in μM): 0.01, 0.1, 0.5, 1, 5, 10, 50 (n = 5 - 7; figure 4.2C). P_{open} was calculated from amplitude histograms generated from 10 s recordings of single-channel activity at a fixed transmembrane potential of 40 mV. The data were fit with a Hill dose-response curve (figure 4.2C). The K_{Ca} channel was reversibly activated by Ca^{2+} (n = 8; figure 4.2).

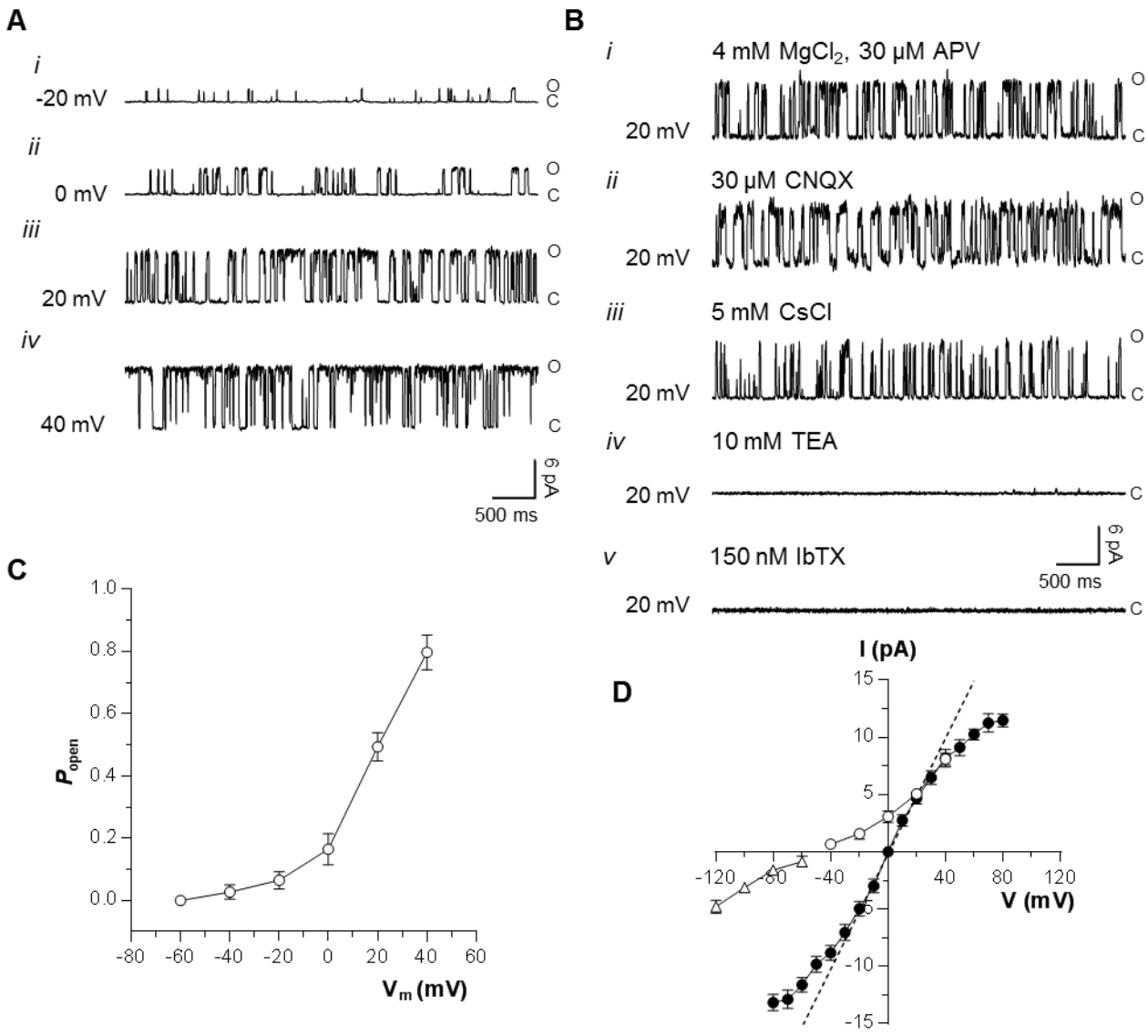

Figure 4.1. Characterization of single-channel K_{Ca} currents in turtle cortical neurons.
(A) Sample recording of single-channel outward currents from cell-attached patches of cortical neurons. Note: The exterior surface of the membrane patch was voltage-clamped to (*i*) 60 mV, (*ii*) 80 mV, (*iii*) 100 mV, and (*iv*) 120 mV. Assuming a cellular V_m of ~ -80 mV, the transmembrane potential of the patch at each holding potential was (*i*) 20 mV, (*ii*) 0 mV, (*iii*) 20 mV, and (*iv*) 40 mV. (B) Sample recordings of cell-attached patches with indicated ion channel/receptor antagonists in the pipette solution. Antagonists: NMDA receptor ($MgCl_2$, APV), AMPA receptor (CNQX), non-specific K^+ channel (CsCl or TEA), specific K_{Ca} channel (IbTX). (C) Voltage dependence of K_{Ca} channels comparing P_{open} versus patch transmembrane potential. (D) Single-channel current amplitude (pA) as a function of patch transmembrane potential (mV). Open circles indicate data from cell-attached patches; solid circles indicate data from excised membrane patches ([KCl] (100 mM) in bath and pipette, $[Ca^{2+}]_e$ was 10 nM, and $[Ca^{2+}]_i$ was 5 µM; open triangles: indicate cell-attached patches with 100 mM [KCl] and 10 nM $[Ca^{2+}]$. For experiments A-C, bath and pipette solutions contained aCSF. For summary graphs C and D, data are mean ± S.E.M., cell-attached patch data are from 20 separate experiments each, and excised patch data are from 10 separate experiments each.

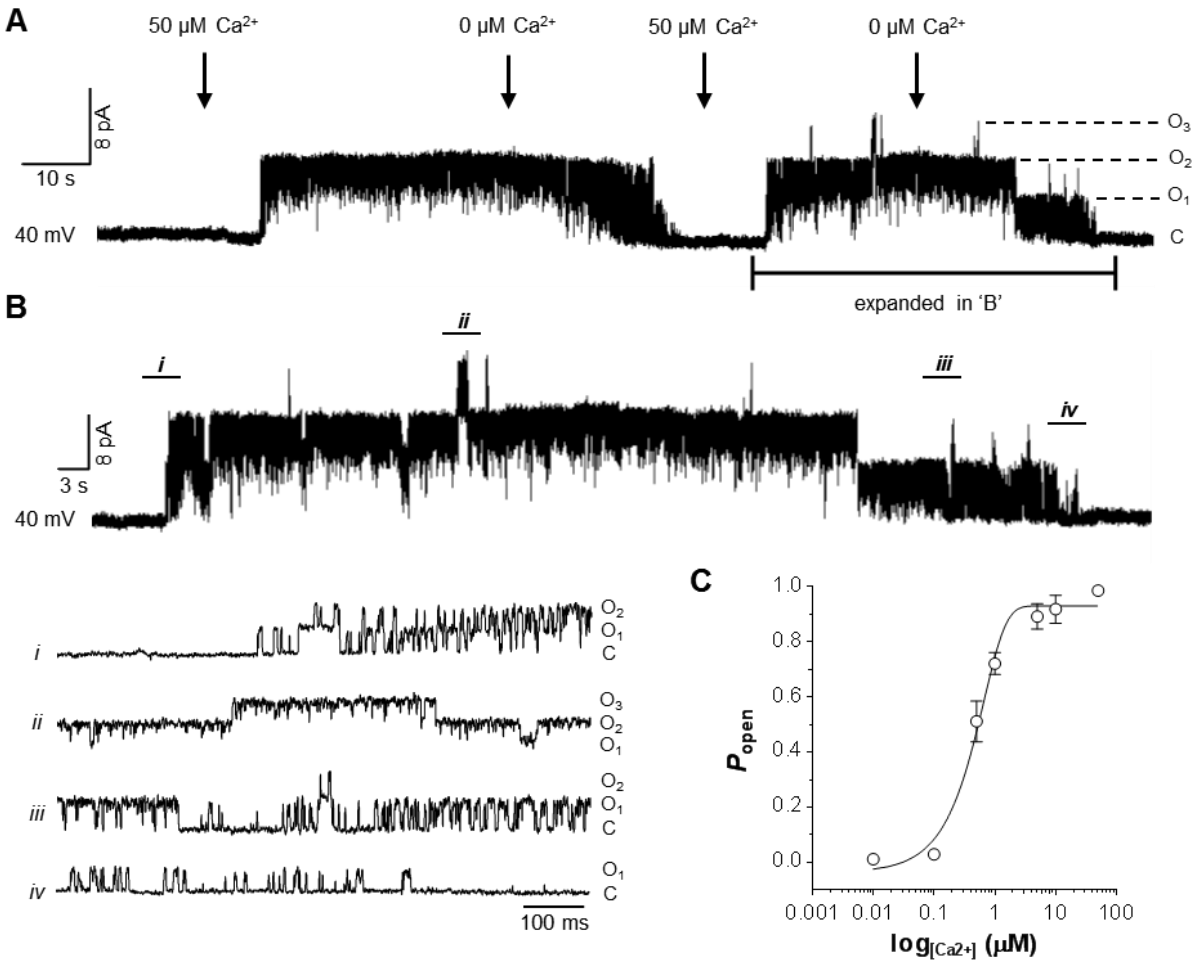

Figure 4.2. K_{Ca} channel activity is reversibly activated by manipulating Ca^{2+} at the intracellular membrane surface.

(A) An expanded view of a single experiment in which the solution bathing the intracellular surface of an excised membrane patch was switched from 0 to 50 μM Ca^{2+}. This relatively high [Ca^{2+}] was used for the fast onset of channel activation and applications were of 1-2 min durations (see Fig. 4). Intracellular bath and pipette solutions contained symmetrical K^+ (100 mM) and the extracellular solution contained a free [Ca^{2+}] of 10 nM. The patch was voltage-clamped at -40 mV, resulting in a transmembrane potential of 40 mV. In this experiment the membrane patch was bathed alternately with 50 μM Ca^{2+} and Ca^{2+}-free solutions to illustrate Ca^{2+}-dependent channel activation. (B) An expansion of the second phase of K_{Ca} activation shown in (A) to illustrate the initiation of repeated channel openings in response to 50 μM Ca^{2+} followed by Ca^{2+} washout. (C) Ca^{2+}-activation curve obtained by exposing the intracellular surface of excised inside-out membrane patches to different free [Ca^{2+}]'s. The pipette solution contained 100 mM KCl and 10 nM free Ca^{2+}. The intracellular bath solution also contained 100 mM KCl but [Ca^{2+}] and [EGTA] were manipulated to generate six solutions with free [Ca^{2+}] ranging from 0 to 50 μM. At each $[Ca^{2+}]_i$, excised patches were held at a transmembrane potential of 40 mV. K_{Ca} channel P_{open} increased with increased $[Ca^{2+}]_i$. Data are mean ± S.E.M. from 5-7 recordings each, and were fitted with a Hill curve.

Upon initial excision of a membrane patch, 50 μM EGTA was added to the intracellular bath solution to ensure that the intracellular surface of the membrane patch was not exposed to Ca^{2+} (figure 4.2). In the absence of Ca^{2+}, channel activity was absent or silenced in excised patches clamped at a transmembrane potential of 40 mV (figure 4.2A, B). To ensure rapid onset of channel activity excised patches were then perfused with 50 μM free Ca^{2+}, which activated the channel within seconds and resulted in continuous channel activity for the duration of Ca^{2+} exposure (figure 4.2A, B). With 50 μM Ca^{2+} at the intracellular surface of the membrane patch, channels were mainly open at patch transmembrane potentials from -80 to +80 mV (not shown). Following 1-2 min of 50 μM Ca^{2+} perfusion, washout with a zero Ca^{2+} intracellular bath solution induced gradual channel closure until no channel activity was observed (figure 4.2A, B).

Effect of anoxia on K_{Ca} channels in cell-attached and excised membrane patches

To determine if K_{Ca} channels are oxygen-sensitive and undergo channel arrest we next examined K_{Ca} single-channel activity following transition to anoxia (figure 4.3 and 4.4). When a cell-attached patch was held at -100 mV (20 mV transmembrane potential), single-channel current amplitude was 6.2 ± 0.5 pA during normoxic conditions (n = 10; figure 4.3A, E) and remained unchanged following a 30 min anoxic treatment (figure 4.3A, C, E). A 60 min normoxic aCSF perfusion did not change K_{Ca} channel mean P_{open} (n = 10; $p = 0.562$; figure 4.3F); however, mean P_{open} significantly decreased 5-fold (from 0.5 ± 0.05 to 0.1 ± 0.03) following 30 min anoxia (n = 10; $p < 0.001$; figure 4.5F). When cortical sheets were reperfused with normoxic aCSF for 30 min following anoxic treatment, mean P_{open} returned to normoxic levels (figure 4.5F). To determine if the K_{Ca} channel is endogenously oxygen-sensitive, membrane patches were isolated from the rest of the cell and K_{Ca} P_{open} was assessed in inside-out membrane patches following a 30 min anoxic perfusion (figure 4.4). K_{Ca} channels required $[Ca^{2+}]_i$ for activation yet continuous Ca^{2+} exposure can cause desensitization; therefore, the effect of pulses of 5 μM Ca^{2+} (just prior to each recording), and continuous application of 5 μM Ca^{2+} on anoxic channel P_{open} was assessed. In experiments where Ca^{2+} was pulsed on, patches were exposed to a continuous 0 $[Ca^{2+}]$ intracellular bathing solution between Ca^{2+} pulses. Under these conditions, when an excised patch was held at -40 mV (40 mV transmembrane potential), current amplitude (~ 8.0 pA) and channel P_{open} (~ 0.9) remained unchanged following a 30 min anoxic perfusion (n = 10 each; figure 4.4E; "Control (0 Ca^{2+})" and "Anoxia (0 Ca^{2+})"). In experiments where excised patches were continuously bathed in 5 μM Ca^{2+} for the entire duration of experiments channel P_{open} gradually decreased over the 60 min duration

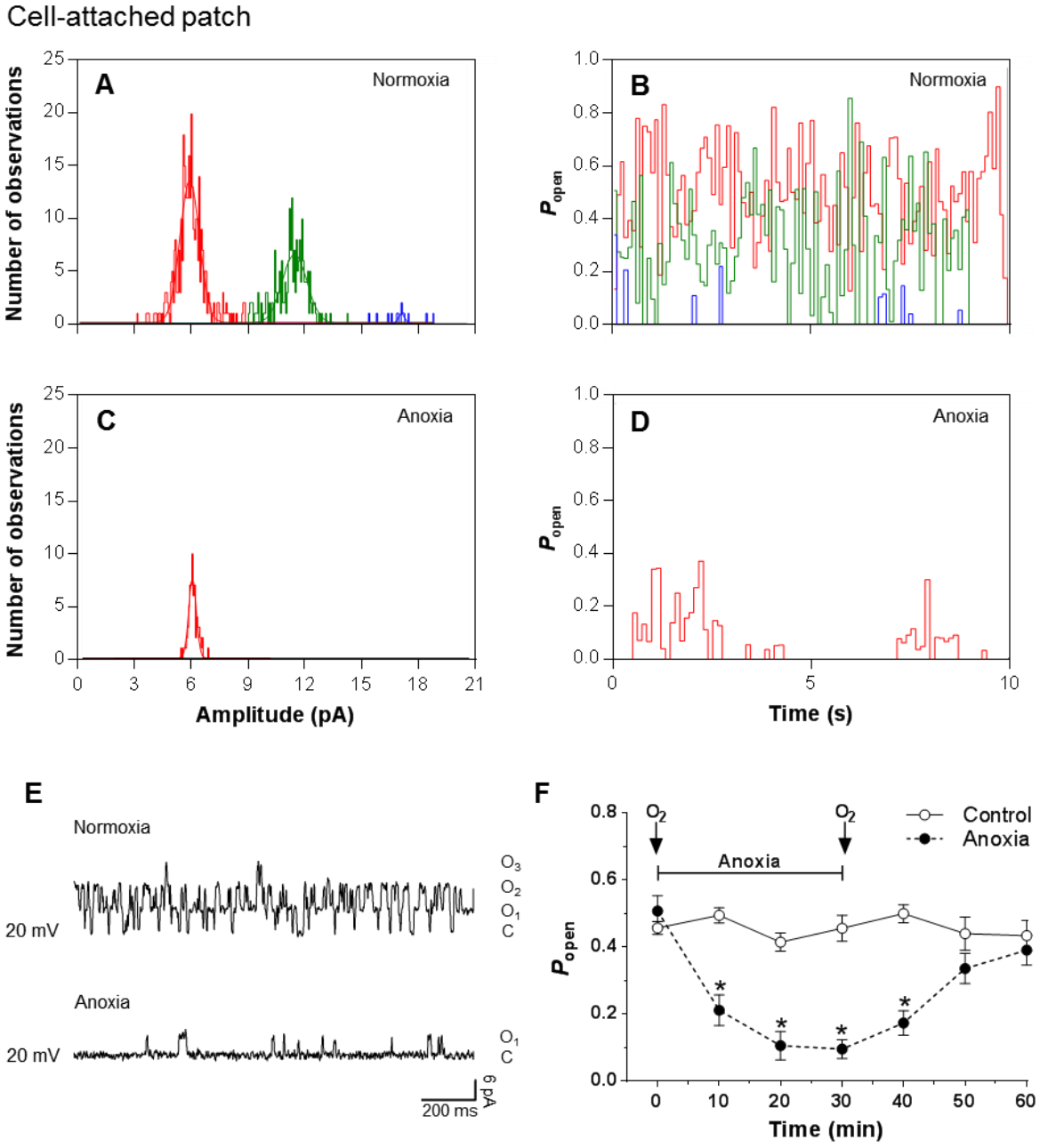

Figure 4.3. Anoxia decreases K_{Ca} channel P_{open} in cell-attached patches.
(A-D) Normoxic and anoxic K_{Ca} open-channel amplitude (A, C) and P_{open} (B, D) histograms were obtained from 10 s single-channel recordings. Note: Normoxia represents data obtained following an initial 15-min normoxic perfusion; anoxia represents data obtained following 30 min anoxic perfusion. There were three channels in this patch (distinguished by red, green, and blue). (E) Segments of single-channel activity from the patch in (A-D) during normoxic and anoxic treatment at a patch V_m of 20 mV. (F) Mean P_{open} following a 15-min normoxic period (Time = 0 min); O_2 labeled arrows indicate normoxic treatment and the black bar indicates the duration of anoxic treatment. Data are mean ± S.E.M. from 10 separate experiments for each treatment. Asterisks indicate a significant effect of anoxia on channel P_{open} compared to control values ($P < 0.05$).

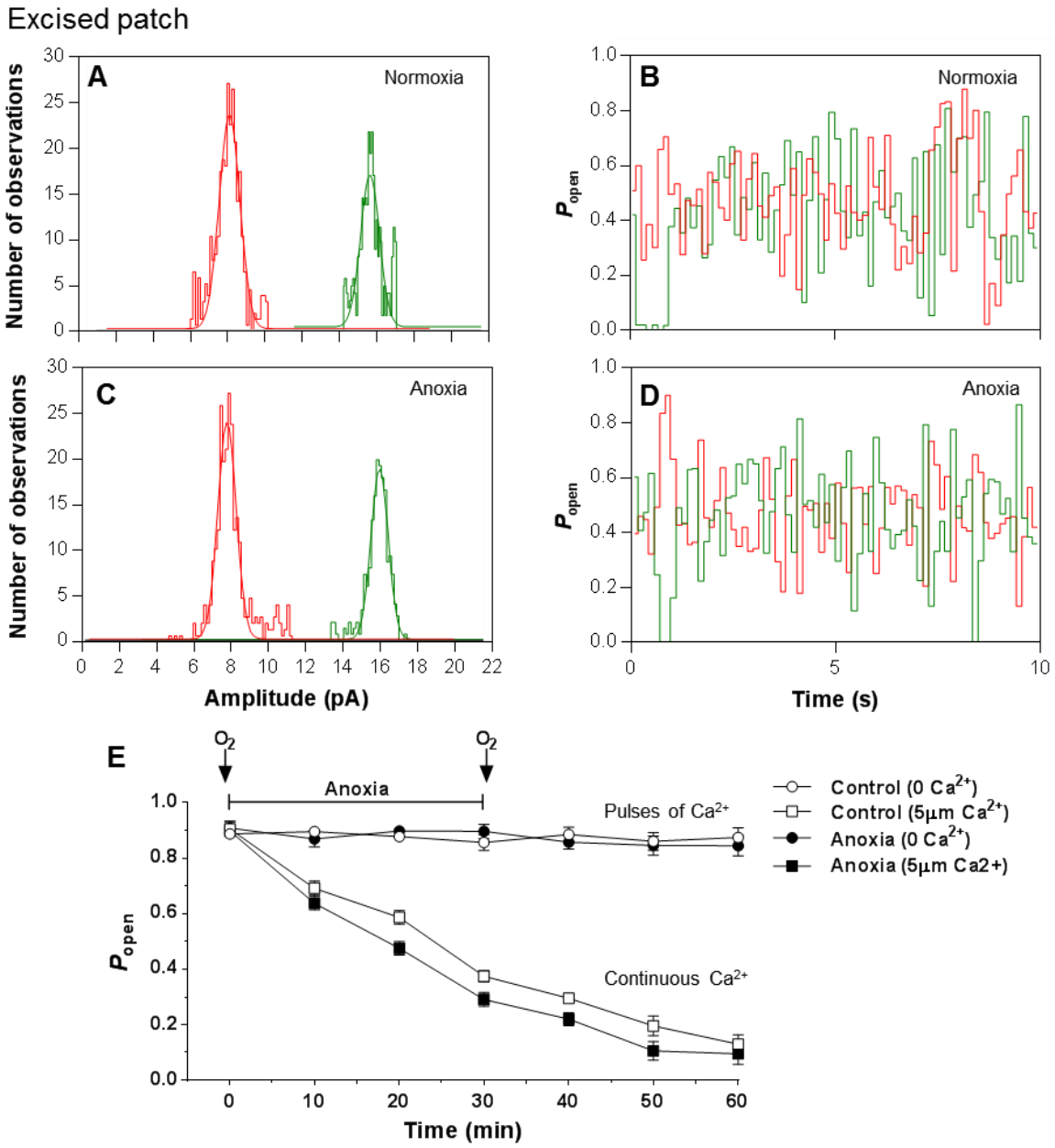

Figure 4.4. Anoxia does not decrease K_{Ca} channel P_{open} in excised membrane patches.
(A-D) Normoxic and anoxic K_{Ca} channel amplitude (A, C) and P_{open} (B, D) histograms were obtained from 10 s single-channel recordings. Green and red colouring indicates two different channels were in this patch. The patch was continuously bathed with a 100 mM K^+, 0 Ca^{2+} solution except prior to recording a 5 µM free Ca^{2+} solution was applied. (E) Mean P_{open} during a 30 min anoxic treatment and recovery. ''Control (0 Ca^{2+})'' and ''Anoxia (0 Ca^{2+})'' represent data obtained from patches exposed to intermittent pulses of 5 µM free Ca^{2+}. ''Control (5 µM Ca^{2+})'' and ''Anoxia (5 µM Ca^{2+})'' represent data obtained from patches where 5 µM Ca^{2+} was continuously perfused. Note: All data was obtained following a 15-min normoxic perfusion; anoxic data was obtained following 30 min anoxic perfusion; black bar indicates the duration of anoxic treatment. Data are mean ± S.E.M. from 10 separate experiments for each treatment.

of experiments irrespective of anoxic exposure (n = 10 each; figure 4.4E; "Control (5 μM Ca^{2+})" and "Anoxia (5 μM Ca^{2+})").

Effect of protein kinase and phosphatase modulators on K_{Ca} channel P_{open}

Phosphorylation of BK channels by PKC decreases P_{open} in mammalian smooth muscle and Purkinje neurons (Zhou *et al.*, 2010; van Welie & du Lac, 2011). Therefore, I postulated that the anoxia-mediated decrease in K_{Ca} P_{open} in turtle cortical neurons (shown in figure 4.3F) is the result of an anoxia-mediated activation of PKC. To test this I pre-incubated cortical sheets with the PKC inhibitor chelerythrine and assessed K_{Ca} channel P_{open} during an anoxic treatment and recovery. Chelerythrine blocked the anoxia-mediated decrease in P_{open} by ~ 80% following 30 min of anoxia (anoxic 0.08 ± 0.02 to anoxic plus chelerythrine 0.45 ± 0.08; n = 5 for each; $p = 0.002$; figure 4.5A), indicating that PKC modulates turtle K_{Ca} channels during anoxia. To assess if activation of PKC under normoxic conditions can mimic the anoxic decrease in K_{Ca} channel P_{open} I treated cortical sheets with phorbol-12-myristate-13-acetate (PMA), a PKC activator. Normoxic application of PMA decreased P_{open} ~ 80% by 30 min of treatment (normoxic 0.4 ± 0.05 to PMA 0.1 ± 0.02; n = 5; $p < 0.001$; figure 4.5B), supporting the previous findings that PKC is involved in regulation of turtle cortical neuron K_{Ca} channels. Mammalian K_{Ca} channels are also regulated by protein phosphatases and the Ca^{2+}-binding protein calmodulin (Fanger *et al.*, 1999; Widmer *et al.*, 2003; van Welie & du Lac, 2011). To test if turtle K_{Ca} channels are regulated by protein phosphatase 1 or 2A I treated cortical sheets with a specific inhibitor of these phosphatases okadaic acid (n = 5; figure 4.5B). To investigate a role for calmodulin I treated cortical sheets with the Ca^{2+}/calmodulin inhibitor calmidazolium (n = 5; data not shown). Neither of these treatments had a significant effect on K_{Ca} P_{open} during normoxia ($p = 0.861$ and 0.457, respectively).

4.4 Discussion

In normoxic mammalian neuronal tissue there is sufficient $[ATP]_i$ for tight regulation of $[Ca^{2+}]$ and $[K^+]$; however, in the absence of compensatory mechanisms a decrease in oxygen availability quickly leads to decreased $[ATP]_i$ and loss of ion homeostasis. Given the important roles of both Ca^{2+} and K^+ in neuronal excitability it is not surprising that a neuronal K_{Ca} current decreases as part of the anoxic defense mechanism in the anoxia-tolerant turtle. In turtle pyramidal neurons

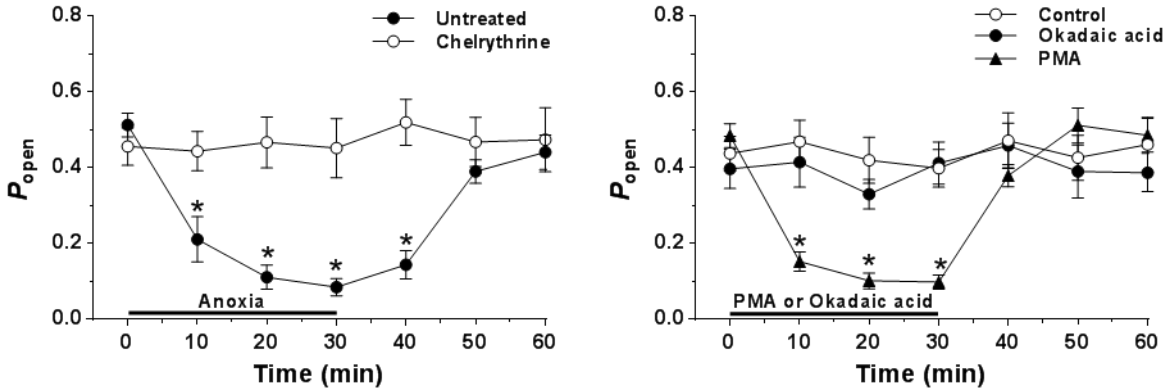

Figure 4.5. The effect of PKC modulation on K_{Ca} channel P_{open} in cell-attached patches.
(A) Summary P_{open} graph showing a 30 min anoxic treatment and a 30 min of anoxia plus PKC inhibitor - chelerythrine (0.5 μM) treatment. (B) Summary P_{open} graph showing a 60 min normoxic control treatment, or a normoxic 30 min application of the PKC activator PMA (0.5 μM), or a normoxic 30 min application of the phosphatase 1 and 2A inhibitor - okadaic acid. Note: Time = 0 min occurs following a 15-min normoxic period. Black line in A indicates the duration of anoxic treatment and in B indicates the duration of either PMA or okadaic acid exposure. Cortical sheets were pre-incubated with chelerythrine and okadaic acid, and these inhibitors were drip applied for the indicated duration. PMA was drip applied only. Asterisks (*) indicate a significant effect of PKC inhibition on channel P_{open} compared to anoxic values (A), and a significant effect of PKC activation during normoxia (B) Data are mean ± S.E.M. from 5-7 separate experiments for each treatment ($P < 0.05$).

$[Ca^{2+}]_i$ increases ~ 10-20% in response to a 30 min anoxia perfusion (Pamenter *et al.*, 2008c; Pamenter *et al.*, 2011); thus, arrest of a K_{Ca} channel would prevent over-activation and reduce K^+ efflux. Massive neuronal K^+ efflux is a characteristic feature of spreading depression (Fanger *et al.*, 1999), an evolutionarily conserved process involved in detrimental human pathologies such as migraine, seizures, and stroke (Van Harreveld *et al.*, 1956; Lauritzen *et al.*, 1988; Rodgers *et al.*, 2007; Dohmen *et al.*, 2008; Rodgers *et al.*, 2010). In the ischemic cortex, anoxic conditions enhance tissue damage by promoting spontaneous SD-like depolarizations and associated waves of increased $[K^+]_o$ that prevent restoration of cellular ATP levels, known as peri-infarct depolarizations (Fabricius *et al.*, 2006; Dohmen *et al.*, 2008; Dreier *et al.*, 2009). Neuronal protection during anoxia may therefore hinge on altered K^+ conductance and tight regulation of the $[K^+]$ gradients in anoxia-tolerant turtles. In this study, I have identified a large-conductance Ca^{2+}-activated K^+ channel (similar to a BK channel in mammals) in turtle cortical neurons and demonstrated a statistically significant reduction in channel P_{open} in response to low oxygen (95% N_2/5% CO_2). Furthermore, it was shown that K_{Ca} channel P_{open} does not decrease in isolated membrane patches, indicating the involvement of intracellular mechanisms in anoxic K_{Ca} channel arrest. Phosphorylation of mammal BK channels by PKC decreases P_{open} and I show that inhibition of PKC in turtle cortical neurons blocks the anoxia-mediated decrease in K_{Ca} channel P_{open}. I propose that decreased K^+ efflux via K_{Ca} channels helps maintain K^+ homeostasis, reduces cellular ATP usage, and promotes survival during anoxic periods.

Ca^{2+}-activated K^+ channels were previously described in turtle cochlear hair cells (Art *et al.*, 1995); however, this is the first study to identify a K_{Ca} channel in the reptile central nervous system. The cell-attached and excised patch I/V curves from this study resemble those generated for mammalian K_{Ca} (Pallotta *et al.*, 1981), and a single-channel slope conductance of 223 pS (in symmetrical potassium) is within the 100-300 pS range for mammalian BK channels (Marty, 1981; Pallotta *et al.*, 1981; Tabares *et al.*, 1985; Egan *et al.*, 1993; Liu *et al.*, 1999). This is also similar to the conductance of turtle cochlear hair cell K_{Ca} channels which is ~ 320 pS (Art *et al.*, 1995). I was able to block single-channel activity with the well-known BK channel blockers TEA and IbTX (Blatz & Magleby, 1987; Candia *et al.*, 1992), indicating similar pharmacological sensitivity as mammalian BK channels. Changing electrode $[K^+]$ in the cell-attached configuration verified K^+ as the current carrier and single-channel P_{open} increased in response to both patch depolarization and bathing Ca^{2+} near the inner membrane surface of excised patches. In cell-attached patches I

did not observe single-channel activity at the cell resting V_m of -80 mV, indicating that resting $[Ca^{2+}]_i$ in intact turtle cortical neurons (~ 120 nM) (Bickler & Buck, 1998) was below the level required for activation. During anoxia, $[Ca^{2+}]_i$ increases to around 150 nM (Bickler & Buck, 1998) which was sufficient to activate the turtle K_{Ca} channel. Thus, arrest of these channels at resting V_m would be appropriate given the increase in $[Ca^{2+}]_i$.

Neuronal BK channels in mammals are involved in fast afterhyperpolarization (fAHP) and are activated immediately following the AP and lasts several tens of milliseconds (Sah & Louise Faber, 2002). The BK channel is a voltage-activated ion channel in which direct calcium binding shifts gating to a more negative cellular V_m (Cui *et al.*, 1997; Braun *et al.*, 2008). BK channel activation typically occurs in response to Ca^{2+} influx via voltage-dependent Ca^{2+} channels, and when free $[Ca^{2+}]_i$ reaches threshold, K_{Ca} channel opening results in K^+ efflux and neuronal hyperpolarization (Sah & Louise Faber, 2002). The regulation of K^+ channels by oxygen tension has been studied in a variety of mammalian cell types (Wyatt & Peers, 1995; López-López *et al.*, 1997; Peers, 1997; López-Barneo *et al.*, 2001); with studies focusing primarily on BK channel inhibition by hypoxia in oxygen-sensing tissues including, neuroendothelial bodies (Youngson *et al.*, 1993), adrenomedullary chromaffin cells (Thompson & Nurse, 1998; Fearon *et al.*, 2002) and carotid body glomus cells (Lopez-Barneo *et al.*, 1993; Williams *et al.*, 2004a). Carotid body glomus cells respond to lowered PO_2 by inhibiting K^+ currents, leading to depolarization and increased cellular excitability, increased cytosolic Ca^{2+}, and increased lung ventilation (Lopez-Barneo *et al.*, 1993; Williams *et al.*, 2004a). We also found inhibition of K_{Ca} channels with lowered oxygen in turtle pyramidal neurons, measured as a decrease in K_{Ca} channel P_{open} at depolarized patch potentials; however, this does not lead to increased AP_f (Pamenter *et al.*, 2011). Turtle pyramidal neurons mildly depolarize (~ 8 mV) during anoxia (Pamenter & Buck, 2008); thus arresting these channels may be even more important since lowered V_m and increased $[Ca^{2+}]_i$ activate them.

Preventing $[K^+]_e$ accumulation is likely important to anoxia-tolerance in the turtle because $[K^+]_e$ accumulation results in V_m depolarization and spreading depression in anoxic/ischemic mammalian neurons (Somjen, 1979; Zhou *et al.*, 2010). In anoxic turtle brain there is a very mild increase in cerebral $[K^+]_e$ (from 2.6 to 3.7 mM; Sick *et al.*, 1982) and a 50% decrease in whole-cell K^+ conductance (Hodgkin & Huxley, 1952; Chih *et al.*, 1989), indicating that K^+ channels are inhibited by anoxia. Predictably a 1.2 mM increase in $[K^+]_e$ results in an ~ 8 mV depolarization in

V_m, precisely what has been measured (Pamenter *et al.*, 2011). Preventing the increase in $[K^+]_e$ would prevent a shift in the equilibrium potential for K^+ (McCartney *et al.*, 2007) and neuronal depolarization. The mild anoxic depolarization in turtle cortical neurons following the transition to anoxia may result from altered conductance states of numerous ions (Pék-Scott & Lutz, 1998; Pamenter & Buck, 2008). Given the hyperpolarizing effects of K_{Ca} during normoxia, blocking this channel likely contributes to stable $[K^+]_e$ and mild depolarization during anoxia in the turtle. Additionally, the anoxia-mediated GABAergic shunt of excitatory current is likely sufficient to counter any further depolarizing effects of decreased K_{Ca} P_{open}. Furthermore, anoxia results in a 40-50% reduction in turtle brain metabolic rate (Doll *et al.*, 1994) which likely reflects a similar decrease in Na^+/K^+ ATPase activity and lowered K^+ uptake.

Mammalian BK channel activity can be differentially regulated by a variety of cytosolic factors; including gases (oxygen, nitric oxide, and carbon monoxide), pH, reactive oxygen species and phosphorylation (Lang *et al.*, 2000; Riesco-Fagundo *et al.*, 2001; Jaggar *et al.*, 2002). In turtle cortical neurons, the anoxic reduction in P_{open} did not occur in excised patches, indicating that K_{Ca} channel modulation by anoxia involves cytosolic oxygen-sensing components potentially including various second messenger pathways. Our findings are supported by studies in mouse neocortical neurons (Liu *et al.*, 1999) and rat carotid body glomus cells (Wyatt & Peers, 1995) where patch excision prevented hypoxic decreases in K_{Ca} channel P_{open}; indicating cytosolic factors are necessary for the hypoxic regulation of K_{Ca} channels. However, an anoxia-mediated decrease in pH could play a role since BK channels in excised patches from mouse neocortical neurons show acute pH sensitivity when pH changes from 7.0 to 6.5 inhibiting P_{open} by ~ 50% (Liu *et al.*, 1999). This is very close to the change in intracellular pH observed in anoxic turtle brain sheets measured with ^{31}P nuclear magnetic resonance spectroscopy (Buck *et al.*, 1998). Mammal BK channel modulation is complex and involves several protein kinases and phosphatases (Egan *et al.*, 1993; Jin *et al.*, 2002a; Jin *et al.*, 2002b; Widmer *et al.*, 2003; Zhou *et al.*, 2010; van Welie & du Lac, 2011); therefore, it is likely that turtle K_{Ca} channels are also regulated by phosphorylation/dephosphorylation. Since I observed an anoxic decrease in P_{open} and there is evidence that phosphorylation of K_{Ca} by PKC decreases P_{open} in mammalian Purkinjie neurons and tracheal tissue I targeted PKC (Widmer *et al.*, 2003; Zhou *et al.*, 2010). Indeed, blocking PKC with chelerythrine during anoxia prevented the anoxia-mediated decrease in P_{open} and during normoxia PKC activation with PMA decreased P_{open}; providing strong evidence for a role of PKC in the

oxygen-sensing mechanism in turtle pyramidal neurons. This PKC is a diacylglycerol and Ca^{2+} activated kinase; therefore, the most direct mechanism of K_{Ca} phosphorylation by PKC, is PKC activation by the rise in cytosolic [Ca^{2+}] resulting from the anoxia-mediated release of Ca^{2+} from mitochondrial stores (Pamenter *et al.*, 2008c). Phosphorylation of K_{Ca} could also change the channels sensitivity to Ca^{2+} as phosphorylation by PKA decreases the BK channel's sensitivity to calcium in mouse neocortical neurons (Liu *et al.*, 1999) but not in rabbit glomus cells (Lopez-Barneo *et al.*, 1988). This was not specifically tested in our study but the lack of a major difference in the inactivation kinetics during continuous Ca^{2+} exposure suggests that sensitivity did not change (figure 4.4E). Anoxia-mediated mitochondrial Ca^{2+} release has also been linked to NMDA and AMPA receptor arrest and involve protein phosphatase 1 and 2A (Shin *et al.*, 2005; Pamenter *et al.*, 2008c; Zivkovic & Buck, 2010) but inhibition of these phosphatases had no effect on normoxic K_{Ca} P_{open}.

In summary, I have provided additional evidence that channel arrest is part of the natural defense mechanism in the anoxia-tolerant turtle brain. Anoxic arrest of K_{Ca} channels indicates that ATP conservation due to channel arrest and homeostatic maintenance of ion gradients is more important to anoxic survival than transient neuronal hyperpolarization. I propose that K_{Ca} channel arrest occurs in response to increased $[Ca^{2+}]_i$ and mild depolarization during anoxia, thereby reducing K^+ efflux and Na^+/K^+-ATPase activity. These data also suggest that K_{Ca} channels are modulated by phosphorylation by PKC in response to low oxygen in turtle brain.

5 Decreases in mitochondrial reactive oxygen species initiate $GABA_A$ receptor-mediated electrical suppression in anoxia-tolerant turtle neurons

Preface

The idea to investigate the effects of anoxic decreases in ROS on $GABA_A$ receptor-mediated electrical suppression was conceived jointly by D. Hogg and L.T. Buck. With the exception of Figure 5.2 panel D all experiments were performed and analyzed by D. Hogg.

Abstract

Anoxia induces hyper-excitability and cell death in mammalian brain but in the anoxia-tolerant western painted turtle (*Chrysemys picta bellii*) neuronal electrical activity is suppressed (i.e., spike arrest), ATP consumption is reduced, and cell death does not occur. Electrical suppression is primarily the result of enhanced γ-aminobutyric acid (GABA) transmission; however, the underlying mechanism responsible for initiating oxygen-sensitive GABAergic spike arrest is unknown. In turtle pyramidal neurons there are three types of $GABA_A$ receptor-mediated currents: spontaneous inhibitory postsynaptic currents (IPSCs), giant IPSCs and tonic currents. The aim of this study was to assess the effects of reactive oxygen species (ROS) scavenging on these three currents since ROS levels naturally decrease with anoxia and may serve as a redox signal to initiate spike arrest. I found that anoxia, pharmacological ROS scavenging, or inhibition of mitochondrial ROS generation enhanced all three types of GABA currents, with tonic currents comprising ~ 50% of the total current. Application of hydrogen peroxide inhibited all three GABA currents, demonstrating a reversible redox-sensitive signaling mechanism. I conclude that anoxia-mediated decreases in mitochondrial ROS production are sufficient to initiate a redox-sensitive inhibitory GABA signaling cascade that suppresses electrical activity when oxygen is limited. This unique strategy for reducing neuronal ATP consumption during anoxia represents a natural mechanism in which to explore therapies to protect mammalian brain from low-oxygen insults.

5.1 Introduction

Upregulation of GABA-mediated inhibition is critical for anoxia-tolerance in turtle brain; however, the oxygen-sensing mechanism(s) responsible for enhanced GABA transmission are unknown. To understand how the turtle brain survives prolonged anoxia it is essential that the oxygen-sensing mechanisms responsible for enhanced GABA transmission be identified. Clues to the potential oxygen sensor(s) can be found in classical oxygen-sensing tissues including, carotid body glomus (type I) cells, PASMCs and adrenomedullary chromaffin cells (AMCs). In these tissues, oxygen sensing is proposed to be the result of perturbations in mitochondrial function and energy state (reviewed in Ward, 2008). Mitochondria are a leading contender as an oxygen sensor because they are the largest consumers of oxygen, and as such are the key determinates of intracellular PO_2. In turtle brain, anoxic increases in mitochondrial Ca^{2+} release have already been linked to channel arrest of NMDA and AMPA receptors which indicates that mitochondria indeed play an oxygen sensing role during anoxia. Mitochondria can act as oxygen sensors because hypoxia or anoxia disrupts electron transfer in the mitochondrial ETC resulting in changes in $[ATP]_i$, ROS generation and overall redox state of the cell (reviewed in Ward, 2008). Any or all of these changes could initiate signalling cascades that activate a variety of processes resulting in protection from anoxia.

The anoxic upregulation of GABA currents occurs in isolated brain sheets; therefore, oxygen-sensitive GABA transmission is intrinsic to the slice. Mitochondria are a potential oxygen-sensor capable of initiating this response because they are ubiquitously expressed throughout the brain. In particular, there is interest in a role for mitochondrial ROS (mROS) as a signal of low oxygen because ROS generation is inherently sensitive to changes in oxygen availability, making it a potentially important component of signalling cascades. Our lab initially became interested in investigating mROS as a signal of the onset of anoxia after reading Schumacker's ROS hypothesis (reviewed in Ward, 2008). However, initial studies revealed that in turtle cerebrocortex ROS do not increase during the transition to anoxia and instead results in the elimination of intracellular ROS ($[ROS]_i$) (Pamenter *et al.*, 2007), a finding that I have recently confirmed (Dukoff *et al.*, 2014).

ROS have long been associated with pathological disease states (e.g., reperfusion injury due to stroke), but more recently evidence has emerged that ROS, and in particular H_2O_2, can regulate a

variety of redox-sensitive proteins and signaling pathways by reversible oxidation of cysteine thiol residues (reviewed in Veal *et al.*, 2007). Under normoxic conditions, $[ROS]_i$ are maintained by the balance between ROS-generating systems and antioxidant enzyme networks (Pitlik *et al.*, 2009; Kahles & Brandes, 2012); however, changes in oxygen availability can alter ROS metabolism resulting in modulation of protein function. ROS can modulate neuronal ionic homeostasis through interactions with several ion transporting systems including: ion channels, ionic pumps, ion exchangers and ion co-transporters (Pitlik *et al.*, 2009). The major effects of ROS on these ion-transporting systems are: oxidation of sulfhydryl groups of transport proteins, lipid peroxidation, and perturbation of oxidative phosphorylation leading to decreases in intracellular [ATP] (Kourie, 1998). Of particular interest is $O_2^{\bullet-}$, which is converted to H_2O_2 in the cytosol (Adam-Vizi, 2005). In mammal, a number of neurotransmitter systems have been found to be redox-sensitive. For example, H_2O_2 suppresses dopamine release in striatal brain slices (Rice, 2011), and Ca^{2+}-dependent exocytosis of glutamate in cortical synaptosomes (Zoccarato *et al.*, 1995). GABA release is also sensitive to ROS with superoxide preventing GABA release in hypothalamus (Chen & Pan, 2007), and oxidants preventing GABA release in spinal cord (Yowtak *et al.*, 2011). In addition, $GABA_A$ receptors are potentiated by reducing agents and inhibited by oxidizing agents (Amato *et al.*, 1999; Calero *et al.*, 2011).

Given the important inhibitory role of GABA during anoxia in turtle brain and the potential for redox regulation of $GABA_A$ receptors I investigated the effects of redox-modulation on GABAergic transmission. Specifically, I assessed the effects of pharmacologically removing ROS on several neuronal electrical parameters of spike arrest (i.e., AP_{th}, AP_f, V_m and G_w) as well as on three different types of $GABA_A$ receptor currents. Since mitochondria are the major producers of ROS in the cell and are potentially important oxygen sensors I also asked whether a decrease in mROS generation is sufficient to initiate GABA-mediated spike arrest.

5.2 Materials and Methods

5.2.1 Experimental design

Experiments were performed in a repeated measurement paired design starting with a 10 min normoxic pre-treatment, followed by 30 min of treatment and 30 min of normoxic recovery unless otherwise stated. H_2O_2, GZ and bicuculline methiodide (BIC) were applied for 5 min. The

electrophysiological protocols used in this chapter are similar to those in Chapter 2 except where indicated. Only new materials and methods specific to this chapter are included in this section.

5.2.2 Electrophysiology

5.2.2.1 Whole-cell and perforated patch clamp recordings

Redox agents react with Ag electrodes to produce voltage offsets (Berman & Awayda, 2013). To reduce potential artifacts in electrophysiological recordings molten AgCl was reapplied often on bath and reference electrodes. When dissolved in aCSF the LJP associated with the ROS scavenger N-(2-Mercaptopropionyl glycine (MPG) and the oxidant H_2O_2 were 16.5 and < 1 mV, respectively. All data have been corrected for these values offline.

5.2.2.2 Measurement of $GABA_A$ receptor currents and charge transfer

To aid in the detection of $GABA_A$ receptor currents, neurons were voltage-clamped at a holding potential of -100 mV and pipette [Cl^-] was increased to 130 mM by equimolar substitution of CsCl for K-gluconate (Note: this is different from the 110 KCl pipette solution used in Chapter 2). Similar to Chapter 2, $GABA_A$ receptor currents were isolated with AP5 (25 μM) and CNQX (25 μM). Turtle pyramidal neurons exhibit two types of phasic $GABA_A$ receptor-mediated currents: fast spontaneous IPSCs (sIPSCs) and slower gIPSCs. Spontaneous IPSCs when recorded in the presence of the voltage-gated Na^+ channel blocker TTX are referred to as miniature IPSCs (mIPSCs). Both sIPSCs and mIPSCs were detected using a threshold search protocol with a trigger level set to 3 times the baseline noise (~ 3 pA). All recordings were visually inspected and only events with a rapid onset (10 to 90% rise time < 5 ms) were included in the analysis. Fast sIPSC and mIPSC data were assessed for 2 min at the end of each treatment period. If required, mIPSCs or sIPSCs were normalized to the normoxic 5 min time point (> 15 min after patch formation).

The amplitude of the tonic GABA current was calculated as the difference between the holding current measured before and after BIC or H_2O_2 application. Tonic currents were measured following a 10 min normoxic control period and after 30 min of treatment. To ensure an accurate measurement of holding current, baseline was sampled at 5 ms epochs every 100 ms over a 10 sec period (Nusser & Mody, 2002; Bright & Smart, 2013). Any baseline points falling on the decay phase of an IPSC were omitted. Two changes in the baseline holding current were calculated and statistically compared. The first measurement was between two 10 sec periods 1 min apart

immediately prior to inhibition of the tonic GABA current, this was the average change in baseline current with no treatment. The second measurement was taken 1 min after BIC or H_2O_2 application; this was the average change in current due to modulation of $GABA_A$ receptors.

Charge transfer (Q (pA × ms); the integrated area under an IPSC) associated with sIPSCs and gIPSCs was calculated according to the equation: $Q_{IPSC} = (f_{treatment} \times Q_{treatment}) \times \Delta t$, where $f_{treatment}$ is the mean frequency (Hz) of the IPSCs, $Q_{treatment}$ is the mean charge transfer (pC) per IPSC, and Δt is time. The charge transfer associated with the tonic current was calculated according to the equation $Q_{TC} = I_{TC} \times \Delta t$, where I_{TC} is the tonic current (pA) (Bai *et al.*, 2001).

5.2.3 Fluorescence imaging

5.2.3.1 Fluorometric assessment of $[ROS]_i$: CM-DCF

Changes in $[ROS]_i$ were assessed using the membrane-permeable ROS sensitive fluorescent indicator 5-(and-6)-chloromethyl-2',7'-dichlorodihydro-fluorescein diacetate, acetyl ester (CM-H_2DCFDA; Invitrogen, Burlington, ON). Cortical sheets were incubated in aCSF containing 5 μM CM-H_2DCFDA (from a 1 mM stock solution in DMSO) for 30 min (4°C) followed by a 30 min wash in aCSF (22°C). During loading the acetate groups on CM-H_2DCFHDA are removed by intracellular esterases yielding the nonfluorescent 5-(and-6)-chloromethyl-2',7'-dichlorodihydro-fluorescein (CM-H_2DCF), and preventing dye leakage (Koopman *et al.*, 2006). Steady state normoxic generation of ROS leads to oxidation of the CM-H_2DCF to fluorescent 5-(and-6)-chloromethyl-2',7'-dichloro-fluorescein (CM-DCF) and a subsequent increase in fluorescence. Cessation of ROS generation results in no change in CM-DCF fluorescence. CM-DCF was excited with a wavelength of 495 nm and fluorescence emission was detected at a wavelength of 520 nm. Cortical sheets were exposed to treatment aCSF for 30 min then reperfused with control aCSF for 20 min or treated with 50 μM H_2O_2 for 5 min. To assess treatment effects on ROS generation the fluorescence at treatment steady state was compared to a linear regression line fit to the 10 min normoxic portion of the trace. Data are presented as percent change expressed relative to that fitted normoxic regression line (Crowe et al., 1995).

5.2.4 Statistics

Analysis of electrophysiological and fluorescent data was performed similar to chapter 2. Either a one-way ANOVA or a Kruskal-Wallis (KW) analysis was used for between group comparisons

where appropriate. Post-hoc analyses consisted of paired *t*-tests, Holms-Sidak or Tukey's. Significance was assessed relative to the 30 min normoxia control point unless otherwise stated. For V_m and GABA current data sets pre-treatment data were not different from normoxic control data; therefore, treatments are compared to 30 min normoxic control data.

5.3 Results

The ROS scavenger MPG and ETC complex IV inhibitor CN decrease $[ROS]_i$

To investigate a role for ROS in modulating GABA receptor currents I first confirmed that $[ROS]_i$ were eliminated by the experimental protocol. Using the ROS sensitive dye CM-DCF I measured changes in fluorescence in cortical brain sheets during normoxia and anoxia, and with and without pharmacological ROS modulation. The rate of change in fluorescence did not change over one hour of normoxic perfusion (0.46 ± 0.5%; n = 8; figure 5.1A, C*i*), indicating maintenance of cellular redox homeostasis. However, anoxia significantly decreased fluorescence compared to normoxic controls (-7.2 ± 1.2%; n = 8; $p < 0.001$; figure 5.1A, C*ii*). To separate the effects of anoxia and decreases in $[ROS]_i$ I pharmacologically eliminated ROS using the general ROS scavenger MPG (0.5 mM) (Leroy *et al.*, 1991). A 30 min normoxic perfusion of MPG significantly decreased fluorescence (-9.1 ± 1.5%; n = 5; $p < 0.001$; figure 5.1A, C*iii*), compared to normoxic controls. The addition of MPG during anoxia did not decrease fluorescence beyond the effects of either anoxia alone or normoxia plus MPG (-9.2 ± 0.9%; n = 5; $p = 0.922$ and $p = 1.000$; figure 5.1A, C*iii*, *iv*). Application of another ROS scavenger *N*-acetylcysteine (NAC; 0.5 mM) mimicked the effects of MPG under each condition (data not shown). Mitochondrial ROS generation is arrested in anoxic cells because there is no oxygen available to remove electrons from the ETC. This could be an important signal to initiate ROS-mediated signalling cascades. To assess if decreases in mROS generation mimic anoxia I treated cortical sheets with cyanide (CN; 0.5 mM), a complex IV (cytochrome c oxidase) inhibitor. There is controversy over the use of complex IV inhibitors and their effects on mROS generation with some studies finding increases in ROS and others finding decreases (Chandel & Schumacker, 2000; Turrens, 2003) Consistent with Pamenter et al. (2007), perfusion of normoxic or anoxic aCSF plus CN decreased CM-DCF fluorescence compared to normoxic or anoxic aCSF plus CN decreased CM-DCF fluorescence compared to normoxic control (-8.6 ± 1.5 and -8.4 ± 0.7% respectively; n = 5 each; $p < 0.001$ for both; figure 5.1A, C*v, vi*). To demonstrate that ROS levels could be experimentally increased I drip applied

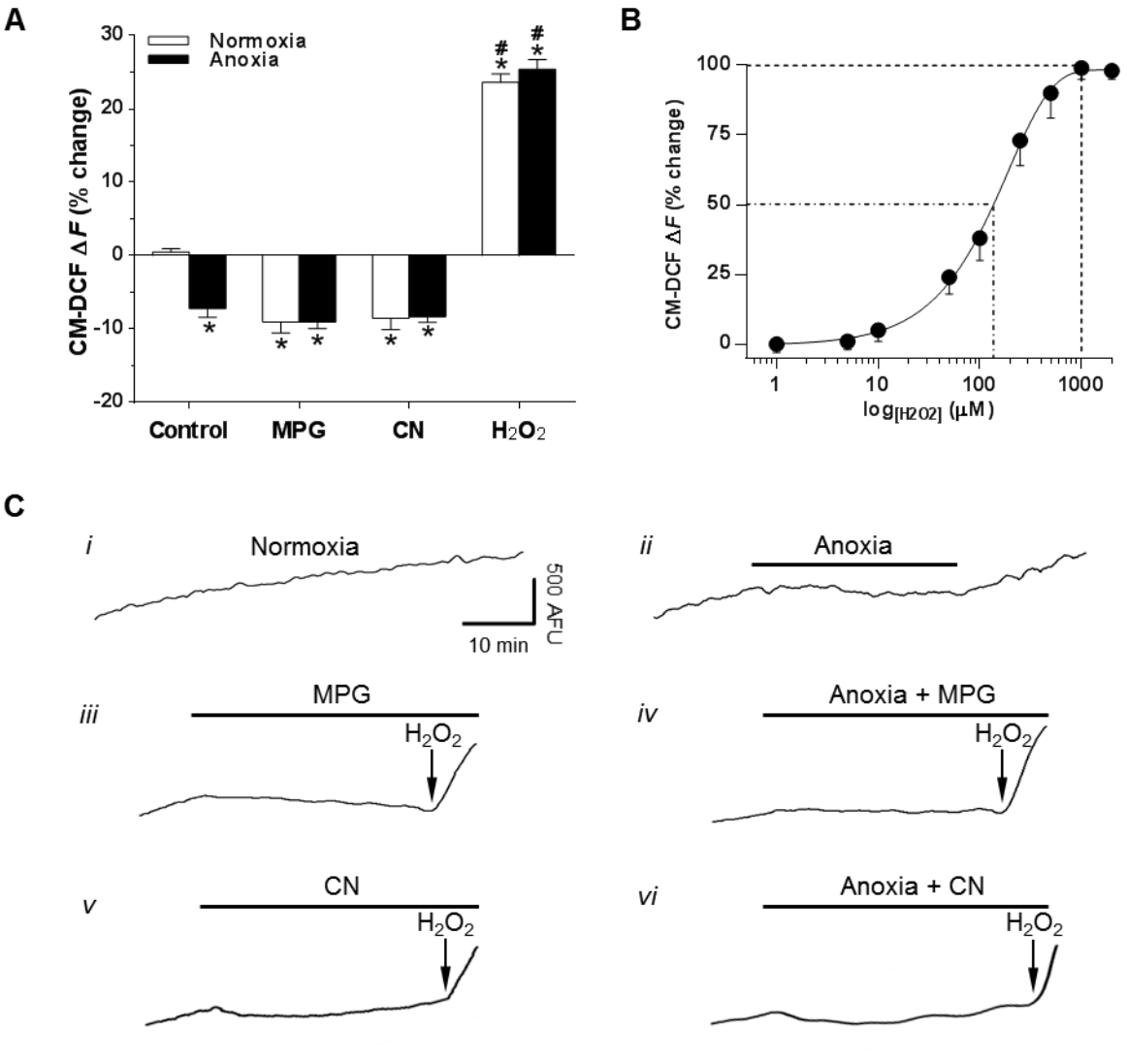

Figure 5.1. Anoxia, ROS scavenging, and inhibition of mitochondrial cytochrome c oxidase with CN decrease $[ROS]_i$.

(A) Summary of treatment induced changes in CM-DCF fluorescence. (B) Dose-response relationship of $[H_2O_2]$ versus ΔCM-DCF fluorescence. (C) Sample CM-DCF fluorescence recordings from (A), neurons treated as indicated. Note: horizontal linear portion of the trace indicates no new ROS generation; black bars represent duration of treatment; arrow indicates onset of H_2O_2 application. Treatments: normoxia 95% O_2/5% CO_2, anoxia 95% N_2/5% CO_2, 0.5 mM MPG, 0.5 mM CN and 50 μM H_2O_2. Data are expressed as means ± S.E.M., n = 4-8 replicates per treatment. Asterisks (*) indicate significant difference from normoxic controls. Pound sign (#) indicates significant difference from anoxic controls ($P < 0.05$).

H_2O_2 and measured CM-DCF fluorescence. It should be noted that *in vitro* studies indicate that DCFH (the non-chloromethylated form of CM-DCFH) is not directly oxidized by H_2O_2 but by peroxidases that require H_2O_2 for the process (Hockberger *et al.*, 1999). Therefore, while changes in CM-DCF are not the direct result of H_2O_2-mediated oxidation they are a useful indicator of general cellular oxidative stress, including H_2O_2-mediated oxidation. Excessive oxidation by H_2O_2 can cause damage to cells so I first determined an appropriate physiological concentration of H_2O_2 to apply. Application of H_2O_2 increased CM-DCF fluorescence in a dose-dependent manner (n = 4-8 each; figure 5.1B), with 50 μM [H_2O_2] being the lowest concentration in which I could detect a significant change in fluorescence. This finding is in agreement with normoxic measurements of H_2O_2 from the media of cultured turtle neurons and is near the reported physiological range of mammalian neuronal intracellular [H_2O_2] ([H_2O_2]$_i$)(1-20 μM) (Hoyt *et al.*, 1997; Lei *et al.*, 1998; Milton *et al.*, 2007). In addition, this concentration did not affect baseline electrophysiological properties of pyramidal neurons, such as V_m, G_w, and AP_{th} indicating it did not induce oxidative damage (Table 3). Compared to normoxic control, a 5 min application of H_2O_2 significantly increased fluorescence during both normoxia and anoxia (23.6 ± 1.1 and 25.4 ± 1.3% respectively; n = 5 each; $p < 0.001$ for both; figure 5.1A, C). Application of H_2O_2 during MPG or CN administration also increased CM-DCF fluorescence confirming sensitivity of the dye to exogenous H_2O_2 under these experimental conditions (figure 5.1C*iii*-*vi*).

Anoxia-mediated decreases in ROS suppress electrical activity

To investigate the role of decreased ROS in GABA-mediated spike arrest I modulated [ROS]$_i$ and measured AP_{th} as an indicator of neuronal excitability. Under normoxic conditions, stepwise current injections elicited APs at a threshold of -45.4 ± 2.0 mV, whereas anoxia significantly depolarized AP_{th} by 33% to -30.3 ± 1.9 mV (n = 10 for both; $p < 0.001$ for both; figure 5.2A). These changes were reversed by reoxygenation and are consistent with previous reports of spike arrest in anoxic turtle brain (see chapter 2; Feng *et al.*, 1988b; Perez-Pinzon *et al.*, 1992b; Pamenter *et al.*, 2008b). Perfusion of MPG under normoxic conditions depolarized AP_{th} compared to normoxic control (-33.1 ± 1.2 mV; n = 10; $p < 0.001$; figure 5.2A, B*i*-*ii*); mimicking anoxia-mediated spike arrest. To evaluate if decreases in [ROS]$_i$ and not other anoxia-induced signals (e.g., decreased ATP) are responsible for GABA-mediated spike arrest I assessed AP_{th} following a bath transition from anoxia to anoxia plus ROS scavenger. ROS scavenging with MPG during anoxia did not induce additional changes in AP_{th} compared to ROS scavenging alone (-30.4 ± 1.4

Table 3. Effect of 50 µM H_2O_2 on electrophysiological properties of pyramidal neurons.

Electrophysiological parameter	Normoxia	H_2O_2
Membrane potential (mV)	-86.3 ± 0.6	-80.3 ± 3.1
Whole-cell conductance (nS)	4.3 ± 0.6	4.4 ± 0.5
Action potential threshold (mV)	-43.5 ± 1.4	-39.3 ± 1.2

Data shown represent the means ± S.E.M. (n = 4 per treatment). A t-test comparing normoxia to H_2O_2 within each measured parameter found the data not to be statistically significant ($P < 0.05$).

mV; n = 10; $p = 0.458$; figure 5.2A). In previous studies, antagonism of $GABA_A$ receptors with GZ prevented the anoxia-mediated depolarization of AP_{th}, highlighting the essential role of these inhibitory receptors during low oxygen stress (see chapter 2; Pamenter *et al.*, 2011; Pamenter *et al.*, 2012b). In the present study, application of GZ to MPG-treated neurons prevented the MPG-mediated depolarization in AP_{th} during anoxia (-38.0 ± 1.7 mV: n = 7; $p = 0.030$) and decreased the change during normoxia (-38.9 ± 2.1 mV; n = 7; $p = 0.172$; figure 5.2A). This demonstrates that similar to anoxia, the MPG-mediated decrease in $[ROS]_i$ alters pyramidal neuron AP_{th} via a GABA-sensitive mechanism. Inhibition of the ETC with CN under normoxic conditions also depolarized AP_{th} compared to normoxic control (-34.5 ± 1.1 mV; n = 10; $p < 0.001$; figure 5.2A) indicating a role for mitochondrial ROS production in spike arrest. Application of GZ to CN treated neurons also prevented the CN induced depolarization in AP_{th} under anoxic conditions (-39.0 ± 1.9; n = 10; p = 0.035). Treatment with H_2O_2 during normoxia did not change AP_{th} relative to normoxic control (-39.8 ± 1.8mV; n = 4; $p = 0.940$); however, H_2O_2 application under anoxic conditions prevented the anoxia-mediated depolarization of AP_{th} (-40.3 ± 3.3 mV; n = 4, $p < 0.008$; figure 5.2A), indicating that increases in $[ROS]_i$ can also prevent spike arrest in turtle cortex.

A subset of pyramidal neurons located in the dorsomedial cortex are spontaneously active (Shen & Kriegstein, 1986). These neurons are well suited to use as a direct measure of spike arrest since decreases in AP_f indicate electrical suppression. Anoxic perfusion decreases AP_f in these neurons (Pamenter *et al.*, 2011); therefore, I assessed the effect of ROS scavenging with MPG on AP_f. Normoxic MPG treatment decreased AP_f from 0.86 ± 0.1 to 0.1 ± 0.1 Hz (n = 6 for both; $p < 0.001$; figure 5.2A, B*i-ii*), and following recovery AP_f returned to baseline levels ($p = 0.146$).

Pharmacological or anoxia-mediated decreases in $[ROS]_i$ shift V_m to E_{GABA} by activating $GABA_A$ receptors.

Anoxia-induced enhancement of GABA transmission activates postsynaptic $GABA_A$ receptors and depolarizes pyramidal neuron V_m to E_{GABA}. To determine if decreases in $[ROS]_i$ alone could mimic the anoxic shift in V_m I treated cortical sheets with pharmacological ROS scavengers. I first repeated baseline measurements of V_m and E_{GABA} in pyramidal neurons using perforated-patch clamp techniques. In passive current clamp recordings, pyramidal neurons had a V_m of -87.3± 1.9 mV (n = 10) under normoxic conditions, and this was hyperpolarized relative to E_{GABA} (-77.6 ± 1.6; n = 10; $p < 0.001$; figure 5.3A). E_{GABA} was not affected by oxygen availability or any

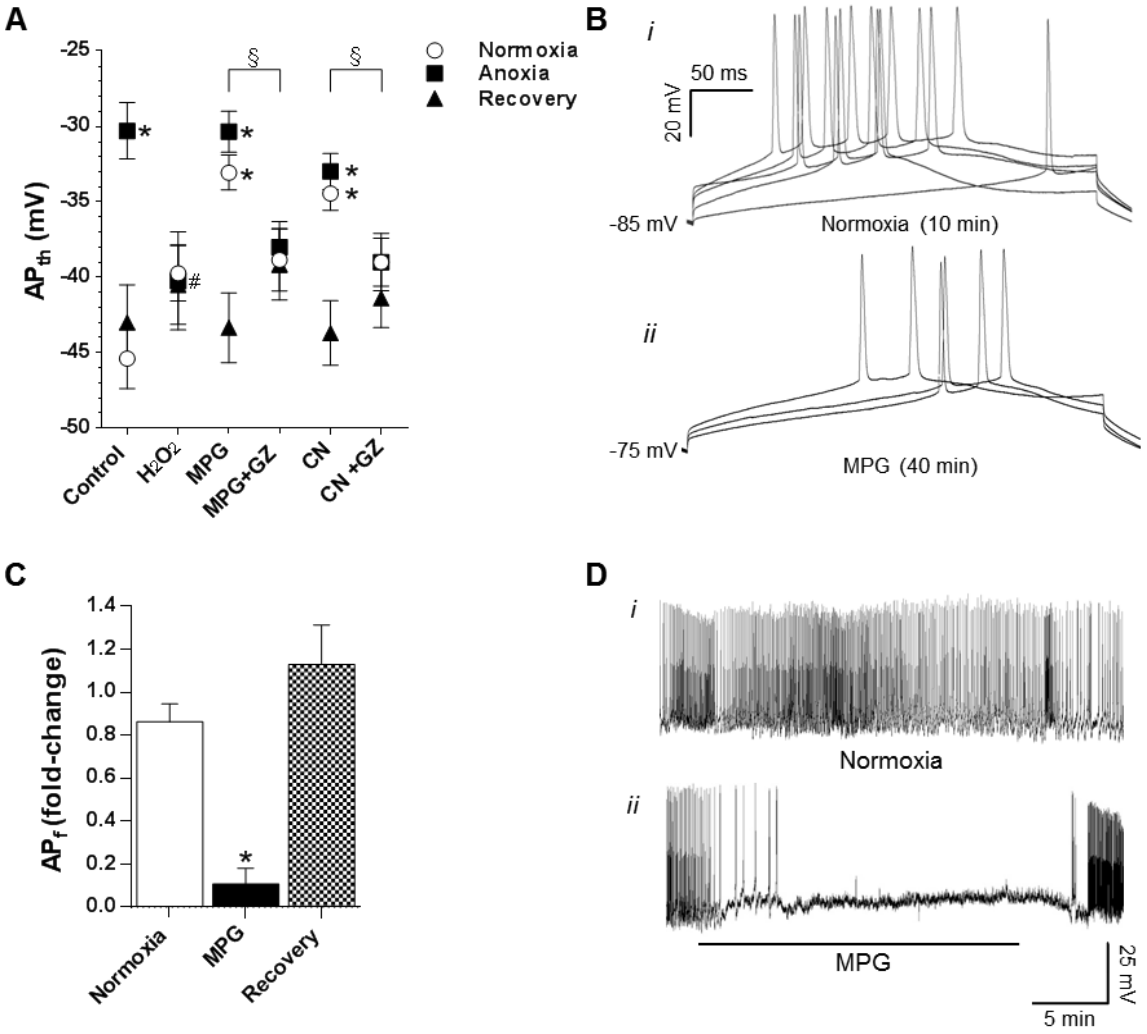

Figure 5.2. Pharmacological or anoxia-mediated decreases in $[ROS]_i$ depolarize AP_{th}; ROS scavenging decreases AP_f in a subset of spontaneously active pyramidal neurons.
(A) Summary graph showing changes in AP_{th} following indicated treatments during transition from normoxia to anoxia and recovery. (B) Sample recordings of APs stimulated by stepwise current injection. (C) Summary of changes in AP_f (Hz) following treatment with the ROS scavenger MPG, and recovery. (D) Sample free running current-clamp recordings of spontaneously firing pyramidal neurons used to generate (C). Black bars represent duration of treatment. Treatments: normoxia 95% O_2/5% CO_2, anoxia 95% N_2/5%, 0.5 mM MPG, 0.5 mM CN, 25 μM GZ, 50 μM H_2O_2. Data are mean ± S.E.M., n = 4-10 separate experiments. Asterisks (*) indicate significant difference from normoxic controls. Pound signs (#) indicate significant difference from anoxic controls. Section symbol (§) indicates significant difference from between indicated anoxic treatments ($P < 0.05$).

pharmacological treatment (n = 4-10; p = 0.508; not shown); therefore, data are compared tonormoxic E_{GABA}. Anoxia depolarized V_m to -77.6 ± 1.5) (n = 9; $p < 0.001$) and it was not different from E_{GABA} (p = 0.986; figure 5.3A, B*ii)*. To determine if decreases in $[ROS]_i$ alone could mimic the anoxic shift in V_m I treated cortical sheets with MPG. Under normoxic conditions MPG treatment depolarized V_m (-77.2 ± 1.4 mV n = 11; $p < 0.001$) to E_{GABA} (p = 0.863; figure 5.3A, B*iii*). Co-treatment with anoxia plus MPG depolarized V_m to -75.3 ± 1.9 mV (n = 11; $p < 0.001$) and V_m was not different from anoxic V_m (p = 0.362) or E_{GABA} (p = 0.336) (figure 5.3A). A subsequent 5 min application of GZ hyperpolarized V_m under normoxic (-83.5 ± 2.8 mV; n = 6; p = 0.018) and anoxic conditions (-85.3 ± 2.1 mV; n = 4; p = 0.001), and hyperpolarized V_m away from E_{GABA} (p = 0.037 and p = 0.019 respectively; figure 5.3A). Since CN-mediated inhibition of complex IV decreases $[ROS]_i$ to a similar extent as anoxia I next tested the effects of CN on V_m and E_{GABA}. CN treatment depolarized V_m (-76.0 ± 2.0 mV; n = 6; $p < 0.001$) and it was not different from E_{GABA} (p = 0.567; figure 5.3A, B*iv*). Co-application of CN and anoxia depolarized V_m compared to normoxic control (-77.0 ± 3.0; n= 5; $p < 0.001$) but not more than anoxia alone (p = 0.855; figure 5.3A). Application of GZ reversed the CN-mediated V_m shift under both normoxic (-83.8 ± 0.9 mV; n = 6; p = 0.009) and anoxic conditions (-84.6 ± 3.0; n = 5; p = 0.026), and V_m was different compared to E_{GABA} (p = 0.028 and p = 0.020 respectively; figure 5.3A). Next I tested whether this effect could be reversed by addition of an oxidant. Application of H_2O_2 did not change V_m under normoxic conditions (-85.3 ± 3.1 mV; n = 4, p = 0.525). However, in anoxic neurons H_2O_2 application hyperpolarized V_m back to normoxic values (-77.5 ± 1.3 to -86.0 ± 1.6 mV; n = 4; p = 0.687; figure 5.3A).

ROS scavengers increase G_w by activating $GABA_A$ receptors.

A GZ-sensitive shift in V_m to E_{GABA} indicates that ROS scavengers activate a $GABA_A$ receptor-mediated shunting current. To confirm this I assessed G_w following perfusion of ROS scavengers or H_2O_2. Compared to normoxia, anoxic treatment caused an increase in G_w from 4.9 ± 0.2 to 7.1 ± 0.4 nS respectively (n = 10 each; $p < 0.001$; figure 5.3C, D). Normoxic MPG treatment increased G_w to 7.5 ± 0.5 nS and this was significantly different from normoxic values (n = 9; $p < 0.001$), but not different from anoxia alone (7.4 ± 0.6 nS; n = 9; p = 0.507). MPG plus anoxia also increased G_w (7.4 ± 0.6 nS; n = 9) but this was not different from anoxia alone indicating activation of a similar pathway (p= 0.578; figure 5.3C, D). Application of GZ to MPG treated normoxic and anoxic neurons decreased G_w to a level not different from normoxic controls (5.6 ±0.4 and 6.0 ±

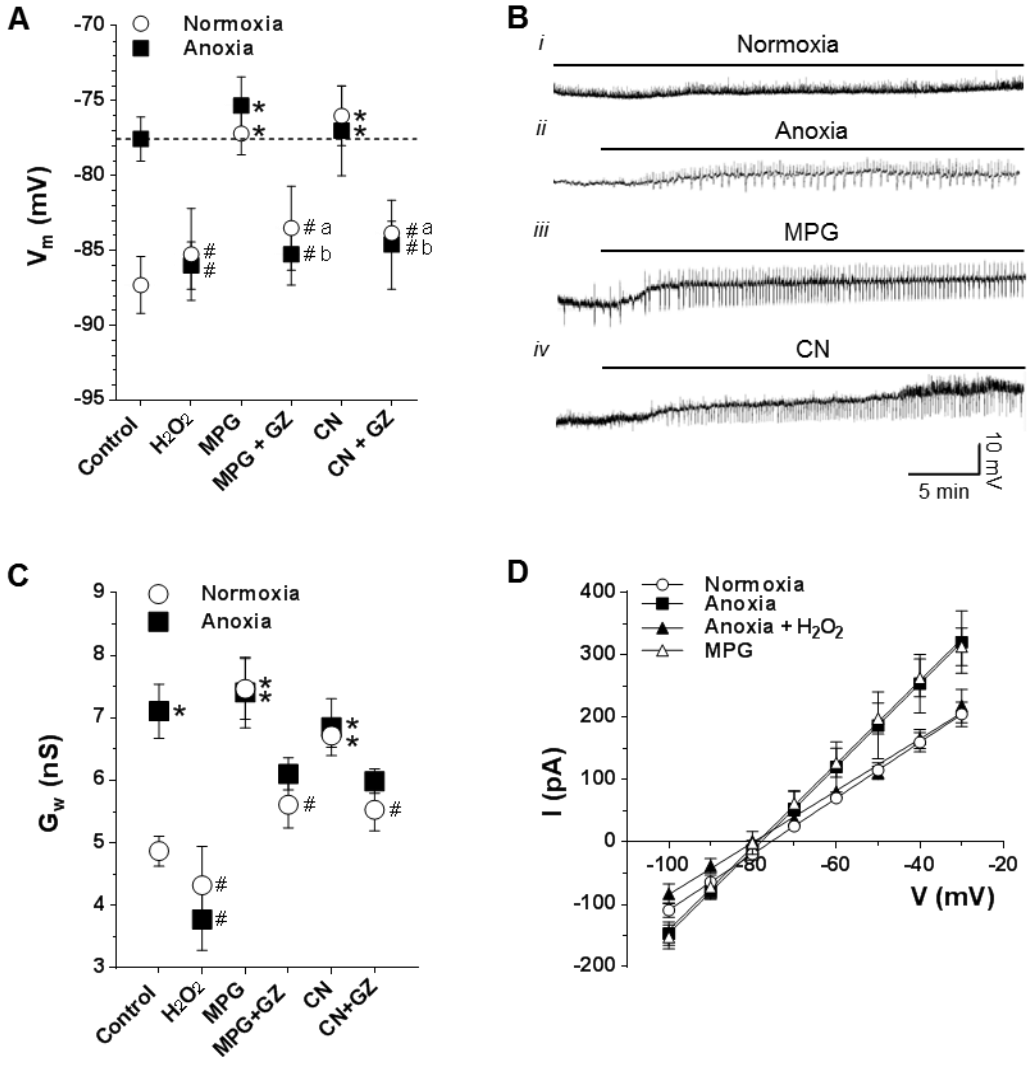

Figure 5.3. Pharmacological or anoxia-mediated decreases in $[ROS]_i$ shift pyramidal neuron V_m to E_{GABA} by activating a GZ-sensitive increase in G_w.

(A) Summary graph showing changes in V_m resulting from indicated treatments, dotted line represents normoxic E_{GABA}. (B) Sample raw traces used to generate (A). Note: spikelets in *ii-iv* are GABAergic gIPSCs. (C) Summary of G_w measured as indicated. (D) I/V relationships from (C). Treatments: normoxia 95% O_2/5% CO_2, anoxia 95% N_2/5% CO_2, 50 µM H_2O_2, 0.5 mM MPG, 25 µM gabazine, 0.5 mM CN. Black bars represent duration of treatment. Data are mean ± S.E.M., n = 4-11 replicates per treatment. Asterisks (*) indicate significant difference from normoxic controls. Dagger (†) indicates significant difference from E_{GABA} in (A). Pound signs (#) indicate significant difference from anoxia in (C) ($P < 0.05$).

0.3 nS, respectively; n = 6 for both; $p = 0.221$ and $p = 0.060$ respectively; figure 5.3C). Under normoxic MPG conditions, GZ treatment caused a statistically significant decrease in G_w ($p = 0.028$); however, under anoxic conditions the decrease was not significant ($p = 0.121$). Compared to normoxic controls CN application increased G_w in normoxic and anoxic neurons (6.7 ± 0.2 and 6.9 ± 0.5 nS; n = 9 each; $p < 0.001$ for both; figure 5.3C); and these values were not different from anoxic controls ($p = 0.472$ and $p = 0.637$ respectively). Subsequent application of GZ to normoxic or anoxic CN treated neurons decreased G_w to levels not different from normoxic controls (4.9 ± 0.5 and 5.3 ± 0.9 nS respectively; n = 6 for both; $p = 0.277$ and $p = 0.067$ respectively); however, G_w values were also not different from normoxic and anoxic CN treatment either ($p = 0.054$ and $p = 0.197$ respectively; figure 5.3C). To test if this effect could be reversed by an oxidant H_2O_2 was applied during normoxia and anoxia. Normoxic H_2O_2 application did not change G_w from normoxic values (4.3 ± 0.6; n = 7; $p = 0.367$; figure 5.3C). However, compared to anoxic control H_2O_2 decreased G_w under anoxic conditions (3.78 ± 0.5 nS; n = 6; $p < 0.001$; figure 5.3C, D).

Decreases in ROS enhance mIPSC frequency

Enhanced GABA transmission can occur through either direct modulation of postsynaptic receptors or by a presynaptic mechanism. To determine which aspects of GABA transmission ROS scavenging regulates we assessed mIPSC amplitude and frequency. Compared to normoxia (-8.2 ± 1.7 pA; n = 6) mIPSC amplitude did not change with anoxia (-5.7 ± 0.9 pA; n = 6) or MPG treatment (-7.8 ± 1.1 pA; n = 6) ($p = 0.369$; figure 5.4A, C). The frequency of mIPSCs was stable within a recording but variable between cells; therefore, this data set was normalized, see methods for details. Compared to normoxia (1.0 ± 0.1; n = 6), anoxia and MPG treatment more than doubled mIPSC frequency (2.4 ± 0.2 and 3.0 ± 0.6 respectively; n = 6 for both; $p = 0.029$ and $p = 0.002$ respectively; figure 5.4B, C; amplitude histograms in figure 5.5).

Decreases in ROS enhance $GABA_A$ receptor sIPSC amplitude

To determine if sIPSCs are sensitive to ROS scavenging and to quantify their roles in GABAergic spike arrest I assessed the effects of ROS depletion on their amplitude and frequency. Spontaneous IPSC frequency did not change following any treatment compared to normoxia (11.1 ± 0.71 Hz; n = 6; $p = 0.431$; figure 5.6A). The amplitude of sIPSCs was stable within a normoxic recording; however, it was variable between cells ranging between -60 to -80 pA. Therefore, this data set was normalized to a previous normoxic segment, see methods for details. Anoxia increased sIPSC

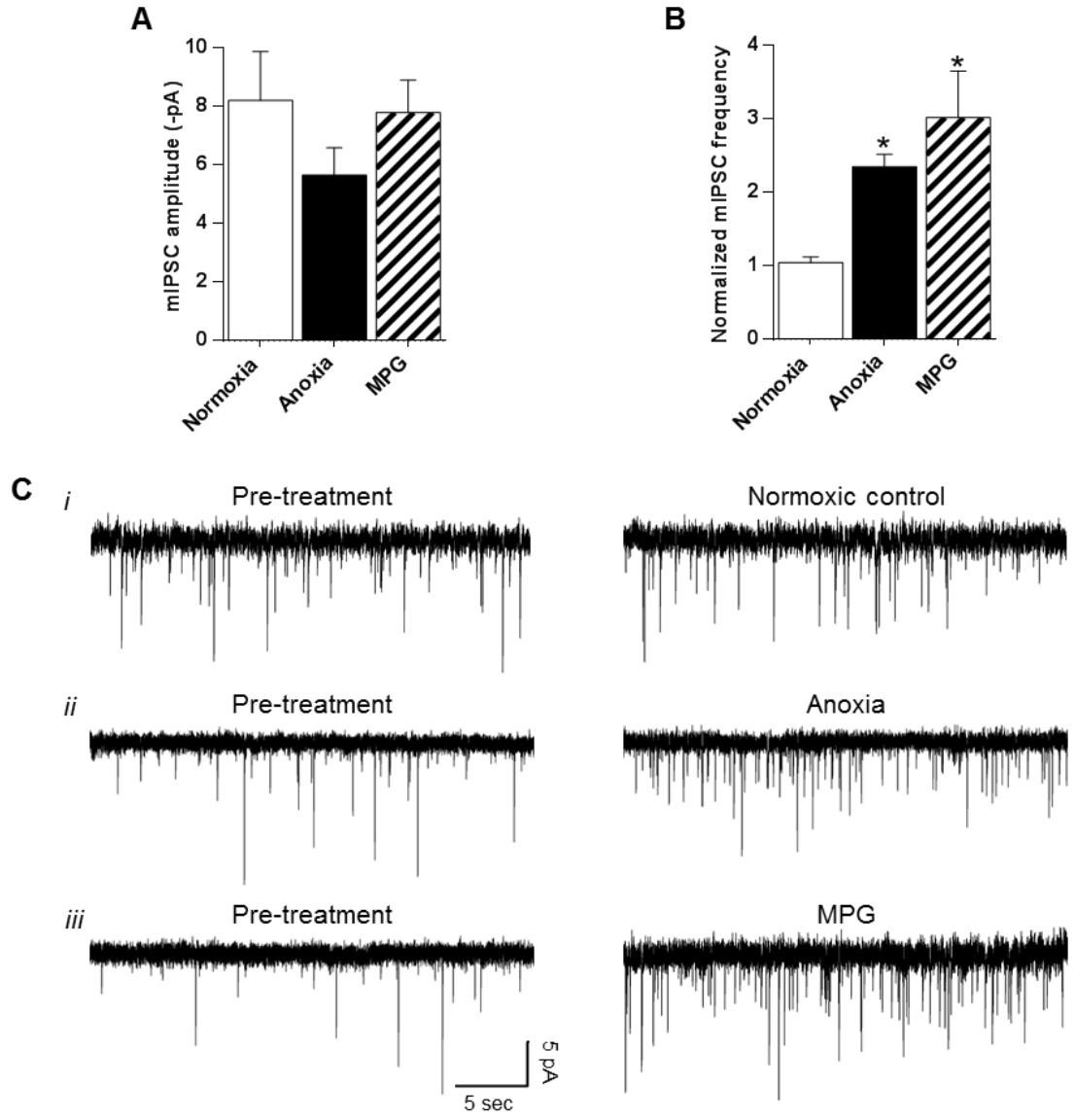

Figure 5.4. Pharmacological and anoxia-mediated decreases in $[ROS]_i$ increase mIPSC frequency but not amplitude in pyramidal neurons.
(A) Summary of mIPSC amplitude following a 30 min treatment with anoxia or the ROS scavenger MPG. (B) Summary of normalized mIPSC frequency under the same conditions as (A). (C) Sample raw traces used to generate (A) and (B). Note: Normoxic pre-treatment (10 min) and treatment (30 min). $GABA_A$ receptor-mediated mIPSCs were enhanced with high $[Cl^-]$ pipette solution (130 mM) and isolated with NMDA and AMPA receptor antagonists (AP5 and CNQX, respectively; 25 μM each), a voltage-gated Na^+ channel inhibitor (TTX; 1 μM), and a glycine receptor antagonist (strychnine; 2 μM). Treatments: normoxia (95% O_2/5% CO_2 bubbled aCSF), anoxia (95% N_2/5% CO_2 bubbled aCSF), MPG (0.5 mM). Data are mean ± S.E.M., n = 6 replicates per treatment. Asterisks (*) indicate significant difference from normoxic controls ($P < 0.05$).

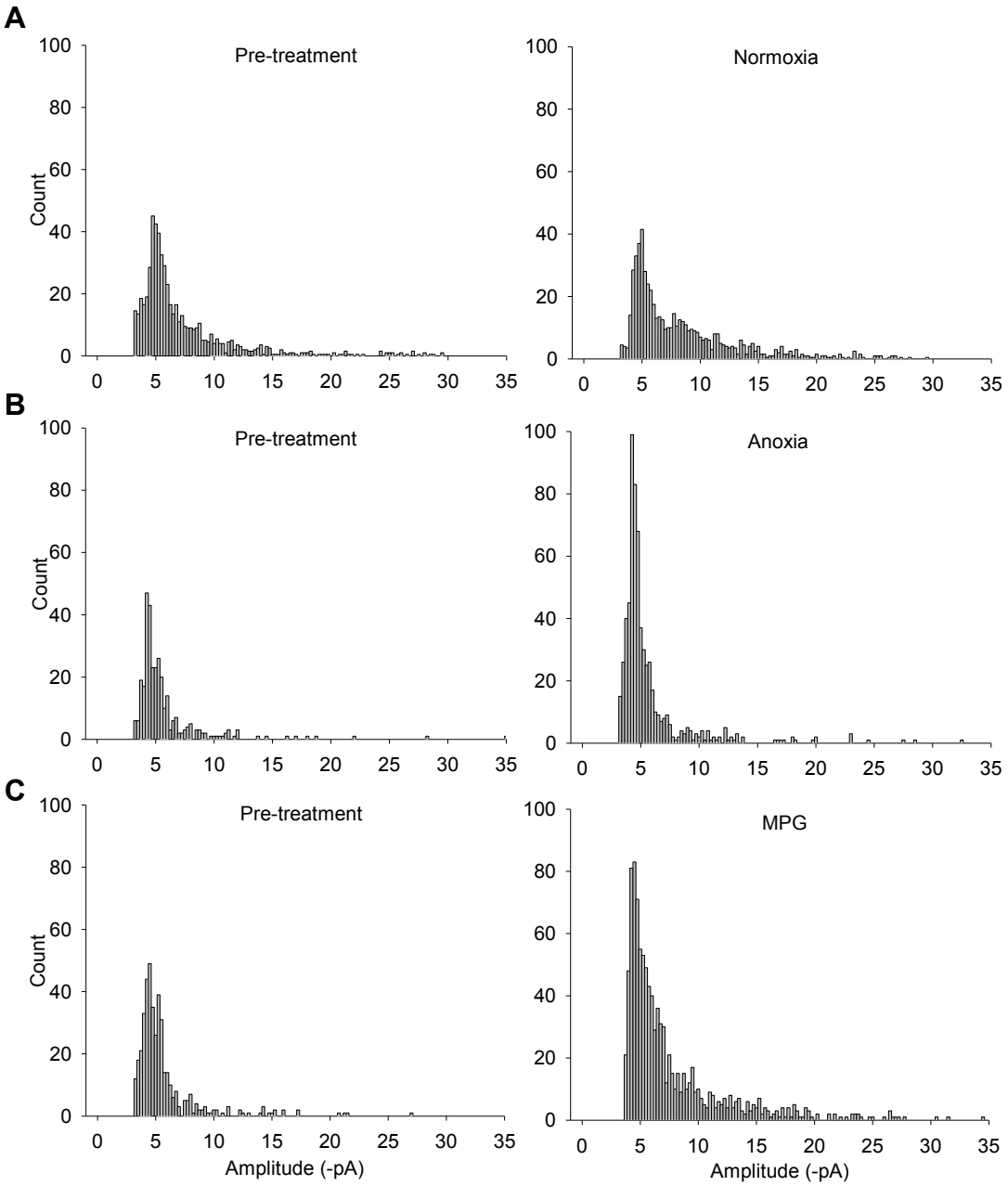

Figure 5.5. Miniature IPSC frequency but not amplitude increases with anoxia and ROS scavenging.

(A-C) Summary amplitude histograms comparing indicated treatment (30 min) to normoxic pre-treatment (10 min). (A) Normoxic control; (B) Anoxia; and (C) MPG. Treatments: normoxia 95% O_2/5% CO_2, anoxia 95% N_2/5%, CO_2, and 0.5 mM MPG. GABAergic mIPSCs were isolated by continuous perfusion of 25 μM AP5, 25 μM CNQX, 1 μM TTX and 2 μM strychnine. To aide in current detection, pipette chloride [Cl^-] was increased to 130 mM and neurons were voltage-clamped at -100 mV. Data are summary of mIPSC events over a 2 min duration, n = 6 replicates per treatment.

amplitude (1.1 ± 0.1 to 1.9 ± 0.1; n = 5 each; $p = 0.006$; figure 5.6B, G*iv-v*) relative to the normoxic control measurements. MPG treatment increased sIPSC amplitude compared to normoxic control (2.0 ± 0.2; n = 7; $p = 0.003$; figure 5.6B). Co-treatment with anoxia plus MPG was not different from anoxia alone (2.1 ± 0.3; n = 7 each; $p = 0.677$; figure 5.6B). CN treatment increased sIPSC amplitude (1.6 ± 0.1; n = 7; $p = 0.044$; figure 5.6B) relative to normoxic control. Co-treatment with anoxia plus CN was not different from anoxia (1.8 ± 0.04; n = 7; and $p = 0.379$; figure 5.6B). Treatment with GZ or BIC eliminated sIPSCs under all treatment conditions (figure 5.6C, G*vi*).

GABA-mediated gIPSC amplitude increases with ROS depletion

Across all treatments the frequency of gIPSCs did not change relative to normoxic frequencies (0.09 ± 0.01 Hz; n = 7; $p = 0.470$; figure 5.6D). Relative to normoxic control (-228.1 ± 11.8 pA; n = 7), anoxia and MPG more than doubled gIPSC peak amplitude (-574.6 ± 93.2 and -515.0 ± 64.0 pA respectively; n = 7 each; $p = 0.013$ and $p = 0.020$ respectively; figure 5.6E, G*i-ii*; amplitude histograms in figure 5.7). Co-application of MPG and anoxia also increased gIPSC amplitude over normoxic control (-675.9 ± 109.4 pA; n = 7; $p < 0.001$) but not more than anoxia alone ($p = 0.397$; figure 5.6E). CN application increased gIPSC amplitude under normoxic (-470.4 ± 52.02 pA; n = 7; $p = 0.047$) and anoxic conditions (-541.0 ± 119.08 pA; n = 7; $p = 0.012$) compared to normoxic control (figure 5.6E, D; figure 5.7). Treatment with GZ or BIC eliminated gIPSCs under all treatment conditions (figure 5.6C, F, G*iii*; figure 5.8C).

Decreases in ROS enhance tonic $GABA_A$ receptor currents

To investigate the role of tonic GABAergic inhibition in anoxia-mediated spike arrest I applied BIC following ROS scavenging treatments. BIC was used to measure tonic $GABA_A$ receptor-mediated currents because the extrasynaptic $GABA_A$ receptors responsible for tonic currents are more sensitive to BIC then they are to GZ (Bai *et al.*, 2001). Under normoxic conditions BIC induced an outward shift in the holding current relative to baseline (19.9 ± 1.9 pA; n = 5; $p = 0.036$; figure 5.8A, C*i*) indicating inhibition of a $GABA_A$ receptor-mediated tonic current. The BIC induced shift in holding current doubled with anoxia and was significantly larger than the normoxic current (40.6 ± 8.2 pA; n = 5; $p = 0.013$; figure 5.8A, C*ii*). Application of BIC to cortical neurons treated with MPG or CN revealed a tonic current that was significantly larger than the normoxic current (43.8 ± 7.3 and 39.0 ± 4.2 pA; n = 5 each; $p = 0.002$ and $p = 0.012$, respectively) but not different from anoxia ($p = 0.666$ and $p = 0.730$, respectively; figure 5.8A, C*iii-iv*).

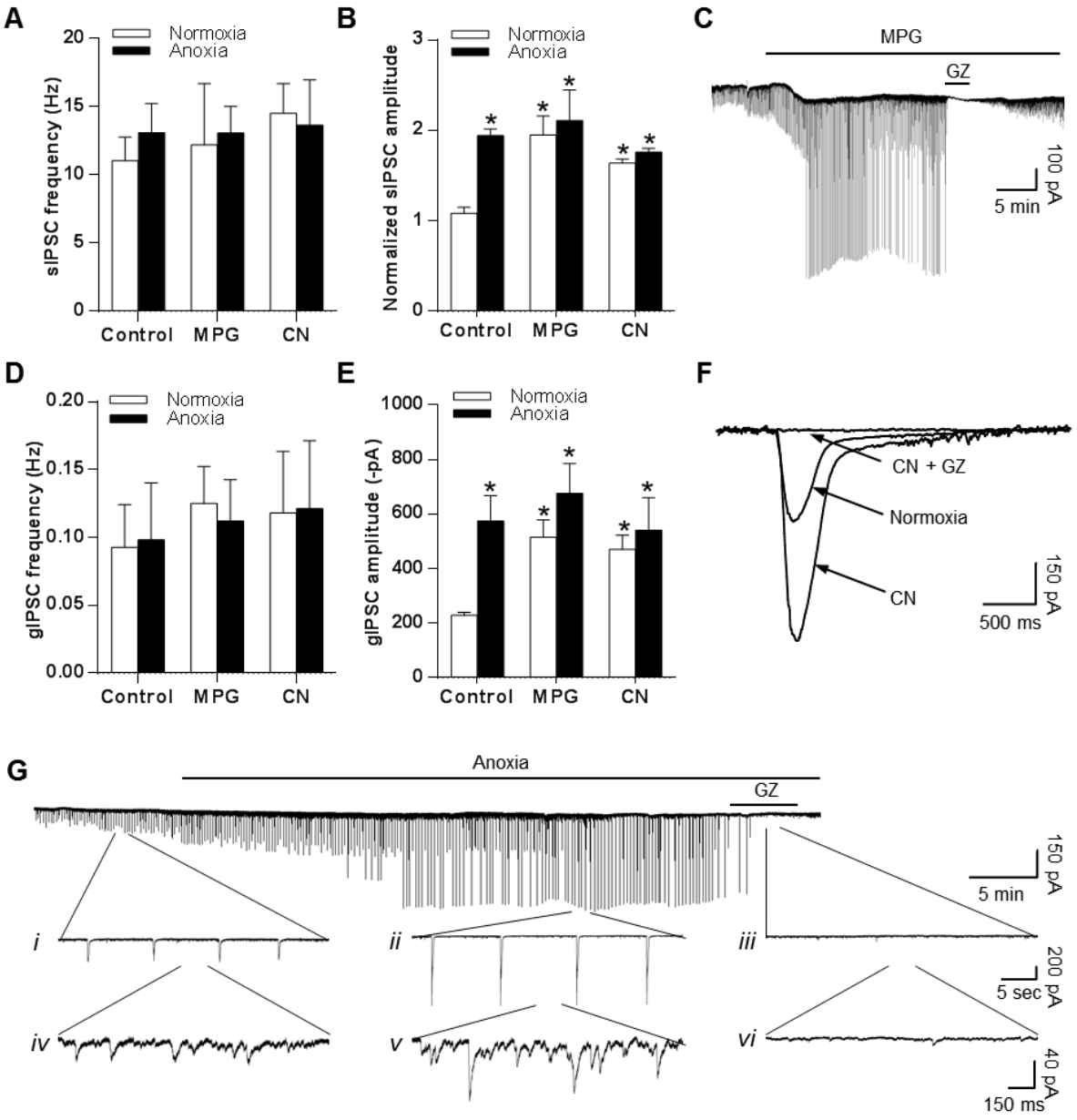
A
sIPSC frequency (Hz)
Normoxia
Anoxia
Control
MPG
CN
B
Normalized sIPSC amplitude
C
MPG
GZ
100 pA
5 min
D
gIPSC frequency (Hz)
E
gIPSC amplitude (-pA)
F
CN + GZ
Normoxia
CN
150 pA
500 ms
G
Anoxia
GZ
150 pA
5 min
i
ii
iii
200 pA
5 sec
iv
v
vi
40 pA
150 ms

Figure 5.6. $GABA_A$ receptor-mediated sIPSCs and gIPSCs are sensitive to pharmacological and anoxia-mediated decreases in $[ROS]_i$ in pyramidal neurons.
(A) Summary of changes in sIPSC frequency in response to indicated treatment. (B) Summary of changes in sIPSC amplitude in response to indicated treatment. (C) Sample raw spontaneous voltage-clamp recording demonstrating MPG-mediated changes in GABA currents. Note: GZ application inhibits all currents demonstrating ROS scavenger-mediated increase in GABA release and activation of $GABA_A$ receptors. (D) Summary of changes in gIPSC frequency in response to indicated treatment. (E) Summary of changes in gIPSC amplitude in response to indicated treatment. (A). (F) Superimposed raw spontaneous gIPSC recordings averaged from 10 events (n = 4 per trace). (G) Sample raw spontaneous voltage-clamp recording demonstrating the change in GABA currents during a transition to anoxia, (*i-iii*) show the effect of anoxia and GZ on gIPSCs, and (*iv-vi*) show the effect of anoxia and GZ on sIPSCs. Cortical sheets were treated with normoxia or anoxia with or without MPG or CN for 30 min. Pyramidal neurons were voltage clamped at -100 mV and $GABA_A$ receptor currents were enhanced with high $[Cl^-]$ pipette solution (130 mM) and isolated with NMDA and AMPA receptor antagonists (AP5 and CNQX, respectively; 25 μM each) Note: due to high pipette chloride, anoxia and ROS scavenging occasionally caused action currents. Black bar denotes treatment duration. Treatments: normoxia (95% O_2/5% CO_2), anoxia (95% N_2/5% CO_2), MPG (0.5 mM), GZ (25 μM), CN (0.5 mM). Data are mean ± S.E.M., n = 5-7 separate experiments. Asterisks (*) indicate significant difference from normoxic controls ($P < 0.05$).

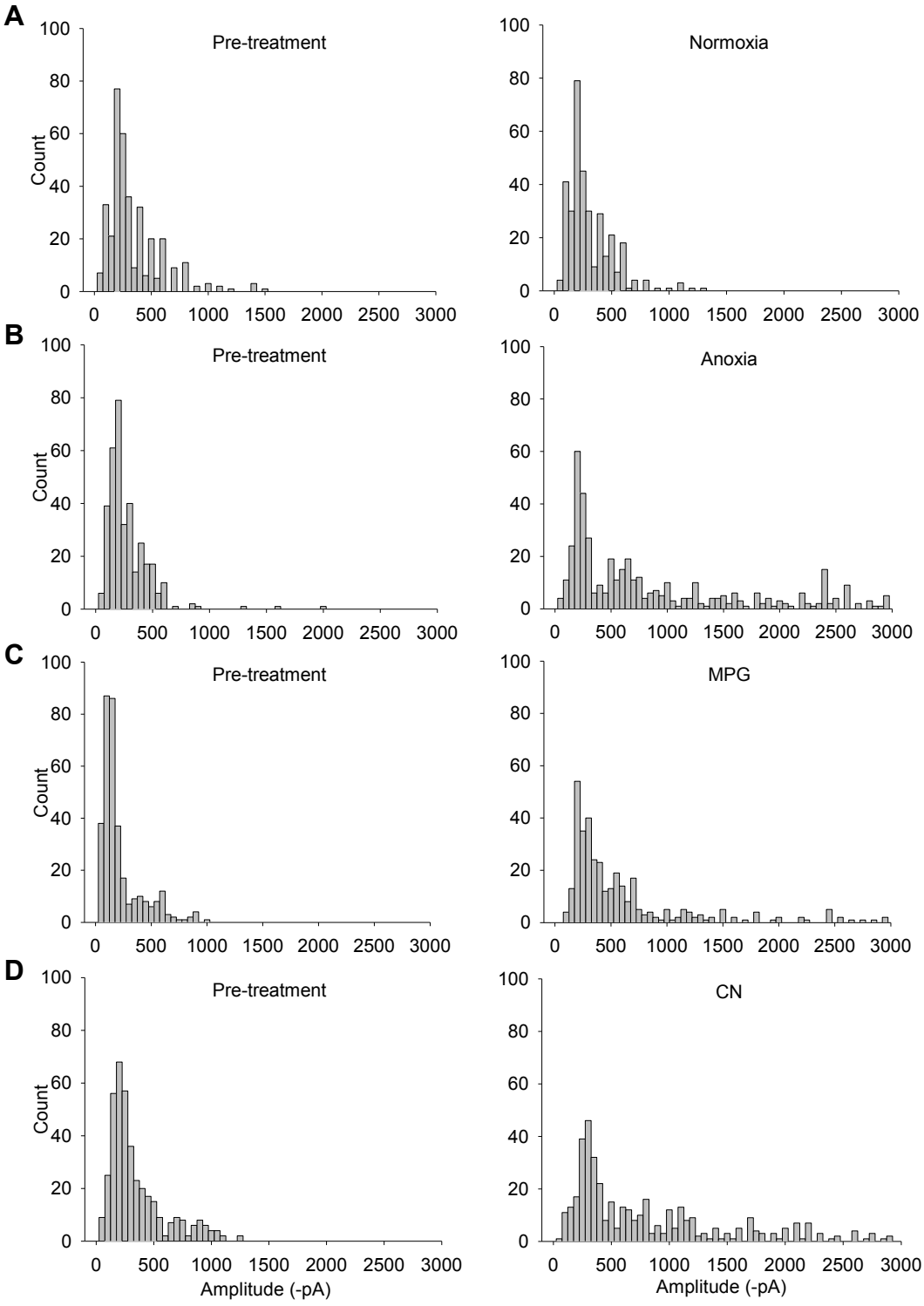

Figure 5.7. Amplitude but not frequency of gIPSCs increases with anoxia and ROS scavenging. (A-D) Summary amplitude histograms (n = 6 each) comparing indicated treatment (30 min) to normoxic pre-treatment (10 min). Pyramidal neurons were voltage clamped at -100 mV and $GABA_A$ receptor currents were enhanced with high [Cl^-] pipette solution (130 mM) and isolated with NMDA and AMPA receptor antagonists (AP5 and CNQX, respectively; 25 μM each). Treatments: normoxia (95% O_2/5% CO_2), anoxia (95% N_2/5% CO_2), MPG (0.5 mM), and CN (0.5 mM).

H_2O_2 inhibits GABA transmission

Since ROS scavenging increases GABA transmission I asked if this effect is reversed by the presence of the oxidant H_2O_2. Following treatment with either normoxia or anoxia, a 5 min application of H_2O_2 completely inhibited sIPSCs and gIPSCs (not shown). Relative to baseline, H_2O_2 induced an outward shift in the holding current under normoxic and anoxic conditions (15.8 ± 2.2 and 33.0 ± 4.2 pA respectively; n = 4 and 5; $p = 0.023$ and $p < 0.001$; figure 5.8B). To assess if GABA transmission can be modulated exclusively by redox agents, H_2O_2 was applied following normoxic MPG or CN treatment. H_2O_2 application abolished MPG or CN-mediated sIPSCs and gIPSCs (see figure 5.8D for MPG example). Relative to baseline, H_2O_2 also induced an outward shift in the holding current in MPG (35.5 ± 5.72 pA; n = 4; $P = 0.006$) or CN treated neurons (31.0 ± 3.1 pA; n = 4; $p = 0.024$; figure 5.8B, D).

Decreases in ROS increase $GABA_A$ receptor-mediated charge transfer

To estimate the relative contribution of GABAergic sIPSC, gIPSC and tonic currents to spike arrest I calculated the charge transfer associated with each current over a 2 min period (figure 5.9A). Under normoxic conditions the charge transfer resulting from sIPSCs was stable for over 30 min (1.1 ± 0.11and 1.2 ± 0.10 μC respectively; n = 6; $p = 0.454$). Anoxia (2.0 ± 0.26 μC; n = 5; $p = 0.012$), MPG (1.8 ± 0.22 μC; n = 7; $p = 0.05$) and CN (2.4 ± 0.60 μC; n = 6; $p < 0.001$) all doubled sIPSC-mediated charge transfer compared to normoxia, consistent with their impact on current amplitude (figure 5.9). Charge transfer resulting from gIPSCs did not change over 30 min of normoxia (1.7 ± 0.23 to 1.7 ± 0.26 μC respectively; n = 7; p = 756) and conducted ~ 50% more current than normoxic sIPSCs. Anoxia (3.3 ± 0.33 μC; n = 7; $p = 0.015$), MPG (3.6 ± 0.63 μC; n = 7; $p = 0.004$), or CN treatment (3.0 ± 0.4 μC; n = 7; $p = 0.04$) doubled charge transfer compared to normoxic gIPSC values (figure 5.9). Charge transfer associated with tonic GABA currents did not change over 30 min of normoxia (2.0 ± 0.12 and 2.4 ± 0.23 μC respectively; n = 7; $p = 151$) and was ~ 40% larger than gIPSCs and ~ 200% larger than sIPSCs under normoxic conditions. Anoxia (4.4 ± 0.78 μC; n = 5; $P = 0.033$), MPG (5.3 ± 0.87 μC; n = 5; $P = 0.004$), or CN treatment (4.7 ± 0.52 μC; n = 5; $p = 0.016$) all doubled charge transfer compared to normoxic tonic GABA currents (figure 5.9). On average charge transfer resulting from tonic currents was ~ 45% larger than gIPSCs and ~ 240% larger than sIPSCs within each treatment condition.

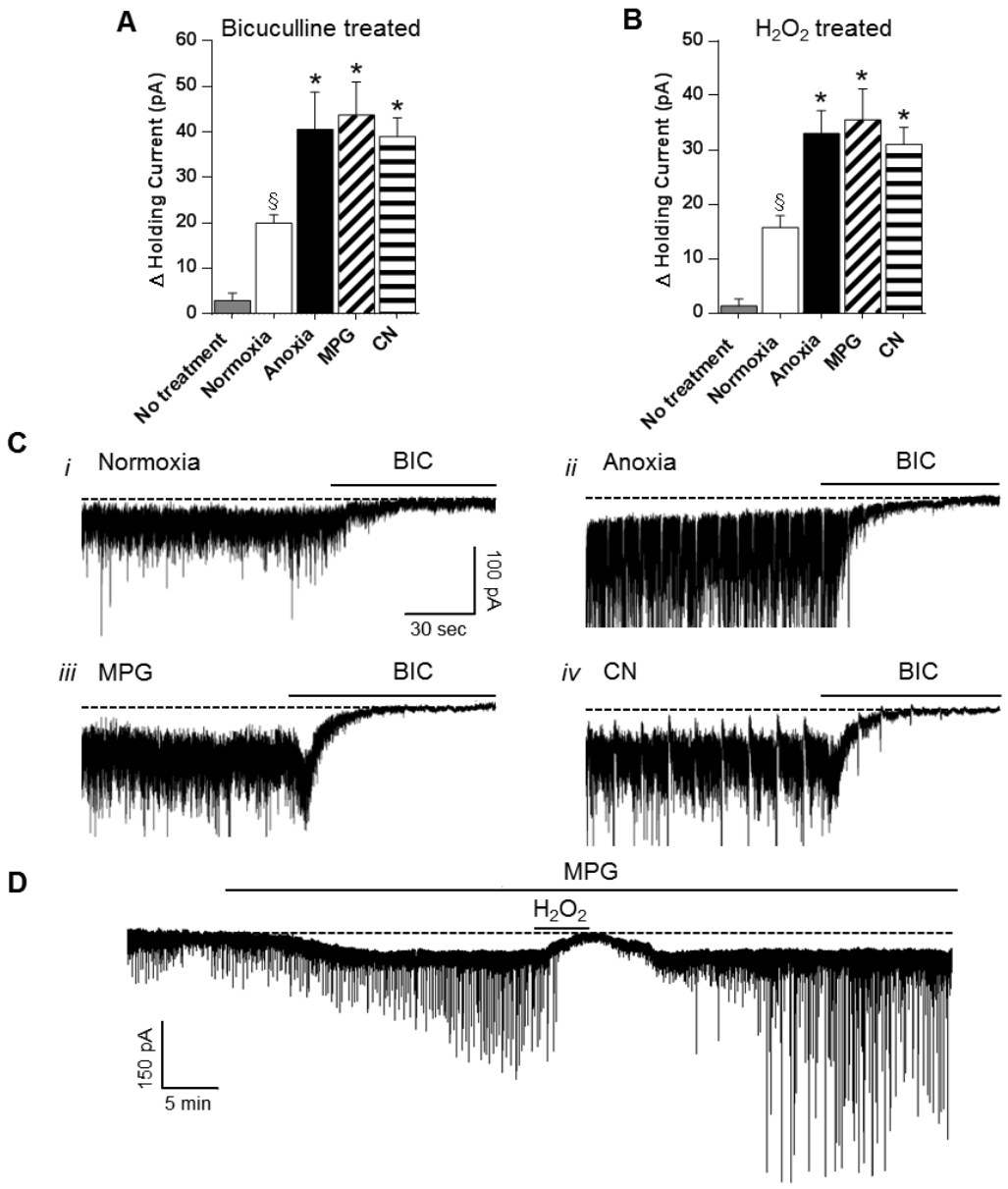

Figure 5.8. $GABA_A$ receptor-mediated tonic currents are modulated by changes in $[ROS]_i$.
(A) Summary of the effects of BIC on tonic $GABA_A$ receptor currents in response to indicated treatment. (B) Summary of the effects of H_2O_2 on tonic $GABA_A$ receptor currents in response to indicated treatment. Note: No treatment (grey bars) in (A) and (B) represent the average change in the holding current prior to application of BIC or H_2O_2, respectively. (C) Sample raw traces used to generate (A). (D) Sample raw trace used to generate (B). Black bar denotes treatment duration. Pyramidal neurons were voltage clamped at -100 mV and $GABA_A$ receptor currents were enhanced with high $[Cl^-]$ pipette solution (130 mM) and isolated with NMDA and AMPA receptor antagonists (AP5 and CNQX, respectively; 25 μM each). Treatments: normoxia (95% O_2/5% CO_2), anoxia (95% N_2/5% CO_2), MPG (0.5 mM), CN (0.5 mM), BIC (100 μM), and H_2O_2 (50 μM). Data are mean ± S.E.M., n = 5-7 replicates per treatment. Section symbol (§) indicates significant difference from baseline. Asterisks (*) indicate significant difference from normoxic controls ($P < 0.05$).

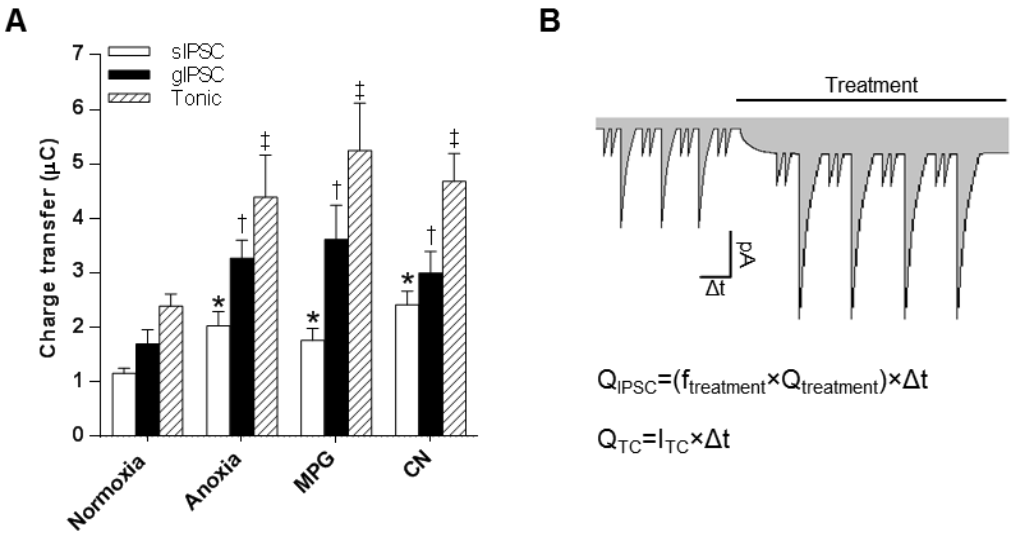

Figure 5.9. Comparison of the pharmacological and anoxia-mediated charge transfer associated with $GABA_A$ receptor-mediated sIPSCs, gIPSCs and tonic currents.
(A) Summary of the cumulated charge transfer resulting from $GABA_A$ receptor sIPSCs, gIPSCs and tonic currents after a 30 min treatment with anoxia, MPG or CN. Note: charge transfer is calculated over a 2 min duration at the end of the treatment period (B) Schematic drawing and equations detail the methods used to calculate charge transfer. Note: grey shading indicates charge transfer associated with $GABA_A$ receptor currents in pyramidal neurons. Charge transfer was calculated from recordings where $GABA_A$ receptor currents were enhanced with high [Cl^-] pipette solution. Black bar denotes treatment duration. For the Q_{IPSC} equation, Q denotes charge transfer (the integrated area under an IPSC (pA × ms)), $f_{treatment}$ is the mean frequency (Hz) of the IPSCs, $Q_{treatment}$ is the mean charge transfer (pC) per IPSC, and Δt is the duration of measurement. For the tonic charge transfer equation I_{TC} is the tonic current (pA) under the indicated treatment. Treatments: normoxia 95% O_2/5% CO_2, anoxia 95% N_2/5%, CO_2, 0.5 mM MPG, 0.5 mM CN. Data are mean ± S.E.M., n = 5-7 replicates per treatment. Asterisks (*) indicate significant difference from normoxic sIPSC. Dagger (†) indicates significant difference from normoxic gIPSC. Double dagger (‡) indicates significant difference from normoxic tonic currents ($P < 0.05$).

5.4 Discussion

In this study, I explore the effects of alterations in $[ROS]_i$ employing three different methods on GABAergic transmission in cortical sheets of an anoxia-tolerant vertebrate. I demonstrate that in turtle cerebrocortex GABAergic transmission is enhanced by pharmacological decreases in $[ROS]_i$ with MPG, and increases in [ROS] with physiological concentrations of H_2O_2 inhibits it. CN-mediated inhibition of mROS generation by inhibition of complex IV of the mitochondrial ETC mimics the effects of both anoxia and pharmacological ROS scavenging, indicating that mitochondria are an *in situ* oxygen sensor capable of enhancing GABAergic transmission. GABA-mediated spike arrest is a critical component of the turtle's anoxia-tolerance strategy and these results identify a unique redox sensitive inhibitory signalling pathway that enables survival during prolonged anoxic stress.

During normoxia, ROS levels are maintained by the balance between ROS-generating and natural ROS-scavenging pathways (Pitlik *et al.*, 2009). Under anoxic conditions however, oxygen is rapidly metabolized by mitochondria resulting in a decrease in $[ROS]_i$ which can modulate ROS-sensitive signalling pathways by shifting cellular redox state. In turtle, this is confirmed by our fluorescent measurement of $[ROS]_i$ which shows ROS generation is inhibited after ~ 10 min of anoxia, and agrees with measurements of bath chamber PO_2 which decreases to ~ 0 mmHg within the same time frame (Dukoff *et al.*, 2014). It is therefore unlikely that there is a significant source of ROS in anoxic neurons and proteins are expected to be in a reduced state or at least not encountering oxidative signals. The free radical scavenger MPG neutralizes ROS as they are generated and provides a general indication of the role of ROS in biological processes. In this study I used MPG to assess the sensitivity of $GABA_A$ receptors to decreases in $[ROS]_i$. The effectiveness of MPG at removing $[ROS]_i$ in turtle cerebrocortex has previously been confirmed (Dukoff *et al.*, 2014); however, as a thiol-based ROS scavenger it may not accurately replicate the physiological effects of ROS under anoxic conditions since MPG may directly reduce cysteine residues on redox-sensitive proteins. However, this is unlikely for two reasons. First, the anoxic application of MPG did not alter the time course or the magnitude of the decrease in $[ROS]_i$. Second, CN which does not directly modulate cysteine residues mimics both anoxia and MPG-mediated changes in CM-DCF fluorescence. An important, although expected finding from this study is that CN application

prevents mROS generation under normoxic conditions indicating that the mitochondrion is the major source of ROS in turtle cortical sheets.

Rather than ROS, it is possible that the anoxic inhibition of mitochondrial ATP production might instead be the signal behind increased GABA transmission since decreases in $[ATP]_i$ and $[ROS]_i$ both occur under anoxic conditions. In particular, one candidate-signalling molecule that increases during anoxia is the ATP metabolite adenosine. In anoxic turtle brain, ATP breaks down into adenosine resulting in increases in $[adenosine]_e$, and this adenosine signal has been identified as a protective neuromodulator in turtle brain (Nillsson & Lutz, 1992). In vertebrate brain adenosine acts as an inhibitory neuromodulator that can decrease neuronal excitability (Bickler & Buck, 2007), and enhance GABA release through agonism of presynaptic adenosine A_{2A} receptors (Shindou *et al.*, 2002). However, decreases in mitochondrial ATP production and increases in extracellular adenosine likely do not initiate enhanced GABA release in anoxic turtle brain for two main reasons. First, the timeline of anoxia induced changes in GABA transmission and ATP/adenosine do not match. In anoxic turtle brain GABA release is enhanced by ~10-20 min of anoxic treatment while $[adenosine]_e$ and $[ATP]_i$ are maintained for ~ 60 min through an increase in anaerobic glycolysis and decreased ATP consumption (Nillsson & Lutz, 1992; Buck *et al.*, 1998). It is important to mention that after 60 min of anoxia $[ATP]_i$ does decrease (~ 20%), and at that time changes in adenylate concentrations are likely relevant neuroprotective molecules (Buck *et al.*, 1998). Second, under normoxic conditions ROS scavenging enhances GABA receptor currents even though oxidative phosphorylation and presumably ATP generation is functional. Another potential competing signal is intracellular acidification resulting from net ATP hydrolysis and anaerobic glycolysis, since in turtle brain intracellular pH decreases by 0.5 or more pH units during anoxia (Buck *et al.*, 1998). However, this is also not likely since ROS scavenger-mediated changes in GABA transmission occur during normoxia when normal pH levels are maintained. Therefore, together these data indicate that decreases in ROS rather than ATP or pH are the inhibitory signal behind increased GABA transmission.

In support of a redox-sensitive GABAergic spike arrest mechanism I demonstrate that under normoxic conditions the pharmacological elimination of ROS induces shunting inhibition by clamping V_m to E_{GABA}. Similar to anoxia, this is likely the result of a $GABA_A$ receptor-mediated increase in G_w because application of GZ decreases G_w and reverses V_m. The inability of GZ to fully reverse MPG and CN-induced changes in G_w is likely the result of the incomplete inhibition

of extrasynaptic $GABA_A$ receptors by GZ (see below). ROS scavenging did not have an effect on E_{GABA}; therefore, GABAergic spike arrest is not the result of modulation of Cl^- regulatory machinery (e.g. KCC2 and NKCC1). Anoxia plus MPG did not have additive effects indicating ROS scavenging and anoxia activate a similar mechanism. Importantly, ROS scavenging alone has the capacity to decrease $AP_f \sim 90\%$ providing direct evidence that decreases in $[ROS]_i$ can initiate spike arrest. Application of H_2O_2 reversed anoxia-induced changes in G_w and V_m indicating that GABA transmission is suppressed by the presence of a strong oxidant. Activation of the $GABA_A$ receptor-mediated electrical shunt by inhibition of mROS generation with CN indicates that anoxic decreases in $[ROS]_i$ likely induces GABA-mediated spike arrest and supports the conclusion that spike arrest results from a mitochondrial based oxygen sensing mechanism.

To determine if GABA release is potentiated by decreases in ROS I measured changes in mIPSC frequency. I found that ROS scavenging and anoxia increase mIPSC frequency 2-3 times indicating GABA release is redox-sensitive. Since vesicular GABA release is primarily Ca^{2+}-dependent, under these experimental conditions a change in mIPSC frequency indicates an increase in presynaptic $[Ca^{2+}]$ (see below for possible mechanisms) (Trigo *et al.*, 2010). Miniature IPSC frequency could also increase as a result of a redox-sensitive insertion of $GABA_A$ receptors into the postsynaptic membrane. This has been shown to occur through Ca^{2+}/calmodulin-dependent protein kinase II phosphorylation of the $GABA_A$ receptor (Saliba *et al.*, 2012). The amplitude of mIPSCs did not change following anoxia or ROS scavenging which indicates that postsynaptic GABA receptors are not redox modulated (Trigo *et al.*, 2010). This is an unexpected finding since GABA transmission has been shown to be redox-sensitive with reducing agents potentiating $GABA_A$ receptors and oxidizing agents inhibiting them (Amato *et al.*, 1999; Calero *et al.*, 2011).

The increase in sIPSC and gIPSC amplitudes could also be the result of an increase in redox-sensitive GABA release. Under anoxic or ROS depleted conditions increased GABA release would lead to temporal synchronization of inhibitory events across multiple synapses and summation of IPSC amplitude. This is particularly evident with sIPSCs which occur at a high frequency (13-14 Hz). Giant IPSCs are a unique $GABA_A$ receptor current in turtle pyramidal neurons with characteristics similar to giant depolarizing potentials in neonatal brain (Ben-Ari *et al.*, 2007) or $GABA_{A,slow}$ currents (Capogna & Pearce, 2011). Giant IPSCs are likely the result of network-driven polysynaptic events because gIPSC frequency does not change and currents last hundreds

of milliseconds. This fits with a redox-sensitive GABA release mechanism because increased simultaneous release of GABA onto dendrites of pyramidal neurons would result in an increase in gIPSC amplitude during anoxia or ROS depletion.

Previously I reported that there is no tonic GABA current in anoxic turtle pyramidal neurons (Chapter 2). In that study I used GZ (25 μM) to antagonize the extrasynaptic $GABA_A$ receptors responsible for tonic currents. Extrasynaptic $GABA_A$ receptors have a different subunit composition than synaptic $GABA_A$ receptors which influences antagonist binding and is the likely reason GZ did not reveal a tonic current (Bai *et al.*, 2001). In this study I applied BIC and determined that there is a tonic GABAergic current under normoxic conditions and this doubles in amplitude following anoxia or ROS scavenging. Importantly, inhibition of mROS generation with CN also doubled this current indicating extrasynaptic $GABA_A$ receptor currents are also regulated by an mROS associated signalling pathway. This finding is consistent with a redox-sensitive increase in GABA release resulting from enhanced synaptic GABA spillover or volume transmission. The analysis of the charge transfer is an important component of this study because it allows a direct comparison of the relative contribution associated with each $GABA_A$ receptor current. This analysis determined that tonic currents are responsible for 45-50% of the total GABAergic charge transfer under all treatment conditions. This highlights the important inhibitory role of extrasynaptic $GABA_A$ receptors during anoxia-mediated spike arrest and shows how tonic GABAergic inhibition is an effective mechanism through which to clamp V_m at E_{GABA}.

In turtle cerebrocortex, GABAergic stellate interneurons are the principal inhibitory neurons responsible for modulation of pyramidal neuron activity (Connors & Kriegstein, 1986); and therefore, the most likely site of a redox-sensitive GABA release mechanism. Enhanced GABA release from stellate interneurons likely results from activation of a local oxygen-sensing mechanism because anoxia and redox-sensitive changes in GABA transmission occur in isolated cortical sheets. Glutamate receptor antagonists do not block GABA transmission indicating that glutamatergic input or feedback excitation from pyramidal neurons is not involved in this mechanism. This is interesting because stellate interneurons receive feedback from pyramidal neurons (Colombe *et al.*, 2004); however, it is possible that the downregulation of glutamatergic signalling during anoxia prevents this (Shin & Buck, 2003). Although the mechanism responsible for oxygen-sensitivity has yet to be elucidated this evidence indicates that in turtle cerebrocortex

the stellate interneuron/pyramidal neuron network is an important inhibitory control point for dampening electrical activity during anoxia.

Mitochondria are appropriately positioned to function as oxygen-sensors and initiators of redox based signalling cascades because they are the primary consumer of cellular oxygen and the most ubiquitous source of cellular ROS (Chen *et al.*, 2003). The presynaptic localization of mitochondria at the membrane and the ROS-sensitive modulation of GABAergic transmission suggest that anoxic decreases in mROS production are a likely signal to initiate GABA-mediated spike arrest. In addition, since $[ROS]_i$ fluctuate with oxygen availability, changes in mROS production could function as an oxygen sensor. Importantly, ROS-mediated signalling would occur simultaneously throughout the brain; and since this mechanism does not require energy during a time when cellular ATP is limited, it constitutes a metabolically inexpensive signal to coordinate the down-regulation of energy consuming processes on a broad scale.

In mammals, several ion channels have been identified as redox-sensitive including voltage-gated potassium channels (Muller & Bittner, 2002), and ATP-sensitive potassium channels (Bao *et al.*, 2009). Since K^+ channel activity has a large influence on V_m, decreases in $[ROS]_i$ could inhibit potassium channels resulting in V_m depolarization and increased GABA release. For example, in pulmonary arteries, hypoxic vasoconstriction is mediated in part by the inhibition of redox-sensitive K^+ channels leading to depolarization of V_m and opening of L-type Ca^{2+} channels (Archer & Michelakis, 2002). In turtle stellate interneurons, a similar mechanism could result in increased GABA release. Alternatively, in turtle pyramidal neurons anoxia depolarizes mitochondrial membrane potential leading to Ca^{2+} release and inhibition of NMDA receptors through a protein phosphatase 1 and 2A-mediated pathway (Shin *et al.*, 2005). Since this Ca^{2+} signal is an integral component of the anoxia tolerance strategy in pyramidal neurons it is possible that it also occurs in presynaptic GABAergic nerve terminals resulting in increased GABA release. A number of second messenger signalling molecules are also redox-sensitive including: PKC (Chu *et al.*, 2003); protein kinase A (PKA) (Humphries *et al.*, 2005); protein kinase G (Burgoyne *et al.*, 2007); protein tyrosine kinase (Klann & Thiels, 1999); tyrosine phosphatase 1B (Denu & Tanner, 1998); protein phosphatase 2A and 2B (Klann & Thiels, 1999); and G proteins (Nishida *et al.*, 2000). Activation of any of these signalling intermediates has the potential to initiate signalling cascades and modulate neuronal firing characteristics via indirect ion channel modification. This is plausible since turtle pyramidal neurons express an oxygen-sensitive Ca^{2+}-activated potassium channel that

is inhibited by a PKC-mediated mechanism that could be regulated by $[ROS]_i$ (Chapter 4; Rodgers-Garlick *et al.*, 2013).

In summary, I have demonstrated that in turtle cerebrocortex GABA release is redox-sensitive and that decreases in $[ROS]_i$ are sufficient and necessary to induce GABAergic spike arrest. Spontaneous IPSCs, gIPSCs and tonic GABA currents all contribute to spike arrest; however, tonic currents are responsible for the majority of charge transfer. I have established that decreases in mitochondria ROS generation are capable of initiating GABA-mediated spike arrest, highlighting a unique ROS-mediated signalling mechanism in a naturally anoxia-tolerant vertebrate. I propose a signalling mechanism in which anoxic decreases in mROS generation activates GABAergic stellate interneurons initiating increased GABA release and inhibition of glutamatergic pyramidal neurons. Further elucidation of this mechanism will lead to a better understanding of redox-sensitive GABA transmission in an anoxia-tolerant vertebrate brain and could potentially produce medically relevant protective measures against anoxic or hypoxic insults in mammalian brain.

6 General discussion and concluding remarks

One of the first recorded scientific studies into the anoxia-tolerance of freshwater turtles dates back over 80 years (Johlin & Moreland, 1933). It was in these studies that turtles were first described as being very tolerant to breathing pure nitrogen, "more so then frogs or newborn mice", and they were considered a useful model organism to work with due to their higher blood volume which aided in analysis of blood sugar and lactic acid measurements. Since those pioneering studies there have been major advancements toward understanding the physiological processes that govern anoxia-tolerance in turtle, and the freshwater turtle is beginning to be more widely recognized as an important model organism through which to investigate natural mechanisms of tolerance to low oxygen. My research has focused on neuroprotective adaptations in the cerebrocortex, and in particular the effects of anoxia on pyramidal neurons because these are the primary excitatory neurons; and therefore, suppressing their activity will reduce the metabolic demands of the brain. Through my research I have been able to advance our understanding of these mechanisms by identifying oxygen-sensitive ion channels and by characterizing the effect of enhanced GABAergic transmission that underlies electrical inhibition in anoxic turtle cerebrocortex. In the remaining section I will discuss my contributions to elucidating the neuroprotective mechanisms leading to channel arrest and spike arrest, and I will conclude with a summary of the pathways involved in protecting turtle brain during anoxia.

When I started my doctoral research I knew that GABAergic neurotransmission was a key component of the turtle's anoxia-tolerant strategy because of the rapid elevation in brain GABA observed during anoxia (Nilsson & Lutz, 1991), and because pharmacological antagonism of $GABA_A$ and $GABA_B$ receptors induced hyperexcitability and cell death (Pamenter *et al.*, 2011). However, the mechanism through which low oxygen levels are sensed in isolated brain sheets and the signalling pathways involved in enhancing GABAergic transmission, as well as the specific effects of GABA on postsynaptic pyramidal neurons were unknown. Since neurotransmission can be modulated by both presynaptic release of transmitter and postsynaptic receptor dynamics it was important to characterize the effects of anoxia on both of these aspects of inhibitory GABA transmission. To investigate the effects of anoxia on presynaptic GABA release I used high Cl^- loaded pyramidal neurons as reporter cells to measure changes in presynaptic release. These experiments identified a unique sphasic $GABA_A$ receptor-mediated giant IPSC and provided the first measurements of anoxia-mediated increases in synaptic GABA release in turtle cerebrocortex.

To confirm that increased GABA release mediates spike arrest I investigated the effect of enhanced GABA transmission on postsynaptic pyramidal neurons. I corroborated previous findings that V_m depolarizes following anoxic perfusion and that this is the result of a $GABA_A$ receptor-mediated increase in whole-cell permeability to Cl^-. This evidence suggested that V_m was shifting to E_{GABA}; however, I needed to confirm this hypothesis. Using perforated patch clamp techniques I measured E_{GABA} and demonstrated that indeed the anoxic increase in G_{Cl} depolarizes V_m to E_{GABA} and induces shunting inhibition. It is important to note that this was the first published measurement of E_{GABA} in a reptile neuron, or an anoxia-tolerant neuron, and it indicates that depolarizing shunting inhibition is more effective than hyperpolarizing inhibition for reducing energy expenditure under anoxic conditions. This is likely because there is a lower ATP demand by membrane ion pumps at a depolarized V_m and because shunting inhibition depolarizes AP_{th} resulting in an increased depolarizing stimulus required to reach threshold.

Once I demonstrated that spike arrest was the result of enhanced synaptic GABA release and activation of postsynaptic $GABA_A$ receptors, the next step was to identity the oxygen sensor and signalling pathway(s) involved in initiating increased GABA release. An ideal candidate for an oxygen sensor in cerebrocortical neurons are mitochondria because they are ubiquitously distributed throughout neurons of the brain, they respond to changing PO_2, and anoxia induced Ca^{2+} release from the mitochondrial matrix had already been shown to initiate channel arrest of glutamate receptors (Pamenter *et al.*, 2008c; Zivkovic & Buck, 2010; Hawrysh & Buck, 2013). Since intracellular ROS decreases with anoxia and CN application (Chapter5; Pamenter *et al.*, 2007) I was interested in whether this could be a signal to increase GABA release. To test this I assessed the effect of anoxia and ROS scavenging on mIPSC activity to determine if GABA release is redox-sensitive. Under these conditions the frequency of mIPSCs increased supporting a redox-sensitive mechanism behind anoxic GABA release in turtle cerebrocortex. Again, this was the first measurement of anoxia-mediated changes in GABAergic mIPSCs in turtle brain. This finding was supported by increases in sIPSC and gIPSC amplitude following ROS scavenging. Application of the mitochondrial ETC inhibitor CN mimicked anoxia and ROS scavenging indicating that decreases in mitochondrial ROS generation is a sufficient signal to activate increased GABA release. Similar to anoxia, ROS scavengers and CN also enhanced a tonic $GABA_A$ receptor current and this was inhibited by application of H_2O_2 indicating that GABA release is reversibly regulated by ROS. Interestingly, while there are examples of a ROS-mediated upregulation of GABAergic

transmission in mammals (Chen & Pan, 2007; Yowtak *et al.*, 2011), this is the first example where a decrease in ROS has been found to increase GABA release. Importantly, the increased GABA release that results from modulation of $[ROS]_i$ mimicked anoxic shunting inhibition in pyramidal neurons supporting a role for mitochondria as the oxygen sensor responsible for initiating spike arrest.

An important finding from these studies was the discovery of $GABA_A$ receptor-mediated *giant* IPSCs. These currents are important not only because they are oxygen-sensitive inhibitory currents that prevent APs during anoxia but also because they provide important information about the mechanism behind GABAergic spike arrest. Since these gIPSCs occur at a fixed frequency in pyramidal neurons throughout the cerebrocortex, and IPSC duration is hundreds of milliseconds, they are presumably the result of the activation of multiple GABAergic synapses by a network of GABAergic interneurons. Giant IPSCs are strikingly similar to the GABA-mediated giant depolarizing potentials (GDPs) that dominate neural activity during early development (Ben-Ari *et al.*, 1989). Indeed, both occur at ~ 0.1 Hz, and are of similar duration (~ 300 ms) (Ben-Ari, 2002). This suggests that in turtle gIPSPs may actually be a retained form of GDPs that have been reassigned to induce electrical suppression and enable anoxia-tolerance. Stellate interneurons are the likely source of this GABA since they are the main GABAergic neurons in the cerebrocortex. Additional support includes the finding that stellate interneurons rhythmically fire bursts of APs, which increase in number of APs per burst with anoxia (Hogg, unpublished). The temporal occurrence of these AP bursts matches that of the gIPSCs in pyramidal neurons indicating that stellate neurons may be the putative oxygen sensing cells in turtle cerebrocortex. Application of NMDA and AMPA receptor antagonists do not block gIPSCs indicating that upstream input from glutamatergic neurons or glutamatergic feedback excitation does not play a role in anoxic increases in GABA release. It is possible that during normoxia stellate activity is inhibited by unknown upstream oxygen sensitive GABAergic neurons, in which a decrease in GABA release during anoxia leads to increased stellate GABA release onto pyramidal neurons (disinhibition). What we do know is that the voltage-gated sodium channel blocker TTX prevents gIPSCs indicting that anoxia signalling involves depolarization of presynaptic nerve terminals and AP-mediated GABA release.

Under voltage-clamp conditions, the large anoxia-mediated increase in gIPSC amplitude indicates this inhibitory mechanism is an important component of the turtle's defense strategy; however, the

specific purpose of these giant releases of GABA has yet to be confirmed. I demonstrated that under physiological conditions V_m shifts to E_{GABA} and gIPSPs become very small; indicating that under anoxic conditions it is activation of extrasynaptic $GABA_A$ receptors and tonic GABA currents, not synaptic $GABA_A$ receptors, which are responsible for shunting inhibition. Therefore, I propose that a major function of the *giant* release of GABA responsible for gIPSCs is to overwhelm synaptic GABA uptake mechanisms resulting in the escape of GABA from the synapse and activation of extrasynaptic $GABA_A$ receptors. This would have the additional effect of activating presynaptic $GABA_B$ receptors on glutamatergic synapses leading to the decrease in glutamatergic activity observed during anoxia. Another potential mechanism for activation of extrasynaptic $GABA_A$ receptors is an anoxia-mediated increase in volume transmission from local GABAergic neurons which could occur concurrently with other GABA release mechanisms; however, this possibility has not been investigated.

Another significant outcome from these studies is the finding that decreases in mROS generation is linked to enhanced GABAergic transmission in anoxic turtle cerebrocortex. These studies identify anoxic decreases in mROS and subsequent decreases in intracellular ROS as an important signal to initiate GABAergic spike arrest. This finding is important not only because it sheds light on the signalling pathways behind increased GABA release, but also because it supports our previous hypothesis that mitochondria are putative oxygen sensors in the turtle cerebrocortex. Furthermore, it demonstrates the versatility of the mitochondria as an oxygen sensor since they can initiate neuroprotective signal cascades simultaneously in both the presynapse and postsynapse. While it is possible that there may be several independent oxygen sensing systems in the turtle brain, the findings from the studies presented in this thesis strongly support the mitochondria as a major oxygen sensor and neuroprotective signalling organelle.

The discovery that turtle cerebrocortex is resistant to an ischemic solution that mimics the penumbral region surrounding an infarct core is significant because it is the first study to test this type of insult in turtle brain. It also demonstrates that anoxia-tolerant turtles are indeed an appropriate model through which important insights into therapies against ischemic brain injury may be found. The finding that enhanced GABA transmission also protects against ischemic insults highlights the incredible robustness of the turtle defense mechanisms and indicates an important area to investigate further in mammals. An interesting result of this study is that in ischemic and high $[K^+]_e$ experiments turtle neurons are electrically quiescent even though V_m was

depolarized past AP_{th}. This indicates that in turtle cerebrocortex GABAergic inhibition dominates over glutamatergic excitation because high $[K^+]_e$ should activate both GABAergic and glutamatergic signalling. Moreover, since antagonism of $GABA_{A+B}$ receptors is required to induce death in ischemic and anoxic neurons, this finding further supports the important role of $GABA_B$ receptor-mediated inhibition of glutamate release under anoxic and ischemic conditions.

My research has primarily focussed on elucidating the role of GABAergic inhibition in spike arrest; however, identification of oxygen sensitive ion channels and the signalling cascades that lead to channel arrest during anoxia is necessary to fully characterize oxygen sensing in turtle brain as well as for a complete understanding of the suite of adaptations turtles use to avoid ECD. My finding that turtle pyramidal neurons express K_{Ca} channels that decrease P_{open} with anoxia is important because it is the first direct measurement of channel arrest of a K^+ channel in anoxic turtle brain. Furthermore, this identifies one of the K^+ channels that contributes to the previously described decreased K^+ leakage during anoxia in turtle brain (Chih *et al.*, 1989; Pék & Lutz, 1997). While it might seem counterintuitive that inhibition of a hyperpolarizing K^+ current is neuroprotective it indicates that preventing accumulation of extracellular K^+ is a priority under anoxic conditions and that GABAergic inhibition is sufficient to prevent excessive AP generation. The finding that PKC, a Ca^{2+}-activated protein kinase, is involved in the regulation of K_{Ca} channels suggests that mitochondrial Ca^{2+} release may be a universal low oxygen signal.

When I started my doctoral research I knew that anoxia induced channel arrest of NMDA and AMPA receptors, and that inhibitory GABA transmission was critical for anoxic survival in turtle brain. However, the presynaptic and postsynaptic mechanisms through which electrical suppression occurs were not well understood. Now we have an improved working model of the mechanisms responsible for anoxia-tolerance, and in this final paragraph I will present my contributions to unravelling the neuroprotective mechanisms behind anoxia-tolerance in turtle brain by summarizing our current understanding of the mechanisms involved in anoxia-mediated electrical suppression in cerebrocortex (Figure 6.1).

At the onset of an anoxic episode blood PO_2 levels begin to decrease. At a PO_2 of ~ 35 mmHg (unpublished observations) there is an increase in activity of GABAergic stellate neurons and this leads to increased synaptic GABA release. Although the oxygen sensor responsible for increased activity may not have been directly confirmed, it is likely the mitochondria because inhibition of

the mROS signal with ROS scavengers or CN mimics the anoxic increases in GABA release. This suggests that in normoxic stellate neurons mitochondrial ROS generation maintains an oxidizing clamp preventing GABA release; this is supported by the finding that H_2O_2 inhibits GABA release. We do know that the signalling pathway involves stellate neuron depolarization and activation of Na_v channels because TTX prevents GABA release (unpublished data). Whether stellate neurons are the oxygen sensing cells of the cerebrocortex is unknown; however, since their AP burst frequency increases during anoxia they are a likely candidate. Stellate neurons are reported to be connected by electrical synapses which would be an effective mechanism to entrain synchronous GABA release throughout the cerebrocortex. Alternatively, stellate neurons could be regulated by another unknown upstream GABAergic oxygen sensing cell which is active under normoxic conditions but inhibited by anoxia. This would lead to disinhibition of stellate neurons and enhanced GABA release. Anoxia-mediated electrical suppression of postsynaptic glutamatergic pyramidal neurons is primarily the result of synaptic vesicular GABA release although decreased/reversed GABA uptake may play a role since inhibition of GABA transporters increased gIPSC amplitude (Chapter 2). Synaptic GABA release activates synaptic and putative-perisynaptic $GABA_A$ receptors causing increases in sIPSCs and gIPSCs. This release of GABA likely saturates GABA uptake transporters and increases $[GABA]_e$. In postsynaptic pyramidal neurons, activation of $GABA_A$ receptors, and in particular extrasynaptic $GABA_A$ receptors, increases G_w, leading to Cl^- efflux and cell shrinking. This depolarizes V_m to E_{GABA} and induces shunting inhibition, which opposes depolarization of V_m to AP_{th} as well as depolarizes AP_{th}. In presynaptic glutamatergic nerve terminals, GABA binding to putative $GABA_B$ receptors activates an inhibitory G-protein which inhibits Ca^{2+} influx and decreases glutamate release, reducing excitatory input into pyramidal neurons.

In pyramidal neurons, in addition to shunting inhibition there is ion channel arrest. Upon onset of anoxia, decreases in mitochondrial ATP production activate mK_{ATP} channels increasing K^+ influx into the matrix and Ψ_m depolarization. This leads to release of matrix Ca^{2+} and an small rise in $[Ca^{2+}]_i$, possibly through activation of the mPTP or modulation of the mitochondrial Ca^{2+} uniporter (Pamenter *et al.*, 2008c; Hawrysh & Buck, 2013). Following protein phosphatase 1/2A-mediated dephosphorylation of the serine residue on the NMDA receptor intracellular C-terminal tail, this Ca^{2+} signal activates calmodulin, which competitively antagonizes binding of α-actinin-2 to the NMDA receptor, resulting in a Ca^{2+}-dependent inactivation of NMDA receptors and delocalization

from the synapse via dissociation from cytoskeletal elements (Shin *et al.*, 2005). AMPA receptors are also inhibited via the same mitochondrial Ca^{2+} release mechanism; however, the exact mode of channel inhibition is unknown (Zivkovic & Buck, 2010). The anoxic increase in intracellular Ca^{2+} also activates PKC which phosphorylates K_{Ca} channels and decreases channel activity.

The studies described within this thesis have significantly increased our understanding of the suite of naturally evolved adaptations that combine to prevent hyperexcitability and cell death in anoxic turtle brain. They have highlighted the critical importance of redox modulation of GABAergic neurotransmission to electrical suppression during anoxia, and have reinforced the important role of channel arrest as a mechanism to reduce ATP expenditure during episodes of low oxygen stress. It is now clear that spike arrest in the anoxia-tolerance turtle brain involves both a decrease in excitatory glutamatergic neurotransmission in pyramidal neurons and an increase in GABAergic neurotransmission. The increased GABA release likely originates from stellate interneurons; therefore, the next step is to directly record from these neurons to better elucidate the oxygen sensing mechanism. A practical insight from my work is that to protect mammal brain from low oxygen injury strategies should include targeting mechanisms in at least these two neuronal sub-types. Once the oxygen-sensing pathways and neuronal circuits involved in upregulating GABA transmission are better understood we will be in a good position to not only understand these incredible physiological adaptations to anoxia present in turtle brain but will also have better tools to develop therapies against low oxygen insults in mammals.

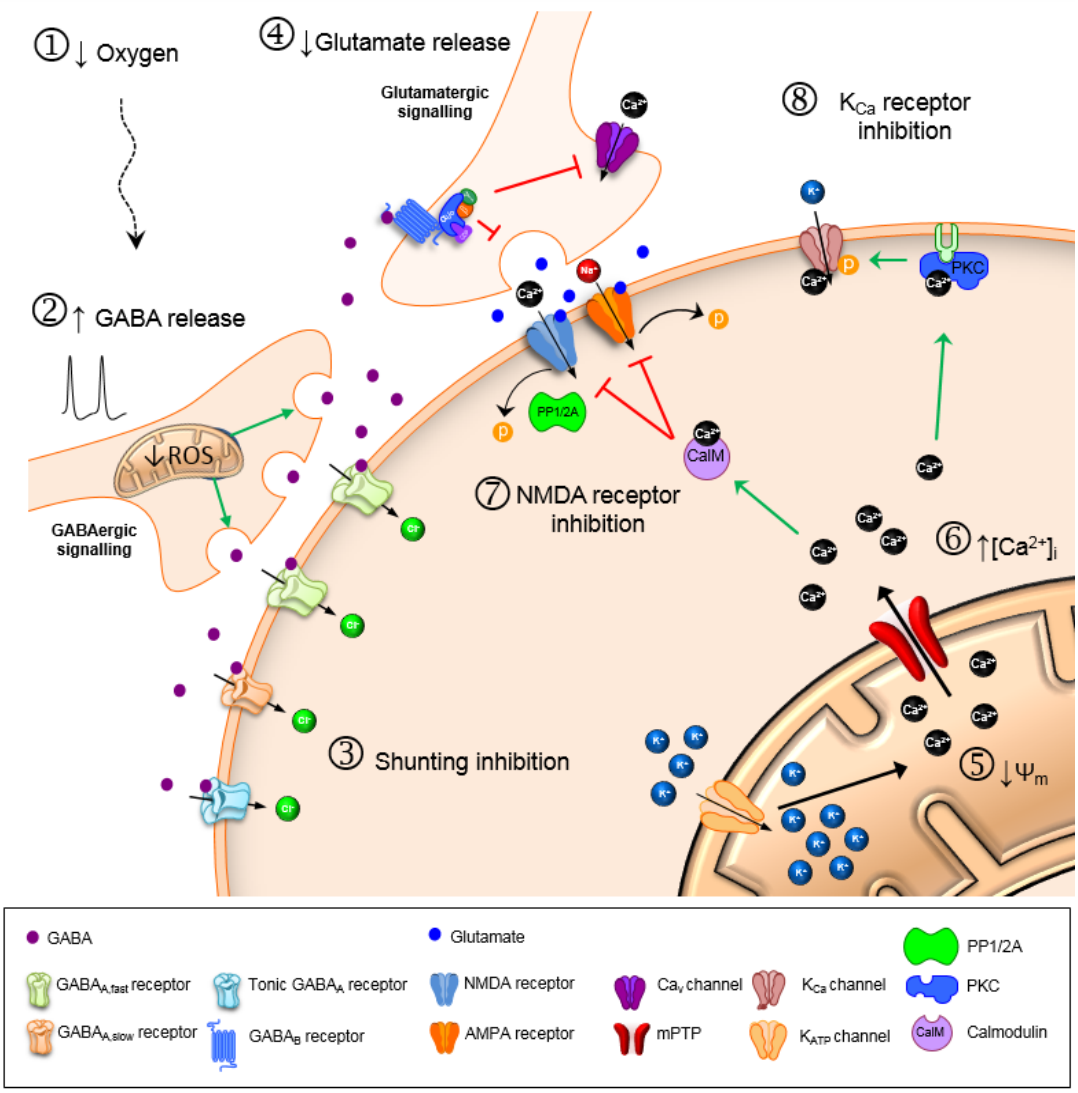

Figure 6.1. General schematic outlining neuroprotective mechanisms that induce electrical suppression in anoxic turtle pyramidal neurons.
Following decreases in blood and tissue PO_2 (1), there is a decrease in stellate neuron $[ROS]_i$ and an increase in burst firing activity (unpublished observations) leading to increased GABA release onto synaptically connected pyramidal neurons (2). Elevated $[GABA]_e$ activates synaptic, putative peri-synaptic, and extrasynaptic $GABA_A$ receptors resulting in a net increase in G_w, and a shift in V_m to E_{GABA} – Shunting inhibition (3). Elevated $[GABA]_e$ activates $GABA_B$ receptors on the presynaptic nerve terminals of glutamatergic neurons inhibiting glutamate release (4). Anoxic inhibition of oxidative ATP production decreases local [ATP] activating mitochondrial ATP-sensitive potassium (mK_{ATP}) channels, and depolarizing mitochondrial membrane potential (Ψ_m) (5). This leads to Ca^{2+} release through opening of the mitochondrial permeability transition pore (mPTP), and an increase in $[Ca^{2+}]_i$ (6). Phosphatases 1/2A dephosphorylate NMDA receptors, and Ca^{2+} activated calmodulin antagonizes binding of α-actinin-2 to the glutamate receptor, leading to inactivation and delocalization of the receptor from the synapse via dissociation from cytoskeletal elements (7); a similar mechanism is likely responsible for decreases in AMPA receptor currents. The increase in $[Ca^{2+}]_i$ also activates protein kinase C (PKC), which phosphorylates calcium-activated potassium channels (K_{Ca}) and decreases channel P_{open} (8). Green arrows indicate activation and red arrows indicate inhibition. Note: for simplicity these mechanisms have been shown occurring all together in one location; however, it is likely that shunting inhibition and channel arrest occur at separate synapses.

7 Appendices

Appendix I: Working concentrations of pharmacological modifiers

Table A. 1. Working concentrations of pharmacological modifiers.

Chemical	Acronym	Working concentration	Description
Calcium chelator			
ethylene glycol tetraacetic acid	EGTA	10-50 μM	Calcium chelator
GABA receptor modulators			
Bicuculline methiodide	BIC	100 μM	$GABA_A$ receptor antagonist
CGP55845	CGP	5 μM	$GABA_B$ receptor antagonist
γ-Aminobutyric acid	GABA	2 mM	$GABA_{A+B}$ receptor agonist
Picrotoxin	PTX	100 μM	$GABA_A$ receptor antagonist
SR-95531(Gabazine)	GZ	25 μM	$GABA_A$ receptor antagonist
GABA transport inhibitor			
SKF 89976A hydrochloride*	SKF	40 μM	GABA transport 1 inhibitor
(*S*)-SNAP-5114*	SNAP	20 μM	GABA transport 2/ 3 inhibitor
Glycine channel modulators			
Strychnine	Stryc	2 uM	Glycine receptor antagonist
Glutamate receptor modulators			
(2R)-amino-5-phosphopentanoate	AP5	25 uM	NMDA receptor antagonist
6-cyano-7-nitroquinoxaline-2, 3-dione	CNQX	25 uM	AMPA receptor antagonist
Sodium channel modulators			
Tetrodotoxin	TTX	1-2 uM	Voltage-gated Na^+ channel inhibitor
Redox modulators			
Hydrogen peroxide	H_2O_2	50 uM	Oxidant
N-acetylcysteine	NAC	0.5 mM	ROS scavenger
N-(2-Mercaptopropionyl) glycine	MPG	0.5 mM	ROS scavenger
Sodium cyanide*	CN	0.5 mM	Mitochondrial complex IV inhibitor

Potassium channel modulators			
Cesium chloride	CsCl	5 mM	K^+ channel antagonist
Iberiotoxin	IbTX	150 nM	K_{Ca} channel antagonist
Tetraethylammonium chloride	TEA	10 mM	Voltage-gated K^+ channel antagonist
Kinase/phosphatase modulators			
Calmidazolium**	CDZ	10 uM / 1 uM	Calmodulin inhibitor
Chelerythrine**	CHT	10 uM / 0.5uM	PKC inhibitor
Okadaic acid**	OA		Phosphatase 1 and 2A inhibitor
Phorbol-12-myristate-13-acetate	PMA	6 uM / 500 nM	PKC activator
		10 uM	

* *Not a direct modulator*

** *Incubation concentration/drip perfusion concentration*

Appendix II: Protocol for neuron identification

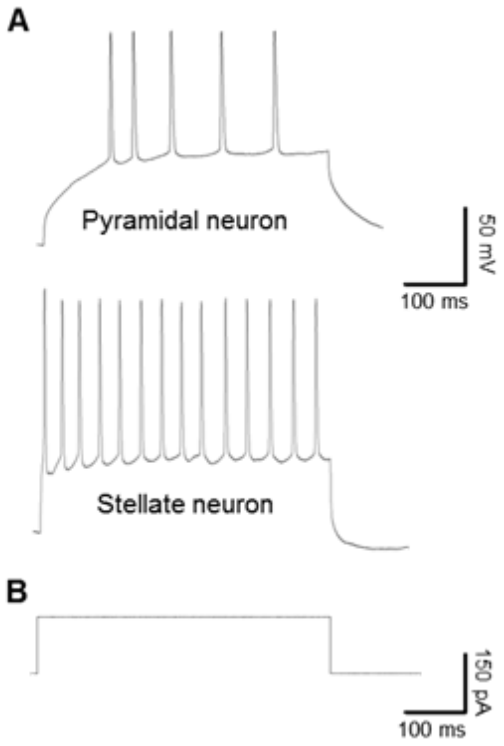

Figure A.1. Pyramidal neurons and stellate neurons can be differentiated by their responses to somatic current injections.
At the beginning of all whole-cell and perforated patch-clamp experiments the type of neuron being recorded from was first identified using a current step protocol. In response to a 450 ms, 150 pA somatic current injection pyramidal neurons fire trains of APs that accommodate while stellate neurons do not. (A) Representative sample traces showing the response of a pyramidal neuron and a stellate neuron to the same current step protocol in the current clamp configuration. (B) Example of the current step protocol used to identify neuron type.

Appendix III: Effect of 95% O_2 vs room air on cortical neurons

Table A.2. Comparison of the effects of 95% O_2/5% CO_2 and room air/5%CO_2 on electrophysiological parameters of cortical pyramidal neurons.

	95% O_2/5% CO_2	room air/5%CO_2
Membrane potential (mV)	-87.3 ± 1.9 (10)	-84.5 ± 4.2(4)
Whole-cell conductance (nS)	4.9 ± 0.2 (10)	4.8 ± 1.1 (4)
Action potential threshold (mV)	-45.4 ± 2.0 (10)	-42.4 ± 1.6 (4)
Giant IPSC amplitude	-228.1 ± 11.8 (7)	-205 ± 15.2 (4)
Giant IPSC frequency	0.09 ± 0.01 (7)	0.11 ± 0.01 (4)
CM-DCF slope of the line (measure of the rate of ROS generation)	15.1 ± 1.2 (7)	12.8 ± 1.1 (4)

Note: For comparison 95% O_2/5% CO_2 data is from chapter 4. Data represent the means ± S.E.M. Parentheses indicate n-value. A t-test comparing 95% O_2/5% CO_2 and room air/5% CO_2 within each measured parameter found the data not to be statistically significant ($P < 0.05$).

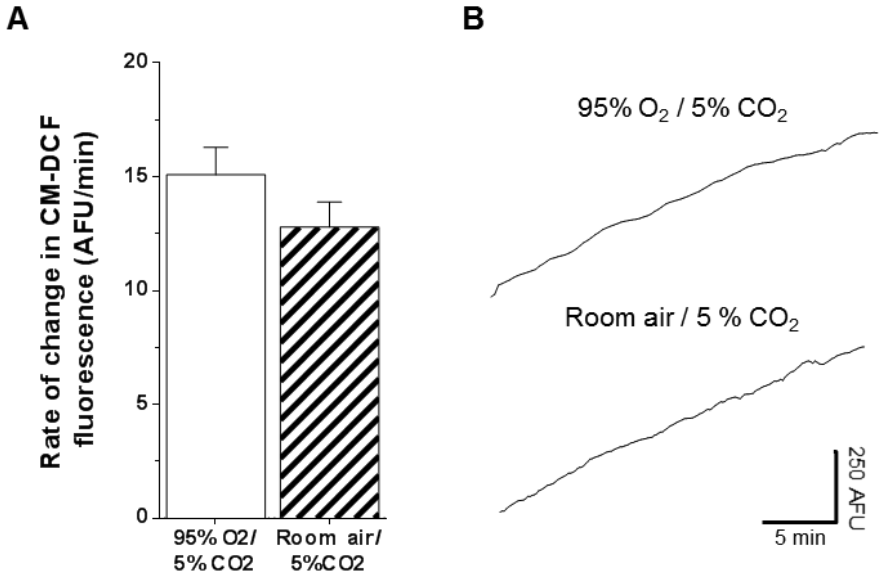

Figure A.2. The rate of $[ROS]_i$ generation is not different in cortical neurons perfused with aCSF equilibrated with 95% O_2/5% CO_2 versus room air/5% CO_2.
(A) Summary of the rate of change in CM-DCF fluorescence over a 30 min experiment. (B) Sample CM-DCF fluorescence traces from (A), cortical sheets were treated as indicated. Note: each trace is averaged from 10 ROI's collected from one recording. The rate of change (equal to the slope of the line) was determined by taking the linear regression of the trace. Data are expressed as means ± S.E.M., n = 4-8 replicates per treatment. A t-test comparing 95% O_2/5% CO_2 and room air/5% CO_2 found the data not to be statistically significant ($P < 0.05$).

References

Aaronson PI, Robertson TP, Knock GA, Becker S, Lewis TH, Snetkov V & Ward JP. (2006). Hypoxic pulmonary vasoconstriction: mechanisms and controversies. *The Journal of physiology* **570,** 53-58.

Abele AE, Scholz KP, Scholz WK & Miller RJ. (1990). Excitotoxicity induced by enhanced excitatory neurotransmission in cultured hippocampal pyramidal neurons. *Neuron* **4,** 413-419.

Aboitiz F & Zamorano F. (2013). Neural progenitors, patterning and ecology in neocortical origins. *Frontiers in Neuroanatomy* **7**.

Adam-Vizi V. (2005). Production of reactive oxygen species in brain mitochondria: Contribution by electron transport chain and non-electron transport chain sources. *Antioxidants & Redox Signaling* **7,** 1140-1149.

Adam-Vizi V & Starkov AA. (2010). Calcium and mitochondrial reactive oxygen species generation: how to read the facts. *Journal of Alzheimer's Disease* **20,** 413-426.

Allen NJ, Rossi DJ & Attwell D. (2004). Sequential release of GABA by exocytosis and reversed uptake leads to neuronal swelling in simulated ischemia of hippocampal slices. *The Journal of neuroscience* **24,** 3837-3849.

Amato A, Connolly CN, Moss SJ & Smart TG. (1999). Modulation of neuronal and recombinant GABAA receptors by redox reagents. *The Journal of Physiology* **517,** 35-50.

Anderson RE, Tan WK, Martin HS & Meyer FB. (1999). Effects of glucose and PaO2 modulation on cortical intracellular acidosis, NADH redox state, and infarction in the ischemic penumbra. *Stroke* **30,** 160-170.

Anderson TR, Jarvis CR, Biedermann AJ, Molnar C & Andrew RD. (2005). Blocking the anoxic depolarization protects without functional compromise following simulated stroke in cortical brain slices. *Journal of Neurophysiology* **93,** 963-979.

Archer S & Michelakis E. (2002). The mechanism (s) of hypoxic pulmonary vasoconstriction: potassium channels, redox O2 sensors, and controversies. *Physiology* **17,** 131-137.

Art J, Wu Y & Fettiplace R. (1995). The calcium-activated potassium channels of turtle hair cells. *The Journal of General Physiology* **105,** 49-72.

Arundine M & Tymianski M. (2004). Molecular mechanisms of glutamate-dependent neurodegeneration in ischemia and traumatic brain injury. *Cellular and Molecular Life Sciences CMLS* **61,** 657-668.

Attwell D & Laughlin SB. (2001). An energy budget for signaling in the grey matter of the brain. *J Cereb Blood Flow Metab* **21,** 1133-1145.

Azevedo FA, Carvalho LR, Grinberg LT, Farfel JM, Ferretti RE, Leite RE, Jacob Filho W, Lent R & Herculano-Houzel S. (2009). Equal numbers of neuronal and nonneuronal cells make the human brain an isometrically scaled-up primate brain. *J Comp Neurol* **513,** 532-541.

Bai D, Zhu G, Pennefather P, Jackson MF, MacDonald JF & Orser BA. (2001). Distinct functional and pharmacological properties of tonic and quantal inhibitory postsynaptic currents mediated by γ-aminobutyric acid A receptors in hippocampal neurons. *Molecular pharmacology* **59,** 814-824.

Bao L, Avshalumov MV, Patel JC, Lee CR, Miller EW, Chang CJ & Rice ME. (2009). Mitochondria Are the Source of Hydrogen Peroxide for Dynamic Brain-Cell Signaling. *Journal of Neuroscience* **29,** 9002-9010.

Belanger M, Allaman I & Magistretti PJ. (2011). Brain Energy Metabolism: Focus on Astrocyte-Neuron Metabolic Cooperation. *Cell Metabolism* **14,** 724-738.

Belkin DA. (1968). Anaerobic brain function: effects of stagnant and anoxic anoxia on persistence of breathing in reptiles. *Science* **162,** 1017-1018.

Ben-Ari Y. (2002). Excitatory actions of GABA during development: the nature of the nurture. *Nature Reviews Neuroscience* **3,** 728-739.

Ben-Ari Y, Cherubini E, Corradetti R & Gaiarsa J. (1989). Giant synaptic potentials in immature rat CA3 hippocampal neurones. *The Journal of Physiology* **416,** 303-325.

Ben-Ari Y, Gaiarsa J-L, Tyzio R & Khazipov R. (2007). GABA: a pioneer transmitter that excites immature neurons and generates primitive oscillations. *Physiological reviews* **87,** 1215-1284.

Bennett AF & Ruben JA. (1979). Endothermy and activity in vertebrates. *Science* **206,** 649-654.

Berman JM & Awayda MS. (2013). Redox artifacts in electrophysiological recordings. *American Journal of Physiology-Cell Physiology* **304,** C604-C613.

Besancon E, Guo S, Lok J, Tymianski M & Lo EH. (2008). Beyond NMDA and AMPA glutamate receptors: emerging mechanisms for ionic imbalance and cell death in stroke. *Trends in pharmacological sciences* **29,** 268-275.

Bickler P. (1998). Reduction of NMDA receptor activity in cerebrocortex of turtles (Chrysemys picta) during 6 wk of anoxia. *American Journal of Physiology-Regulatory, Integrative and Comparative Physiology* **275,** R86-R91.

Bickler PE. (1992). Effects of temperature and anoxia on regional cerebral blood flow in turtles. *Am J Physiol* **262,** R538-541.

Bickler PE & Buck LT. (1998). Adaptations of vertebrate neurons to hypoxia and anoxia: maintaining critical Ca2+ concentrations. *Journal of experimental biology* **201,** 1141-1152.

Bickler PE & Buck LT. (2007). Hypoxia tolerance in reptiles, amphibians, and fishes: Life with variable oxygen availability. *Annual Review of Physiology* **69,** 145-170.

Bickler PE, Donohoe PH & Buck LT. (2000). Hypoxia-induced silencing of NMDA receptors in turtle neurons. *The Journal of Neuroscience* **20,** 3522-3528.

Blaesse P, Airaksinen MS, Rivera C & Kaila K. (2009). Cation-chloride cotransporters and neuronal function. *Neuron* **61,** 820-838.

Blanton MG, Lo Turco JJ & Kriegstein AR. (1989a). Whole cell recording from neurons in slices of reptilian and mammalian cerebral cortex. *Journal of Neuroscience Methods* **30,** 203-210.

Blanton MG, Loturco JJ & Kriegstein AR. (1989b). Whole cell recording from neuron in slices of reptillian and mammalian cerebral-cortex. *Journal of Neuroscience Methods* **30,** 203-210.

Blatz A & Magleby K. (1987). Calcium-activated potassium channels. *Trends in Neurosciences* **10,** 463-467.

Borden LA. (1996). GABA Transporter Heterogeneity: Pharmacology and cellular localization. *Neurochemistry International* **29,** 335-356.

Boudker O, Ryan RM, Yernool D, Shimamoto K & Gouaux E. (2007). Coupling substrate and ion binding to extracellular gate of a sodium-dependent aspartate transporter. *Nature* **445,** 387-393.

Brady S, Siegel G, Albers RW & Price D. (2005). *Basic neurochemistry: molecular, cellular and medical aspects*. Academic Press.

Braitenberg V & Schüz A. (1998). *Cortex: Statistics and Geometry of Neuronal Connectivity. 2nd thoroughly revised edition of: Anatomy of the Cortex*. Springer Verlag.

Branston N, Symon L, Crockard H & Pasztor E. (1974). Relationship between the cortical evoked potential and local cortical blood flow following acute middle cerebral artery occlusion in the baboon. *Experimental neurology* **45,** 195-208.

Braun M, Ramracheya R, Bengtsson M, Zhang Q, Karanauskaite J, Partridge C, Johnson PR & Rorsman P. (2008). Voltage-gated ion channels in human pancreatic β-cells: electrophysiological characterization and role in insulin secretion. *Diabetes* **57,** 1618-1628.

Brickley SG, Cull-Candy SG & Farrant M. (1999). Single-channel properties of synaptic and extrasynaptic GABAA receptors suggest differential targeting of receptor subtypes. *The Journal of neuroscience* **19,** 2960-2973.

Bright DP & Smart TG. (2013). Methods for recording and measuring tonic GABAa receptor-mediated inhibition. *Frontiers in neural circuits* **7**.

Brooks S & Storey K. (1993). Protein kinase C in turtle brain: changes in enzyme activity during anoxia. *Journal of Comparative Physiology B* **163,** 84-88.

Brooks SPJ & Storey KB. (1990). Phosphofructokinase from a vertebrate facultative anaerobe: effects of temperature and anoxia on the kinetic parameters of the purified enzyme from turtle white muscle. *Biochimica et Biophysica Acta (BBA) - Protein Structure and Molecular Enzymology* **1037,** 161-164.

Broughton BR, Reutens DC & Sobey CG. (2009). Apoptotic mechanisms after cerebral ischemia. *Stroke* **40,** e331-e339.

Buck L, Espanol M, Litt L & Bickler P. (1998). Reversible decreases in ATP and PCr concentrations in anoxic turtle brain. *Comparative Biochemistry and Physiology Part A: Molecular & Integrative Physiology* **120,** 633-639.

Buck L & Hochachka P. (1993). Anoxic suppression of Na+-K+-ATPase and constant membrane potential in hepatocytes: support for channel arrest. *American Journal of Physiology* **265,** R1020-R1020.

Buck L, Hochachka P, Schon A & Gnaiger E. (1993). Microcalorimetric measurement of reversible metabolic suppression induced by anoxia in isolated hepatocytes. *American Journal of Physiology-Regulatory, Integrative and Comparative Physiology* **265,** R1014-R1019.

Buck LT & Bickler PE. (1998). Adenosine and anoxia reduce N-methyl-D-aspartate receptor open probability in turtle cerebrocortex. *Journal of Experimental Biology* **201,** 289-297.

Burgoyne JR, Madhani M, Cuello F, Charles RL, Brennan JP, Schroder E, Browning DD & Eaton P. (2007). Cysteine redox sensor in PKGI alpha enables oxidant-induced activation. *Science* **317,** 1393-1397.

Calero CI, Vickers E, Moraga Cid G, Aguayo LG, von Gersdorff H & Calvo DJ. (2011). Allosteric modulation of retinal GABA receptors by ascorbic acid. *J Neurosci* **31,** 9672-9682.

Candia S, Garcia ML & Latorre R. (1992). Mode of action of iberiotoxin, a potent blocker of the large conductance Ca (2+)-activated K+ channel. *Biophysical Journal* **63,** 583.

Canfield DE. (2005). The early history of atmospheric oxygen: Homage to Robert A. Garrels. *Annual Review of Earth and Planetary Sciences* **33,** 1-36.

Capogna M & Pearce RA. (2011). $GABA_{A, slow:}$ causes and consequences. *Trends in neurosciences* **34,** 101-112.

Chandel NS & Schumacker PT. (2000). Cellular oxygen sensing by mitochondria: old questions, new insight. *Journal of Applied Physiology* **88,** 1880-1889.

Chen Q & Pan HL. (2007). Signaling mechanisms of angiotensin II-induced attenuation of GABAergic input to hypothalamic presympathetic neurons. *Journal of Neurophysiology* **97,** 3279-3287.

Chen Q, Vazquez EJ, Moghaddas S, Hoppel CL & Lesnefsky EJ. (2003). Production of reactive oxygen species by mitochondria central role of complex III. *Journal of Biological Chemistry* **278,** 36027-36031.

Chih C-p, Rosenthal M & Sick TJ. (1989). Ion leakage is reduced during anoxia in turtle brain: a potential survival strategy. *Brain* **10,** 17.

Choi DW. (1992). Excitotoxic cell-death. *Journal of Neurobiology* **23,** 1261-1276.

Choi Y-B & Lipton S. (2000). Redox modulation of the NMDA receptor. *Cellular and Molecular Life Sciences CMLS* **57,** 1535-1541.

Chu F, Ward NE & O'Brian CA. (2003). PKC isozyme S-cysteinylation by cystine stimulates the pro-apoptotic isozyme PKC delta and inactivates the oncogenic isozyme PKC epsilon. *Carcinogenesis* **24,** 317-325.

Clapham DE. (2007). Calcium signaling. *Cell* **131,** 1047-1058.

Clark VM & Miller Jr A. (1973). Studies on anaerobic metabolism in the fresh-water turtle (*Pseudemys scripta elegans*). *Comparative Biochemistry and Physiology Part A: Physiology* **44,** 55-62.

Clarke DD & Sokoloff L. (1999). Circulation and energy metabolism of the brain. *Basic neurochemistry: molecular, cellular and medical aspects* **6,** 637-669.

Cobb S, Buhl E, Halasy K, Paulsen O & Somogyi P. (1995). Synchronization of neuronal activity in hippocampus by individual GABAergic interneurons.

Colombe JB, Sylvester J, Block J & Ulinski PS. (2004). Subpial and stellate cells: two populations of interneurons in turtle visual cortex. *J Comp Neurol* **471,** 333-351.

Connors BW & Kriegstein AR. (1986). Cellular physiology of the turtle visal cortex: Distinctive properties of pyramidal and stellate neurons. *Journal of Neuroscience* **6,** 164-177.

Costa C, Leone G, Saulle E, Pisani F, Bernardi G & Calabresi P. (2004). Coactivation of GABAA and GABAB receptor results in neuroprotection during in vitro ischemia. *Stroke* **35,** 596-600.

Crowe WE, Altamirano J, Huerto L & Alvarezleefmans FJ. (1995). Volume changes in single N1E-115 neuroblastoma-cells measured with a fluorescent probe. *Neuroscience* **69,** 283-296.

Cui J, Cox D & Aldrich R. (1997). Intrinsic voltage dependence and Ca2+ regulation of mslo large conductance Ca-activated K+ channels. *The Journal of general physiology* **109,** 647-673.

Cunha R. (2001). Adenosine as a neuromodulator and as a homeostatic regulator in the nervous system: different roles, different sources and different receptors. *Neurochemistry international* **38,** 107-125.

D'Agostino DP, Putnam RW & Dean JB. (2007). Superoxide ($\cdot O_2^-$) Production in CA1 Neurons of Rat Hippocampal Slices Exposed to Graded Levels of Oxygen. *Journal of neurophysiology* **98,** 1030-1041.

Danbolt NC. (2001). Glutamate uptake. *Progress in neurobiology* **65,** 1-105.

Dean JB, Mulkey DK, Garcia III AJ, Putnam RW & Henderson III RA. (2003). Neuronal sensitivity to hyperoxia, hypercapnia, and inert gases at hyperbaric pressures. *Journal of Applied Physiology* **95,** 883-909.

DeFazio RA, Keros S, Quick MW & Hablitz JJ. (2000). Potassium-coupled chloride cotransport controls intracellular chloride in rat neocortical pyramidal neurons. *Journal of Neuroscience* **20,** 8069-8076.

Denu JM & Tanner KG. (1998). Specific and reversible inactivation of protein tyrosine phosphatases by hydrogen peroxide: Evidence for a sulfenic acid intermediate and implications for redox regulation. *Biochemistry* **37,** 5633-5642.

Desan PH. (1984). The organization of the cerebral cortex of the pond turtle, Pseudemys scripta elegans. Harvard University.

Dienel GA. (2012). Brain lactate metabolism: the discoveries and the controversies. *J Cereb Blood Flow Metab* **32,** 1107-1138.

Dixon KC. (1937). The Pasteur effect and its mechanism. *Biological Reviews* **12,** 431-460.

Dohmen C, Sakowitz OW, Fabricius M, Bosche B, Reithmeier T, Ernestus RI, Brinker G, Dreier JP, Woitzik J & Strong AJ. (2008). Spreading depolarizations occur in human ischemic stroke with high incidence. *Annals of neurology* **63,** 720-728.

Doll C, Hochachka P & Hand S. (1994). A microcalorimetric study of turtle cortical slices: insights into brain metabolic depression. *Journal of experimental biology* **191,** 141-153.

Doll C, Hochachka P & Reiner P. (1991). Effects of anoxia and metabolic arrest on turtle and rat cortical neurons. *American Journal of Physiology-Regulatory, Integrative and Comparative Physiology* **260,** R747-R755.

Dreier JP, Major S, Manning A, Woitzik J, Drenckhahn C, Steinbrink J, Tolias C, Oliveira-Ferreira AI, Fabricius M & Hartings JA. (2009). Cortical spreading ischaemia is a novel process involved in ischaemic damage in patients with aneurysmal subarachnoid haemorrhage. *Brain* **132,** 1866-1881.

Drew K, Harris M, LaManna J, Smith M, Zhu X & Ma Y. (2004). Hypoxia tolerance in mammalian heterotherms. *Journal of Experimental Biology* **207,** 3155-3162.

Duchen MR. (1999). Contributions of mitochondria to animal physiology: from homeostatic sensor to calcium signalling and cell death. *The Journal of physiology* **516,** 1-17.

Dukoff DJ, Hogg DW, Hawrysh PJ & Buck LT. (2014). Scavenging ROS dramatically increase NMDA receptor whole-cell currents in painted turtle cortical neurons. *The Journal of experimental biology* **217,** 3346-3355.

Edinger AL & Thompson CB. (2004). Death by design: apoptosis, necrosis and autophagy. *Current Opinion in Cell Biology* **16,** 663-669.

Egan TM, Dagan D & Levitan IB. (1993). Properties and modulation of a calcium-activated potassium channel in rat olfactory bulb neurons. *Journal of neurophysiology* **69,** 1433-1433.

Else PL & Hulbert AJ. (1987). Evolution of mammalian endothermic metabolism:"leaky" membranes as a source of heat. *Am J Physiol* **253,** R1-7.

Erecińska M & Silver IA. (1994). Ions and energy in mammalian brain. *Progress in neurobiology* **43,** 37-71.

Essrich C, Lorez M, Benson JA, Fritschy J-M & Lüscher B. (1998). Postsynaptic clustering of major GABAA receptor subtypes requires the γ2 subunit and gephyrin. *Nature neuroscience* **1,** 563-571.

Fabricius M, Fuhr S, Bhatia R, Boutelle M, Hashemi P, Strong AJ & Lauritzen M. (2006). Cortical spreading depression and peri-infarct depolarization in acutely injured human cerebral cortex. *Brain* **129,** 778-790.

Fanger CM, Ghanshani S, Logsdon NJ, Rauer H, Kalman K, Zhou J, Beckingham K, Chandy KG, Cahalan MD & Aiyar J. (1999). Calmodulin mediates calcium-dependent activation of the intermediate conductance KCa channel, IKCa1. *Journal of Biological Chemistry* **274,** 5746-5754.

Fearon IM, Thompson RJ, Samjoo I, Vollmer C, Doering LC & Nurse CA. (2002). O2− sensitive K+ channels in immortalised rat chromaffin-cell-derived MAH cells. *The Journal of physiology* **545,** 807-818.

Feng Z, Rosenthal M & Sick TJ. (1988a). Suppression of evoked-potentials with continued ion-transport during anoxia in turtle brain. *American Journal of Physiology-Regulatory, Integrative and Comparative Physiology* **255,** R478-R484.

Feng ZC, Rosenthal M & Sick TJ. (1988b). Suppression of evoked-potentials with continued ion-transport during anoxia in turtle brain. *American Journal of Physiology* **255,** R478-R484.

Fernandes JA, Lutz PL, Tannenbaum A, Todorov AT, Liebovitch L & Vertes R. (1997). Electroencephalogram activity in the anoxic turtle brain. *American Journal of Physiology* **273,** 911-919.

Galeffi F, Sinnar S & Schwartz-Bloom RD. (2000). Diazepam promotes ATP recovery and prevents cytochrome c release in hippocampal slices after in vitro ischemia. *Journal of neurochemistry* **75,** 1242-1249.

Galluzzi L, Maiuri M, Vitale I, Zischka H, Castedo M, Zitvogel L & Kroemer G. (2007). Cell death modalities: classification and pathophysiological implications. *Cell death and differentiation* **14,** 1237-1242.

Gardner-Medwin A. (1981). Possible roles of vertebrate neuroglia in potassium dynamics, spreading depression and migraine. *Journal of experimental Biology* **95,** 111-127.

Gassmann M & Bettler B. (2012). Regulation of neuronal GABAB receptor functions by subunit composition. *Nature Reviews Neuroscience* **13,** 380-394.

Gerber U & Gahwiler BH. (1994). *GABAB and adenosine receptors mediate enhancement of the K+ current, IAHP, by reducing adenylyl cyclase activity in rat CA3 hippocampal neurons*, vol. 72.

Ghai HS & Buck LT. (1999). Acute reduction in whole cell conductance in anoxic turtle brain. *American Journal of Physiology-Regulatory Integrative and Comparative Physiology* **277,** R887-R893.

Ginsberg MD. (2008). Neuroprotection for ischemic stroke: past, present and future. *Neuropharmacology* **55,** 363-389.

Gnaiger E. (2003). Oxygen conformance of cellular respiration. In *Hypoxia*, pp. 39-55. Springer.

Gray R & Johnston D. (1985). Rectification of single GABA-gated chloride channels in adult hippocampal neurons. *METHODS* **13,** 16.

Gribkoff VK, Starrett JE & Dworetzky SI. (2001). Maxi-K potassium channels: form, function, and modulation of a class of endogenous regulators of intracellular calcium. *The Neuroscientist* **7,** 166-177.

Gunter TE, Yule DI, Gunter KK, Eliseev RA & Salter JD. (2004). Calcium and mitochondria. *FEBS letters* **567,** 96-102.

Guppy M & Withers P. (1999). Metabolic depression in animals: physiological perspectives and biochemical generalizations. *Biological Reviews of the Cambridge Philosophical Society* **74,** 1-40.

Hamann S, Kiilgaard JF, Litman T, Alvarez-Leefmans FJ, Winther BR & Zeuthen T. (2002). Measurement of cell volume changes by fluorescence self-quenching. *Journal of fluorescence* **12,** 139-145.

Hansen AJ. (1985). Effect of anoxia on ion distribution in the brain. *Physiological Reviews* **65,** 101-148.

Hansen AJ & Nedergaard M. (1988). Brain ion homeostasis in cerebral ischemia. *Neurochemical pathology* **9,** 195-209.

Hardie DG, Hawley SA & Scott JW. (2006). AMP-activated protein kinase–development of the energy sensor concept. *The Journal of physiology* **574,** 7-15.

Harris JJ, Jolivet R & Attwell D. (2012). Synaptic energy use and supply. *Neuron* **75,** 762-777.

Hashimoto T & Kuriyama K. (1997). In vivo evidence that GABAB receptors are negatively coupled to adenylate cyclase in rat striatum. *Journal of neurochemistry* **69,** 365-370.

Hawrysh PJ & Buck LT. (2013). Anoxia-mediated calcium release through the mitochondrial permeability transition pore silences NMDA receptor currents in turtle neurons. *The Journal of experimental biology* **216,** 4375-4387.

Hazel JR. (1995). Thermal adaptation in biological membranes: is homeoviscous adaptation the explanation? *Annual Review of Physiology* **57,** 19-42.

Henze D & Buzsaki G. (2001). Action potential threshold of hippocampal pyramidal cells< i> in vivo</i> is increased by recent spiking activity. *Neuroscience* **105,** 121-130.

Herbert CV & Jackson DC. (1985). Temperature effects on the responses to prolonged submergence in the turtle Chrysemys picta bellii. II. Metabolic rate, blood acid-base and ionic changes, and cardiovascular function in aerated and anoxic water. *Physiological Zoology***,** 670-681.

Hewitt SA, Wamsteeker JI, Kurz EU & Bains JS. (2009). Altered chloride homeostasis removes synaptic inhibitory constraint of the stress axis. *Nature Neuroscience* **12,** 438-443.

Hochachka PW. (1986). Defense strategies against hypoxia and hypothermia. *Science* **231,** 234-241.

Hochachka PW & Somero GN. (1984). *Biochemical adaptation*. Princeton University Press Princeton.

Hockberger PE, Skimina TA, Centonze VE, Lavin C, Chu S, Dadras S, Reddy JK & White JG. (1999). Activation of flavin-containing oxidases underlies light-induced production of H2O2 in mammalian cells. *Proceedings of the National Academy of Sciences* **96,** 6255-6260.

Hodgkin AL & Huxley AF. (1952). A quantitative description of membrane current and its application to conduction and excitation in nerve. *The Journal of physiology* **117,** 500.

Hogg D, Hawrysh P & Buck L. (2014). Environmental remodelling of GABAergic and glutamatergic neurotransmission: Rise of the anoxia-tolerant turtle brain. *Journal of Thermal Biology*.

Howarth C, Gleeson P & Attwell D. (2012). Updated energy budgets for neural computation in the neocortex and cerebellum. *Journal of Cerebral Blood Flow and Metabolism* **32,** 1222-1232.

Hoyt KR, Gallagher AJ, Hastings TG & Reynolds IJ. (1997). Characterization of hydrogen peroxide toxicity in cultured rat forebrain neurons. *Neurochemical Research* **22,** 333-340.

Humphries KM, Deal MS & Taylor SS. (2005). Enhanced dephosphorylation of cAMP-dependent protein kinase by oxidation and thiol modification. *Journal of Biological Chemistry* **280,** 2750-2758.

Hylland P & Nilsson GE. (1999). Extracellular levels of amino acid neurotransmitters during anoxia and forced energy deficiency in crucian carp brain. *Brain research* **823,** 49-58.

Hylland P, Nilsson GE & Lutz PL. (1994). Time course of anoxia-induced increase in cerebral blood flow rate in turtles: evidence for a role of adenosine. *Journal of Cerebral Blood Flow & Metabolism* **14,** 877-881.

Ikonomidou C & Turski L. (2002). Why did NMDA receptor antagonists fail clinical trials for stroke and traumatic brain injury? *The Lancet Neurology* **1,** 383-386.

Inglefield JR & Schwartz-Bloom RD. (1999). Fluorescence imaging of changes in intracellular chloride in living brain slices. *Methods* **18,** 197-203.

Jackson DC. (1968). Metabolic depression and oxygen depletion in diving turtle. *Journal of Applied Physiology* **24,** 503-&.

Jackson DC. (2000). Living without oxygen: lessons from the freshwater turtle. *Comparative Biochemistry and Physiology Part A: Molecular & Integrative Physiology* **125,** 299-315.

Jackson DC. (2002). Hibernating without oxygen: physiological adaptations of the painted turtle. *The Journal of physiology* **543,** 731-737.

Jackson DC & Heisler N. (1983). Intracelular and extracellular acid-base and electrolyte status of submerged anoxic turteles at 3° C. *Respiration physiology* **53,** 187-201.

Jackson DC & Ultsch GR. (1982). Long-term submergence at 3 C of the turtle, Chrysemys picta bellii, in normoxic and severely hypoxic water: II. Extracellular ionic responses to extreme lactic acidosis. *Journal of Experimental Biology* **96,** 29-43.

Jackson MB & Redman SJ. (2003). Calcium dynamics, buffering, and buffer saturation in the boutons of dentate granule-cell axons in the hilus. *The Journal of neuroscience* **23,** 1612-1621.

Jaggar JH, Leffler CW, Cheranov SY, Tcheranova D, Shuyu E & Cheng X. (2002). Carbon monoxide dilates cerebral arterioles by enhancing the coupling of Ca2+ sparks to Ca2+-activated K+ channels. *Circulation research* **91,** 610-617.

Jiang C, Agulian S & Haddad GG. (1991). O_2 tension in adult and neonatal brain slices under several experimental conditions. *Brain research* **568,** 159-164.

Jiang J & Amara SG. (2011). New views of glutamate transporter structure and function: advances and challenges. *Neuropharmacology* **60,** 172-181.

Jin P, Weiger TM & Levitan IB. (2002a). Reciprocal modulation between the α and β4 subunits of hSlo calcium-dependent potassium channels. *Journal of Biological Chemistry* **277,** 43724-43729.

Jin P, Weiger TM, Wu Y & Levitan IB. (2002b). Phosphorylation-dependent functional coupling of hSlo calcium-dependent potassium channel and its hβ4 subunit. *Journal of Biological Chemistry* **277,** 10014-10020.

Johlin J & Moreland FB. (1933). Studies of the blood picture of the turtle after complete anoxia. *Journal of Biological Chemistry* **103,** 107-114.

Kahles T & Brandes RP. (2012). NADPH oxidases as therapeutic targets in ischemic stroke. *Cellular and Molecular Life Sciences* **69,** 2345-2363.

Kaila K. (1994). Ionic basis of $GABA_A$ receptor channel function in the nervous system. *Progress in neurobiology* **42,** 489-537.

Kaila K, Voipio J, Paalasmaa P, Pasternack M & Deisz R. (1993). The role of bicarbonate in GABAA receptor-mediated IPSPs of rat neocortical neurones. *The Journal of Physiology* **464,** 273-289.

Kanter ED, Kapur A & Haberly LB. (1996). A dendritic GABAA-mediated IPSP regulates facilitation of NMDA-mediated responses to burst stimulation of afferent fibers in piriform cortex. *The Journal of neuroscience* **16,** 307-312.

Kapur A, Pearce R, Lytton W & Haberly L. (1997). GABAA-mediated IPSCs in piriform cortex have fast and slow components with different properties and locations on pyramidal cells. *Journal of neurophysiology* **78,** 2531-2545.

Kemp PJ. (2006). Detecting acute changes in oxygen: will the real sensor please stand up? *Experimental physiology* **91,** 829-834.

Kemp PJ, Lewis A, Hartness ME, Searle GJ, Miller P, O'Kelly I & Peers C. (2002). Airway chemotransduction: from oxygen sensor to cellular effector. *American journal of respiratory and critical care medicine* **166,** S17-S24.

Kesaraju S & Milton SL. (2009). Preliminary evidence of neuronal regeneration in the anoxia tolerant vertebrate brain. *Experimental neurology* **215,** 401-403.

Klann E & Thiels E. (1999). Modulation of protein kinases and protein phosphatases by reactive oxygen species: Implications for hippocampal synaptic plasticity. *Progress in Neuro-Psychopharmacology & Biological Psychiatry* **23,** 359-376.

Koch C & Poggio T. (1983). A Theoretical Analysis of Electrical Properties of Spines. *Proceedings of the Royal Society of London Series B, Biological Sciences* **218,** 455-477.

Koch C, Poggio T & Torre V. (1983). Non-linear interactions in a dendritic tree - localization, timing, and role in information-processing. *Proceedings of the National Academy of Sciences of the United States of America-Biological Sciences* **80,** 2799-2802.

Koopman WJ, Verkaart S, van Emst-de Vries SE, Grefte S, Smeitink JA & Willems PH. (2006). Simultaneous quantification of oxidative stress and cell spreading using 5-(and-6)-chloromethyl-2′, 7′-dichlorofluorescein. *Cytometry Part A* **69,** 1184-1192.

Kornau H-C. (2006). GABAB receptors and synaptic modulation. *Cell and tissue research* **326,** 517-533.

Kourie JI. (1998). Interaction of reactive oxygen species with ion transport mechanisms. *American Journal of Physiology - Cell Physiology* **275,** C1-C24.

Kriegstein AR & Connors BW. (1986a). Cellular physiology of the turtle visal cortex - Synaptic properties and intrinsic circuitry. *Journal of Neuroscience* **6,** 178-191.

Kriegstein AR & Connors BW. (1986b). Cellular physiology of the turtle visual cortex: synaptic properties and intrinsic circuitry. *The Journal of neuroscience* **6,** 178-191.

Krivoruchko A & Storey KB. (2010). Forever young: mechanisms of natural anoxia tolerance and potential links to longevity. *Oxidative medicine and cellular longevity* **3,** 186-198.

Lahiri S, Roy A, Baby S, Hoshi T, Semenza G & Prabhakar N. (2006). Oxygen sensing in the body. *Progress in biophysics and molecular biology* **91,** 249-286.

Lambert N & Grover L. (1995). The mechanism of biphasic GABA responses. *Science* **269,** 928-929.

Lampe JW & Becker LB. (2011). State of the art in therapeutic hypothermia. *Annual review of medicine* **62,** 79-93.

Land SC, Buck LT & Hochachka PW. (1993). Response of protein synthesis to anoxia and recovery in anoxia-tolerant hepatocytes. *American Journal of Physiology* **265,** R41-R41.

Lane N. (2005). *Power, sex, suicide: mitochondria and the meaning of life*. Oxford University Press.

Lang R, Harvey J, McPhee G & Klemm M. (2000). Nitric oxide and thiol reagent modulation of Ca2+-activated K+ (BKCa) channels in myocytes of the guinea-pig taenia caeci. *The Journal of physiology* **525,** 363-376.

Larkum ME, Watanabe S, Lasser-Ross N, Rhodes P & Ross WN. (2008). Dendritic properties of turtle pyramidal neurons. *Journal of neurophysiology* **99,** 683-694.

Larson J & Park TJ. (2009). Extreme hypoxia tolerance of naked mole-rat brain. *Neuroreport* **20,** 1634-1637.

Lauritzen M, Rice ME, Okada Y & Nicholson C. (1988). Quisqualate, kainate and NMDA can initiate spreading depression in the turtle cerebellum. *Brain Research* **475,** 317-327.

Lei BP, Adachi N & Arai T. (1998). Measurement of the extracellular H2O2 in the brain by microdialysis. *Brain Research Protocols* **3,** 33-36.

Leitch E, Coaker J, Young C, Mehta V & Sernagor E. (2005). GABA type-A activity controls its own developmental polarity switch in the maturing retina. *The Journal of neuroscience* **25,** 4801-4805.

Leroy P, Nicolas A, Gavriloff C, Matt M, Netter P, Bannwarth B, Hercelin B & Mazza M. (1991). Determination of 2-mercaptoproprionyl glycine and its metabolite, 2-mercaptopropionic acid, in plasma by ion-pair reversed-phase high performance liquid-chromatography with postcolumn derivatization. *Journal of Chromatography-Biomedical Applications* **564,** 258-265.

Li H, Siegel RE & Schwartz RD. (1993). Rapid decline of GABAA receptor subunit mRNA expression in hippocampus following transient cerebral ischemia in the gerbil. *Hippocampus* **3,** 527-537.

Lipton P. (1999). Ischemic cell death in brain neurons. *Physiol Rev* **79,** 1431-1568.

Liu H, Moczydlowski E & Haddad GG. (1999). O2 deprivation inhibits Ca2+-activated K+ channels via cytosolic factors in mice neocortical neurons. *Journal of Clinical Investigation* **104,** 577-588.

Lo EH. (2008). A new penumbra: transitioning from injury into repair after stroke. *Nature medicine* **14,** 497-500.

Lopez-Barneo J, Benot A & Urena J. (1993). Oxygen sensing and the electrophysiology of arterial chemoreceptor cells. *Physiology* **8,** 191-195.

Lopez-Barneo J, Lopez-Lopez JR, Urena J & Gonzalez C. (1988). Chemotransduction in the carotid body: K+ current modulated by PO2 in type I chemoreceptor cells. *Science* **241,** 580-582.

López-Barneo J, Pardal R & Ortega-Sáenz P. (2001). Cellular mechanism of oxygen sensing. *Annual Review of Physiology* **63,** 259-287.

López-López J, Gonzalez C & Perez-Garcia M. (1997). Properties of ionic currents from isolated adult rat carotid body chemoreceptor cells: effect of hypoxia. *The Journal of Physiology* **499,** 429-441.

Lutz PL & Kabler S. (1997). Release of adenosine and ATP in the brain of the freshwater turtle *Trachemys scripta* during long-term anoxia. *Brain research* **769,** 281-286.

Lutz PL & Nilsson GE. (1997). *The brain without oxygen*. Springer, Berlin.

Lutz PL, Nilsson GE & Prentice HM. (2003). *The brain without oxygen: causes of failure-physiological and molecular mechanisms for survival*. Springer.

Magistretti PJ & Allaman I. (2013). Brain energy metabolism. In *Neuroscience in the 21st Century*, pp. 1591-1620. Springer.

Magleby KL. (2003). Gating Mechanism of BK (Slo1) Channels So Near, Yet So Far. *The Journal of general physiology* **121,** 81-96.

Martin WF & Mentel M. (2010). The origin of mitochondria. *Nature*.

Marty A. (1981). Ca-dependent K channels with large unitary conductance in chromaffin cell membranes.

McCartney MR, Deeb TZ, Henderson TN & Hales TG. (2007). Tonically active GABAA receptors in hippocampal pyramidal neurons exhibit constitutive GABA-independent gating. *Molecular pharmacology* **71,** 539-548.

Mehrani H & Storey KB. (1995). cAMP-dependent protein kinase and anoxia survival in turtles: purification and properties of liver PKA. *Molecular and cellular biochemistry* **145,** 81-88.

Milton SL, Nayak G, Kesaraju S, Kara L & Prentice HM. (2007). Suppression of reactive oxygen species production enhances neuronal survival in vitro and in vivo in the anoxia-tolerant turtle Trachemys scripta. *Journal of Neurochemistry* **101,** 993-1001.

Mink JW, Blumenschine RJ & Adams DB. (1981). Ratio of central nervous-system to body metabolism in vertebrates - its constancy and functional basis. *American Journal of Physiology* **241,** R203-R212.

Mitchell SJ & Silver RA. (2003). Shunting Inhibition Modulates Neuronal Gain during Synaptic Excitation. *Neuron* **38,** 433-445.

Mittmann N, Seung SJ, Hill MD, Phillips SJ, Hachinski V, Cote R, Buck BH, Mackey A, Gladstone DJ, Howse DC, Shuaib A & Sharma M. (2012). Impact of disability status on ischemic stroke costs in Canada in the first year. *Can J Neurol Sci* **39,** 793-800.

Muir KW. (2006). Glutamate-based therapeutic approaches: clinical trials with NMDA antagonists. *Current opinion in pharmacology* **6,** 53-60.

Muller W & Bittner K. (2002). Differential oxidative modulation of voltage-dependent K+ currents in rat hippocampal neurons. *Journal of Neurophysiology* **87,** 2990-2995.

Nedergaard M & Hansen AJ. (1993). Characterization of cortical depolarizations evoked in focal cerebral ischemia. *Journal of Cerebral Blood Flow & Metabolism* **13,** 568-574.

Neher E. (1992). Correction for liquid junction potentials in patch-clamp experiments. *Methods in Enzymology* **207,** 123-131.

Nicholls DG & Budd SL. (2000). Mitochondria and neuronal survival. *Physiol Rev* **80,** 315-360.

Nicol S, Glass M & Heisler N. (1983). Comparison of directly determined and calculated plasma bicarbonate concentration in the turtle *Chrysemys picta bellii* at different temperatures. *Journal of experimental biology* **107,** 521-525.

Nillsson GE & Lutz PL. (1992). Short communication: adenosine release in the anoxic turtle brain: a possible mechanism for anoxic survival. *Journal of Experimental Biology* **162,** 345-351.

Nilsson GE & Lutz PL. (1991). Release of inhibitory neurotransmitters in response to anoxia in turtle brain. *American Journal of Physiology-Regulatory, Integrative and Comparative Physiology* **261,** R32-R37.

Nilsson GE & Renshaw GM. (2004). Hypoxic survival strategies in two fishes: extreme anoxia tolerance in the North European crucian carp and natural hypoxic preconditioning in a coral-reef shark. *Journal of Experimental Biology* **207,** 3131-3139.

Nishida M, Maruyama Y, Tanaka R, Kontani K, Nagao T & Kurose H. (2000). G alpha(i) and G alpha(o) are target proteins of reactive oxygen species. *Nature* **408,** 492-495.

Numann R, Catterall WA & Scheuer T. (1991). Functional modulation of brain sodium channels by protein kinase C phosphorylation. *Science* **254,** 115-118.

Nusser Z & Mody I. (2002). Selective modulation of tonic and phasic inhibitions in dentate gyrus granule cells. *Journal of neurophysiology* **87,** 2624-2628.

Olsen RW, DeLorey T, Siegel G, Agranoff B, Albers R, Fisher S & Uhler M. (1999). GABA and glycine. *Basic neurochemistry Molecular, cellular and medical aspects***,** 335-346.

Otmakhova NA & Lisman JE. (2004). Contribution of Ih and GABAB to synaptically induced afterhyperpolarizations in CA1: a brake on the NMDA response. *Journal of neurophysiology* **92,** 2027-2039.

Pakkenberg B, Pelvig D, Marner L, Bundgaard MJ, Gundersen HJG, Nyengaard JR & Regeur L. (2003). Aging and the human neocortex. *Experimental Gerontology* **38,** 95-99.

Pallotta BS, Magleby KL & Barrett JN. (1981). Single channel recordings of Ca2+-activated K+ currents in rat muscle cell culture.

Pamenter ME, Ali SS, Tang Q, Finley JC, Gu XQ, Dugan LL & Haddad GG. (2012a). An *in vitro* ischemic penumbral mimic perfusate increases NADPH oxidase-mediated superoxide production in cultured hippocampal neurons. *Brain research* **1452,** 165-172.

Pamenter ME & Buck LT. (2008). Neuronal membrane potential is mildly depolarized in the anoxic turtle cortex. *Comparative Biochemistry and Physiology Part A: Molecular & Integrative Physiology* **150,** 410-414.

Pamenter ME, Hogg DW, Gu XQ, Buck LT & Haddad GG. (2012b). Painted turtle cortex is resistant to an in vitro mimic of the ischemic mammalian penumbra. *Journal of Cerebral Blood Flow & Metabolism* **32,** 2033-2043.

Pamenter ME, Hogg DW, Ormond J, Shin DS, Woodin MA & Buck LT. (2011). Endogenous GABAA and GABAB receptor-mediated electrical suppression is critical to neuronal anoxia tolerance. *Proceedings of the National Academy of Sciences* **108,** 11274-11279.

Pamenter ME, Perkins GA, McGinness AK, Gu XQ, Ellisman MH & Haddad GG. (2012c). Autophagy and Apoptosis Are Differentially Induced in Neurons and Astrocytes Treated with an In Vitro Mimic of the Ischemic Penumbra. *PLoS ONE* **7,** e51469.

Pamenter ME, Richards MD & Buck LT. (2007). Anoxia-induced changes in reactive oxygen species and cyclic nucleotides in the painted turtle. *Journal of Comparative Physiology B: Biochemical, Systemic, and Environmental Physiology* **177,** 473-481.

Pamenter ME, Shin DS-H & Buck LT. (2008a). Adenosine A1 receptor activation mediates NMDA receptor activity in a pertussis toxin-sensitive manner during normoxia but not anoxia in turtle cortical neurons. *Brain research* **1213,** 27-34.

Pamenter ME, Shin DSH & Buck LT. (2008b). AMPA receptors undergo channel arrest in the anoxic turtle cortex. *American Journal of Physiology-Regulatory Integrative and Comparative Physiology* **294,** R606-R613.

Pamenter ME, Shin DSH, Cooray M & Buck LT. (2008c). Mitochondrial ATP-sensitive K+ channels regulate NMDAR activity in the cortex of the anoxic western painted turtle. *Journal of Physiology-London* **586,** 1043-1058.

Peers C. (1997). Oxygen-sensitive ion channels. *Trends in pharmacological sciences* **18,** 405-408.

Pék-Scott M & Lutz PL. (1998). ATP-sensitive K+ channel activation provides transient protection to the anoxic turtle brain. *American Journal of Physiology-Regulatory, Integrative and Comparative Physiology* **275,** R2023-R2027.

Pék M & Lutz PL. (1997). Role for adenosine in channel arrest in the anoxic turtle brain. *Journal of Experimental Biology* **200,** 1913-1917.

Perez-Pinzon M, Rosenthal M, Sick TJ, Lutz PL, Pablo J & Mash D. (1992a). Downregulation of sodium channels during anoxia: a putative survival strategy of turtle brain. *American Journal of Physiology-Regulatory, Integrative and Comparative Physiology* **262,** R712-R715.

Perez-Pinzon MA, Chan CY, Rosenthal M & Sick TJ. (1992b). Membrane and synaptic activity during anoxia in the isolated turtle cerebellum. *American Journal of Physiology-Regulatory, Integrative and Comparative Physiology* **263,** R1057-R1063.

Pitlik TN, Bulai PM, Denisov AA, Afanasenkov DS & Cherenkevich SN. (2009). Redox regulation of ionic homeostasis in neurons. *Neurochemical Journal* **3,** 87-92.

Ponganis PJ, Meir JU & Williams CL. (2011). In pursuit of Irving and Scholander: a review of oxygen store management in seals and penguins. *Journal of Experimental Biology* **214,** 3325-3339.

Pouille F & Scanziani M. (2001). Enforcement of temporal fidelity in pyramidal cells by somatic feed-forward inhibition. *Science* **293,** 1159-1163.

Qian N & Sejnowski TJ. (1990). When is an inhibitory synapse effective? *Proceedings of the National Academy of Sciences* **87,** 8145-8149.

Ramaglia V & Buck LT. (2004). Time-dependent expression of heat shock proteins 70 and 90 in tissues of the anoxic western painted turtle. *Journal of experimental biology* **207,** 3775-3784.

Rice ME. (2011). H2O2: A Dynamic Neuromodulator. *Neuroscientist* **17,** 389-406.

Rice ME, Lee EJ & Choy Y. (1995). High Levels of Ascorbic Acid, Not Glutathione, in the CNS of Anoxia-Tolerant Reptiles Contrasted with Levels in Anoxia-Intolerant Species. *Journal of neurochemistry* **64,** 1790-1799.

Rider MH, Hussain N, Dilworth SM & Storey KB. (2009). Phosphorylation of translation factors in response to anoxia in turtles, Trachemys scripta elegans: role of the AMP-activated protein kinase and target of rapamycin signalling pathways. *Molecular and cellular biochemistry* **332,** 207-213.

Riesco-Fagundo A, Perez-Garcia M, Gonzalez C & Lopez-Lopez J. (2001). O2 modulates large-conductance Ca2+-dependent K+ channels of rat chemoreceptor cells by a membrane-restricted and CO-sensitive mechanism. *Circulation research* **89,** 430-436.

Rivera C, Voipio J, Payne JA, Ruusuvuori E, Lahtinen H, Lamsa K, Pirvola U, Saarma M & Kaila K. (1999). The K+/Cl− co-transporter KCC2 renders GABA hyperpolarizing during neuronal maturation. *Nature* **397,** 251-255.

Rizzuto R & Pozzan T. (2006). Microdomains of intracellular Ca2+: molecular determinants and functional consequences. *Physiological reviews* **86,** 369-408.

Rodgers-Garlick CI, Hogg DW & Buck LT. (2013). Oxygen-sensitive reduction in Ca2+-activated K+ channel open probability in turtle cerebrocortex. *Neuroscience* **237,** 243-254.

Rodgers CI, Armstrong GA & Robertson RM. (2010). Coma in response to environmental stress in the locust: a model for cortical spreading depression. *Journal of insect physiology* **56,** 980-990.

Rodgers CI, Armstrong GA, Shoemaker KL, LaBrie JD, Moyes CD & Robertson RM. (2007). Stress preconditioning of spreading depression in the locust CNS. *PLoS One* **2,** e1366.

Rollinson N, Tattersall GJ & Brooks RJ. (2008). Overwintering habitats of a northern population of Painted Turtles (Chrysemys picta): winter temperature selection and dissolved oxygen concentrations. *Journal of Herpetology* **42,** 312-321.

Rossi DJ, Oshima T & Attwell D. (2000). Glutamate release in severe brain ischaemia is mainly by reversed uptake. *Nature* **403,** 316-321.

Rudolph U & Knoflach F. (2011). Beyond classical benzodiazepines: novel therapeutic potential of GABAA receptor subtypes. *Nat Rev Drug Discov* **10,** 685-697.

Sah P & Louise Faber E. (2002). Channels underlying neuronal calcium-activated potassium currents. *Progress in neurobiology* **66,** 345-353.

Saliba RS, Kretschmannova K & Moss SJ. (2012). Activity-dependent phosphorylation of GABA(A) receptors regulates receptor insertion and tonic current. *Embo Journal* **31,** 2937-2951.

Scheuer T. (2011). Regulation of sodium channel activity by phosphorylation. In *Seminars in cell & developmental biology*, pp. 160-165. Elsevier.

Schiene K, Bruehl C, Zilles K, Qu M, Hagemann G, Kraemer M & Witte OW. (1996). Neuronal Hyperexcitability and Reduction of GABAA-Receptor Expression in the Surround of Cerebral Photothrombosis. *J Cereb Blood Flow Metab* **16,** 906-914.

Semyanov A, Walker MC, Kullmann DM & Silver RA. (2004). Tonically active GABAA receptors: modulating gain and maintaining the tone. *Trends in Neurosciences* **27,** 262-269.

Senior A. (1988). ATP synthesis by oxidative phosphorylation. *Physiol Rev* **68,** 177-231.

Shen JM & Kriegstein AR. (1986). Turtle Hippocampal Cortex Contains Distinct Cell Types, Burst-Firing Neurons, and an Epileptogenic Subfield. *Journal of Neurophysiology* **56**.

Shepherd GM. (2011). The microcircuit concept applied to cortical evolution: from three-layer to six-layer cortex. *Frontiers in neuroanatomy* **5**.

Shin DS-H, Wilkie MP, Pamenter ME & Buck LT. (2005). Calcium and protein phosphatase 1/2A attenuate *N*-methyl-d-aspartate receptor activity in the anoxic turtle cortex. *Comparative Biochemistry and Physiology Part A: Molecular & Integrative Physiology* **142,** 50-57.

Shin DSH & Buck LT. (2003). Effect of anoxia and pharmacological anoxia on whole-cell NMDA receptor currents in cortical neurons from the western painted turtle. *Physiological and Biochemical Zoology* **76,** 41-51.

Shindou T, Nonaka H, Richardson PJ, Mori A, Kase H & Ichimura M. (2002). Presynaptic adenosine A2A receptors enhance GABAergic synaptic transmission via a cyclic AMP dependent mechanism in the rat globus pallidus. *British journal of pharmacology* **136,** 296-302.

Shulman RG & Rothman DL. (2004). *Brain Energetics and Neuronal Activity: Applications to FMRI and Medicine*. John Wiley & Sons.

Shulman RG, Rothman DL, Behar KL & Hyder F. (2004). Energetic basis of brain activity: implications for neuroimaging. *Trends in Neurosciences* **27,** 489-495.

Sick TJ, Rosenthal M, LaManna JC & Lutz PL. (1982). Brain potassium ion homeostasis, anoxia, and metabolic inhibition in turtles and rats. *Am J Physiol* **243,** R281-R288.

Siesjo BK. (1978). Brain energy metabolism.

Siesjö BK. (1992). Pathophysiology and treatment of focal cerebral ischemia: Part I: Pathophysiology. *Journal of neurosurgery* **77,** 169-184.

Sigel E & Steinmann ME. (2012). Structure, function, and modulation of GABAA receptors. *Journal of Biological Chemistry* **287,** 40224-40231.

Simonds WF. (1999). G protein regulation of adenylate cyclase. *Trends in pharmacological sciences* **20,** 66-73.

Somjen GG. (1979). Extracellular potassium in the mammalian central nervous system. *Annual review of physiology* **41,** 159-177.

Staley KJ & Mody I. (1992). Shunting of excitatory input to dentate gyms granule cells by a depolarizing GABA A receptor-mediated postsynaptic conductance. *J Neurophysiol* **68,** 197-212.

Staples JF & Buck LT. (2009). Matching cellular metabolic supply and demand in energy-stressed animals. *Comparative Biochemistry and Physiology a-Molecular & Integrative Physiology* **153,** 95-105.

Stensløkken K-O, Ellefsen S, Stecyk JA, Dahl MB, Nilsson GE & Vaage J. (2008). Differential regulation of AMP-activated kinase and AKT kinase in response to oxygen availability in crucian carp (Carassius carassius). *American Journal of Physiology-Regulatory, Integrative and Comparative Physiology* **295,** R1803-R1814.

Stone TW. (1981). Physiological roles for adenosine and adenosine 5′-triphosphate in the nervous system. *Neuroscience* **6,** 523-555.

Stys PK, Waxman SG & Ransom BR. (1991). Na+-Ca2+ exchanger mediates Ca2+ influx during anoxia in mammalian central nervous system white matter. *Annals of neurology* **30,** 375-380.

Sylvester J, Shimoda LA, Aaronson PI & Ward JP. (2012). Hypoxic pulmonary vasoconstriction. *Physiological Reviews* **92,** 367-520.

Tabares L, López-Barneo J & de Miguel C. (1985). Calcium-and voltage-activated potassium channels in adrenocortical cell membranes. *Biochimica et Biophysica Acta (BBA)-Biomembranes* **814,** 96-102.

Thompson JW, Prentice HM & Lutz PL. (2007a). Regulation of extracellular glutamate levels in the long-term anoxic turtle striatum: coordinated activity of glutamate transporters, adenosine, K ATP+ channels and GABA. *Journal of biomedical science* **14,** 809-817.

Thompson R, Buttigieg J, Zhang M & Nurse C. (2007b). A rotenone-sensitive site and H_2O_2 are key components of hypoxia-sensing in neonatal rat adrenomedullary chromaffin cells. *Neuroscience* **145,** 130-141.

Thompson RJ & Nurse CA. (1998). Anoxia differentially modulates multiple K+ currents and depolarizes neonatal rat adrenal chromaffin cells. *The Journal of physiology* **512,** 421-434.

Thompson SM & Gahwiler BH. (1989). Activity-Dependent Disinhibition. II. Effects of Extracellular Potassium, Furosemide, and Membrane Potential on E&-in Hippocampal CA3 Neurons.

Trigo FF, Bouhours B, Rostaing P, Papageorgiou G, Corrie JE, Triller A, Ogden D & Marty A. (2010). Presynaptic miniature GABAergic currents in developing interneurons. *Neuron* **66,** 235-247.

Turrens JF. (2003). Mitochondrial formation of reactive oxygen species. *Journal of Physiology-London* **552,** 335-344.

Ulinski P. (2007). Visual Cortex of Turtles. In *Evolution of Nervous Systems*, ed. Kaas JH, pp. 195-201. Elsevier.

Ultsch GR. (1989). Ecology and physiology of hibernation and overwintering among freshwater fishes, turtles, and snakes. *Biological Reviews* **64,** 435-515.

Ultsch GR & Jackson DC. (1982). Long-term submergence at 3 C of the turtle, Chrysemys picta bellii, in normoxic and severely hypoxic water: I. Survival, gas exchange and acid-base status. *Journal of Experimental Biology* **96,** 11-28.

Van Harreveld A, Stamm J & Christensen E. (1956). Spreading depression in rabbit, cat and monkey. *Am J Physiol* **184,** 312-320.

van Welie I & du Lac S. (2011). Bidirectional control of BK channel open probability by CAMKII and PKC in medial vestibular nucleus neurons. *Journal of neurophysiology* **105,** 1651-1659.

Van Wylen DG, Park T, Rubio R & Berne RM. (1986). Increases in cerebral interstitial fluid adenosine concentration during hypoxia, local potassium infusion, and ischemia. *Journal of Cerebral Blood Flow & Metabolism* **6,** 522-528.

Veal EA, Day AM & Morgan BA. (2007). Hydrogen peroxide sensing and signaling. *Molecular cell* **26,** 1-14.

Verdoorn TA, Draguhn A, Ymer S, Seeburg PH & Sakmann B. (1990). Functional-propreties of recombinant rat GABA-A receptors depend upon subunit composition. *Neuron* **4,** 919-928.

Vornanen M & Paajanen V. (2006). Seasonal changes in glycogen content and Na+-K+-ATPase activity in the brain of crucian carp. *American Journal of Physiology-Regulatory, Integrative and Comparative Physiology* **291,** R1482-R1489.

Ward J. (2008). Oxygen sensors in context. *Biochimica et Biophysica Acta (BBA)-Bioenergetics* **1777,** 1-14.

Warner DS, Sheng H & Batinić-Haberle I. (2004). Oxidants, antioxidants and the ischemic brain. *Journal of experimental biology* **207,** 3221-3231.

Warren DE & Jackson DC. (2008). Lactate metabolism in anoxic turtles: an integrative review. *Journal of Comparative Physiology B* **178,** 133-148.

Wasser JS, Warburton SJ & Jackson DC. (1991). Extracellular and intracellular acid-base effects of submergence anoxia and nitrogen breathing in turtles. *Respiration physiology* **83,** 239-252.

Watanabe M, Wake H, Moorhouse AJ & Nabekura J. (2009). Clustering of Neuronal K+-Cl-Cotransporters in Lipid Rafts by Tyrosine Phosphorylation. *Journal of Biological Chemistry* **284,** 27980-27988.

Weir EK, López-Barneo J, Buckler KJ & Archer SL. (2005). Acute oxygen-sensing mechanisms. *New England Journal of Medicine* **353,** 2042-2055.

Widmer HA, Rowe IC & Shipston MJ. (2003). Conditional protein phosphorylation regulates BK channel activity in rat cerebellar Purkinje neurons. *The Journal of physiology* **552,** 379-391.

Wilkie MP, Pamenter ME, Alkabie S, Carapic D, Shin DS & Buck LT. (2008). Evidence of anoxia-induced channel arrest in the brain of the goldfish (< i> Carassius auratus</i>). *Comparative Biochemistry and Physiology Part C: Toxicology & Pharmacology* **148,** 355-362.

Williams GS, Boyman L, Chikando AC, Khairallah RJ & Lederer W. (2013). Mitochondrial calcium uptake. *Proceedings of the National Academy of Sciences* **110,** 10479-10486.

Williams SE, Wootton P, Mason HS, Bould J, Iles DE, Riccardi D, Peers C & Kemp PJ. (2004a). Hemoxygenase-2 is an oxygen sensor for a calcium-sensitive potassium channel. *Science* **306,** 2093-2097.

Williams SEJ, Wootton P, Mason HS, Bould J, Iles DE, Riccardi D, Peers C & Kemp PJ. (2004b). Hemoxygenase-2 Is an Oxygen Sensor for a Calcium-Sensitive Potassium Channel. *Science* **306,** 2093-2097.

Willmore W & Storey K. (1997a). Antioxidant systems and anoxia tolerance in a freshwater turtle Trachemys scripta elegans. *Molecular and cellular biochemistry* **170,** 177-185.

Willmore WG & Storey KB. (1997b). Glutathione systems and anoxia tolerance in turtles. *American Journal of Physiology-Regulatory Integrative and Comparative Physiology* **42,** R219.

Wyatt CN & Buckler KJ. (2004). The effect of mitochondrial inhibitors on membrane currents in isolated neonatal rat carotid body type I cells. *The Journal of physiology* **556,** 175-191.

Wyatt CN, Mustard KJ, Pearson SA, Dallas ML, Atkinson L, Kumar P, Peers C, Hardie DG & Evans AM. (2007). AMP-activated protein kinase mediates carotid body excitation by hypoxia. *Journal of Biological Chemistry* **282,** 8092-8098.

Wyatt CN & Peers C. (1995). Ca^{2+}-activated K+ channels in isolated type I cells of the neonatal rat carotid body. *The Journal of Physiology* **483,** 559-565.

Yao H, Shu Y, Wang J, Brinkman BC & Haddad GG. (2007). Factors influencing cell fate in the infarct rim. *Journal of neurochemistry* **100,** 1224-1233.

Youngson C, Nurse C, Yeger H & Cutz E. (1993). Oxygen sensing in airway chemoreceptors. *Nature* **365,** 153-155.

Yowtak J, Lee KY, Kim HY, Wang JG, Kim HK, Chung K & Chung JM. (2011). Reactive oxygen species contribute to neuropathic pain by reducing spinal GABA release. *Pain* **152,** 844-852.

Yu Y, Hill AP & McCormick DA. (2012). Warm body temperature facilitates energy efficient cortical action potentials. *PLoS computational biology* **8,** e1002456.

Zhou N, Gordon GR, Feighan D & MacVicar BA. (2010). Transient swelling, acidification, and mitochondrial depolarization occurs in neurons but not astrocytes during spreading depression. *Cerebral Cortex* **20,** 2614-2624.

Zivkovic G & Buck LT. (2010). Regulation of AMPA receptor currents by mitochondrial ATP-sensitive K+ channels in anoxic turtle neurons. *Journal of neurophysiology* **104,** 1913-1922.

Zoccarato F, Valente M & Alexandre A. (1995). Hydrogen peroxide induces a long lasting inhibition of the Ca2+ dependent glutamate release in cerebralcortical synaptosomes without interfering with cytosolic Ca2+. *Journal of Neurochemistry* **64,** 2552-2558.